Dispositifs médicaux intelligents à base d'hydrogel de polysaccharide obtenus par Impression 4D

Michel Habib

THÈSE POUR OBTENIR LE GRADE DE DOCTEUR DE L'UNIVERSITÉ DE MONTPELLIER

En Sciences des Procédés des matériaux, bioproduits et aliments

École doctorale GAIA

Unité de recherche de l'Institut Charles Gerhardt de Montpellier, UMR 5253

Dispositifs médicaux intelligents à base d'hydrogel de polysaccharide obtenus par Impression 4D

Présentée par Michel HABIB
Le 17 Octobre 2024

Sous la direction du
Dr. Tahmer SHARKAWI, Pr. Audrey TOURRETTE et Dr. Sébastien BLANQUER

Devant le jury composé de

Rachel AUZELY-VELTY, Professeur, Université Grenoble Alpes	Rapporteur
Etienne FLEURY, Professeur, INSA Lyon	Rapporteur
Sophie FULLANA-GIROD, Professeur, Université de Toulouse III Paul Sabatier	Examinateur
Michel BOISSIERE, Maître de Conférence, Université de Cergy-Pontoise	Examinateur
Tahmer SHARKAWI, Professeur, Université de Montpellier	Directeur de thèse
Audrey TOURRETTE, Professeur, Université de Toulouse III Paul Sabatier	Co-directeur de thèse
Sébastien BLANQUER, Chargé de Recherches, Université de Montpellier	Co-encadrant de thèse
Céline POCHAT, Maître de Conférence, Université de Montpellier	Invitée

UNIVERSITÉ DE MONTPELLIER

To the ones who believed

"Words offer the means to meaning, and for those who will listen, the enunciation of truth"

V

"Bettering yourself is intelligence. Bettering others is virtue. Bettering the world is enlightenment."

Matshona Dhliwayo

"We must all face the choice between what is right and what is easy"

J.K. Rowling

TABLE OF CONTENTS / TABLEAU DE MATIERES

ABRÉVIATIONS

AAc	acrylic acid
Alg-MA	methacrylated alginate
Alg-MA	methacrylated alginate
Alg-Na^+	Sodium alginate
BSED	backscattered electron detector
CEC	critical entanglement concentration
CMC	carboxymethyl cellulose
CMC	critical micellar concentration
CS	chitosan
DCM	dicholomethane
Dextran-MA	dextran methacrylate
DIW	direct ink writing
DLP	digital light processing
DM	degree of modification
DMA	dopamine methacrylamide
DMAAm	N,N-dimethyl acrylamide
DMAEMA	dimethylaminoethyl methacrylate
DMAPMA	N-[3-(dimethylamino) propyl] methacrylamide
EDTA	ethylenediaminetetraacetic acid tetrasodium
EG	ethylene glycol
G	guluronic
GC	gel content
Gel-MA	methacrylated gelatin
GO	graphene oxide
HABI	hexaarylbiimidazole
HVA	high viscosity sodium alginate
LAP	lithium phenyl-2,4,6-trimethylbenzoylphosphinate
LCST	lower critical solution temperature
LVA	low viscosity sodium alginate
M	mannuronic
MA	methacrylic anhydride

MA	methacrylic anhydride
MA-BSA	methacrylated bovine serum albumin
MAPBA	methacrylamidophenylboronic acid
MC	methyl cellulose
Mc	mesh size
Mn	number average molecular weight
MVA	medium viscosity sodium alginate
Mw	weight average molecular weight
NAGA	N-acryloylglycinamide
NdFeB	neodymium iron boron magnetic
NFC	nanofibrilated cellulose
NiPAAm	N-isopropylacrylamide
NIR	near infra red
Oalg-MA	oxidized methacrylated alginate
PAAc	poly(acrylic acid)
PAAm	poly(acrylamide)
PBS	phosphate buffer solution
PDI	polydispersity index
PDMAPMA	poly(N-[3-(dimethylamino) propyl] methacrylamide)
PDMS	poly(dimethyl siloxane)
PEG	poly(ethylene glycol)
PEtOx	poly(2-ethyl-2-oxazoline)
PG	propylene glycol
PHEAm	poly(N-hydroxyethylacrylamide)
PHEMA	poly(2-hydroxyethyl methacrylate)
PiPrOx	poly(2-isopropyl-2-oxazoline
PMEO$_2$MA	poly(2-(2-methoxyethoxy) ethyl methacrylate)
PNAGA	poly(N-acryloylglycinamide)
PNiPAAm	poly(N-isopropylacrylamide)
PVA	Poly(vinylalcohol)
Q	swelling degree
R_H	hydrodynamic radius
SANS	small-angle neutron scattering

SD	standard deviation
SEM	scanning electron microscopy
SLA	stereolithography
SMP	shape memory polymer
SP	spiropyran
TDA	Taylor dispersion analysis
TEA	triethylamine
TGA	thermogravimetric analysis
UCST	upper critical solution temperature
UV	ultraviolet
VHB	very high bond
VPTT	volume phase transition temperature

INTRODUCTION GENERALE

Introduction Générale

Les maladies chroniques et les besoins en soins personnalisés augmentent de façon exponentielle, et les avancées dans les technologies biomédicales sont essentielles pour répondre à ces défis. Ces applications couvrent un large éventail, allant des dispositifs médicaux implantables (soit dans le cadre de traitement thérapeutique ou encore dans le contexte de reconstruction/réparation tissulaire), aux systèmes de délivrance de médicaments ciblés (administration précise et contrôlée de biomolécules actives). Les technologies biomédicales, comme les prothèses intelligentes et les organes artificiels, repoussent les limites de ce qui est possible, offrant aux patients une qualité de vie améliorée et des options de traitement plus efficaces.

Dans ce contexte, les hydrogels se révèlent particulièrement précieux en raison de leur capacité à imiter les propriétés naturelles des tissus humains, ce qui est crucial pour des applications comme l'ingénierie tissulaire ou encore la cicatrisation des plaies. De plus, les hydrogels ont l'avantage d'être employé comme de puissant et efficace système de délivrance contrôlée de principes actifs, minimisant les effets secondaires et augmentant l'efficacité des traitements. Ces applications biomédicales sont essentielles pour le développement de nouvelles thérapies et dispositifs, permettant de répondre aux besoins médicaux non satisfaits et d'améliorer les soins de santé à un niveau global.

Les hydrogels intelligents, ou hydrogels sensibles aux stimuli, représentent une avancée majeure dans le domaine des applications biomédicales. Ces matériaux ont la capacité de réagir de manière contrôlée à des changements dans leur environnement, tels que la température, le pH, la lumière ou les champs électriques et magnétiques. Cette réactivité permet aux hydrogels intelligents de s'adapter et de répondre de manière dynamique aux conditions spécifiques du corps humain.

L'utilisation d'hydrogels stimulables dans les applications biomédicales a ouvert de nouvelles perspectives dans la conception de matériaux capables de répondre de manière dynamique à leur environnement. Ces hydrogels, qui réagissent à des stimuli externes peuvent être conçus pour se déformer, changer de forme, ou même se déplacer en réponse à ces stimulations. Cette capacité de transformation permet de développer des dispositifs médicaux qui ne se contentent

pas de réagir passivement à leur environnement, mais qui peuvent également adopter des configurations optimisées en fonction des conditions locales.

La technologie d'impression 4D pousse encore plus loin le potentiel de déformation de ces hydrogels stimulables. Contrairement à l'impression 3D traditionnelle, qui produit des objets statiques en trois dimensions, l'impression 4D permet de créer des structures qui peuvent évoluer et changer de propriétés dans le temps sous l'effet de stimuli spécifiques. En intégrant des hydrogels stimulables dans cette technologie, il est possible de concevoir des matériaux intelligents qui changent de forme après leur fabrication, permettant des applications en chirurgie mini-invasive comme des implants qui se déploient progressivement une fois implantés, ou des scaffolds tissulaires qui s'adaptent aux besoins de régénération du patient. Cette capacité à concevoir des matériaux qui non seulement réagissent, mais qui évoluent activement, ouvre la voie à des innovations médicales qui pourraient transformer la manière dont les traitements sont administrés et personnalisés, rendant la médecine de demain plus réactive et adaptable.

La majorité des hydrogels intelligents pour l’impression 4D sont actuellement à base de polymères synthétiques, tels que le poly(acrylamide) (PAAm), le poly(N-isopropylacrylamide) (PNiPAAm), ou les dérivés du polyéthylène glycol (PEG). Ces polymères synthétiques sont largement utilisés en raison de leur facilité de fabrication, leur stabilité chimique, leur imprimabilité et la possibilité de moduler leurs propriétés en fonction des besoins spécifiques des applications. Cependant, malgré leurs avantages, ces polymères synthétiques peuvent présenter des limitations, notamment en termes de biodégradabilité et parfois de biocompatibilité, ce qui est un obstacle lorsqu'ils sont utilisés dans des applications *in vivo* à long terme.

En revanche, l'impression 4D utilisant des hydrogels naturels est beaucoup moins courante dans la littérature. Pourtant, les polymères naturels, tels que les polysaccharides ou protéines, offrent des avantages significatifs pour les applications biomédicales, notamment en matière de biocompatibilité et de biodégradabilité. Ces polymères, dérivés de sources naturelles, sont souvent mieux tolérés par l'organisme, réduisant ainsi le risque de réaction immunitaire ou d'inflammation. De plus, les polymères naturels offrent de nombreuses fonctionnalités chimiques, permettant ainsi des modifications afin de faire varier ces propriétés. Malgré ces derniers avantages, les hydrogels naturels présentent souvent des propriétés mécaniques

insuffisantes, réduisant ainsi leur efficacité dans des applications spécifiques. Bien que des modifications chimiques puissent améliorer ces caractéristiques, elles se révèlent généralement insuffisantes pour satisfaire pleinement certaines exigences. En outre, en raison de leur faible solubilité et de leur viscosité élevée en solution, l'imprimabilité des polymères naturels pose un réel défi.

Ainsi, l'impression 4D utilisant des hydrogels à base de polysaccharides représente un enjeu considérable, en raison des obstacles techniques et des propriétés complexes de ces matériaux. C'est dans ce contexte que ce projet de thèse s'inscrit, visant à explorer et à surmonter ces défis pour développer des dispositifs innovantes et viables à base d'alginate dans ce domaine en pleine expansion.

L'alginate de sodium est un polysaccharide naturel extrait des algues brunes. C'est un polysaccharide statistique de deux unités de répétitions : mannuronate (M) et guluronate (G). Chaque monomère est composé de deux groupes hydroxyles (-OH) et une fonction carboxylique ($-COO^-$, Na^+). L'alginate est sensible au pH et aux ions. À pH bas, les groupements carboxyles sont protonés, ce qui limite ça solubilité dans l'eau. À pH neutre ou élevé, ces groupements carboxyles sont déprotonés, favorisant ça solubilité dans l'eau ainsi que la formation de liaisons ioniques avec des cations multivalents tels que le calcium (Fe^{3+}, Cu^{2+}, Ca^{2+}, Mn^{2+}) entre les blocs G. La présence de ces cations permet la réticulation physiquement des chaînes d'alginate par la formation de "zones d'œufs" ou "egg-box", où les ions calcium agissent comme nœud de réticulation en formant des liaisons ioniques. Ce mécanisme de gélification crée un réseau tridimensionnel stable et résistant. Grâce à sa capacité de gélification, l'alginate est largement utilisé dans le domaine de la santé. Tel que cité précédemment, la présence de groupements fonctionnels permet une modification chimique, conduisant à une réticulation chimique des chaînes ce qui entraîne de nouvelles propriétés. En exploitant ces caractéristiques, il est possible de préparer une résine (mélange de solvant, polymère et photo-amorceur) réticulable sous UV afin de générer des hydrogels avec de nouvelles propriétés que nous allons particulièrement étudier dans cette thèse dans l'objectif de l'utiliser avec des techniques de fabrication additive par photo-polymérisation tel que la stéréolitographie. L'alginate répond au cahier de charge de polysaccharide sensible à un stimulus, biocompatible et présente un potentiel pour l'impression par stéréolithographie dans des conditions modérées (température ambiante et pH neutre).

De cette étude sur les hydrogels stimulables et imprimés à base d'alginate, notre objectif est de cibler le développement de **dispositifs médicaux intelligents en impression 4D**. Avant de passer à la fabrication en 3D de ces hydrogels, il est impératif de développer une résine adaptée aux exigences spécifiques de ce processus. La résine joue un rôle critique dans la fabrication additive, influençant la précision, la résolution et les propriétés finales de l'objet imprimé en 3D. En optimisant la formulation de la résine à base d'alginate, il sera possible de développer une nouvelle génération de dispositifs et de thérapies biomédicales par impression 3D.

Dans cet objectif, le **chapitre I** du manuscrit se concentre sur l'état de l'art au sujet de la conception d'actuateurs intelligents à base d'hydrogel pour des potentielles applications biomédicales. Cette étude s'intéresse dans un premier temps aux polymères utilisés et aux différents stimuli auxquels ils répondent. Ensuite, les différentes méthodes de fabrication des actuateurs suivant différentes échelles géométriques (incluant des structures 1D, 2D et 3D), ainsi que le contrôle de leur actuation sont explorées.

Le **chapitre II** présente une étude approfondie sur l'élaboration d'hydrogels à base d'alginate obtenus par double réticulation physique et chimique par photo-polymérisation. L'influence de différents paramètres est étudiée, notamment celle de la masse molaire et du degré de méthacrylation sur les propriétés de ces hydrogels d'alginate. D'autres propriétés remarquables liées à la réticulation duale de l'alginate ont été également démontrées.

Le **chapitre III** se focalise sur l'optimisation du procédé d'impression 4D de la résine à base d'alginate. La conception d'actuateurs par contrôle du gradient de réticulation permet de générer différentes déformations programmées sur diverses géométries. Les comportements de changement de formes ont également été démontrés sur des structures 3D.

Dans la perspective d'apporter une réponse thermique aux hydrogels d'alginate par l'hybridation avec un hydrogel thermo-sensible, nous nous sommes penchés, dans le **chapitre IV,** sur l'influence de la méthacrylation dans le comportement thermique de plusieurs Pluronics. À travers une étude rhéologique approfondie, les diagrammes de phases des Pluronics modifiés P123, P104 et F127 ont été élaborés afin d'obtenir des hydrogels thermo-sensibles.

Enfin, le **chapitre V** étudie l'impression 4D des hydrogels à base d'alginate, dont les propriétés mécaniques sont renforcées par l'incorporation de Pluronic F127 méthacrylé dans la résine. Le

changement de forme programmé a permis de développer et de démontrer des preuves de concept pour des dispositifs médicaux adaptés à ces changements de formes.

CHAPTER I / CHAPITRE I

Introduction Chapitre I

Le chapitre 1 se concentre sur un état de l'art des hydrogels stimulables et des divers stimuli utilisés dans le domaine biomédical. Ces matériaux, capables de répondre à des stimuli externes tels que la température, le pH et/ou la lumière, présentent un fort potentiel pour la conception de dispositifs médicaux innovants. Le chapitre explore les bases de la construction d'actuateurs hydrogels, en examinant le choix des polymères appropriés et les méthodes de fabrication avancées, comme les systèmes bicouches ou par l'impression 4D, pour obtenir des configurations spécifiques et programmées.

De plus, ce chapitre aborde le contrôle de l'actuation de ces hydrogels, un élément essentiel pour le développement de dispositifs médicaux fonctionnels programmés. Il met en lumière les techniques permettant d'ajuster les paramètres de fabrication, tels que le degré de réticulation ou la distribution spatiale des réseaux polymériques, afin de diriger la déformation du matériau en réponse à un stimulus donné, et ainsi concevoir des dispositifs médicaux adaptés à des applications spécifiques.

Chapter I

Stimuli Responsive Hydrogel Actuators for Biomedical Applications: Design to Actuation

1. INTRODUCTION

Hydrogels are a class of materials that have gained significant attention in various fields such as biomedical engineering, agriculture, soft robotics and environmental science due to their unique properties.[1,2] Hydrogels are a 3D crosslinked hydrophilic networks that can retain a large amount of water. They can be obtained by various crosslinking methods including physical crosslinking (hydrogel bonding, hydrophobic interactions or ionic interactions) or chemical crosslinking (covalent bonds obtained during curing process).[3]The polymeric structures can be based on synthetic or natural polymers. Furthermore, based on the nature of the matrix, stimuli responsive hydrogels can be chosen to exhibit a conformational change under an external stimulus such as temperature, pH, ionic strength, light, magnetic field.[4] Hence, once crosslinked, the conformational change of the matrix will be translated by a modification of the hydrogel's properties (color, mechanical properties, fluorescence, etc…) or swelling behavior (swelling / shrinking).[5] In this review, the responsive behavior is focused on the volumetric change of the hydrogel that could potentially be translated into a mechanical motion leading to smart hydrogel actuators as represented in Figure I-1 to be used for the conception of medical devices.

The significance of hydrogel actuators lies in their ability to undergo large, reversible, programmed shape deformation in response to an external stimulus.[6] These soft materials capable of mimicking the dynamic behavior of biological systems offer many advantages in robotics due their flexibility and adaptability for various tasks. For biomedical engineering they can be used as drug delivery systems, or three-dimensional scaffolds for cell growth and tissue engineering due to their tunable mechanical properties. Adapting a hydrogel actuator system to a specific application is no easy task. It is crucial to understand the behavior of the hydrogel system, study its swelling/shrinking behavior, tune its mechanical properties before translating the volumetric change into a physical motion. The importance of shape deformation in hydrogels cannot be overstated. It is the key mechanism through which these materials undergo

dynamic responses to external stimuli allowing them to perform a wide range of tasks in the biomedical field.[7]

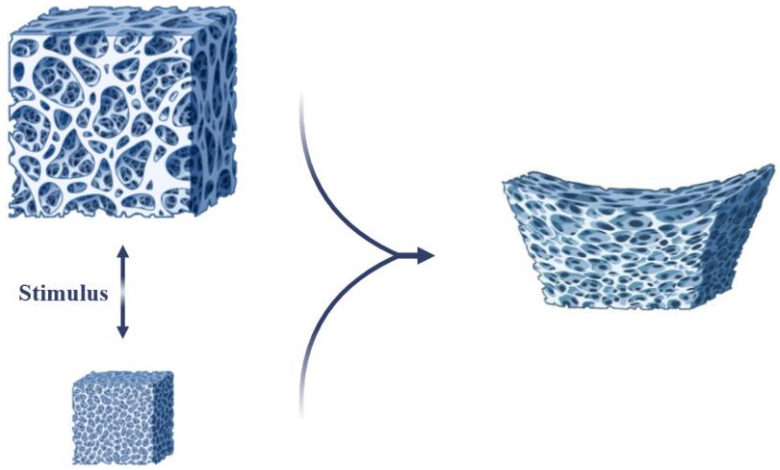

Figure I-1. Schematic illustration of the swelling / shrinking of a hydrogel under the influence of an external stimulus that can be used to develop shape changing hydrogels.

This chapter focus on understanding how to design and engineer a hydrogel actuator to meet certain requirements in term of shape morphing while focusing on biocompatible systems with potential biomedical applications. In the first part the different mechanisms behind the swelling / shrinking ability of smart hydrogels will be investigated taking into account simple mono-stimuli responsive hydrogels as examples. Next, the principles to transform the swelling / shrinking ability of smart hydrogels into a 3D deformation to obtain hydrogel actuators (devices capable of transforming shape over time) will be explained following a mathematical model. The relationship between the conception and the shape morphing will be addressed based on the preparation techniques ranging from simple bilayer structures to complex 4D printed architectures. As originally defined by Tibbits, 4D printing is the process in which a 3D printed shape (strand, film or three dimensional structure) morph into another using water as its activation energy.[8] The examples represented in this part focus on the shape morphing aspects of hydrogels that have potential as biomedical devices. Finally, some biomedical applications of hydrogel actuators will be discussed with the remaining challenges at hand.

2. STIMULI RESPONSIVE HYDROGELS

Stimuli-responsive hydrogels can be obtained by crosslinking stimuli-sensitive precursors, such as monomers or macromers. Hence, the conformational changes of the chains' structure induced by the external stimulus will result in the variation of the water uptake of the

hydrogel. The most commonly studied stimuli systems (temperature, pH and light) as well as multi-stimuli systems used as potential biomedical applications will be investigated in this part.

2.1. Thermo-responsive hydrogels

The widely studied stimulus in these crosslinked matrices is temperature. Thermo-responsive hydrogel networks can be obtained by crosslinking polymers that can undergo phase transitions *via* different mechanisms including thermally induced coil-to-globule transition, temperature induced self-assembly and thermo-induced helical conformational change as illustrated in Figure I-2.[9]

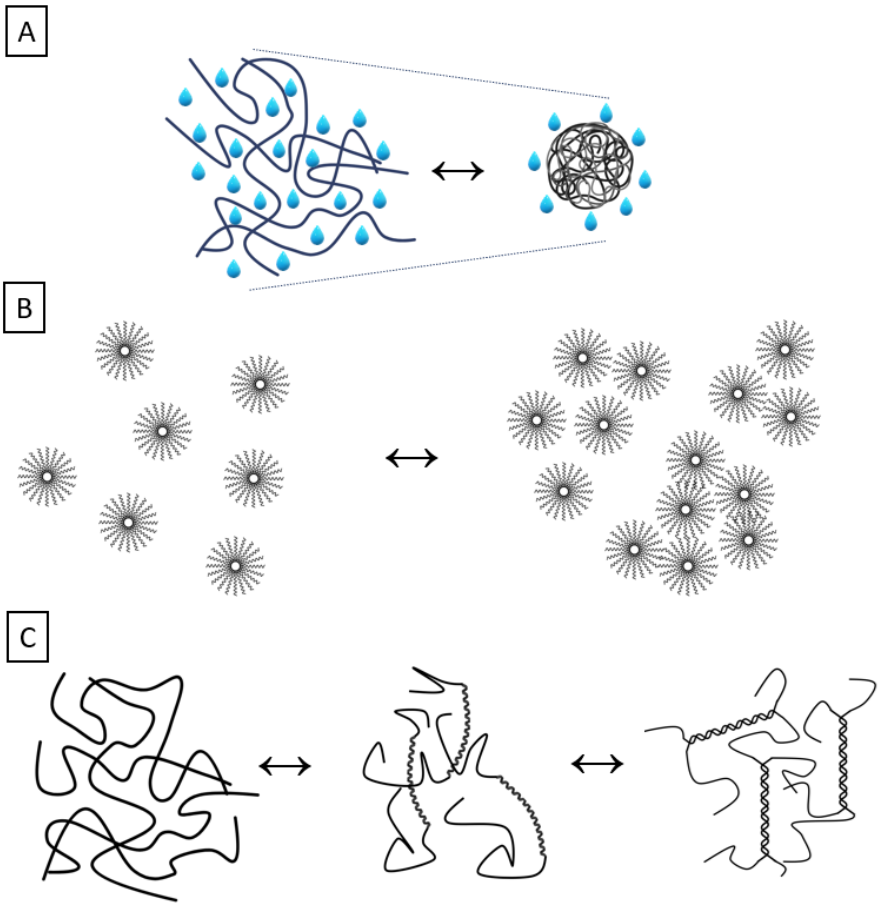

Figure I-2: Schematic illustration of A) volume phase transition from hydrated chains to compact structure B) micelles induced auto assembly and C) sol-gel transition upon temperature variation with the formation of helices and double helices.

Thermally induced coil-to-globule transition

Thermally induced coil-to-globule transitions occurs on polymers where the hydration state of the chains is highly dependent on temperature.[10,11] Such type of polymers are classically divided into two groups: lower critical solution temperature (LCST) where the

polymer is hydrated below the LCST (where polymer-solvent interactions are favored) and precipitates above it (favoring polymer-polymer interactions), and the upper critical solution temperature (UCST) where the polymer is in a hydrated state above the UCST and in a compact state below it, as illustrated in Figure I-2A. Crosslinking these types of polymers results in a thermo-responsive hydrogels exhibiting a volume phase transition temperature (VPTT). In the case of LCST polymer, the hydrogel swells below the VPTT and shrinks above it. The opposite transformation is observed for UCST based polymer network.

Temperature induced self-assembly

Some amphiphilic block copolymers can self-assemble in water to form micelles, liposomes or polymersomes.[12–14] Certain micellar structures demonstrate a thermal response where the organizational state of the micelles is highly dependent on temperature variations as illustrated in Figure I-2B. Increasing the temperature will favor the hydrophobic interaction leading to a specific assembly of the micelles in water. Crosslinking the micelles can result in the formation of a thermo-responsive hydrogel where the water uptake will be directly influenced by the temperature-dependent organization of the micellar.

Thermo-induced helical conformational change

Another form of thermal behavior can be observed on several polysaccharides and polypeptides where the chains undergo a conformational change with temperature variation .[15,16] When heated the chains are present in a random coil state that form helices upon cooling. Further cooling will result in the formation of a double or triples helix structures through hydrogen bond interactions that stabilizes the network trapping water in the physically crosslinked network as illustrated in Figure I-2C. This physical change is observed for example on carrageenan, gellan gum, agarose and agar agar which are widely used in the biomedical field.[15] The thermal response of these polysaccharides is mainly used to obtain a physical crosslinked hydrogels and rarely as an external stimulus to control the swelling behavior.

Temperature is one of the most extensively studied stimuli in smart hydrogels due to its precise control over the swelling/shrinking behavior. Additionally, the temperature response can be tuned to occur in physiological conditions promoting their utility in the biomedical field. Some examples of strictly temperature responsive hydrogel systems and the range of their swelling / shrinking response are summarized in Table I-1 that can be used as potential for biomedical applications.

Table I-1. Temperature responsive hydrogel networks and the water uptake variation upon temperature variation.

Mechanism	Network	Swelling degree variation	Temperature variation	Ref
Thermally induced coil-to-globule transition	**poly(N-isopropylacrylamide) / F127**	up to 90% loss	10 to 40°C	[17]
	poly(2-ethyl-2-oxazoline) , poly(2-isopropyl-2-oxazoline)	up to 90% loss	20 to 70°C	[18]
	poly(N-acryloylglycinamide)	up to 55% diameter increase	10 to 70°C	[19]
	poly(allylurea-co-allylamine)	up to 90% gain	27 to 60°C	[20]
	poly(N-t-butylacrylamide-co-acrylamide)	up to 95% loss	10 to 40°C	[21]
	Poly(oligo (ethylene glycol) -co- oligo (propylene glycol))	up to 90% loss	10 to 60°C	[22]
	poly(vinylcaprolactone-co-ulfobetaineMA)	up to 20% gain	4 and 37°C	[23]
Temperature induced self-assembly	**F127**	Up to 80% loss	10 to 50°C	[24,25]
Thermo-induced helical conformational change	**Agarose**	N/A	42 to 20°C	[26]

2.2. pH/ionic strength responsive hydrogels

pH-sensitivity occurs in polymeric chains that contain functional groups, such as typical carboxylic acid or amine groups, which can be protonated or deprotonated. In a

crosslinked system, the overall charge density of the network will be highly dependent on the pH.[27] Increasing the charge density through protonation or deprotonation of functional groups will cause an expansion of the hydrogel. This expansion results from the enhanced electrostatic repulsion between the charged moieties and the osmotic pressure generated by the counter ions. Whereas upon decreasing the charge density on the polymeric chain, hydrogen bonds will be formed between the functional groups collapsing the chains. The swelling behavior of these hydrogels can be tuned by varying the pH of the medium as well as the ionic strength of the solution. Some examples of hydrogels systems that are only pH responsive and have potential for biomedical applications are summarized in Table I-2.

Table I-2. pH / ionic strength responsive hydrogel networks and the water uptake variation upon pH variation.

Network	Swelling degree variation	pH variation	Ref
poly(acrylic acid)	up to 95% gain	1 to 7	[28,29]
poly(ethoxytriethyleneglycol monomethacrylatelmethyl methacrylate)	up to 50% gain	3 to 10	[30]
Modified Dextran-MA	up to 60% gain	1 to 7	[31]
poly(organophosphazene)	up to 80% gain	4 to 10	[32]
Poly(N-acryloyl-L -alanine)	up to 90% gain	2 to 12	[33]
Carboxy methyl cellulose (CMC) / chitosan (CS)	up to 85% gain	2 to 7	[34]
poly(EG vinyl ether -co- butyl vinyl ether -co – acrylic acid)	95% gain	2 to 9	[35]
poly(N-vinyl-2-pyrrolidone/itaconic acid)	up to 90% gain	4 to 10	[36]

2.3. Light responsive hydrogels

Light responsiveness typically results in color changes due to the presence of fluorescent moieties within the hydrogel network.[37,38] However, it can also be used as a mean

to tune the hydrogel water uptake by introducing photochromic groups such as azobenzene[39], spiropyran (SP)[40] that changes configurations under UV light.[41,42] Moreover, light sensitivity can be added to a thermo-responsive network throughout the addition of particles exhibiting a photo-thermal effect leading to multi-stimuli responsive systems, which will be developed in the upcoming part. Light as a non-invasive tool for biomedical application can be used as an external stimulus to control the swelling behavior of hydrogels.[43]

2.4. Multi-stimuli responsive systems

While single-stimuli responsive systems offer promising volumetric change upon a specific trigger, more complex and smarter systems can be designed to adapt to several external stimuli.[44] Multi-stimuli responsive systems can be achieved by polymerizing monomers that change conformation under multiple conditions, copolymerizing monomers/macromers that respond to different stimuli, or developing polymer composites with stimuli-responsive particles embedded in the matrix.[45] These advanced systems exhibit enhanced functionality and versatility, making them highly suitable for diverse and demanding applications. For example, Zhai *et al.* obtained dual temperature and pH responsive hydrogel by incorporating kappa-carrageenan in a PNiPAAm network.[46] This particular combination demonstrates dual temperature response where the hydrogel swells when reaching the sol-gel transition of k-carrageenan and shrinks when reaching the VPTT of poly(N-isopropylacrylamide) (PNiPAAm). In addition, the presence of sulfonic groups on k-carrageenan will induce a pH sensitivity upon protonation/deprotonation. Pei *et al.* crosslinked dopamine methacrylamide (DMA), methacrylamidophenylboronic acid (MAPBA) and dimethylaminoethyl methacrylate (DMAEMA) to obtain a multi responsive hydrogel.[47] The swelling degree of the hydrogel is dependent on temperature, pH (from DMAEMA) and glucose concentration (from dissociation of borate ester bonds in DMA- MAPBA).

In addition to copolymerization, multi-stimuli response can be attained in hydrogel composites by the integration of sensitive particles. For instance, light sensitivity can be added to a thermo-responsive network throughout the addition of photo-thermal particles such as graphene oxide (GO) or gold nanorods.[46] When exposed to irradiation, these particles absorb the light and transform it into heat raising the temperature above the transition temperature of the thermo-sensitive network. For example, Shiotani *et al.* shrunk PNIPAAm based hydrogels containing gold nanorods upon irradiation of selective zones.[48] Ghavami *et al.* incorporated Fe_3O_4 particles in a dual pH and thermo-responsive poly(2-dimethylamino-ethyl methacrylate-g-salep) hydrogel to provide an additionnal magnetic response.[49] More multi-stimuli responsive

hydrogels systems are presented in Table I-3 with the respective stimuli and water uptake variation upon stimulus.

Table I-3. Multi-stimuli responsive hydrogel networks and the water uptake variation in the presence or absence of each stimulus.

Network	Stimuli	Ref
PNiPAAm and Kappa carrageenan	temperature + pH	[46]
poly(DMA -co- MAPBA -co-DMAEMA)	pH + temperature + glucose	[47]
Alginate / kappa-Carrageenan	pH + ions	[50]
poly(ethylene glycol diglycidyl ether -co-cystamine)	pH + temperature	[51]
Hemicellulose -g- acrylic acid	pH + ionic strength	[52]
poly(2-dimethylamino) ethyl methacrylate-g-salep/Fe_3O_4	pH + temperature + magnetic	[49]
PNiPAAm - GO	Temperature + light	[53]
PNiPAAm-Gold nanorods	Temperature + light	[48]
PNiPAAm-Gold nanorods	Temperature + light	[54]

As seen in this part, stimuli responsive hydrogels showcase adaptability and versatility. Their ability to respond to various external stimuli such as temperature, pH and/or light allows them to be tuned for various biomedical applications such as drug delivery or tissue engineering. However, the application of simuli responsive hydrogels comes with its own advantages and disadvantages as sumerized in Table I-4. For instance, temperature response is fast and reversible but can be constrained by environmental conditions. pH is compatible with biological systems but lacks precision as the response occurs on a wide range of pH values. Light response offers a precise spatial control but is limited to the penetration depth. Furthermore, they can offer non-invasive activation, precise spatial control or targeted response. Conversly, these hydrogels face challenges such as limited operational ranges, slow/fast response time, unknown

stability in physiological conditions or complex manufacturing processes. Based on the specific application, the range of deformation can be tuned by properly choosing the hydrogel network and the stimulus. The potential of hydrogels exhibiting a volumetric change, can go beyond the shrinking/expansion and can be used as a tool to generate a specific action or motion upon the deformation.

Table I-4. Advantages and limitation of temperature, pH, light and multi-stimuli responsive hydrogels.

Stimulus Type	Advantages	Limitations
Thermal	• Reversible actuation • Compatibility with biological systems • Precise control over temperature	• Limited spatial control • Sensitivity to environmental conditions • Energy consumption
pH	• Reversibility of shape changes • Compatibility with biological systems	• Limited by ions diffusion into network • Sensitivity to solution conditions • Broad pH range
Light	• Precise spatial control • Fast response times • Reversibility of shape changes	• Limited penetration depth • Potential photo-toxicity • Wavelength specificity
Multi-stimuli	• Versatility and specificity • Reversibility of shape changes • Precise control over actuation	• Sensitivity to solution conditions • Potential toxicity

3. HYDROGEL ACTUATORS CONCEPTION

The importance of smart hydrogels lies in the ability to translate the volumetric change into a mechanical motion under an external stimulus. The actuating mechanism of soft actuators is due to an anisotropic expansion profile across a given architecture. This difference in physical behavior will create internal stresses forcing the system to deform generating a bending,

twisting or rolling motion. The greater the expansion difference is, the more accentuated the deformation will be. The anisotropic volumetric changes can be obtained by building a bilayer hydrogel structure or by 3D printing technology.

3.1. Bilayer constructs

A common method to obtain such deformations is by building a bilayer system composed of two hydrogels with different physical or chemical properties. [55] By choosing a stimuli responsive layer, the swelling behavior can be tuned by the application of the external stimulus. Hence, the differential swelling or the shrinking of the hydrogels will be triggered upon stimulus. This difference in swelling behavior for bilayer systems will cause the system to deform towards the layer with the lowest expansion coefficient as illustrated in Figure I-3.

The common method to prepare bilayer hydrogel actuators is through a two steps process. It involves curing the first hydrogel layer in a mold and on top of it, the second layer will be cured. The crosslinking mainly occurs under UV light in the presence of a photo-initiator by a free radical polymerization.

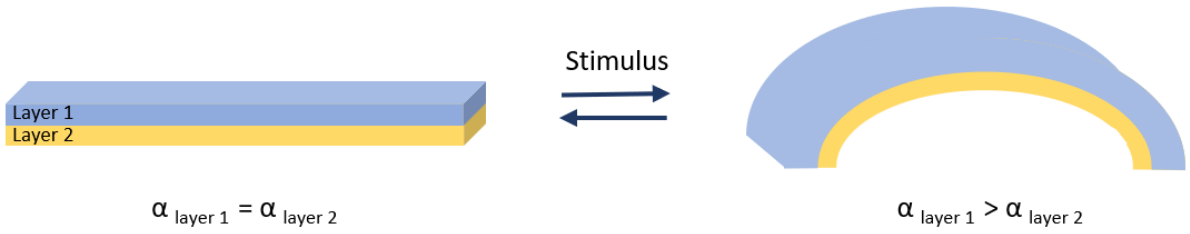

Figure I-3. Schematic illustration of the concept of a bilayer actuator where upon stimulus layer 1 expands more than layer 2 inducing a 3D deformation.

The presence of diverse polymeric materials has led to a wide range of possible bilayer constructs. Numerous combinations of hydrogels are possible to obtain mono-stimuli responsive actuators or multi-stimuli responsive actuators.

Single stimuli responsive bilayer hydrogel actuators are obtained by combining a responsive layer (known as the active layer) which exhibit a volumetric change upon stimulus with another layer (known as the passive layer) that shows little to no volume change. Hence, upon stimulus, the two layers will have different physical behavior that creates internal stresses forcing the system to bend towards the layer with the lowest expansion as depicted in Figure I-3. For instance, Shin *et al.* developed a system composed of PNiPAAm as the active layer and a poly(acrylamide) (PAAm) as the passive layer that bends when the temperature goes above the

LCST of PNIPAM as observed Figure I-4A.[56] As temperature increases, the PNiPAAm layer will shrink resulting in the bending of the bilayer hydrogel system leading to grippers that are able to carry a block having 22 times their weight. Similarly, Han *et al.* developed a bilayer actuator based on PAAc as the active layer and PAAm as the passive layer.[57] Due to the pH response of PAAc, the hydrogel actuator demonstrates a strong actuation upon pH variation as seen in Figure I-4B. By decreasing the pH, protonation of the carboxyl group in the PAAc layer occurs that favors strong hydrogen bonds formation resulting in the shrinkage of the PAAc layer hence bending of the hydrogel.

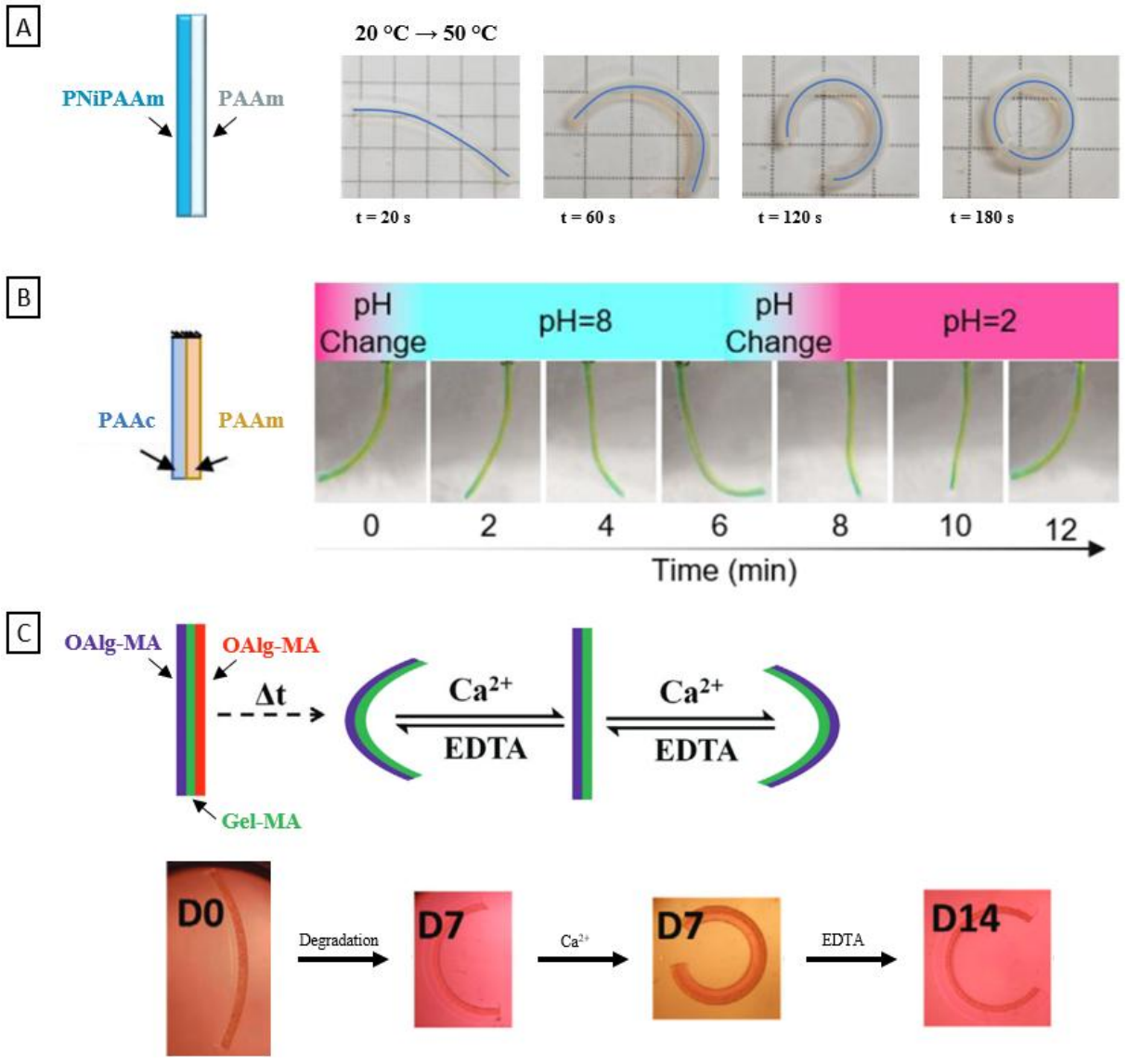

Figure I-4. Actuation of a A) PNiPAAm / PAAm bilayer actuator upon heating [56], B) PAAc / PAAm bilayer under pH variation [57], C) oxidized methacrylated alginate (OAlg-MA) and methacrylated gelatin (Gel-MA) trilayer hydrogel upon degradation or in the presence of ions.[58]

Multiple stimuli responsive hydrogel actuators can be obtained by either combining two layers that responds each to a specific stimulus or by choosing an active layer that respond to several stimuli. Taking advantage of the diversity in hydrogel materials and their different response to environmental change, complex systems can be built. For example, taken as temperature responsive layer the commonly used PNiPAAm, various assemblies can be made. Combining with poly(N-[3-(dimethylamino) propyl] methacrylamide) (PDMAPMA), a thermal and pH sensitive system can be obtained.[59] Alternatively, to create a temperature-solvent dual responsive actuator, poly(N-hydroxyethylacrylamide) (PHEAm) can be used as a second active layer alongside PNiPAAm as a first layer.[60] Designing hydrogel actuating can become increasingly complex, where Ding *et al.* developed a trilayer actuator based on oxidized methacrylated alginate (OAlg-MA) and methacrylated gelatin (Gel-MA).[58] The swelling behavior of the alginate layer varies with the degradation rate. In this case, the Gel-MA layer represents the passive layer that is sandwiched between two OAlg-MA active layers. As seen in Figure I-4C, as the first layer degrades, the actuators exhibit a strong actuation. Moreover, the system demonstrates a sensitivity to calcium ions due to the unique property of alginate to complex with Ca^{2+}. So, in presence of calcium ions in solution, the hydrogel reverses its bending direction revealing a multi-stimuli response. More biocompatible stimuli responsive hydrogel actuators that have potential in the biomedical field are summarized in Table I-5.

Bilayer hydrogel actuators are primarily designed using synthetic polymers due to their tunable properties and consistent performance. These synthetic materials, such as PNiPAAm, poly(acrylamide) (PAAm) and poly(acrylic acid) (PAAc) allow for precise control over the actuator's responsiveness and mechanical strength. However, there are a few notable examples where natural polymers are used. Natural polymers like some polysaccharides are sometimes used to enhance biocompatibility and biodegradability, making them suitable for specific biomedical applications.[61,62] Despite the predominance of synthetic polymers, the incorporation of natural polymers in bilayer hydrogel actuators is gaining interest for applications requiring sustainable and environmentally friendly materials.

While bilayer hydrogel actuators are promising, their architectural complexity is limited to sheets/films. This paves the way for 3D printing, a manufacturing process that offers significant structural advantages. 3D printing enables the creation of dynamic, adaptive structures that transform over time upon stimulus, leading to more sophisticated and functional architectures and setting the stagefor innovative 4D printing processes.

Table I-5. Mono and multi-stimuli responsive bilayer hydrogel actuators and the corresponding stimulus for biomedical applications.

	Bilayer system	Stimuli	Potential application	Ref
Mono-stimuli responsive actuators	PNiPAAm / PAAm	Temperature	Biomimetic robotics	[56]
	PAAc / PAAm	pH	Drug delivery	[57]
	poly(methacrylic acid) /poly(2-hydroxyethyl methacrylate) (PHEMA)	pH	Drug delivery	[63]
	polysiccinimide / polycaprolactone	hydrolysis	Cell delivery and Tissue engineering	[64]
Multi-stimuli responsive actuators	PNiPAAm / poly(N-hydroxyethylacrylamide)	Temperature and solvent	Drug delivery	[60]
	poly(NiPAAm -co-DMAPMA)	Temperature and pH	Drug delivery	[59]
	CS / (cellulose / CMC)	pH and ionic strength	Drug delivery, lenses	[65]
	poly(3-(1-(4-vinylbenzyl)-1H-imidazol-3-ium-3-yl) propane-1-sulfonate)/ poly(butyl acrylate)	Salt and solvent	Biomimetic robotics	[66]
	Alginate methacrylate (Alg-MA) / Gel-MA	Oxidation and ions	Tissue engineering	[58]

3.2. Perspective of hydrogel actuators with 4D Printing

Besides film casting, bilayer constructs or mold curing, anisotropic hydrogels can be obtained *via* various 4D printing processes. 4D printing is an innovative manufacturing process where the printed materials are programmed to shape morph throughout time when exposed to an external stimulus. Programming during the printing process of hydrogel actuators is a crucial aspect to develop 4D printing hydrogel actuators. The process involves strategically controlling the hydrogels architecture, composition and alignment during the printing phase in order to encode the desired shape transformation. From the existing 3D printing techniques, the two common ones used for hydrogel printing are direct ink writing (DIW) and stereolithography (SLA). Each printing technique requires specific properties in the hydrogel ink to achieve optimal results. For direct ink writing (DIW), the ink must possess shear-thinning properties to allow for smooth extrusion through a nozzle while maintaining structural integrity post-deposition. Conversely, SLA printing necessitates a photocurable resin, which crosslinks upon light exposure, enabling the precise formation of complex structures layer by layer. These distinct requirements ensure that the hydrogel actuators obtained have a good resolution printing, ultimately enhancing their performance in 4D applications as illustrated in Figure I-5.

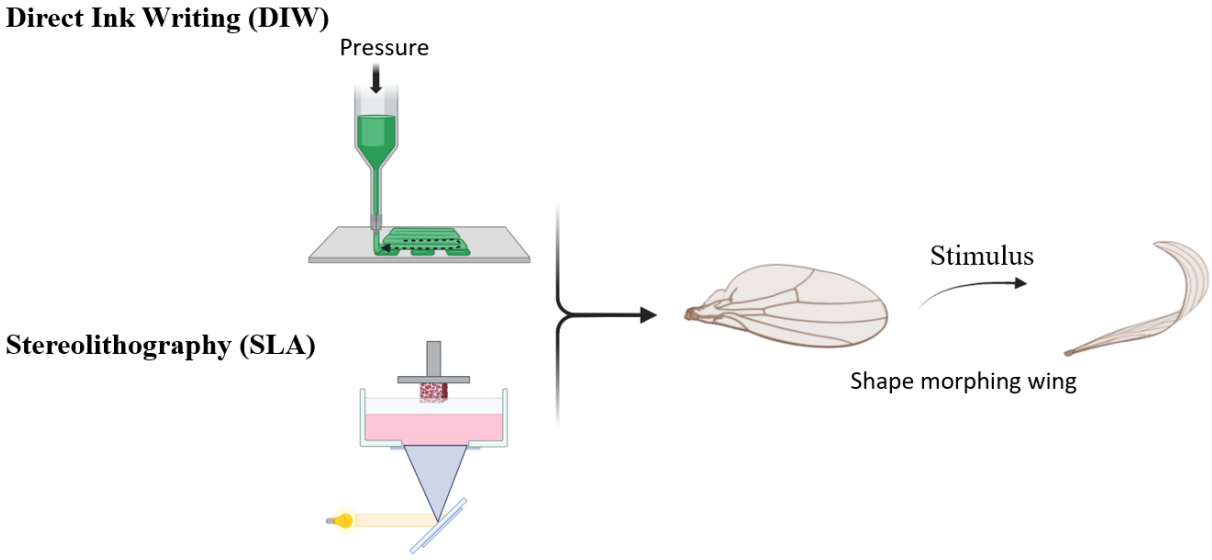

Figure I-5. Schematic illustration of stereolithography and direct ink writing printing techniques to obtained shape morphing structures such as the illustrated wing.

3.2.1. Direct ink writing (DIW) process for 4D printed actuators

In DIW printing, the resin needed is liquid and should have specific viscosity adapted to the machine. The viscous hydrogel precursor is extruded through a precision-controlled nozzle onto a substrate in a layer-by-layer fashion as illustrated in Figure I-5. The resin

deposition path is pre-programmed in the design file. Each layer is cured under light or by chemical reaction to obtain a crosslinked network. The object is built up gradually as successive layers cure on top of each other.

Programming in DIW involves tuning the printing speed and pressure of deposition. By doing so, the local density of the hydrogel can be adjusted. The crosslinking density can be controlled spatially creating an anisotropic swelling gradient in the hydrogel's architecture.

By tuning the rheological properties of the ink, Liu *et al.* designed various shape morphing structures upon temperature variation.[67] The actuation mechanism is governed by the differential swelling behavior of PNiPAAm and PAAm hydrogels. The multi-material system, exhibit PNiPAAm part and PAAm parts as seen in Figure I-6A. In this system, PNiPAAm plays the role of the active section, whereas PAAm is the passive one upon temperature variations. By alternating the PNiPAAm and PAAm design regions, controlled bending of a tube can be achieved, or a valve can be opened. The bioinspired shape morphing architectures show promising results for biomedical engineering. Another strategy to obtain a stimuli responsive shape morphing behavior is by blending polymers. For example, Guo *et al.* 4D printed thermo-sensitive hydrogels based on PAAm and agarose nanofibers.[68] Although agarose is not chemically crosslinked in the PAAm matrix, the thermal behavior of the polysaccharide can still be exploited. As seen in Figure I-6B, initially above the sol-gel temperature of agarose, the hydrogel shape can be manually deformed and the deformation can be fixed when cooled below the sol-gel temperature of agarose. Hence, upon reheating, the hydrogel deforms and regains its initial non-deformed structure. Due to the biocompatibility of the resin, these 4D printed systems demonstrates potential as medical devices that can be deformed around body temperature. DIW has the significant advantage to manufacture multi-material systems by simply using several printing nozzles. For example, to favor the usage in biomedical applications, Narupai *et al.* developed multi-material multi-stimuli responsive 4D printed hydrogel structures based on methacrylated bovine serum albumin (MA-BSA).[69] The multi-stimuli response comes from the formulation of various inks based on the biodegradable MA-BSA used to construct a single structure. A temperature responsive hydrogel results from the mix MA-BSA/PNiPAAm while the pH response results from the combination of MA-BSA/PDMAEMA. As seen in Figure I-6C, a 3D printed bilayer hydrogel film composed of a thermo-sensitive layer and a pH sensitive layer demonstrates rolling upon temperature change and an accentuated deformation upon both temperature and pH variations. The presence of MA-BSA in both inks improves the biocompatible and biodegradable aspect that is desired for

biomedical applications. More 4D printed hydrogels systems obtained *via* DIW are summarized in Table I-6 as promising candidates for biomedical applications.

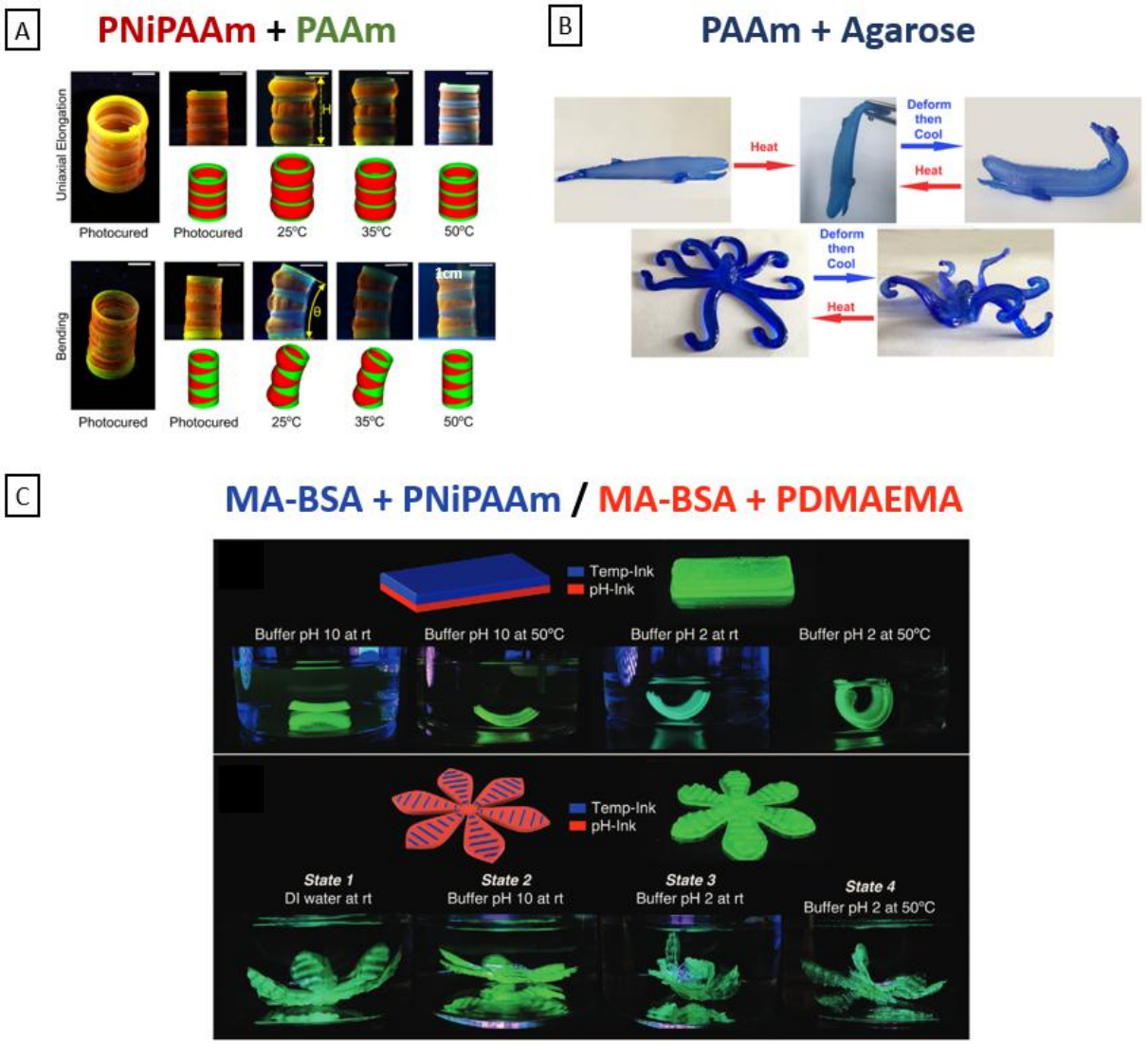

Figure I-6. A) Shape morphing of a PNiPAAm / PAAm multi-material tube by heating [67], B) temperature induced shape deformation of a PAAm / Agarose hydrogels [68], C) pH and temperature induced rolling of a MA-BSA based hydrogel actuators [69] obtained by DIW printing.

Table I-6. 4D printed stimuli responsive hydrogels and the water uptake/volumetric change upon stimulus obtained by DIW as potential for biomedical applications.

Network	Water uptake variation / volumetric change	Potential application	ref
PNiPAAm / PAAm	up to 60%	Medical applications	[67,70,71]
PAAm / Agarose	NA	Medical devices	[68]
Alg-MA / DMAEMA	up to 35 % size	vascular stents	[72]
Alginate / MC	up to 50%	Biomedical engineering	[73]
MA-BSA + PNiPAAm / MA-BSA + PDMAEMA	up to 15%	Drug delivery, biomedical devices	[69]
Alg-MA or Hyaluronic acid methacrylate	NA	Tissue engineering and regenerative medicine	[74]

3.2.2. Stereolithography (SLA) process for 4D printed actuators

SLA is an advanced 3D printing technology that uses light to cure a photosensitive resin, layer by layer, to build a three-dimensional architecture. Once the hydrogel precursor is placed in the tank, the platform moves downwards to reach the desired layer thickness. The layer is then cured by a laser according to the .stl design file. After each layer curing, the platform moves upward allowing the resin to flow underneath. The process is repeated until the entire object is completed as illustrated Figure I-5.

Even though the development of multi-materials in SLA remains complex compared to DIW, by varying the light intensity or curing time between the layers can lead to anisotropic photo-crosslinking profile with desires non-uniform shape morphing. By creating different degrees of

crosslinking in an architecture, the swelling behavior will differ regionally creating internal stress in the system that will force it to deform.[75]

The importance of SLA printing lies in its ability to obtain more complex geometries with high resolution. For example, Dutta et Cohn printed a porous cube hydrogel that is able to change aspect ratio on command by pH and/or temperature variations.[76] The F127-MA/PAAc acid hybrid hydrogel shrinks in acidic media or when heated around body temperature for potential biomedical devices applications as seen in Figure I-7A. Ji *et al.* constructed various 4D printed structures such as programmable self-folding architectures or thermal activated gripper.[75] The PHEMA/poly(2-(2-methoxyethoxy) ethyl methacrylate) ($PMEO_2MA$) based hydrogels can transform from 1D strip, 2D sheets or 3D architectures into more complex 3D structures as observed in Figure I-7B. Shiblee *et al.* developed temperature responsive actuator based on poly (N,N-dimethyl acrylamide-co-stearyl acrylate).[77] By tuning the composition of the monomers various swelling behaviors were obtained. By increasing the sterearyl acrylate content, the thermo-responsiveness of the hydrogels almost disappeared which allows them to 3D print bisectional actuator, where the active part is N,N-dimethyl acrylamide (DMAAm) rich and the passive part is stearyl acrylate rich. The actuator demonstrates a strong actuation upon heating due the difference on swelling behavior between the two sections. More 4D printed hydrogels systems obtained *via* SLA printing are summarized in Table I-7 as promising candidates for biomedical applications.

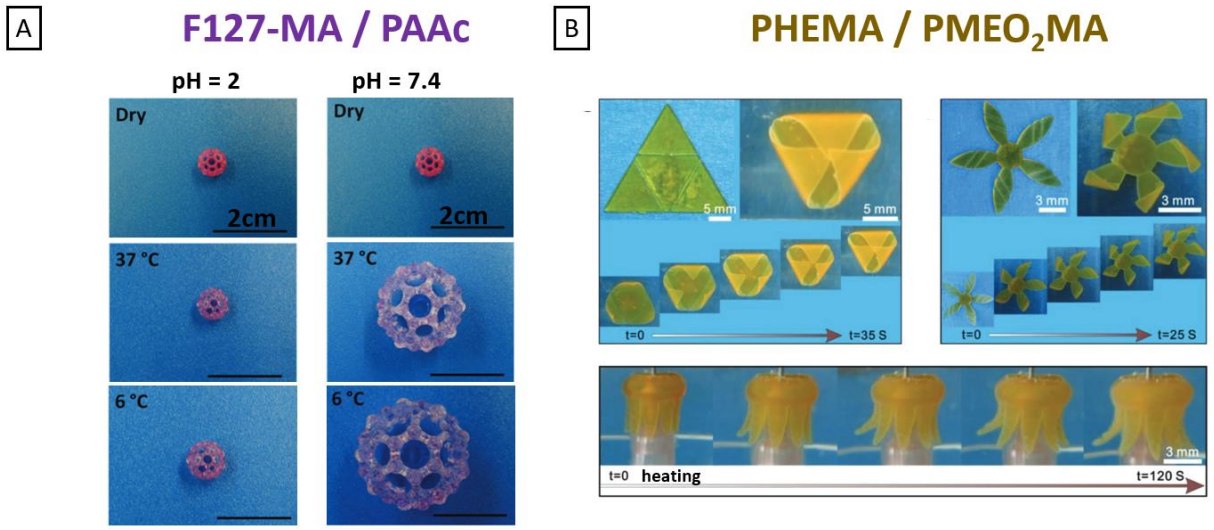

Figure I-7. A) pH and temperature induced deformation of a F127-MA / PAAc based hydrogel [76], B) self-rolling and temperature induced actuation of a PHEMA / $PMEO_2MA$ hydrogels [75] obtained by SLA printing.

Table I-7. 4D printed stimuli responsive hydrogels and the water uptake/volumetric change upon stimulus obtained by SLA printing as potential for biomedical applications.

Network	Water uptake variation / volumetric change	Potential application	Ref
F127-MA / PAAc	up to 80%	Medical devices	[76]
poly(DMAAm-co-stearyl acrylate)	up to 20%	Bionic devices	[77]
PHEMA / PMEO$_2$MA	up to 80%	Tissue engineering	[75]
poly(EG dimethacrylate) / PAAc	up to 50%	Tissue engineering, smart biosensors	[78]
poly(EG diacrylate) / PAAc	up to 55%	Drug delivery	[79]

As seen in this part, various methods can be used to obtain shape changing hydrogel systems. For biomedical applications, it is important to choose the appropriate stimulus compatible to physiological conditions. For simple execution, bilayer hydrogels can be used, while for more complex designs and architectures, 3D printing techniques demonstrates higher potential. Understanding the fabrication process is only part of the equation; equally important is the ability to manipulate these actuators to achieve the desired movements and responses, which is the focus of the next part.

4. ACTUATION CONTROL

After discussing the preparation methods for hydrogel actuators, it is crucial to explore how the degree and direction of their actuation can be precisely controlled. The next section will delve into the strategies and techniques used to control the actuation degree and direction, which are key factors in optimizing the performance and functionality of hydrogel-based systems especially as biomedical devices. Some factors affecting the orientation include the design parameters following Timoshenko's model, layer patterning and fibers alignment will be discussed in this part.

4.1. Timoshenko's Principle

An interesting aspect of bilayer hydrogel actuators lies in the ability to predict the radius of curvature using Timoshenko's model.[80,81] The model is designed for bi-metal thermostats deformation upon heating; however, it can be adapted to hydrogels by modifying the thermal expansion coefficient.

$$\frac{1}{\rho} = \frac{6\,(\alpha_2 - \alpha_1)\,(1+m)^2}{h\left(3(1+m)^2+(1+mn)\left(m^2+\frac{1}{mn}\right)\right)} \qquad \textbf{(Equation I-1)}$$

Where:

ρ: inner radius of the curved strip

α_i: xy linear expansion coefficient of layer i

a_i: thickness of layer i

h: total thickness of the strip

m: ratio between the thickness of layer 2 and layer 1

n: ratio of Young's modulus of layer 2 and layer 1

Several design parameters can be seen to influence the degree of bending of bilayer systems such as the total thickness of the actuator and the ratio of each layer. The linear expansion coefficient and the Young's modulus are imposed by the chosen chemistry and the degree of crosslinking. To obtain the strongest deformation possible, in other words the smallest radius of curvature, the layers chosen should have the highest expansion coefficient difference but with a similar Young's modulus. In terms of design, the highest curvature is obtained for layers having the same thickness and an overall small thickness. Zhao *et al.* studied the influence of geometry and the mechanical properties on bilayer hydrogel actuator composed of GO-PNiPAAm and poly(vinyl alcohol) (PVA).[82] By varying the amount of nanofibrillated cellulose (NFC) in the PNiPAAm, the mechanical properties were varied. By increasing the NFC content (NFC0 and NFC3 for 0 and 5 mg/mL respectively), the Young's modulus increased and resulted in decreasing the radius of curvature as seen in Figure I-8A according to Timoshenko's principle. In addition, it was observed that thinner hydrogels exhibit a stronger actuation than wider ones. Similarly, Wang *et al.*, studied the influence of the composition and geometry on the actuation of a thermo and solvent responsive PNiPAAm / PHEAm bilayer hydrogel actuator.[60] Similar trends corresponding to Timoshenko's principle were observed. Improving the mechanical properties of one of the layers will results in a lower radius of

curvature. In addition to, thicker hydrogels demonstrate a lower radius of curvature compared to thinner ones as seen in Figure I-8B.

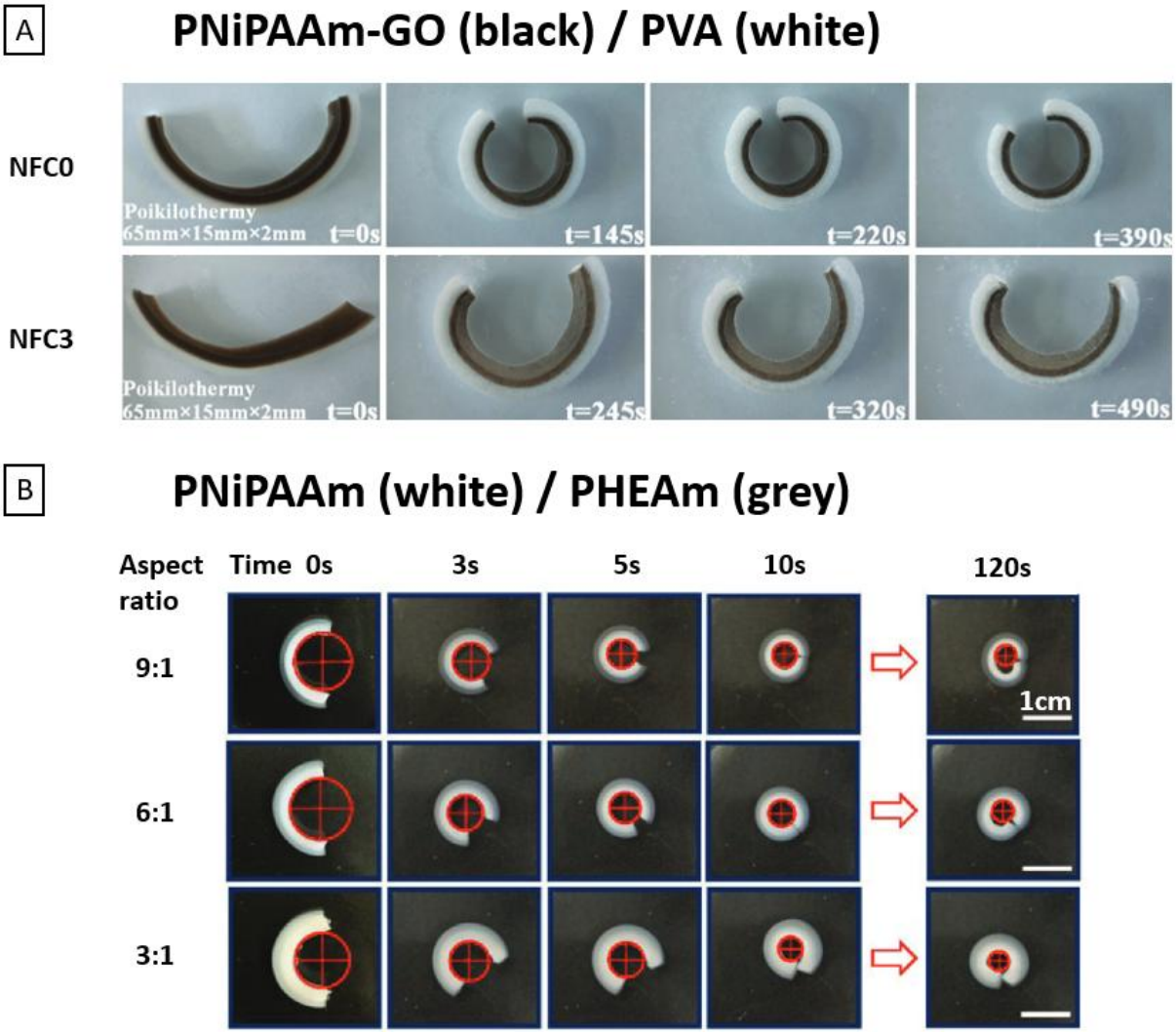

Figure I-8. A) Temperature response of PNiPAAm-GO / PVA bilayer hydrogel actuators with various concentration of NFC (0 and 5 mg/mL) when heated from 32 to 50°C [82] and B) the dynamic thermal actuation of a PNiPAAm / PHEAm bilayer hydrogel actuator with varying thickness aspect ratio when heated from room temperature to 40 °C [60].

By studying the swelling behavior and the mechanical properties of each layer before assembly, the radius of curvature can be predicted. The geometrical aspect of the device can be tuned to adapt to the proper application which is crucial in the biomedical field.

4.2. Patterning

By controlling the swelling behavior in the hydrogel matrix, shape deformation can be programmed.[83] By building a bilayer system or crosslinking gradient, a bending motion is obtained.[64] The degree of bending can be controlled by varying the design parameters of the actuator according to Timoshenko's formula as previously seen. More complex shape deformation can be obtained by tuning the anisotropic swelling behavior of the system. Instead of uniform building blocks, patterning can be applied in a specific layer in order to control or limit the swelling behavior or alternating sections with different swelling behaviors. For example, on a bilayer hydrogel, applying a patterned active layer at various angles more specific transformation can be obtained. Wang *et al.* controlled the deformation of a PNiPAAm / PAAm-CS bilayer actuators by tuning the design and pattern orientation.[84] As seen in Figure I-9A, by patterning the PNiPAAm layer on top of PAAm-CS layer, cylinder, helices or cone-like deformation can be obtained. The direction of the patterned layer, will influence the direction of the stresses induced from the difference of expansion between the layers resulting in more complex shape transformation. Another similar strategy can be applied by limiting the swelling behavior at a specific direction. This can be achieved by the addition of rigid fibers on the top of a hydrogel. The presence of these fiber will limit the expansion of the hydrogel in the direction of the fibers' alignment, hence generating internal stresses at the surface in the direction orthogonal to the fibers that forces the system to deform. Han *et al.* applied parallel elastomer strips on top of PNiPAAm / PAAc bilayer hydrogel actuators to control the shape deformation.[57] As seen in Figure I-9B, the rolling direction can be controlled by varying the fibers alignment angle. At a 90° angle, a rolling motion is obtained due to the parallel stresses induced by swelling difference, whereas at a 45° angle, twisting motion occurs cause of the tilted direction of the internal stress in the hydrogel. Another strategy to generate internal stresses at controlled direction is by alternating the active and passive sections in a same layer. Shang et Theato alternated PNiPAAm and PAAc sections having a crosslinking gradient to obtain various complex 3D deformation.[85] The deformation is generated by the crosslinking gradient present and the direction of the motion is controlled by the pattern's orientation. As observed in Figure I-9C, bending, rolling or folding motions can be generated by varying the pattern's design.

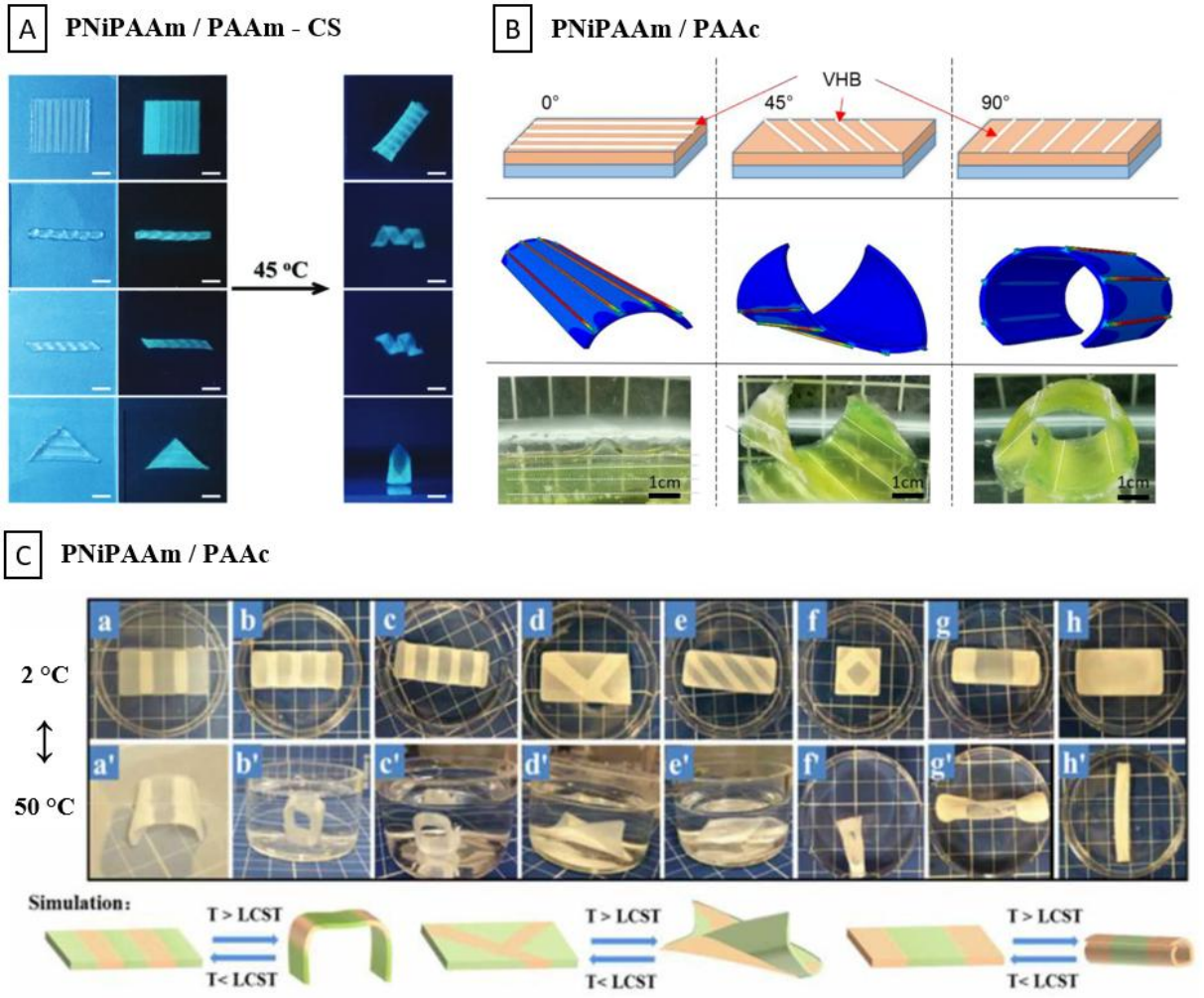

Figure I-9. A) Patterning of PNiPAAm layer on top of PAAm-CS at different orientation [84], B) very high bond (VHB) elastomer strips on top of a PNiPAAm / PAAc bilayer hydrogel to control the deformation angle [57] and C) alternating patterns configuration of a PNiPAAm / PAAc hydrogel to reveal the programmed shape deformation [85] upon stimulus.

4.3. Fiber alignment

Besides design parameters, the shape deformation can be controlled by incorporating micro fibers in the hydrogel matrix that can be aligned. By aligning the fibers, the swelling of the hydrogel will be lowered in the direction parallel to the orientation demonstrating an anisotropic expansion profile. By patterning different section with various alignment direction, various controlled shape deformations can be obtained. Erb *et al.* controlled the deformation of a PNiPAAm bilayer hydrogel by aligning Al_2O_3 platelets coated with iron oxide nanoparticles.[80] The particles were aligned by an external magnetic field before and during curing under UV light leading to the rolling of the hydrogel upon heating as observed in Figure I-10A. The alignment of the particles can be achieved during the preparation process itself, without the need for external manipulation for example through shear-induce alignment via

DIW.[86] Sydney Gladman *et al.* 4D printed PNiPAAm by incorporating NFC and obtained various complex deformation mimicking natural phenomena.[87] During the extrusion process, the NFC align according to the trajectory of the nozzle's path paving the way to designing and programming numerous structures such as the opening and closing of a flower as observed in Figure I-10B.

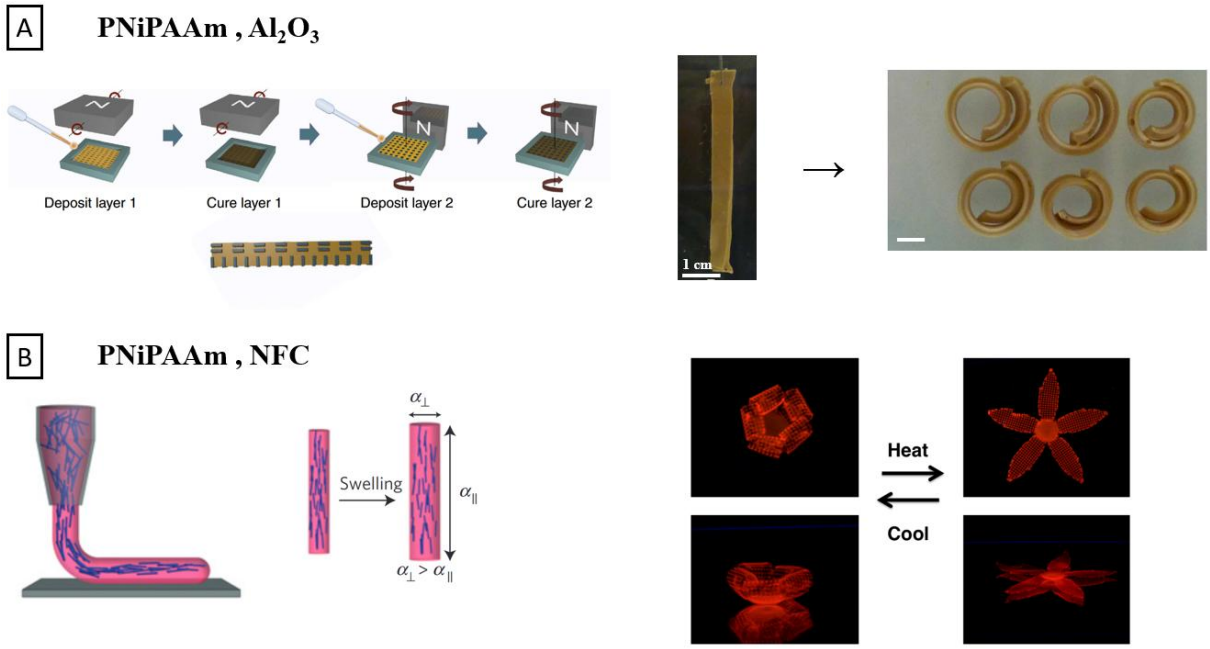

Figure I-10. A) Step by step process of the alignment of alumina nanoparticles under an external magnetic field and curing of PNiPAAm hydrogel strip to obtain a self-rolling actuator when hydrated [80] and B) shear induced alignment of NFC fibrils in PNiPAAm hydrogels as a building block to obtain control deformation with temperature variation [87].

5. HYDROGEL ACTUATORS AS BIOMEDICAL DEVICES

Hydrogel actuators are perfect candidates in the field of personalized biomedical devices due to their versatility and adaptability. These actuators can be tailored from a variety of materials as previously seen, allowing customization to address specific medical challenges. The diverse range of hydrogels—each with unique properties such as varying stiffness, swelling behavior, and biocompatibility—enables the design of devices that can precisely mimic different tissue types or respond to specific environmental changes. Moreover, hydrogel actuators can be engineered to respond to a variety of stimuli, including temperature, pH, light, or electrical signals, making them highly adaptable to changing conditions within the body. This flexibility not only enhances the performance and effectiveness of biomedical devices but also supports the development of next-generation solutions in areas like drug delivery,

regenerative medicine, and soft robotics, where precise, personalized interaction with biological tissues is essential. Duan *et al.* designed a CS / CMC bilayer hydrogel that can be used a smart lens with tunable focal point or even for drug delivery.[65] The bending direction was seen to be pH dependent. Below pH value of 3.6, CS has higher swelling than CMC which induces curling towards the CMC layer. While for a pH higher than 3.6, CMC has the higher swelling degree inducing actuation towards de CS layer. By modulating the pH level, different curvatures are obtained leading to various focal length of the bioinspired lens device as observed in Figure I-11A. Ge *et al.* 4D printed using SLA by digital light processing (DLP) a smart stent based on PAAm and modified commercial VeroClear.[88] The particular design as observed in Figure I-11B, offers a dual functionality where the modified VeroClear part (yellow) will be responsible for the expansion of the device in physiological conditions and the PAAm part (red) will be used a drug delivery vehicle. The thermo responsive stent exhibit a reversible shape memory aspect at 30 °C that is suitable for biomedical application. The device can be manipulated at high temperature to form a compact form that is maintained at lower temperature. Once the smart stent is placed in physiological conditions, it will expand to regain its initial shape. In addition, a red dye simulating a drug was encapsulated in the PAAm part of the device show a fast release response upon implantation. Hu et al. 4D printed using DIW a multi- responsive soft robot based on PNiPAAm and neodymium iron boron magnetic (NdFeB) particles.[89] The soft robot can be manipulated magnetically to move as observed in Figure I-11C in a complex human stomach model. Upon NIR irradiation, the gripper closes entrapping the cargo in it. It can be further manipulated to move and release the cargo at target zones.

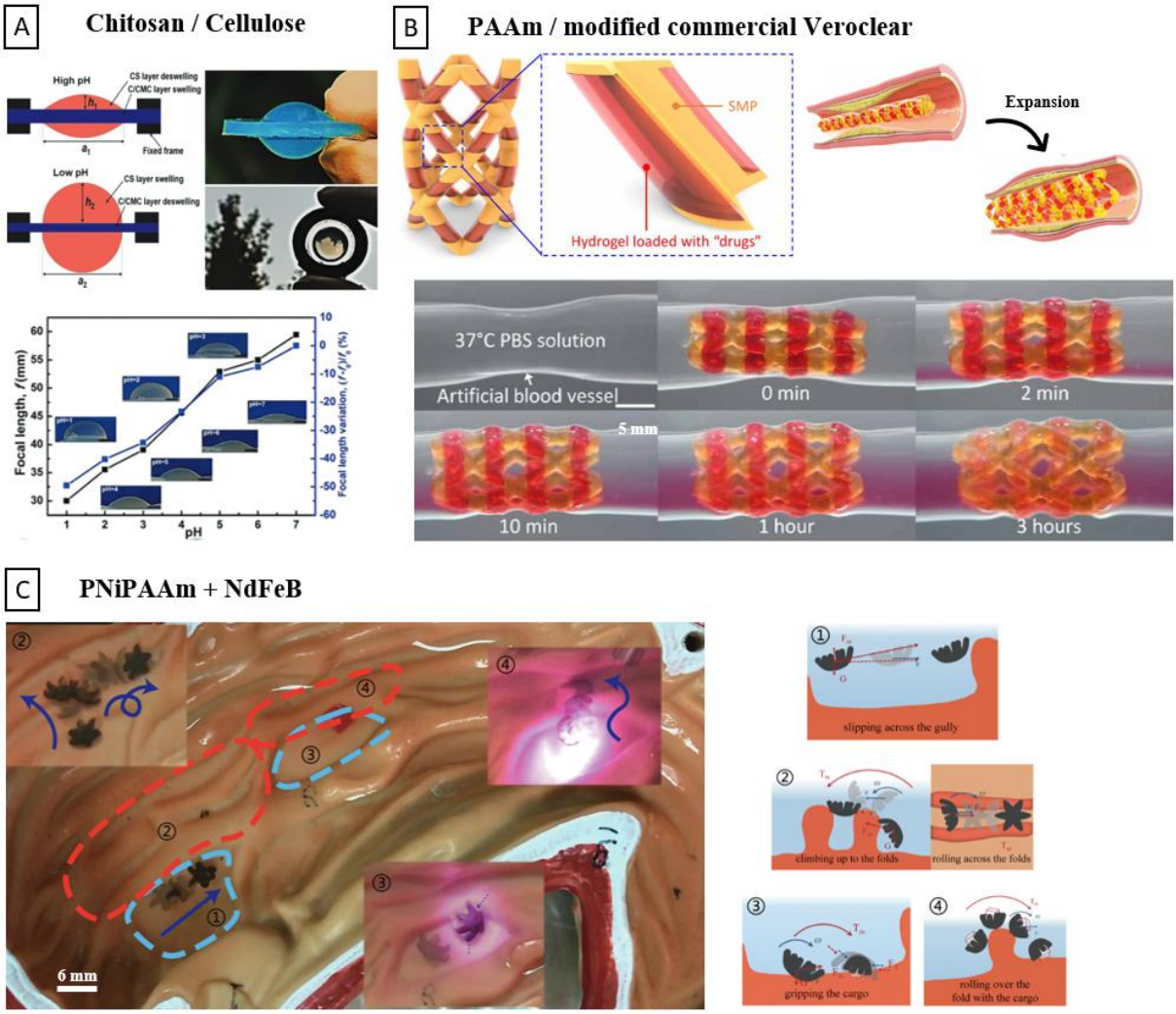

Figure I-11. A) pH response chitosan / cellulose bilayer smart lens with adaptable focal length [65]. B) 4D printed smart stent based on shape memory polymer (SMP) base on commercial VeroClear (yellow parts) and red dye loaded PAAm hydrogel part (red parts) expanding and releasing the dye in physiological media [88]. C) Smart soft robot based on PNiPAAm and neodymium iron boron magnetic particles moving and entrapping a cargo in stomach like model under light and magnetic stimuli [89].

6. CONCLUSION

The development of hydrogel actuators for biomedical applications represents a significant advancement in the field of soft and responsive materials. The selection of the polymer matrix plays a crucial role in determining the mechanical properties, biocompatibility, and responsiveness of these actuators. The ability to precisely control actuation through various stimuli (pH, temperature, and light) offers versatile functionality, enabling hydrogel actuators to adapt to specific biomedical environments and tasks. The preparation techniques, including simple bilayer structures, to more complex DIW and SLA printing processes, provide robust

and scalable methods for fabricating hydrogel actuators with complex geometries and tailored properties. These techniques allow for the integration of multiple functionalities within a single actuator, enhancing their potential for practical applications. Controlling the actuation of hydrogel-based systems is achieved through careful design and material selection, enabling predictable and reversible on-demand movements. The integration of these actuators in biomedical applications has been demonstrated through practical examples, that underscore the potential of hydrogel actuators to revolutionize various aspects of healthcare, offering solutions that are both innovative and responsive to the dynamic needs of biological systems.

Overall, hydrogel actuators present a promising avenue for the future of biomedical engineering, with ongoing research poised to expand their capabilities and applications further. Continued advancements in material science, fabrication techniques, and stimulus control will be essential in realizing the full potential of these smart, adaptable systems in real-world biomedical settings.

7. RESEARCH STRATEGY

In developing hydrogel actuators for biomedical applications, our research strategy centers on leveraging the strengths of natural polymers. While the majority of hydrogel actuators have traditionally relied on synthetic polymers such as PAAm, PAAc or PNiPAAm due to their well-characterized properties and ease of manipulation, there is growing interest in incorporating natural polymers. Natural polymers offer distinct advantages, including inherent biocompatibility and biodegradability, making them particularly appealing for biomedical applications. However, the challenge lies in modifying these natural polymers to achieve the desired mechanical strength, stimuli responsiveness, and processability.

Given these considerations, we have chosen to focus on alginate-based hydrogels in our research. Alginate, a polysaccharide derived from brown seaweed, has demonstrated significant potential due to its biocompatibility and its characteristic capability to complex with multi-valent cations such as Ca^{2+}. To harness these properties in a hydrogel actuator, our strategy involves chemically modifying alginate to produce a photo-crosslinkable resin suitable for advanced fabrication techniques. Specifically, we will explore the methacrylation of alginate, which introduces methacrylate groups into the polymer backbone, enabling the formation of crosslinked networks upon exposure to UV. This modification not only retains the beneficial properties of alginate but also provides the necessary functionality for stereolithography-based 3D printing which is the most studied technique in the team *Chimie et Matériaux*

MacroMoléculaires (C3M) of ICGM. SLA is particularly well-suited for creating complex, finely detailed hydrogel structures, making it an ideal choice for fabricating actuators with intricate designs and responsive features. By combining methacrylated alginate with SLA printing, we aim to develop hydrogel actuators that exhibit precise control over their shape, mechanical properties, and responsiveness to stimuli. The first critical step in this research will involve the synthesis and characterization of methacrylated alginate to ensure it meets the requirements for photo-crosslinking and 3D printing. This will involve optimizing the degree of methacrylation to balance crosslinking density with the desired flexibility and responsiveness of the hydrogel. In addition, the mechanical properties will be improved by blending alginate with Pluronic. Subsequent steps will include evaluating the printing parameters, refining the actuator designs, and assessing the performance of the resulting hydrogel actuators in relevant biomedical scenarios as illustrated in Figure I-12. Through this approach, we aim to contribute to the development of advanced hydrogel actuators that combine the best attributes of natural polymers with the precision of cutting-edge fabrication technologies.

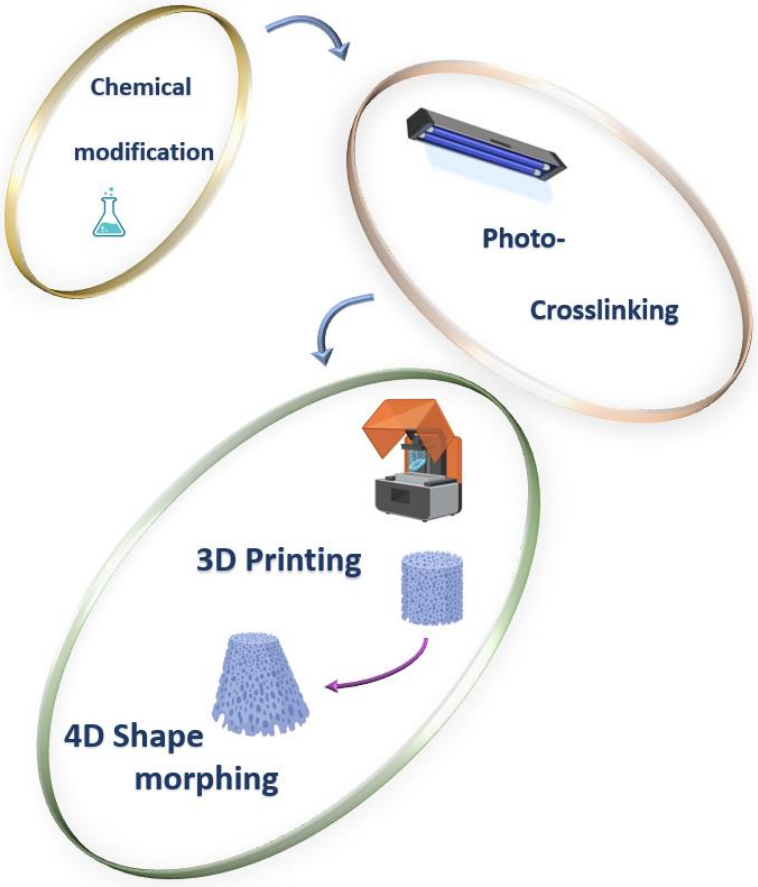

Figure I-12. Schematic illustration of the research strategy leading to 4D printing.

REFERENCES

[1] W. A. Laftah, S. Hashim, A. N. Ibrahim, *Polymer-Plastics Technology and Engineering* **2011**, *50*, 1475.

[2] H. M. El-Husseiny, E. A. Mady, L. Hamabe, A. Abugomaa, K. Shimada, T. Yoshida, T. Tanaka, A. Yokoi, M. Elbadawy, R. Tanaka, *Materials Today Bio* **2022**, *13*, 100186.

[3] F. Ullah, M. B. H. Othman, F. Javed, Z. Ahmad, H. Md. Akil, *Materials Science and Engineering: C* **2015**, *57*, 414.

[4] C. Echeverria, S. Fernandes, M. Godinho, J. Borges, P. Soares, *Gels* **2018**, *4*, 54.

[5] M. C. Koetting, J. T. Peters, S. D. Steichen, N. A. Peppas, *Materials Science and Engineering: R: Reports* **2015**, *93*, 1.

[6] W. Li, Q. Guan, M. Li, E. Saiz, X. Hou, *Progress in Polymer Science* **2023**, *140*, 101665.

[7] Q. Shi, H. Liu, D. Tang, Y. Li, X. Li, F. Xu, *NPG Asia Mater* **2019**, *11*, 64.

[8] S. Tibbits, *Architectural Design* **2014**, *84*, 116.

[9] F. Xin, Q. Lyu, *Gels* **2022**, *9*, 7.

[10] Y. Yuan, K. Raheja, N. B. Milbrandt, S. Beilharz, S. Tene, S. Oshabaheebwa, U. A. Gurkan, A. C. S. Samia, M. Karayilan, *RSC Appl. Polym.* **2023**, *1*, 158.

[11] J. Seuring, S. Agarwal, *Macromol. Rapid Commun.* **2012**, *33*, 1898.

[12] J. D. Jang, C. Do, J. Bang, Y. S. Han, T.-H. Kim, *Polymers* **2019**, *11*, 63.

[13] J. Wu, Y. S. Thio, F. S. Bates, *J Polym Sci B Polym Phys* **2005**, *43*, 1950.

[14] G. Wanka, H. Hoffmann, W. Ulbricht, *Macromolecules* **1994**, *27*, 4145.

[15] S. Graham, P. F. Marina, A. Blencowe, *Carbohydrate Polymers* **2019**, *207*, 143.

[16] H. J. Chung, T. G. Park, *Nano Today* **2009**, *4*, 429.

[17] T. Jayaramudu, K. Varaprasad, E. R. Sadiku, J. Amalraj, *Colloids and Surfaces A: Physicochemical and Engineering Aspects* **2019**, *572*, 307.

[18] D. Segiet, A. Stockmann, J. Sadowski, F. Katzenberg, J. C. Tiller, *Macromol. Chem. Phys.* **2021**, *222*, 2100157.

[19] D. Yang, M. Viitasuo, F. Pooch, H. Tenhu, S. Hietala, *Polym. Chem.* **2018**, *9*, 517.

[20] N. Shimada, S. Kidoaki, A. Maruyama, *RSC Adv.* **2014**, *4*, 52346.

[21] V. Ozturk, O. Okay, *Polymer* **2002**, *43*, 5017.

[22] E. Suljovrujic, M. Krstic, Z. Rogic Miladinovic, S. Petrovic, A. Leskovac, G. Stamboliev, *Reactive and Functional Polymers* **2023**, *189*, 105612.

[23] B. Yang, C. Wang, Y. Zhang, L. Ye, Y. Qian, Y. Shu, J. Wang, J. Li, F. Yao, *Polym. Chem.* **2015**, *6*, 3431.

[24] J. B. Lee, J. J. Yoon, D. S. Lee, T. G. Park, *Journal of Biomaterials Science, Polymer Edition* **2004**, *15*, 1571.

[25] M. R. Kim, T. G. Park, *Journal of Controlled Release* **2002**, *80*, 69.

[26] I. D. Paepe, H. Declercq, M. Cornelissen, E. Schacht, *Polym. Int.* **2002**, *51*, 867.

[27] M. R. Bayat, M. Baghani, *Journal of Intelligent Material Systems and Structures* **2021**, *32*, 2349.

[28] R. Khan, M. Zaman, A. Salawi, M. A. Khan, M. O. Iqbal, R. Riaz, M. M. Ahmed, M. H. Butt, M. N. Alvi, Y. Almoshari, M. Alshamrani, *Gels* **2022**, *8*, 281.

[29] X. Gao, C. He, C. Xiao, X. Zhuang, X. Chen, *Materials Letters* **2012**, *77*, 74.

[30] B. Vázquez, M. Gurruchaga, I. Gon˜i, J. San Román, *Biomaterials* **1997**, *18*, 521.

[31] M. Giannuzzo, M. Feeney, P. Paolicelli, M. A. Casadei, *Journal of Drug Delivery Science and Technology* **2006**, *16*, 49.

[32] H. R. Allcock, A. M. A. Ambrosio, *Biomaterials* **1996**, *17*, 2295.

[33] R. Cheng, J. Liu, P. Xie, Y. Wu, J. Deng, *Polymer* **2015**, *68*, 246.

[34] Long Zhao, H. Mitomo, F. Yosh, *Journal of Bioactive and Compatible Polymers* **2008**, *23*, 319.

[35] M. Gümüşderelioğlu, D. Kesgin, *International Journal of Pharmaceutics* **2005**, *288*, 273.

[36] K.-S. Chen, Y.-A. Ku, H.-R. Lin, T.-R. Yan, D.-C. Sheu, T.-M. Chen, F.-H. Lin, *Materials Chemistry and Physics* **2005**, *91*, 484.

[37] B. Wang, X. Xiao, Y. Zhang, L. Liao, *European Polymer Journal* **2019**, *116*, 545.

[38] S. Long, F. Chen, H. Ren, Y. Hu, C. Chen, Y. Huang, X. Li, *Polymers* **2024**, *16*, 1031.

[39] K. Unger, P. Salzmann, C. Masciullo, M. Cecchini, G. Koller, A. M. Coclite, *ACS Appl. Mater. Interfaces* **2017**, *9*, 17408.

[40] W. Francis, A. Dunne, C. Delaney, L. Florea, D. Diamond, *Sensors and Actuators B: Chemical* **2017**, *250*, 608.

[41] K. Homma, A. C. Chang, S. Yamamoto, R. Tamate, T. Ueki, J. Nakanishi, *Acta Biomaterialia* **2021**, *132*, 103.

[42] J. Volarić, J. Buter, A. M. Schulte, K.-O. van den Berg, E. Santamaría-Aranda, W. Szymanski, B. L. Feringa, *The Journal of Organic Chemistry* **2022**, *87*, 14319.

[43] M. Luo, X. Zhang, J. Wu, J. Zhao, *Carbohydrate Polymers* **2021**, *266*, 118097.

[44] Q. Zheng, C. Xu, Z. Jiang, M. Zhu, C. Chen, F. Fu, *Front. Chem.* **2021**, *9*, 650358.

[45] A. Pourjavadi, R. Heydarpour, Z. M. Tehrani, *New J. Chem.* **2021**, *45*, 15705.

[46] M. Zhai, Y. Zhang, J. Ren, M. Yi, H. Ha, J. F. Kennedy, *Carbohydrate Polymers* **2004**, *58*, 35.

[47] X. Pei, L. Fang, W. Chen, X. Wen, L. Bai, X. Ba, *Macro Chemistry & Physics* **2021**, *222*, 2000339.

[48] A. Shiotani, T. Mori, T. Niidome, Y. Niidome, Y. Katayama, *Langmuir* **2007**, *23*, 4012.

[49] Somayeh Ghavami, G. R. Bardajee, A. Mirshokraie, K. Didehban, *Polym. Sci. Ser. B* **2019**, *61*, 376.

[50] M. Anees Ur Rehman Qureshi, N. Arshad, A. Rasool, N. K. Janjua, M. S. Butt, M. Naqeeb Ur Rehman Qureshi, H. Ismail, *R. Soc. Open Sci.* **2024**, *11*, 231952.

[51] S. Komatsu, M. Tago, Y. Ando, T.-A. Asoh, A. Kikuchi, *Journal of Controlled Release* **2021**, *331*, 1.

[52] J. Du, B. Li, C. Li, Y. Zhang, G. Yu, H. Wang, X. Mu, *International Journal of Biological Macromolecules* **2016**, *88*, 451.

[53] K. Shi, Z. Liu, Y.-Y. Wei, W. Wang, X.-J. Ju, R. Xie, L.-Y. Chu, *ACS Appl. Mater. Interfaces* **2015**, *7*, 27289.

[54] Y. Qu, B. Y. Chu, J. R. Peng, J. F. Liao, T. T. Qi, K. Shi, X. N. Zhang, Y. Q. Wei, Z. Y. Qian, *NPG Asia Mater* **2015**, *7*, e207.

[55] S. Basak, A. Bandyopadhyay, *RSC Appl. Polym.* **2024**, *2*, 583.

[56] Y. Shin, J. Choi, J.-H. Na, S. Y. Kim, *Polymer* **2020**, 123163.

[57] Z. Han, P. Wang, G. Mao, T. Yin, D. Zhong, B. Yiming, X. Hu, Z. Jia, G. Nian, S. Qu, W. Yang, *ACS Appl. Mater. Interfaces* **2020**, *12*, 12010.

[58] A. Ding, O. Jeon, R. Tang, Y. B. Lee, S. J. Lee, E. Alsberg, *Adv. Sci.* **2021**, 2004616.

[59] G. Gao, L. Wang, Y. Cong, Z. Wang, Y. Zhou, R. Wang, J. Chen, J. Fu, *ACS Omega* **2018**, *3*, 17914.

[60] X. Wang, H. Huang, H. Liu, F. Rehfeldt, X. Wang, K. Zhang, *Macromol. Chem. Phys.* **2019**, *220*, 1800562.

[61] A. Sood, A. Gupta, G. Agrawal, *Carbohydrate Polymer Technologies and Applications* **2021**, *2*, 100067.

[62] A. Berradi, F. Aziz, M. E. Achaby, N. Ouazzani, L. Mandi, *Polymers* **2023**, *15*, 2908.

[63] H. He, J. Guan, J. L. Lee, *Journal of Controlled Release* **2006**, *110*, 339.

[64] S. Zakharchenko, E. Sperling, L. Ionov, *Biomacromolecules* **2011**, *12*, 2211.

[65] J. Duan, X. Liang, K. Zhu, J. Guo, L. Zhang, *Soft Matter* **2017**, *13*, 345.

[66] S. Xiao, X. He, J. Qian, X. Wu, G. Huang, H. Jiang, Z. He, J. Yang, *Ind. Eng. Chem. Res.* **2020**, *59*, 7646.

[67] J. Liu, O. Erol, A. Pantula, W. Liu, Z. Jiang, K. Kobayashi, D. Chatterjee, N. Hibino, L. H. Romer, S. H. Kang, T. D. Nguyen, D. H. Gracias, *ACS Appl. Mater. Interfaces* **2019**, *11*, 8492.

[68] J. Guo, R. Zhang, L. Zhang, X. Cao, *ACS Macro Lett.* **2018**, *7*, 442.

[69] B. Narupai, P. T. Smith, A. Nelson, *Adv Funct Materials* **2021**, *31*, 2011012.

[70] J. Liu, W. Liu, A. Pantula, Z. Wang, D. H. Gracias, T. D. Nguyen, *Extreme Mechanics Letters* **2019**, *30*, 100514.

[71] T. Uchida, H. Onoe, *Micromachines* **2019**, *10*, 433.

[72] P. Cao, L. Tao, J. Gong, T. Wang, Q. Wang, J. Ju, Y. Zhang, *ACS Appl. Polym. Mater.* **2021**, *3*, 6167.

[73] J. Lai, X. Ye, J. Liu, C. Wang, J. Li, X. Wang, M. Ma, M. Wang, *Materials & Design* **2021**, *205*, 109699.

[74] A. Kirillova, R. Maxson, G. Stoychev, C. T. Gomillion, L. Ionov, *Adv. Mater.* **2017**, *29*, 1703443.

[75] Z. Ji, C. Yan, B. Yu, X. Zhang, M. Cai, X. Jia, X. Wang, F. Zhou, *Adv. Mater. Technol.* **2019**, *4*, 1800713.

[76] S. Dutta, D. Cohn, *J. Mater. Chem. B* **2017**, *5*, 9514.

[77] M. N. I. Shiblee, K. Ahmed, M. Kawakami, H. Furukawa, *Adv. Mater. Technol.* **2019**, *4*, 1900071.

[78] C. Garcia, A. Gallardo, D. López, C. Elvira, A. Azzahti, E. Lopez-Martinez, A. L. Cortajarena, C. M. González-Henríquez, M. A. Sarabia-Vallejos, J. Rodríguez-Hernández, *ACS Appl. Bio Mater.* **2018**, *1*, 1337.

[79] J. W. Yu, J. Jung, Y.-M. Choi, J. H. Choi, J. Yu, J. K. Lee, N.-H. You, M. Goh, *Polym. Chem.* **2016**, *7*, 36.

[80] R. M. Erb, J. S. Sander, R. Grisch, A. R. Studart, *Nat Commun* **2013**, *4*, 1712.

[81] F. Momeni, J. Ni, *Engineering* **2020**, *6*, 1035.

[82] Q. Zhao, Y. Liang, L. Ren, Z. Yu, Z. Zhang, F. Qiu, L. Ren, *J. Mater. Chem. B* **2018**, *6*, 1260.

[83] X. Le, W. Lu, J. Zhang, T. Chen, *Advanced Science* **2019**, *6*, 1801584.

[84] L. Wang, Y. Jian, X. Le, W. Lu, C. Ma, J. Zhang, Y. Huang, C.-F. Huang, T. Chen, *Chem. Commun.* **2018**, *54*, 1229.

[85] J. Shang, P. Theato, *Soft Matter* **2018**, *14*, 8401.

[86] A. Gevorkian, S. M. Morozova, S. Kheiri, N. Khuu, H. Chen, E. Young, N. Yan, E. Kumacheva, *Adv. Funct. Mater.* **2021**, 2010743.

[87] A. Sydney Gladman, E. A. Matsumoto, R. G. Nuzzo, L. Mahadevan, J. A. Lewis, *Nature Mater* **2016**, *15*, 413.

[88] Q. Ge, Z. Chen, J. Cheng, B. Zhang, Y.-F. Zhang, H. Li, X. He, C. Yuan, J. Liu, S. Magdassi, S. Qu, *Sci. Adv.* **2021**, *7*, eaba4261.

[89] X. Hu, Z. Ge, X. Wang, N. Jiao, S. Tung, L. Liu, *Composites Part B: Engineering* **2022**, *228*, 109451.

CHAPTER II / CHAPITRE II

Introduction Chapitre II

Ce chapitre explore la conception et l'optimisation de réseaux d'hydrogels basés sur l'alginate de sodium, un polysaccharide naturel reconnu pour ses propriétés biocompatibles et biodégradables. L'accent est mis sur la modification chimique de l'alginate par greffage de motifs méthacryliques, permettant de créer des hydrogels photo-réticulables dont les propriétés mécaniques et de gonflement peuvent être finement ajustées en fonction de la masse molaire de l'alginate et du degré de méthacrylation. La méthacrylation est réalisée spécifiquement sur les groupements hydroxyle, afin de conserver les fonctions acides carboxyliques intactes, ce qui permet de les complexer avec des ions multivalents, notamment le Ca^{2+}.

L'étude examine également l'introduction d'une réticulation secondaire par l'ajout d'ions Ca^{2+}, visant à renforcer les propriétés mécaniques et à induire des changements de volume rapides et réversibles des hydrogels. Ce double réseau réticulé est présenté comme une base prometteuse pour la conception d'actuateurs auto-repliables et de systèmes auto-réparables, ouvrant la voie à des applications avancées dans le domaine des matériaux intelligents.

Chapter II

Dual Cross-Linked Stimuli-Responsive Alginate-Based Hydrogels

KEYWORDS

Hydrogels, polysaccharide, Sodium alginate, dual crosslinking, stimuli-responsive, structure-property relationship.

ABSTRACT

Sodium alginate with different molecular weights (55, 170 and 320 $kg.mol^{-1}$) were chemically modified by grafting methacrylic moieties onto the hydroxyl groups of the alginate backbone. The methacrylation was optimized to obtain different degrees of modification. Chemically crosslinked hydrogels were obtained following UV light irradiation in the presence of a photo-initiator. The swelling behavior and the mechanical properties were observed to depend both on the degree of methacrylation and the alginate molecular weight. Due to the chain entanglement present in high viscosity sodium alginate, lower degrees of modification were required to tune the hydrogels properties. Moreover, in the presence of Ca^{2+}, secondary crosslinking was introduced by the coordination of the alginates guluronate moieties with the Ca^{2+} ions. The addition of this secondary crosslinking caused fast volume shrinkage and a reinforcement of the mechanical properties. The secondary crosslinking was reversible and the hydrogels regained their original shape for at least three cycles. Additionally, the dual crosslinked network can be used to induce adhesion between hydrogels and serve as a building block for self-folding actuators.

1. INTRODUCTION

Polysaccharides, like cellulose, starch, chitosan, alginate, agarose, are naturally occurring polymer chains extracted from natural resources. These natural polymers show sufficient biocompatibility allowing their use in biomedical applications such as wound dressing, tissue engineering, drug delivery etc.[1] These polymers are naturally abundant, can be relatively easily chemically modified and for the most part of them, can be processed in water thus avoiding the use of toxic organic solvents. However, due to their various structural heterogeneities, it is important to understand the different structure-property relationships in order to control and adapt the different properties for the desired application. For instance, understanding the swelling behavior is crucial for drug delivery applications, particularly concerning drug release kinetics. Similarly, understanding the elasticity modules is important for wound healing, and exploring shape morphing possibilities is significantly useful for tissue engineering in order to align with specific mechanical or tissue filling requirements. These properties are often correlated with the nature and degree of crosslinking of these natural polymers.

Sodium alginate is a commonly used polysaccharide in the biomedical field. It is known to complex/coordinate with multivalent cations such as Fe^{3+}, Cu^{2+}, Ca^{2+} , Mn^{2+} leading to the formation of physically crosslinked hydrogels.[2-4] However, alginate physical hydrogels demonstrate weak stability in physiological media resulting from the dissociation of the matrix due to the Na^{+} - Ca^{2+} ion exchange.[5] Stable chemical crosslinking of alginate can be obtained via photo-crosslinking after introduction of methacrylate moieties onto the hydroxyl or carboxyl groups present on the backbone.[6] Furthermore, increases in methacrylation degrees ranging from 8% to 25% have been reported to result in a notable increase in the compression modulus from 35 to 175 kPa for alginates [7]). Modifying the swelling and mechanical properties of sugar-based hydrogels can also be achieved by the introduction of a secondary crosslinking to the polymer network.[8-12] For instance, the shear storage modulus showed a hundredfold improvement with the introduction of a secondary crosslinking for alginates.[13] This dual crosslinking mechanism thus represents an interesting strategy to induce stimuli-responsive behaviors for smart hydrogels. Early research combined chemical and ionic crosslinking of alginate to improve the performance and properties of drug delivery microspheres.[14-15] Kim et *al*. reported chemically photo-crosslinked alginate hydrogels by functionalizing the carboxyl group with tyramine hydrochloride. The mechanical performance of the hydrogels were further reinforced by the introduction of calcium ions.[16] Similarly, Gao *et al.* prepared dual-crosslinked

alginate fibers using a microfluidic fabrication system.[17] The dual crosslinked network enhanced the tensile strength of the fibers and improved their stability in physiological conditions compared to simple physically crosslinked alginate networks. Fenn *et al.* used dual crosslinking on alginate beads to control the release of doxorubicin hydrochloride as a controlled drug delivery system.[14] They found that dual crosslinking might not be beneficial for the drug encapsulation efficiency due to the entrapment of the drug inside the dual crosslinked network. Incorporating physical crosslinking in alginate hydrogels have been used to enhance the mechanical properties for cell compatibility.[13, 16, 18]

In most of these studies the structure-property correlations of dual crosslinking alginate systems have not been fully reported. Furthermore, none of these studies report the combined physical and mechanical crosslinking of alginate as means to promote hydrogel repair and induce volume and shape deformation for potential actuators. Indeed, the reported dual-crosslinked alginate systems often lack information on the alginate's structural properties such as the molecular mass M_w and/or monomer composition (Guluronic/Mannuronic (G/M) ratio). In this work, three Sodium alginates (Alg-Na^+) having a similar G/M ratio but different molecular mass were chemically modified in order to obtain chemically crosslinked networks. The influence of both different degrees of modification and the reversibility of the physical crosslinking on the network's properties was evaluated. The swelling behavior as well as the mechanical properties were assessed in both water and phosphate buffered solutions (PBS). Finally, dual crosslinking was used as a mean to induce self-healing and to prepare self-folding actuators with specific shape deformation.

2. MATERIALS & METHODS

2.1. Materials

Sodium alginate (Alg-Na^+) of medium (MVA) and high viscosity (HVA) having G/M = 0.6 - 0.7 were generously donated by Algaia (Saint Lo, FRANCE). Low viscosity sodium alginate (LVA) was purchased from Sigma-Aldrich. Characterization of the Alg-Na^+ samples can be found in the supplementary information section (Figure II-S1 & Table II-S1). Methacrylic anhydride (MA), calcium chloride ($CaCl_2$), ethylenediaminetetraacetic acid tetrasodium salt dihydrate (EDTA $4Na^+$, $2H_2O$) and phosphate buffered saline (PBS) were purchased from Sigma-Aldrich. Triethylamine (TEA) was purchased from Fisher Chemicals. Milli-Q water (conductivity = 18.2 mΩ.cm at 23°C) was used during this study. Lithium

phenyl-2,4,6-trimethylbenzoylphosphinate (LAP) was synthesized as described in literature[19]. All chemicals were used without further purification unless mentioned otherwise.

2.2. Methods

Sodium alginate chemical modification

Methacrylated alginate (Alg-MA) was obtained by reacting Alg-Na^+ with methacrylic anhydride (MA). A 2 % (w/v) aqueous Alg-Na^+ was prepared by dissolving 1 g of Alg-Na^+ in 50 mL of milli-q water in a 250 mL round bottom flask under magnetic stirring (700 rpm). In order to obtain a homogeneous mixture, the solution was left to stir for 4 hours at 20°C. TEA was then added at different molar equivalents (2, 10, 20, 40 and 60 eq.) with respect to MA and the solution was left to stir for 30 minutes to ensure complete homogenization. Finally, MA was added at different molar equivalents (1, 5, 10, 20 and 30 eq.) with respect to the sugar units. The reaction was carried for the first 4 hours in an ice bath and then for the next 20 hours at 24°C. Alg-MA was isolated by precipitating the mixture in cold acetone followed by drying at 24°C under reduced pressure. Different degrees of methacrylation were obtained by varying the amounts of added MA or TEA:MA as summarized in Figure II-2a. The different Alg-MA will be denoted by LVAx, MVAx or HVAx where LVA, MVA and HVA represents low viscosity alginate (54 000 $g.mol^{-1}$), medium viscosity alginate (170 000 $g.mol^{-1}$) and high viscosity alginate (320 000 $g.mol^{-1}$) respectively and x the degree of modification (DM) by methacrylate moieties per sugar unit (in %).

^{1}H NMR characterization

^{1}H NMR was used to quantify the degree of modification (DM). 20 mg of Alg-MA was dissolved in 1mL of D_2O and left to stir for 1 hour to obtain a homogeneous solution. The ^{1}H NMR spectra were recorded on a Bruker Avance I 400 MHz (64 scans, 5 s relaxation time). The DM, defined as the number of methacrylates per sugar moiety, was calculated as the ratio of the protons of methacrylate (1.95 ppm, 5.8 ppm and 6.2 ppm) and H_{G1} proton of the alginate using the following equation.

$$DM\ (\%) = G\% * \frac{I_{H\ vinyl\ 6.2\ ppm}}{I_{H_G\ 5\ ppm}} \qquad \text{(Equation 1)}$$

Where I_H represents the intensity of vinyl protons of the grafted methacrylate at 6.2 ppm, $I_{H_{G1}}$ represents the intensity of the anomeric protons of the guluronic moieties and G% represents the fraction of guluronic units in the polysaccharide. The G% is calculated by comparing the anomeric G proton at 5.8 ppm with the anomeric M proton at 4.47 ppm.

Hydrogel preparation

The photo-crosslinkable aqueous alginate resin comprised of a 3 % (w/v) Alg-MA and 0.12 % (w/v) LAP as the photo-initiator. The alginate resin was injected in a cylindrical Teflon mold (10 mm diameter and 4 mm thickness) and covered with a glass slide to ensure a flat surface and avoid solvent evaporation. Photo-crosslinking was performed under UV light at 365 nm for 20 minutes using a UV Crosslinker Bio-Link chamber (Thermo Fischer, France) at 2-3 $mW.cm^{-2}$. Prior to the swelling and mechanical assays, the hydrogels were allowed to swell in water for 8 hours (with two water change) to ensure the removal of all unreacted species. Subsequently, they were then dried on a Teflon sheet in a 45°C oven for 24 hours until a constant weight was reached.

Gel content (GC)

Hydrogels were used directly after UV curing. Upon photo-crosslinking, the hydrogels were dried on a Teflon sheet in a 45°C oven for 24 hours until a constant weight was achieved. The dry mass was recorded and denoted as $m_{dry\ 1}$. Subsequently, the hydrogel was allowed to swell in water for 24 hours (with two water changes) followed by oven drying. The mass of the dry washed hydrogels was recorded and denoted as $m_{dry\ 2}$. The gel content (GC) was calculated using the following equation.[20]

$$GC = 100 * \frac{m_{dry\ 2}}{m_{\ dry\ 1}} \qquad \text{(Equation 2)}$$

Swelling kinetics

A washed dry hydrogel disk was placed in 40 mL of Milli-Q water at 24°C. The hydrogel was then weighed at different time intervals after removing excess water with a wet KimTech paper. Between measurements, the gel was re-immersed in the Milli-Q water at 24°C. The swelling degree (Q) was calculated using the following equation.

$$Q = \frac{m_{swollen\ at\ time\ t}}{m_{\ dry}} \qquad \text{(Equation 3)}$$

Cyclic swelling

The equilibrium cyclic swelling degrees were measured using the washed dried hydrogels as starting material with both EDTA and PBS as decomplexing solutions. The cycles comprised of the following sequences: 1) water, 2) 10% (w/v) aq. $CaCl_2$ solution and 3) 1% (w/v) aq EDTA solution or PBS to mimic physiological conditions. Steps 2 and 3 were repeated for 2 extra cycles. For each measurement, the hydrogel was left to swell in the specific media

for 24 hours at 24 ºC. The swelling degree was calculated using equation 2. The values are represented as the mean of triplicate sets. The standard deviation was found to be around 20% for each value. The error bars are not shown on the figures to avoid their superposition and maintain clear reading.

Compression testing

Compression tests of the swollen hydrogels were conducted on an Instron 3366L5885 mechanical tester equipped with a 100N load cell. Cylindrical samples (10 mm diameter and 4 mm thickness) were prepared in a Teflon mold as previously described. The samples were washed, dried and then left to swell in water for 24 hours. Hydrogels were taken at different steps of the cyclic swelling and the dimensions were measured using a caliper. The compression speed was set at 1 $mm.s^{-1}$ with a 200 ms sampling time. Each value is represented by the mean ± standard deviation (SD) (n = 3). Young's modulus was calculated as the slope at 3% deformation.

Rheological frequency sweeps

All tests were performed on a Thermo Fisher HAAKE MARS 60 rheometer using an 8 mm parallel circular sanded plate-plate geometry. The samples were cylindrical disks (8 mm diameter and 1mm thickness) matching the plates' diameter and the fixed gap value respectively. Frequency sweeps were done between 1 and 10 rad/s in the linear viscoelastic domain at a constant 5% strain at 25°C.

Induced hydrogel repair

The hydrogels were left to swell in water for different time intervals to vary the swelling degree. They were then cut in half, rearranged in the desired architecture and glued with few microliters of 10% (w/v) aqueous $CaCl_2$ solution. Calcium was left to diffuse for 30 seconds before manually extending the hydrogel to test its stability.

The efficiency of the induced hydrogel healing was evaluated by tensile testing. The tensile tests were performed on an Instron 3366L5885 mechanical tester equipped with a 100 N load cell. The tensile speed was set at 1 $mm.s^{-1}$ with 200 ms sampling time.

Actuator preparation

Alginate-based actuators were first built by establishing a dual-crosslinking gradient. The gradient was achieved by allowing calcium diffusion from the top surface of the hydrogel for an optimized period of 5 seconds. Before curing, the methacrylated alginate resin was placed in a mold measuring 30mm x15 mm, with thicknesses of 0.5, 0.75 and 1 mm. Calcium was left

to diffuse for 5 seconds on the surface of the resin, by applying a wetted filter paper with a 5 % (w/v) $CaCl_2$ solution. Subsequently, the surface of the mold was covered with a glass slide to ensure a flat surface and avoid water evaporation, followed by photo-crosslinking under UV (365 nm) for 20 minutes.

Next, hydrogel films were patterned to achieve alternating sections of single (chemically) and dual (chemical and physical) crosslinked section. The hydrogels were allowed to swell in water for 3 hours to ensure that the equilibrium swelling degree was reached.

3. RESULTS & DISCUSSION

3.1. Sodium alginate chemical modification

The addition of a photo-sensitive function on the alginate's backbone provides the ability to obtain a chemically crosslinked network under UV irradiation and a photo-initiator. The common method of functionalization is by grafting methacrylate groups on the hydroxyl or carboxyl of the polysaccharides' unit.[1] The reaction commonly occurs in the presence of methacrylic anhydride, glycidyl methacrylate, 2-aminoethyl methacrylate or by microwave assisted methacrylation.[12, 21] Reaction conditions requires either careful control of pH with concentrated NaOH, very long reaction times to favor ring opening over the transesterification reaction, the use of organic cosolvent or complex apparatus with careful temperature control.[21] As stated previously, the methacrylation was done on three batches of sodium alginate having various molecular weights and denoted as LVA; MVA and HVA for low viscosity alginate (54 000 $g.mol^{-1}$), medium viscosity alginate (170 000 $g.mol^{-1}$) and high viscosity alginate (320 000 $g.mol^{-1}$) respectively. For a fixed concentration in water, increasing the molecular weight of the alginate backbone will result in an increase of the viscosity of the solution (Figure II-S4) because of the formation of notable chain entanglements thus justifying the chosen the nomenclature.

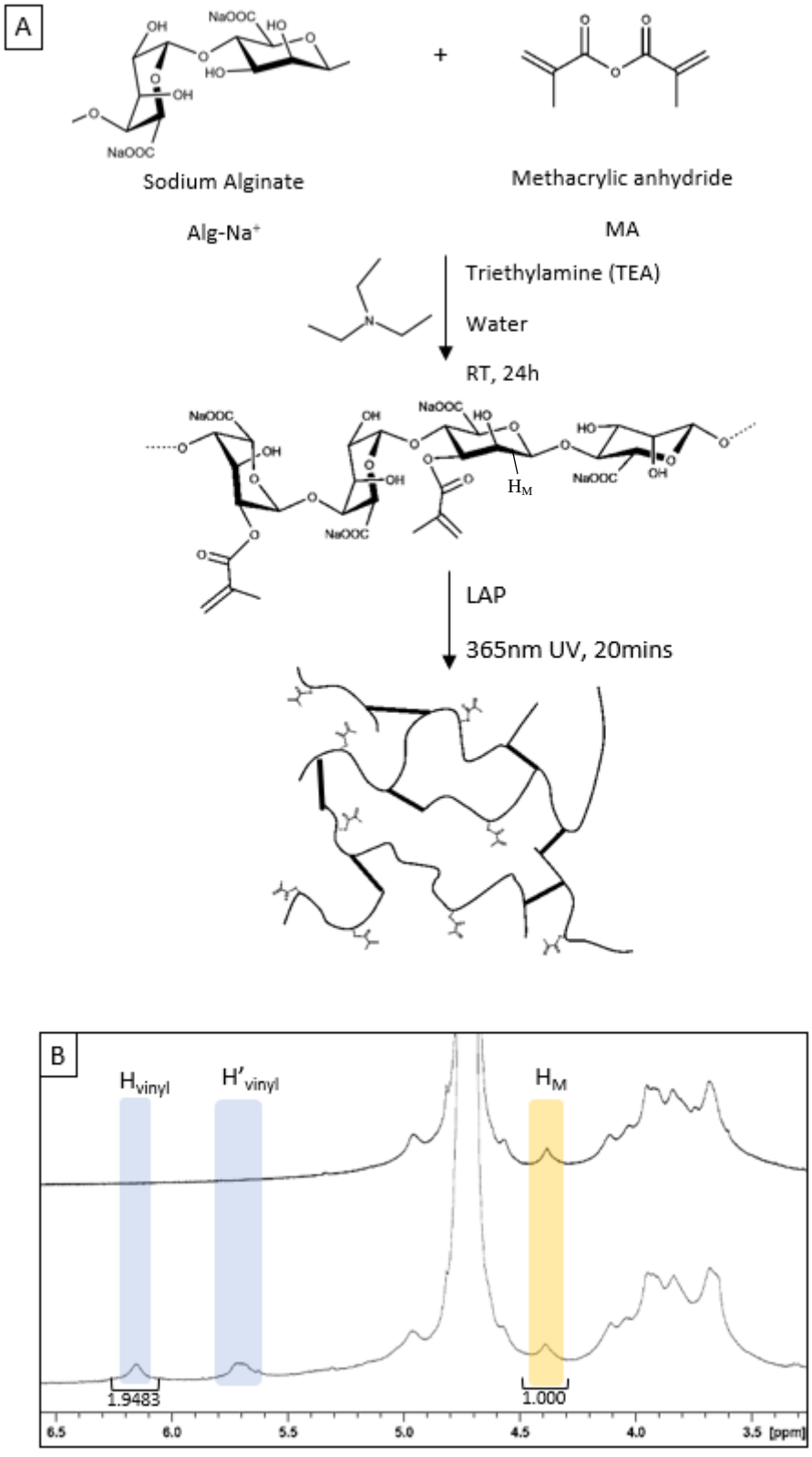

Figure II-1. A) Schematic illustration of the methacrylation of sodium alginate and its photo-crosslinking and B) NMR spectra of native MVA (top) and methacrylated MVA80 (bottom).

In order to obtain the photo-crosslinkable sodium alginate resin, methacrylic moieties were grafted on the alginate backbone by reacting the hydroxyl groups with methacrylic anhydride as shown in Figure II-1. Grafting the methacrylic moieties on the hydroxyl groups allows the carboxylic acids to remain available to coordinate with Ca^{2+} ions providing a secondary reversible crosslinking in the hydrogel matrix.[22] During methacrylation, methacrylic acid is released as a byproduct of the reaction or as a result of the hydrolysis of the methacrylic anhydride. To avoid a drastic drop in pH, which could lead to the formation of alginic acid and its precipitation,[5] TEA was used as a poor nucleophilic base in order to neutralize the acids formed while simultaneously preventing the hydrolysis of the formed esters.

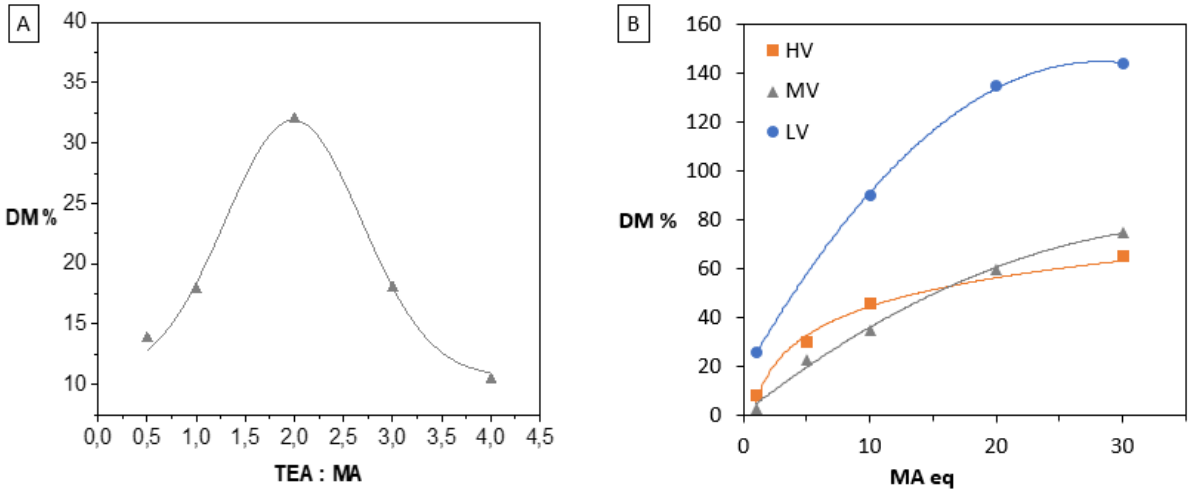

Figure II-2. Influence of A) TEA/MA ratio for a fixed MA = 10 eq on the DM of MVA and B) MA equivalence for a fixed TEA/MA = 2 eq on the DM of LVA, MVA and HVA (The percentage is calculated based on the number of modifications per sugar unit. Considering that each unit has two hydroxyl groups, the maximum percentage reaches 200%).

The successful methacrylation can be observed on the ^{1}H NMR spectra as shown in Figure II-S1. The vinyl protons of the grafted methacrylates appear at 5.8 and 6.2 ppm while the methyl protons appear at 1.9 ppm. Two main parameters were found to influence the DM as illustrated in Figure II-2: the molar ratio TEA/MA and the equivalent amount of added MA. For MVA, an increase in the TEA/MA molar ratio leads to an increase in DM until a peak of 33% is reached at TEA/MA = 2 eq.; subsequently, it decreases to 10% for 4 eq TEA. At low TEA/MA molar ratio, insufficient TEA is present to neutralize the methacrylic acids formed, resulting in a drop in pH. This causes an increase in the viscosity due to hydrogen bonding between the protonated carboxylic acid functions, limiting access of MA to the hydroxyl groups thus leading to lower DM. At TEA/MA ≥ 2eq, triethylamine catalyzes the hydrolysis of the anhydride compared to

nucleophilic acyl substitution reaction, favoring the formation of methacrylic acid rather than grafting on the alginate backbone and resulting in lower DM.[23] In addition, a large excess of MA is used to achieve higher DM. A logarithmic increase is observed until a plateau is achieved due to the steric hindrance caused by the grafted methacrylic moieties.[12, 24] The same tendency is observed for the low viscosity sodium alginate (54 000 $g.mol^{-1}$) but with higher DM values. Decreasing the molecular weight of alginate will increase the number of hydroxyl groups present at the chain ends providing more reactive sites for the methacrylation and allowing for a lower viscosity of the reaction medium, thus favoring a more homogeneous methacrylation.

3.2. Photo-crosslinking of methacrylated alginate

Alginate-based hydrogels are commonly obtained *via* the physical crosslinking of the polysaccharide with Ca^{2+}.[3, 25-26] These ionically crosslinked hydrogels have weak stability in physiological media, thus limiting their applications in the biomedical field.[5] Chemical crosslinking provides the formation of a stable matrix where the ionic crosslinking can be further used as a mean to tune the hydrogel's properties.

The hydrogels were prepared by photo-polymerization of the functionalized alginate in presence of lithium phenyl-2,4,6-trimethylbenzoylphosphinate (LAP) as a known cytocompatible photo-initiator under UV light.[27] The amount of LAP and irradiation time were optimized as represented in Figure II-S2-S3. Alginate with different molecular weights and various degrees of methacrylation were used in order to study the influence of these parameters. The weight percentage of Alg-MA and LAP were kept at 3% (w/v) and 3.75% (w/w) respectively. To form the crosslinked network, Alg-MA underwent free radical polymerization under UV light forming crosslinking bridges between the methacrylate groups. The resulting hydrogels showed diverse physical characteristics, from soft and elastic to hard and brittle depending on the degree of modification.

The gel content (GC), defined as the percentage of Alg-MA present in the crosslinked matrix after washing, was seen to be dependent on both the alginate molecular weight and the degree of modification. As seen in Figure II-3, an increase in the alginate molecular weight and/or the degree of crosslinking led to an increase in the gel content of the hydrogels. For example, for MVA, increasing the DM from 20 to 60% resulted in an increase of the gel content from 60 to 90%. The presence of more methacrylate moieties on the alginate backbone improved the crosslink density between the methacrylate groups. Furthermore, for LVA higher DMs are needed to achieve significant gel contents. For a 54 000 $g.mol^{-1}$ Alg-Na^{+} (LVA), at DM of 90%,

the GC is around 70%, compared to Alg-Na^+ of 320 000 $g.mol^{-1}$ (HVA) where the GC reaches 92% for a 75% degree of modification. In fact, for high molecular weight alginates a lower degree of modification is needed for crosslinking due to the increase in chain entanglements providing additional physical crosslinking. Chain overlapping is dependent on the backbone's molecular weight (Figure II-S4, Table II-S3). Increasing the molecular weight of the Alg-Na^+ will result in a decrease of the critical overlapping concentration, facilitating the formation of a stable chemical network even with low DM's.[28]

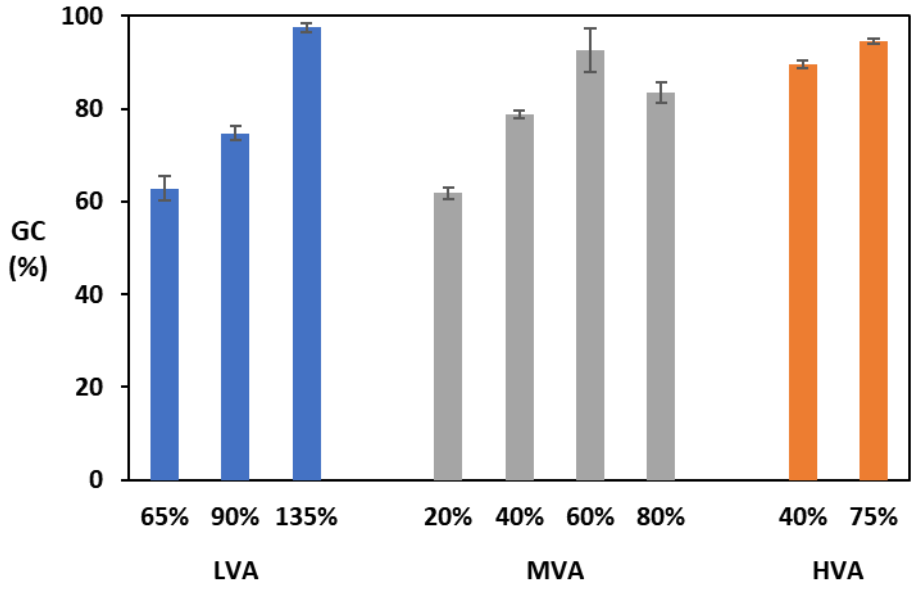

Figure II-3. Gel content of the hydrogels as function of the Alg Mw and DM.

3.3. Cyclic shape morphing of alginate hydrogels

To investigate the influence of the crosslinking density on the hydrogels swelling ability; the swelling degree of hydrogels with various methacrylated alginates were determined at different conditions. Firstly, the swelling behavior of the chemically crosslinked hydrogels was determined in water for 24 hours (the equilibrium is reached in 1 hour (Figure II-S5). Secondly, additional crosslinking was introduced to the chemically crosslinked network upon submerging the hydrogel in a $CaCl_2$ solution. Water uptake of the dual crosslinked network was then measured. The secondary ionic crosslinking is reversible upon submerging the hydrogels in an EDTA-rich solution. EDTA is a Ca^{2+} chelating molecule which extracts the calcium ions from the alginate hydrogels. To better undertand the behavior of the system in physiological conditions, the cyclic swelling was also studied between PBS and a 10 % (w/v) aqueous solution

of $CaCl_2$. PBS also plays the role of a calcium decomplexing agent due to the Na^+ - Ca^{2+} ion exchange.[29]

As seen in Figure II-5, upon submerging the chemically crosslinked hydrogels in water significantly different swelling degrees are observed. Both the DM and the alginate molecular weight directly influence the swelling degree. In water, an increase of the DM will decrease the water uptake due to a higher degree of crosslinking. For example, increasing the DM of MVA (170 000 $g.mol^{-1}$) from 40 to 80% decreases the swelling ratio from 160 to 50. Moreover, for LVA (54 000 $g.mol^{-1}$), higher degrees of crosslinking are needed to significantly modify the swelling behavior. An increase of the DM from 55% to 140% leads to a decrease of the water uptake from 115 to 30. For similar degrees of methacrylation, increasing the sodium alginate molecular weights yields lower swelling degrees which can be explained by further chain entanglements with longer polysaccharide chains. For instance, LVA60 has a 130 swelling degree which is significantly higher than 80 for MVA60. This influence of the degree of methacrylation and the alginate molecular weight on the hydrogel matrix is also confirmed by comparing the mesh sizes by rheology (Table II-S5). The same tendency is observed for HVA (320 000 $g.mol^{-1}$) hydrogels, however hydrogels with lower DM were too fragile to be handled. The same correlation between the DM and alginate -molecular weight is observed in PBS. It is important to note that the swelling capacity in PBS is lower than in water due to the higher ionic strength of the solution.[30-32] In the presence of salt rich media, the negatively charged alginate backbone interacts with the positively charged counterions limiting the repulsion force between the negatively charged carboxylic groups thus leading to lower swelling degrees.

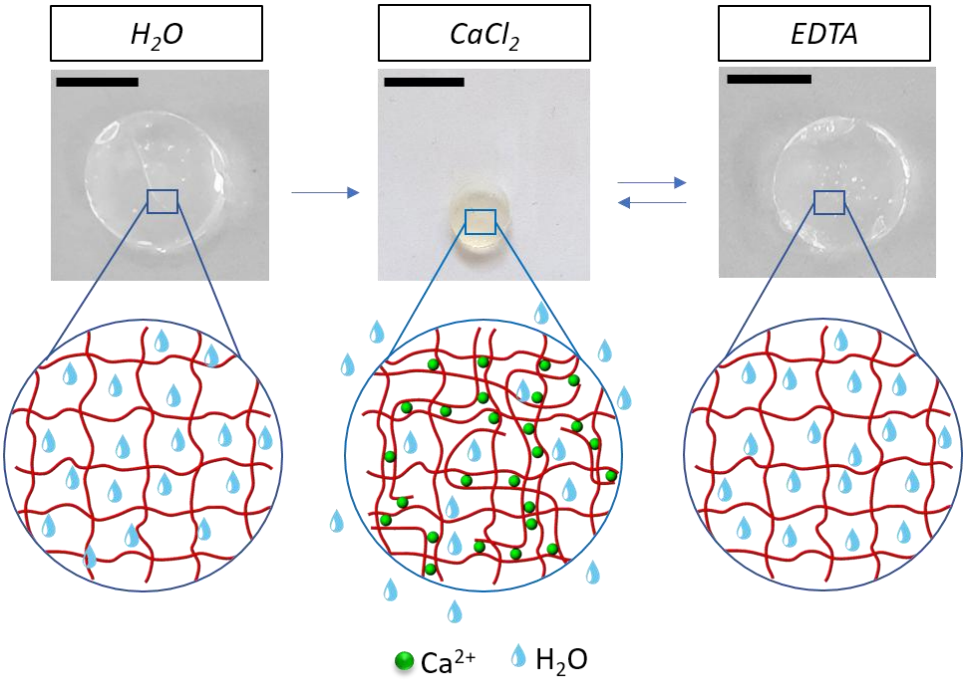

Figure II-4. Pictures and illustrations of the cycling shape morphing of MVA40 in water.

The secondary crosslinking was introduced into the matrix after immersing the swollen hydrogels in a $CaCl_2$ solution where the swelling degree drastically drops. When the hydrogels are surrounded by Ca^{2+} rich solution, the calcium will diffuse inside the hydrogel's matrix and will coordinate between the free carboxylic acids of guluronate moieties bringing the chains closer to each other. This secondary crosslinking expels the water from the matrix as illustrated in Figure II-4 by the shrinking the hydrogels by more than two times their original dimensions. For LVA (54 000 $g.mol^{-1}$) the swelling degree decreases from 120 to 50 and from 45 to 10 for a DM of 60% and 90% respectively, upon the addition of the secondary crosslinking as shown in Figure II-5a.

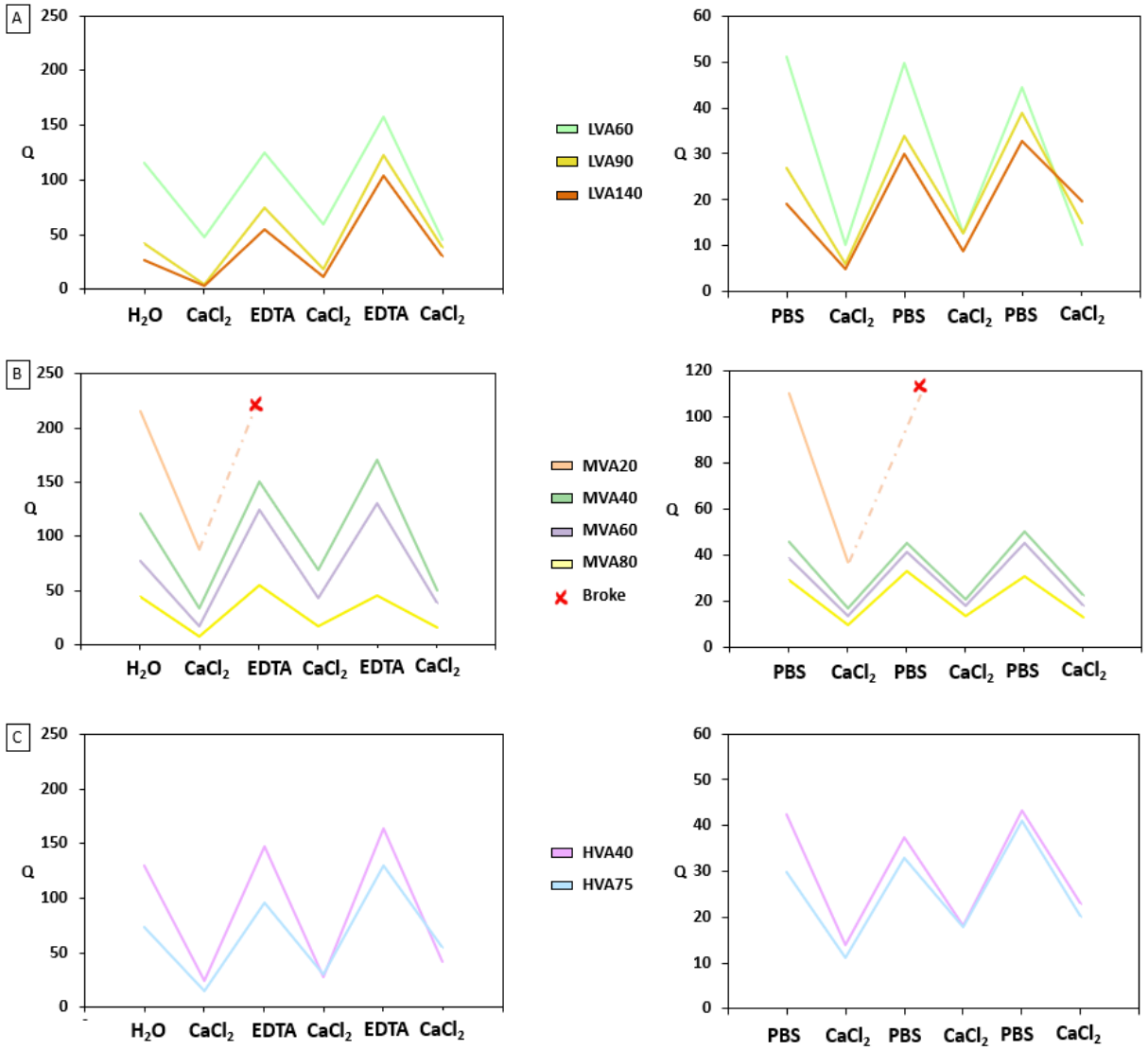

Figure II-5. Cyclic swelling behavior of a) LVA b) MVA and c) HVA alginate hydrogels in water and PBS. The standard deviation (n=5) was found to be between 10 and 20%. The error bars are not shown on the figures to avoid their superposition and maintain a clear reading.

The secondary physical crosslinking is reversible in the presence of EDTA as seen in Figure II-5. As EDTA has a stronger affinity for the calcium than sodium alginate, calcium ions will be extracted from the dual-crosslinking hydrogels reversing the physical crosslinking. This will allow water to re-diffuse into the hydrogels that can regain their initial swelling degree and shape. The swelling/shrinking behavior was reversible for at least 3 cycles despite a slight increase in the swelling over the cycles. This is explained in the literature by the cyclic-induced stress resulting from cycling between relaxation and contraction states.[33-34]

3.4. Influence of dual crosslinking on the mechanical properties

One of the main advantages of chemically crosslinked networks is the ability to tune the mechanical properties by modifying the degree of crosslinking.[35] As previously seen, the swelling behavior is directly affected by the DM. The same correlation can be extrapolated to the mechanical properties. The mechanical behavior of the hydrogels was studied by compression tests and rheological characterization.

By increasing the degree of methacrylation from 60 % to 140% for LVA (54 000 $g.mol^{-1}$), the compression modulus in water increases from 0.047 to 0.524 MPa respectively. The storage modulus G' also increases from 1 kPa to 95 kPa respectively. This increase is due to the higher degree of crosslinking forming a tighter network as correlated with the decrease of the water uptake. The same tendency is observed for the MVA (170 000 $g.mol^{-1}$) and HVA (320 000 $g.mol^{-1}$) hydrogels (Figure II-6). The impact of chain entanglements can also be seen in the mechanical properties, where the compression modulus of HVA75 hydrogel is higher than for LVA90. Increased chain entanglement adds additional interactions between the chains, contributing to an enhancement in the mechanical properties. Hence, the mechanical properties of the hydrogels can be tuned by either modifying the degree of methacrylation or the molecular weight of the alginate. Furthermore, the introduction of a secondary crosslinking by calcium ions significantly improves the compression modulus by up to 100 times resulting from a much denser network as seen for the compression modulus of MVA40 wich increases from 0.004 MPa to 2.5 MPa. The improvement is also seen for the other hydrogels when having dual-crosslinked hydrogels. Analysis of Table II-1 reveals that the storage and loss modulus of various alginates exhibit negligible changes over the course of the study, except for the low crosslinked networks of LVA60 and MVA20, where rheological values are markedly lower compared to the others. This distinct behavior is also evident in the swelling study, with LVA60 and MVA20 showing significantly higher swelling ratios in water (Figure II-5). Conversely, the other degrees of methacrylation display relatively minor differences in the swelling ratio among them. Similarly to the compression measurements, dual-crosslinked hydrogels exhibit significantly higher storage and loss modulus compared to their simple-photocrosslinked counterparts. Additionally, tan δ indicates higher dissipation for the dual-crosslinked systems.

Finally, upon extracting calcium ions from the system with EDTA, the compression modulus decreases as the hydrogels re-swells. The reversibility of the reinforcement of the mechanical

properties by the addition of calcium ions was also observed for the hydrogels previously swollen in PBS.

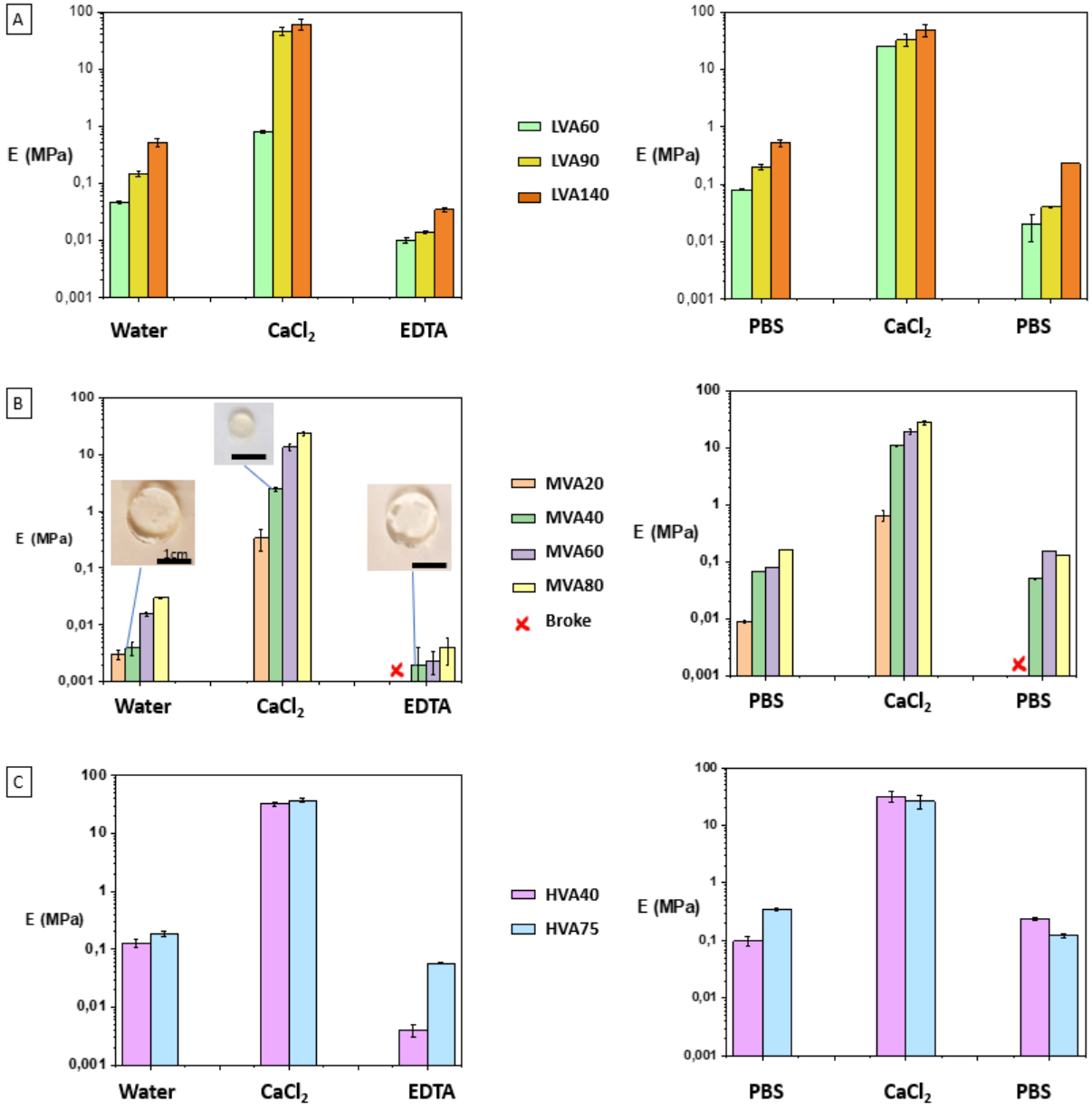

Figure II-6. Compression modulus A) LVA B) MVA and C) HVA alginate hydrogels in water and PBS at different points of the cycling swelling.

Table II-1. Storage modulus, loss modulus and tan δ of LV, MV and HV hydrogels at different swelling states.

		Water			**$CaCl_2$**			**PBS**			**$CaCl_2$**		
	DM (%)	G' (kPa)	G" (kPa)	tan δ	G' (kPa)	G" (kPa)	tan δ	G' (kPa)	G" (kPa)	tan δ	G' (kPa)	G" (kPa)	tan δ
LVA	**60**	1.05	0.086	0.08	10.60	6.39	0.60	1.66	0.10	0.06	94.92	24.86	0.26
	90	43.6	3.05	0.07	69.0	17.7	0.26	23.05	1.38	0.06	33.1	8.18	0.25
	140	95.22	6.73	0.07	72.0	10.06	0.14	45.96	1.83	0.04	85.92	1.63	0.19
MVA	**20**	1.33	0.18	0.14	23.1	3.74	0.16	1.08	0.12	0.11	38.93	9.93	0.26
	40	41.15	3.82	0.09	111.24	31.5	0.28	4.09	0.12	0.03	61.25	15.98	0.26
	60	57.06	4.11	0.07	175.88	44.29	0.25	12.47	0.37	0.03	172.99	51.76	0.3
	80	64.17	5.78	0.09	187.53	51.65	0.26	18.44	0.38	0.02	230.62	52.78	0.23
HVA	**40**	21.83	1.64	0.08	15.30	4.84	0.32	6.78	0.38	0.06	49.24	14.98	0.31
	75	35.6	2.04	0.057	18.24	2.85	0.16	9.91	0.31	0.03	82.43	30.12	0.37

3.5. Ion induced hydrogel repair

In addition to shape and mechanical properties modifications, this study showed that controlling dual crosslinking can also be used to induce healing/auto assembly behavior of the hydrogels. Physical crosslinking can be used as a tool to repair/adhere hydrogels together.[36-37] By simply cutting the hydrogel MVA60 and rearranging the pieces to the desired architecture, the addition of a $CaCl_2$ solution at the interface of the two pieces can induce complexation at the interface thereby facilitating hydrogel repair (Figure II-7a). Four cylindrical hydrogels were cut and the pieces were rearranged to obtain a snake-like structure and subsequently "healed" with the addition of a $CaCl_2$ solution at the interface of the pieces. However, it was observed that the healed interface of the hydrogel is stable up until a certain threshold of water uptake and tends to dissociate past this threshold certainly due to the increased stress induced by the water uptake and associated swelling. In addition, it was also observed that the induced hydrogel repair is more efficient at lower initial water uptake ratios. In a reduced swollen state, the polymer chains are closer to each other which facilitates the coordination between two separate carboxylic groups of two different chains. The limiting swelling degree above which the induced healing does not work anymore was found to be around 30 across all samples. This can be used as a tool to control the release of parts of the hydrogel in order to control its shape

throughout time. To evaluate the efficiency of the induced hydrogel repair, tensile testing was done on a water swollen native sample and an identical sample which was cut in half and then repaired with a $CaCl_2$ solution as observed in Figure II-7b. The sample that underwent the ion induced hydrogel repair demonstrates slightly improved mechanical properties. In fact, Young's modulus increased from 0.27 MPa to 0.87 MPa for the native and the healed sample respectively. Moreover, the stress at break increased by almost 30% for the healed sample compared to the native one. This improvement of the mechanical properties is explained by the localized dual-crosslinking around the healed area. The calcium ions diffuse in the targeted area creating a localized improvement in the mechanical properties which is reflected in testing of the whole sample.

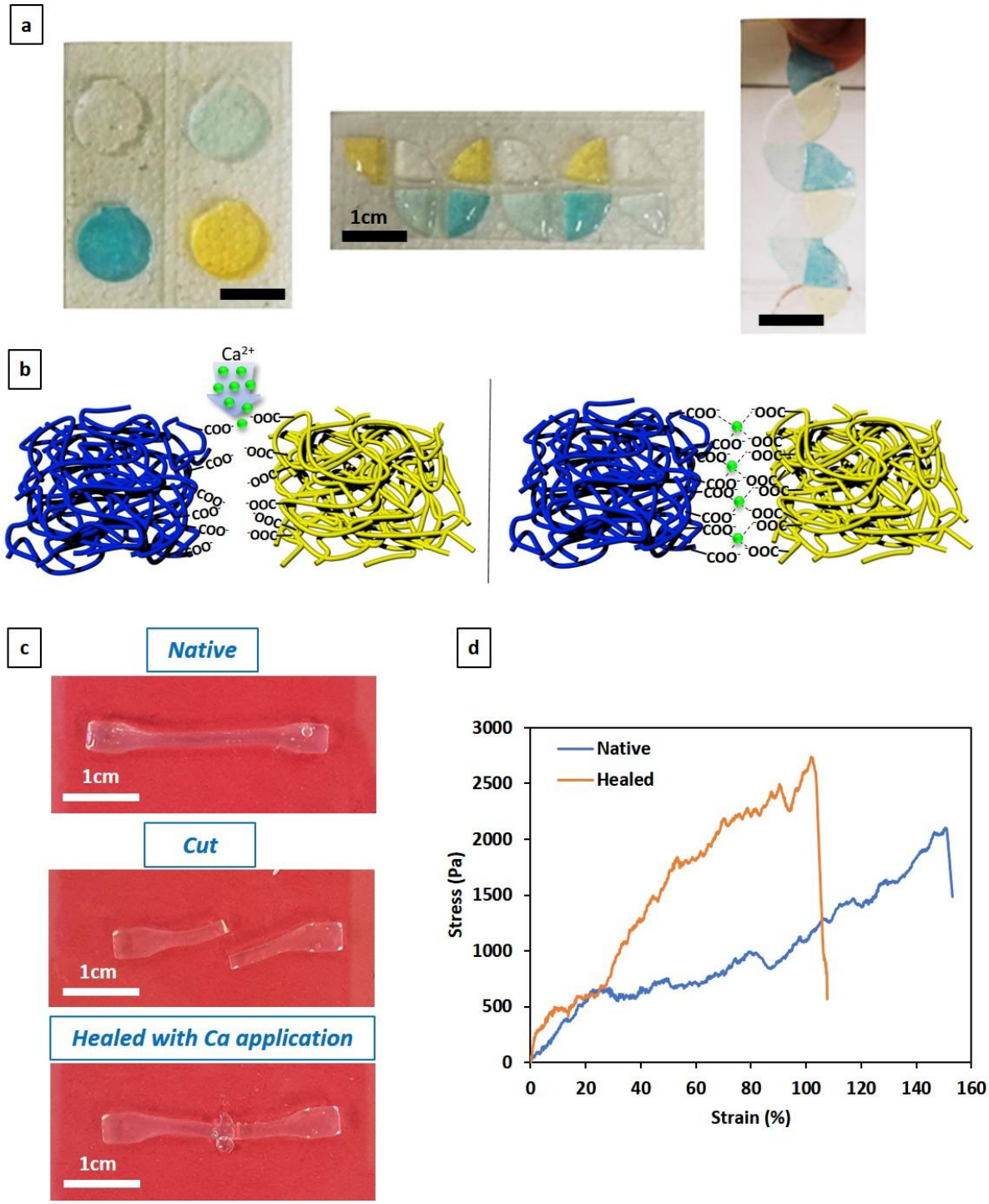

Figure II-7. a) Pictures of the nduced hydrogel repair used to transform MVA60 hydrogels from disk-shape structures to a snake-like architecture and b) schematic illustration of the ionic repairing surface to srface, c) tensile testing sample repaired by calcium application, and d) evaluation of the induced healing efficency by tensile testing.

3.6. Controlled dual crosslinking as an actuating mechanism

Hydrogel actuators have the ability to change shape in aqueous media.[38-39] They are mainly built by combining one layer with a high swelling degree with another showing little to no volume change. The anisotropic swelling behavior in the bilayer system creates mechanical stresses at the interface of the layers forcing the system to bend. Bilayer hydrogel actuators are limited by the stability of the adhesion between the two layers. Stable systems can be obtained by a two steps polymerization where one layer is cured on top of the other, phase separation or the use of glue.[40-42] For each method, the chemistry of each layer should be carefully selected to ensure a strong interpenetrating network which brings certain limitations in the design. Herein, we used calcium diffusion as a mean to prepare alginate actuators creating a gradient of dual-crosslinking with a calcium rich phase and a calcium poor/free phase. The described system is obtained via a simple one step preparation without any risk of delamination as the preparation does not involve the bilayer systems as described in the literature.[43-44] For instance, Kirillova et al. reported self-folding alginate films through direct ink writing printing process creating a bilayer system.[45] They also obtained self-folding films with modified hyaluronic acid where the actuating mechanism is more related to the hydrogel film preparation process than to the exploitation of the crosslinking chemistry.

Here we leverage the significant difference in the swelling degree between the simple chemically crosslinked alginate network and the dual-crosslinked one as a mean to induce shape deformation. A dual-crosslinking gradient was obtained by the calcium diffusion from the top surface of the hydrogel films. Contrary to bilayer systems, there is no risk of delamination with this strategy to induce a swelling gradient. Different self-folding actuators were obtained using LVA90 by varying the thickness of the hydrogel film (0.5 mm, 0.7 mm and 1 mm) and maintaining the same calcium diffusion time. The diffusion time was fixed at 5 seconds using a wetted filter paper with a 5% (w/v) $CaCl_2$ solution to obtain a dual-crosslinking gradient. It was noticed that more than 5 seconds resulted in the full dual crosslinking of the hydrogels where no shape deformation was observed. The dual-crosslinking gradient across the hydrogel creates an anisotropic swelling degree in the hydrogels resulting in the bending of the system towards the denser dual-crosslinked section. As illustrated in Figure II-8, upon submerging in water, several tube diameters can be obtained ranging from 2.7 mm to 5.5 mm, by simply increasing the thickness of the hydrogel. The correlation between the thickness of the hydrogel and the radius of curvature was confirmed by Timoshenko's formula that simulates the deformation of bilayer thermostats or bilayer hydrogels (Figure II-S5).[46-47]

Furthermore, complex shape deformations can be obtained by patterning the hydrogels.[48] Patterning creates local anisotropic swelling degrees which can result in more complex shape transformations such as induced rolling, twisting or curling deformations based on the pattern's direction on a PNIPAM/PAAc bilayer systems as reported by Shang *et al*. By locally patterning the hydrogel with Ca^{2+} to achieve dual-crosslinked alternating regions, specific deformations can be induced. For instance, when creating alternating sections between dual crosslinked and simple chemically crosslinked regions in a 45° pattern, a helical deformation is observed. Conversely, the same alternating sections in a 90° pattern results in a tubular shape-like deformation, as depicted in Figure II-8. This distinctive behavior arises from the orientation of the resulting stress during swelling.

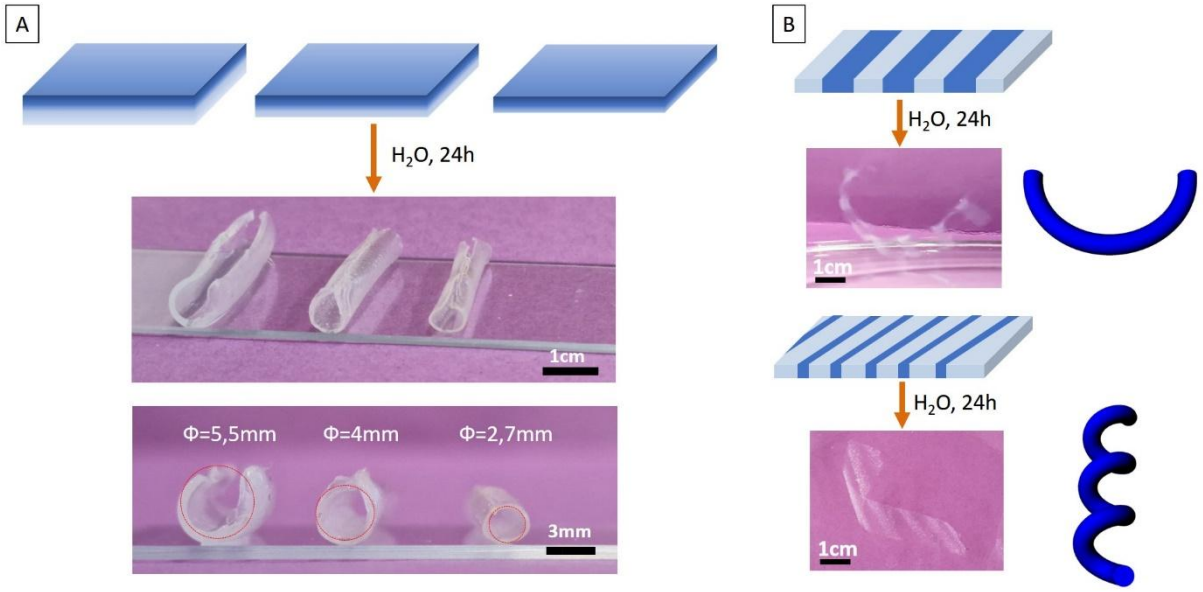

Figure II-8. LVA90 hydrogel actuators obtained by A) gradient dual-crosslinking (film thickness 1 mm, 0.7 mm, 0.5 mm from left to right) and B) patterned dual-crosslinking representing curving and helicoidal actuation. The shade blue represents the dual crosslinking.

4. CONCLUSION

In this study, the structure-property relationship of modified alginate hydrogels under ionic stimulation was investigated. Alginate hydrogels were obtained by chemically modifying sodium alginate with methacrylic anhydride in the presence of TEA under mild conditions. The reaction was optimized to obtain various degrees of methacrylation for sodium alginate of different molecular weights (LVA; MVA and HVA). By modifying the amount of added MA, several DM were obtained up to 140%, 80% and 75% for LVA (54 000 $g.mol^{-1}$), MVA (170 000

$g.mol^{-1}$) and HVA (320 000 $g.mol^{-1}$) respectively. Hydrogels were then obtained by photo crosslinking in the presence of LAP as photo-initiator under UV light. The water uptake and compression modulus were seen to be directly influenced by the DM. Increasing the DM resulted in a higher degree of crosslinking leading to a lower swelling degree and a higher compression modulus. In addition, increasing the molecular mass of the alginate backbone will reinforce the mechanical properties due to higher chain overlapping. The addition of secondary crosslinking was then thoroughly investigated as a tool to tune the swelling, the water uptake and the mechanical properties. Additionally, this study demonstrated the use of this secondary crosslinking as a mean to allow healing as well as shape deformation of previously chemically crosslinked alginate hydrogels. Several self-folding actuators were built to obtain tubes with different diameters when modifying the thickness of the hydrogels. Moreover, complex architecture such as helices can be obtained by patterning the hydrogels at a specific angle. This study contributes to the understanding of the structural properties of the alginate hydrogels gels and stimulated changes through the control of dual crosslinking. This is an interesting strategy to induce stimuli-responsive behaviors for smart hydrogels such as a bioinks for 4D printing processes.

Supplementary Information Chapter II

Dual Cross-Linked Stimuli-Responsive Alginate-Based Hydrogels

Polysaccharide Characterization

G/M composition

The guluronic content of each sample was determined using ^{1}H-NMR, 400MHz. In order to obtain a more detailed NMR spectra, the sodium alginates were depolymerized in the presence of hydrogen peroxide following the procedure described by Mao et al.[49] Briefly, a 2% (w/v) Alg-Na^{+} solution was prepared to which H_2O_2 was added to a final concentration of 3% (w/w). The solutions were magnetically stirred at 600 rpm under a hood at 25°C for 2 hours. The alginate was precipitated in acetone and dried under reduced pressure overnight.

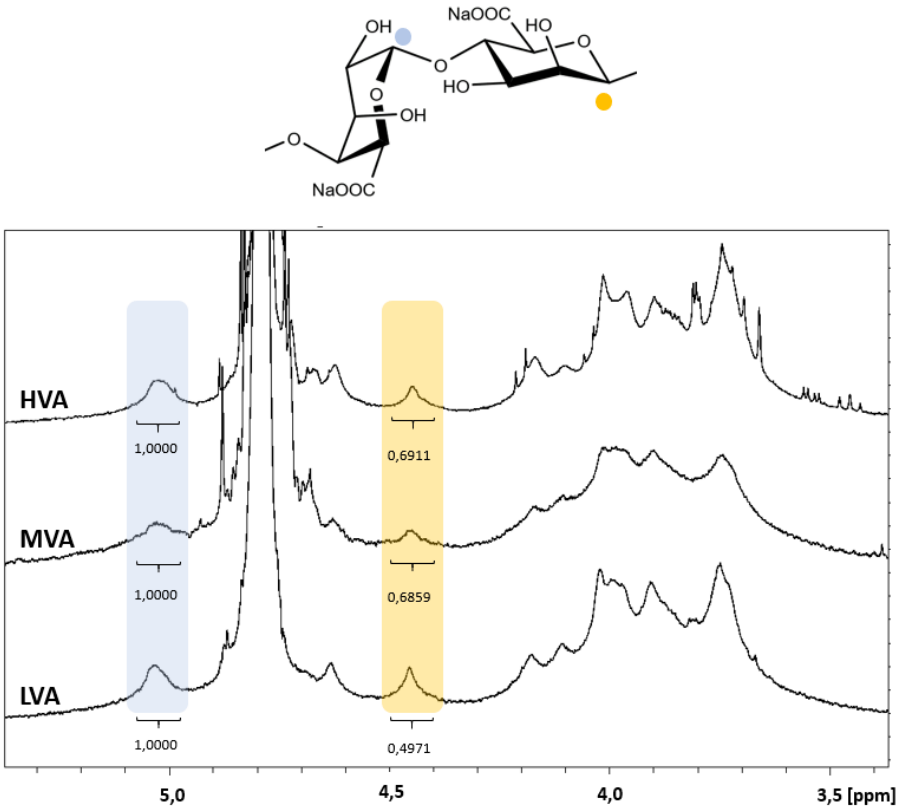

Figure II-S1. ^{1}H NMR spectra of sodium alginate LVA, MVA and HVA in D_2O, 5s relaxation time and 120 scans.

The percentage of guluronate units was determined by comparing the integral of H_G peaks at 5.1 ppm to the H_M at 4.45 ppm as illustrated in Figure II-S1. The G% was calculated according to equation II-S1 and the results are summarized in Table II-S1.

Table II-S1. Guluronic percentage in LVA, MVA and HVA

$$G\% = 100 * \frac{I_{H_G}}{I_{H_G} + I_{H_M}} \quad \text{(Equation II-S1)}$$

	M_w g/mol	**G%**
LVA	55 000	65
MVA	170 000	60
HVA	320 000	60

Molecular Weight

The average number molecular weight of each sodium alginate was calculated from the hydrodynamic radius obtained by Taylor Dispersion Analysis (TDA). The analysis was performed with solutions at a concentration of 2 g/L in PBS 10 mM (pH = 7.6) under the following experimental conditions: Agilent 7100 capillary electrophoresis equipment, hydrodynamic injection at 50 mbar, injection time of 6s, mobilization pressure at 30 mbar, and UV detection at a wavelength of 200 nm.

Table II-S2. The number average molecular weight (Mn), weight average molecular weight (Mw) and the polydispersity index (PDI) of the low, medium and high molecular weight Alg-Na^+.

Alg-Na^+		**Mn g/mol**	**Mw g/mol**	***Đ***
Low viscosity (LV)	Native	53 000	66 000	1.25
	DM90	55 000	66 000	1.20
Medium viscosity (MV)	Native	178 000	183 000	1.03
	DM40	151 000	156 000	1.03
High viscosity (HV)	Native	314 000	320 000	1.02
	DM40	267 000	270 000	1.01

Hydrogel Optimization process

The amount of LAP and irradiation time were optimized on the MVA40 samples by following the volumetric change the hydrogel. LAP concentration was increased with a fixed irradiation time of 10 minutes. Figure II-S2 illustrates that the increase in LAP results in a decrease in the volume expansion. This is attributed to a higher crosslinking degree thus limiting water uptake. For subsequent studies, the initiator content was set at 3.75 % (w/w) relative to the polymer. This value represents the midpoint of the plateau observed between 2 and 5.5 % (w/w).

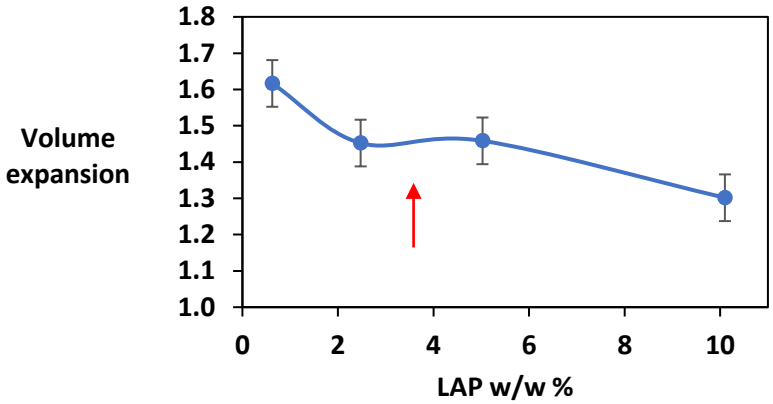

Figure II-S2. Influence of the photoinitiator amount on the expansion of the MVA40 hydrogels with a fixed time of 10 minutes irradiation.

After fixing the amount of the photoinitiator, the irradiation time was optimized by following the gel content of the MVA40 hydrogel under the following conditions: 365nm UV light wavelength with a constant light intensity of 2-3 mW/cm^2 as set by the UV chamber. As illustrated in Figure II-S3, the highest gel content was achieved after 20 minutes of irradiation. Therefore, a LAP concentration 3.75% (w/w) and a 20-minute irradiation time was used for all hydrogel precursor resins.

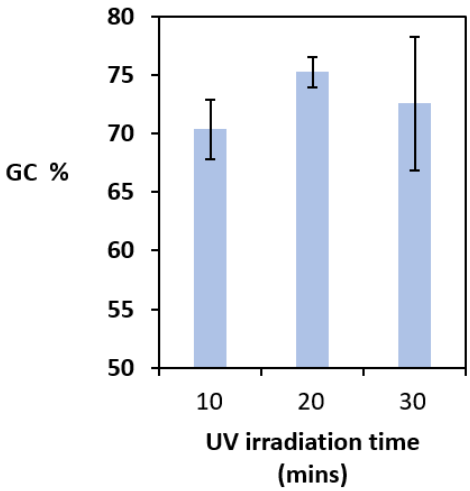

Figure II-S3. Gel content as function of a 365 nm UV irradiation time for MVA40 hydrogels.

Critical Entanglement Concentration

Viscosity measurements were conducted using a Thermo Fisher HAAKE MARS 60 rheometer with a cone-plate geometry (angle 2°, diameter 3.5 cm, and truncation length of 100 μm).

The critical entanglement concentration (CEC) was determined as the cross-section point (slope change) identified through successive dilutions from relatively high concentrations, associated with viscous solutions, confirming that the system was above the CEC. The CEC values were found to be 2% for LVA, 1% for MVA, and 0.1% for HVA.

The specific viscosity was calculated using Equation II-S2 based on the viscosities obtained through rheological measurements at infinite shear rate[28]. This value corresponds to the point where the viscosity reaches a constant value, as illustrated for HVA in Figure S4b.

$$\eta_{sp} = \frac{\eta_{\infty}}{\eta_{water}} - 1 \qquad \text{(Equation II-S2)}$$

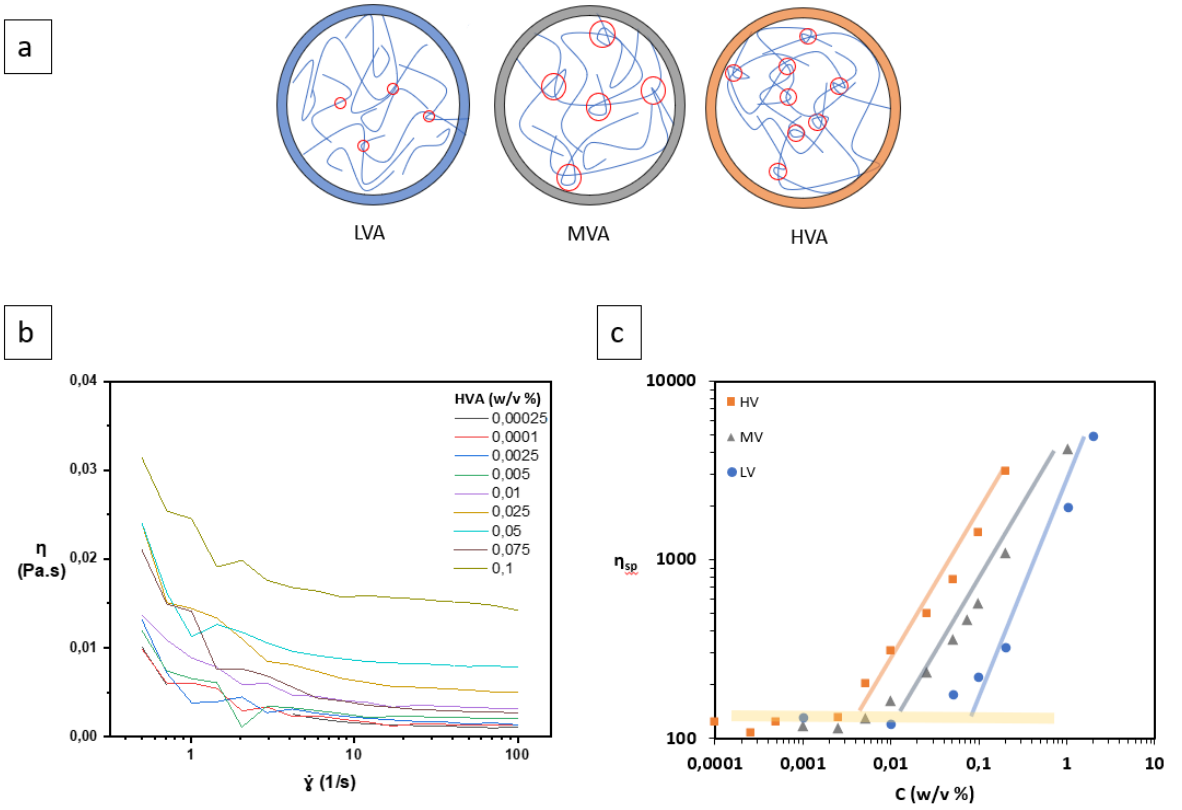

Figure II-S4. a) Schematic representation of the physical entanglements (red circles) in LVA, MVA and HVA matrix, b) dynamic viscosity of HVA at different concentrations with increasing shear rate and c) specific viscosity measurement at the plateau for high shear rate for LVA, MVA and HVA.

Table II-S3. Critical entanglement concentration for LVA, MVA and HVA.

Alg	CEC (w/v%)
LVA	0,09
MVA	0,011
HVA	0,005

Swelling kinetics

The swelling kinetics were investigated by measuring the hydrogel weight gain in water from the dry state weight. The swelling profiles of the different hydrogels are depicted in Figure II-S5.

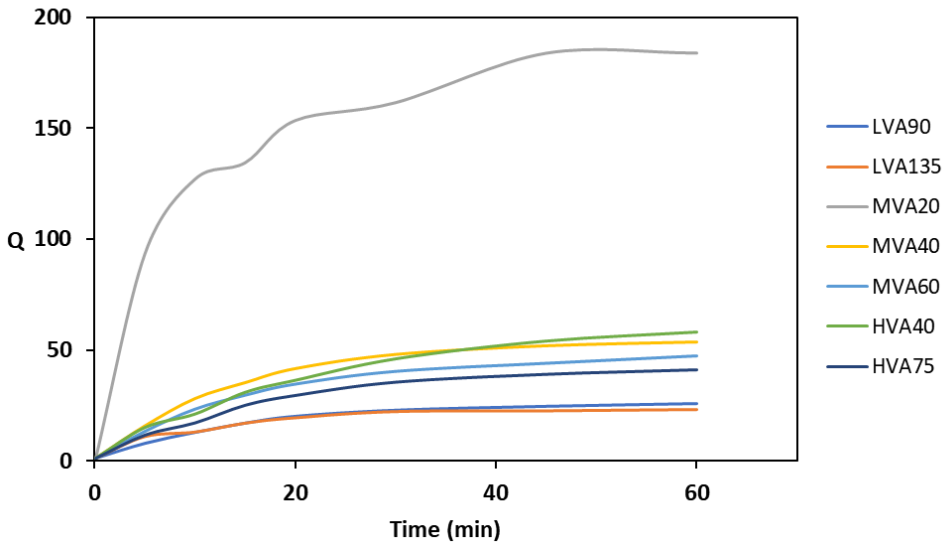

Figure II-S5. Swelling kinetics for LVA, MVA and HVA hydrogels in water.

From the swelling kinetics, the water diffusion coefficient could be deduced using Fickian's equation II-S3; where *t* is the time, m_t is the weight of the hydrogel at a time *t*, m_∞ is the weight of the hydrogel at equilibrium, *k* is the characteristic constant of the hydrogel and n the constant describing the water diffusion mechanism.[30,50]

$$\frac{m_t}{m_\infty} = k * t^n \qquad \text{(Equation II-S3)}$$

The diffusion coefficients D, as reported in Table II-S4, can then be deduced using equation II-S4, where *a* is the initial diameter of the sample, which is valid for the first 20% of total swelling for cylindrical samples.

$$k = 4 * \left(\frac{D}{\pi * a^2}\right)^{0,5}$$ (Equation II-S4)

Table II-S4. Water diffusion coefficient in LVA, MVA and HVA hydrogels.

Alginate	DM (%)	Diffusion Coefficient (m/s)
LVA	90	6,4E-16
	135	8,7E-16
MVA	20	1,4E-15
	40	6,4E-16
	60	6,3E-16
HVA	40	4,3E-16
	75	5,4E-16

Rheology

The linear viscoelastic domain was determined through frequency and deformation sweeps on LVA60 (Figure II-S6a, b, and c). The conditions were kept constant at 5% deformation, and the frequency sweep ranged from 1 to 10 rad/s, as illustrated for HVA75 (Figure II-S6d).

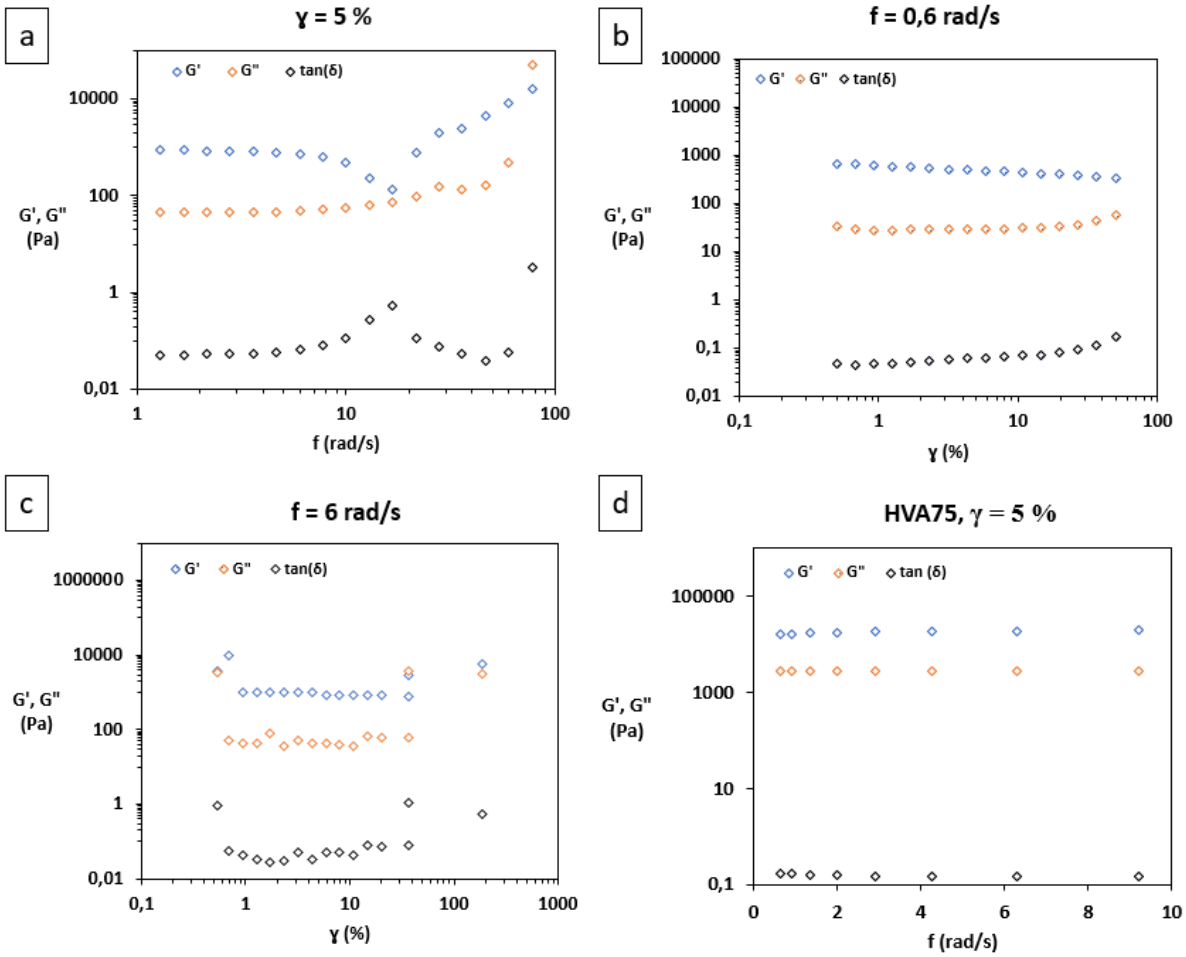

Figure II-S6. a) Frequency sweep at 5% deformation, b) Deformation sweep at 0.6 rad/s frequency, c) Deformation sweep at 6 rad/s for LVA60, and d) Frequency sweep for HVA75 at 5% deformation.

Cross-linking density was evaluated by calculating the specific volume of the mesh using equation II-S5:[12,51]

$$\vartheta_e = \frac{G' * N_A}{R * T} \qquad \text{(Equation II-S5)}$$

Where ϑ_e is the specific volume of the mesh in m^{-3}, G' is the storage modulus in the linear regime in Pa, N_A is the Avogadro's number, R is the gas constant and T is the temperature at which G' was measured (298 K). Mesh size (Mc) in nm was calculated (Equation II-S6) from the specific volume assuming a cubic unit between the crosslinking point.

$$Mc = \sqrt[3]{\vartheta_e} * 10^9 \qquad \text{(Equation II-S6)}$$

The results are shown in table II-S5.

Table II-S5. Specific volume between the crosslinking points and mesh size of the different hydrogels at equilibrium in water.

	DM (%)	ϑ_e x 10^{24} (m^{-3})	Mc (nm)
LVA	65	0,2	16,4
	90	9,5	4,7
	140	20,7	3,6
MVA	20	0,3	15,2
	40	8,9	4,8
	60	12,4	4,3
	80	13,5	4,2
HVA	40	4,7	6,0
	75	7,7	5,1

Curvature prediction for bilayer systems

The radius of curvature for bilayer systems can be predicted using the simplified Timoshenko's equation (equation II-S7).[46] Where ρ is the radius of curvature, Δα is the difference of expansion between the layers, m is the ratio between the thicknesses of layer 1 to layer 2, h is the total thickness of the sample and n the ratio of the Young's modulus of layer 1 to layer 2.

$$\frac{1}{\rho} = \frac{24\,(\Delta\alpha)(1+m)^2}{h\,(3(1+m)^2+(1+mn)(m^2+\frac{1}{mn}))} \qquad \text{(Equation II-S7)}$$

In order to correlate the deformation tendency of the crosslinking gradient created in the hydrogel films, the system can be represented as a bilayer system where the thickness of the first dual crosslinked layer is fixed given that calcium ions were allowed to diffuse for the same duration for all hydrogels and the thickness of the chemically crosslinked layer (layer 2) is varied. The correlation between the radius of curvature and the thickness of layer 2 for a fixed layer 1 is represented in Figure II-S6.

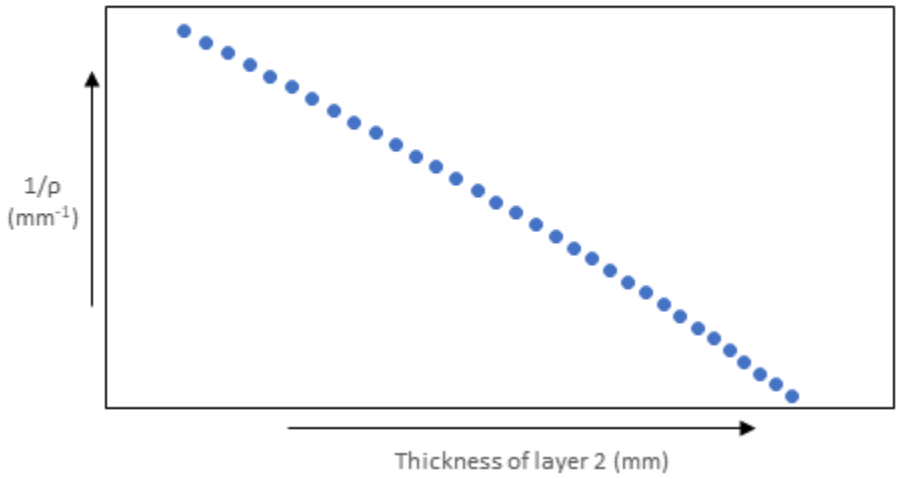

Figure II-S7. Influence of the thickness of layer 2 on the radius of curvature for a fixed layer 1.

REFERENCES

1. Luo, M. C.; Zhang, X. Y.; Wu, J.; Zhao, J. M., Modifications of polysaccharide-based biomaterials under structure-property relationship for biomedical applications. *Carbohyd Polym* **2021,** *266*, 118097.

2. Gamella, M.; Privman, M.; Bakshi, S.; Melman, A.; Katz, E., DNA Release from Fe-Cross-Linked Alginate Films Triggered by Logically Processed Biomolecular Signals: Integration of Biomolecular Computing and Actuation. *Chemphyschem* **2017,** *18* (13), 1811-1821.

3. Ouwerx, C.; Velings, N.; Mestdagh, M. M.; Axelos, M. A. V., Physico-chemical properties and rheology of alginate gel beads formed with various divalent cations. *Polym Gels Netw* **1998,** *6* (5), 393-408.

4. Scheja, S.; Domanskyi, S.; Gamella, M.; Wormwood, K. L.; Darie, C. C.; Poghossian, A.; Schöning, M. J.; Melman, A.; Privman, V.; Katz, E., Glucose-Triggered Insulin Release from Fe-Cross-linked Alginate Hydrogel: Experimental Study and Theoretical Modeling. *Chemphyschem* **2017,** *18* (12), 1541-1551.

5. Lee, K. Y.; Mooney, D. J., Alginate: Properties and biomedical applications. *Prog Polym Sci* **2012,** *37* (1), 106-126.

6. Li, S. J.; Xiong, Q. P.; Lai, X. P.; Li, X.; Wan, M.; Zhang, J. N.; Yan, Y. J.; Cao, M.; Lu, L.; Guan, J. M.; Zhang, D. Y.; Lin, Y., Molecular Modification of Polysaccharides and Resulting Bioactivities. *Compr Rev Food Sci F* **2016,** *15* (2), 237-250.

7. Jeon, O.; Bouhadir, K. H.; Mansour, J. M.; Alsberg, E., Photocrosslinked alginate hydrogels with tunable biodegradation rates and mechanical properties. *Biomaterials* **2009,** *30* (14), 2724-2734.

8. Hachet, E.; Van Den Berghe, H.; Bayma, E.; Block, M. R.; Auzély-Velty, R., Design of Biomimetic Cell-Interactive Substrates Using Hyaluronic Acid Hydrogels with Tunable Mechanical Properties. *Biomacromolecules* **2012,** *13* (6), 1818-1827.

9. Mihaila, S. M.; Gaharwar, A. K.; Reis, R. L.; Marques, A. P.; Gomes, M. E.; Khademhosseini, A., Photocrosslinkable Kappa-Carrageenan Hydrogels for Tissue Engineering Applications. *Adv Healthc Mater* **2013,** *2* (6), 895-907.

10. De Paepe, I.; Declercq, H.; Cornelissen, M.; Schacht, E., Novel hydrogels based on methacrylate-modified agarose. *Polym Int* **2002,** *51* (10), 867-870.

11. Sahraro, M.; Barikani, M.; Daemi, H., Mechanical reinforcement of gellan gum polyelectrolyte hydrogels by cationic polyurethane soft nanoparticles. *Carbohyd Polym* **2018,** *187*, 102-109.

12. Zanon, M.; Chiappone, A.; Garino, N.; Canta, M.; Frascella, F.; Hakkarainen, M.; Pirri, C. F.; Sangermano, M., Microwave-assisted methacrylation of chitosan for 3D printable hydrogels in tissue engineering. *Mater Adv* **2022,** *3* (1), 514-525.

13. Samorezov, J. E.; Morlock, C. M.; Alsberg, E., Dual Ionic and Photo-Crosslinked Alginate Hydrogels for Micropatterned Spatial Control of Material Properties and Cell Behavior. *Bioconjugate Chem* **2015,** *26* (7), 1339-1347.

14. Fenn, S. L.; Miao, T. X.; Scherrer, R. M.; Oldinski, R. A., Dual-Cross-Linked Methacrylated Alginate Sub-Microspheres for Intracellular Chemotherapeutic Delivery. *Acs Appl Mater Inter* **2016,** *8* (28), 17775-17783.

15. Mahou, R.; Borcard, F.; Crivelli, V.; Montanari, E.; Passemard, S.; Noverraz, F.; Gerber-Lemaire, S.; Buehler, L.; Wandrey, C., Tuning the Properties of Hydrogel Microspheres by Adding Chemical Cross-linking Functionality to Sodium Alginate. *Chem Mater* **2015,** *27* (12), 4380-4389.

16. Kim, E.; Kim, M. H.; Song, J. H.; Kang, C.; Park, W. H., Dual crosslinked alginate hydrogels by riboflavin as photoinitiator. *Int J Biol Macromol* **2020,** *154*, 989-998.

17. Gao, Y. J.; Jin, X. Y., Dual Crosslinked Methacrylated Alginate Hydrogel Micron Fibers and Tissue Constructs for Cell Biology. *Mar Drugs* **2019,** *17* (10), 557.

18. Tahir, I.; Floreani, R., Dual-Crosslinked Alginate-Based Hydrogels with Tunable Mechanical Properties for Cultured Meat. *Foods* **2022,** *11* (18), 2829.

19. Majima, T.; Schnabel, W.; Weber, W., Phenyl-2,4,6-Trimethylbenzoylphosphinates as Water-Soluble Photoinitiators - Generation and Reactivity of O=P(C6h5)(O-) Radical-Anions. *Makromol Chem* **1991,** *192* (10), 2307-2315.

20. Jalil, A.; Khan, S.; Naeem, F.; Haider, M. S.; Sarwar, S.; Riaz, A.; Ranjha, N. M., The structural, morphological and thermal properties of grafted pH-sensitive interpenetrating highly porous polymeric composites of sodium alginate/acrylic acid copolymers for controlled delivery of diclofenac potassium. *Des Monomers Polym* **2017,** *20*, 308-324.

21. Ilhan, G. T.; Irmak, G.; Gümüsderelioglu, M., Microwave assisted methacrylation of

carrageenan: A bioink for cartilage tissue engineering. *Int J Biol Macromol* **2020,** *164*, 3523-3534.

22. Schweiger, R. G., Acetylation of Alginic Acid .1. Preparation and Viscosities of Algin Acetates. *J Org Chem* **1962,** *27* (5), 1786-1789.

23. Cooper, W. C.; Chilukoorie, A.; Polam, S.; Scott, D.; Wiseman, F., A comparative study on the hydrolysis of acetic anhydride and N,N-dimethylformamide: Kinetic isotope effect, transition-state structure, polarity, and solvent effect. *J Phys Org Chem* **2017,** *30* (12), e3701.

24. Gerola, A. P.; Silva, D. C.; Matsushita, A. F. Y.; Borges, O.; Rubira, A. F.; Muniz, E. C.; Valente, A. J. M., The effect of methacrylation on the behavior of Gum Arabic as pH-responsive matrix for colon-specific drug delivery. *Eur Polym J* **2016,** *78*, 326-339.

25. Gao, X. P.; Zhang, Y.; Zhao, Y. M., Zinc oxide templating of porous alginate beads for the recovery of gold ions. *Carbohyd Polym* **2018,** *200*, 297-304.

26. Kuo, C. K.; Ma, P. X., Maintaining dimensions and mechanical properties of ionically crosslinked alginate hydrogel scaffolds. *J Biomed Mater Res A* **2008,** *84a* (4), 899-907.

27. Fairbanks, B. D.; Schwartz, M. P.; Bowman, C. N.; Anseth, K. S., Photoinitiated polymerization of PEG-diacrylate with lithium phenyl-2,4,6-trimethylbenzoylphosphinate: polymerization rate and cytocompatibility. *Biomaterials* **2009,** *30* (35), 6702-6707.

28. Smidsrod, O., Solution Properties of Alginate. *Carbohyd Res* **1970,** *13* (3), 359-372.

29. Zhao, J.; Zhao, X.; Guo, B. L.; Ma, P. X., Multifunctional Interpenetrating Polymer Network Hydrogels Based on Methacrylated Alginate for the Delivery of Small Molecule Drugs and Sustained Release of Protein. *Biomacromolecules* **2014,** *15* (9), 3246-3252.

30. Bajpai, S. K.; Johnson, S., Superabsorbent hydrogels for removal of divalent toxic ions. Part I: Synthesis and swelling characterization. *React Funct Polym* **2005,** *62* (3), 271-283.

31. Drozdov, A. D.; Christiansen, J. D., Modeling the effects of pH and ionic strength on swelling of anionic polyelectrolyte gels. *Model Simul Mater Sc* **2015,** *23* (5), 055005.

32. Roy, P. K.; Swami, V.; Kumar, D.; Rajagopal, C., Removal of Toxic Metals Using Superabsorbent Polyelectrolytic Hydrogels. *J Appl Polym Sci* **2011,** *122* (4), 2415-2423.

33. Bui, T. Q.; Cao, V. D.; Wang, W.; Nguyen, T. H.; Kjoniksen, A. L., Energy Lost in a Hydrogel Osmotic Engine Due to a Pressure Drop. *Ind Eng Chem Res* **2021,** *60* (36), 13348-13357.

34. Zhang, Y.; Zhang, Y. Y.; Wang, Q.; Fan, X. R., Preparation and Properties of a Chitosan-Hyaluronic Acid-Polypyrrole Conductive Hydrogel Catalyzed by Laccase. *J Polym Environ* **2017,** *25* (3), 526-532.

35. Jeon, O.; Song, S. J.; Lee, K. J.; Park, M. H.; Lee, S. H.; Hahn, S. K.; Kim, S.; Kim, B. S., Mechanical properties and degradation behaviors of hyaluronic acid hydrogels cross-linked at various cross-linking densities. *Carbohyd Polym* **2007,** *70* (3), 251-257.

36. Miao, T. X.; Fenn, S. L.; Charron, P. N.; Oldinski, R. A., Self-Healing and Thermoresponsive Dual-Cross-Linked Alginate Hydrogels Based on Supramolecular Inclusion Complexes. *Biomacromolecules* **2015,** *16* (12), 3740-3750.

37. Wei, Z. J.; He, J.; Liang, T.; Oh, H.; Athas, J.; Tong, Z.; Wang, C. Y.; Nie, Z. H., Autonomous self-healing of poly(acrylic acid) hydrogels induced by the migration of ferric ions. *Polym Chem-Uk* **2013,** *4* (17), 4601-4605.

38. Han, Z. L.; Wang, P.; Mao, G. Y.; Yin, T. H.; Zhong, D. M.; Yiming, B. R. B.; Hu, X. C.; Jia, Z.; Nian, G. D.; Qu, S. X.; Yang, W., Dual pH-Responsive Hydrogel Actuator for Lipophilic Drug Delivery. *Acs Appl Mater Inter* **2020,** *12* (10), 12010-12017.

39. Wang, L.; Jian, Y. K.; Le, X. X.; Lu, W.; Ma, C. X.; Zhang, J. W.; Huang, Y. J.; Huang, C. F.; Chen, T., Actuating and memorizing bilayer hydrogels for a self-deformed shape memory function. *Chem Commun* **2018,** *54* (10), 1229-1232.

40. Shin, Y.; Choi, J.; Na, J. H.; Kim, S. Y., Thermally triggered soft actuators based on a bilayer hydrogel synthesized by gamma ray irradiation. *Polymer* **2021,** *212*, 123163.

41. Xiao, S. W.; Zhang, M. Z.; He, X. M.; Huang, L.; Zhang, Y. X.; Ren, B. P.; Zhong, M. Q.; Chang, Y.; Yang, J. T.; Zheng, J., Dual Salt- and Thermoresponsive Programmable Bilayer Hydrogel Actuators with Pseudo-Interpenetrating Double-Network Structures. *Acs Appl Mater Inter* **2018,** *10* (25), 21642-21653.

42. Ma, C. X.; Lu, W.; Yang, X. X.; He, J.; Le, X. X.; Wang, L.; Zhang, J. W.; Serpe, M. J.; Huang, Y. J.; Chen, T., Bioinspired Anisotropic Hydrogel Actuators with On-Off Switchable and Color-Tunable Fluorescence Behaviors. *Adv Funct Mater* **2018,** *28* (7), 1704568.

43. Le, X. X.; Lu, W.; Zhang, J. W.; Chen, T., Recent Progress in Biomimetic Anisotropic Hydrogel Actuators. *Adv Sci* **2019,** *6* (5), 1801584.

44. Han, Z.; Zhang, J. W., Rapid-Responsive Hydrogel Actuators with Hierarchical Structures: Strategies and Applications. *Acs Appl Polym Mater* **2023,** *5* (7), 4605-4620.

45. Kirillova, A.; Maxson, R.; Stoychev, G.; Gomillion, C. T.; Ionov, L., 4D Biofabrication Using Shape-Morphing Hydrogels. *Adv Mater* **2017,** *29* (46), 1703443.

46. Timoshenko, S., Analysis of bi-metal thermostats. *J Opt Soc Am Rev Sci* **1925,** *11* (3), 233-255.

47. Wang, X. J.; Huang, H. Q.; Liu, H.; Rehfeldt, F.; Wang, X. H.; Zhang, K., Multi-Responsive Bilayer Hydrogel Actuators with Programmable and Precisely Tunable Motions. *Macromol Chem Phys* **2019,** *220* (6), 1800562.

48. Shang, J. J.; Theato, P., Smart composite hydrogel with pH-, ionic strength- and temperature-induced actuation. *Soft Matter* **2018,** *14* (41), 8401-8407.

49. Mao, S. R.; Zhang, T. T.; Sun, W.; Ren, X. H., The depolymerization of sodium alginate by oxidative degradation. *Pharm Dev Technol* **2012,** *17* (6), 763-769

50. Ritger, P. L.; Peppas, N. A., A simple equation for description of solute release I. Fickian and non-fickian release from non-swellable devices in the form of slabs, spheres, cylinders or discs. *Journal of Controlled Release* **1987,** *5* (1), 23-26.

51. Noe, C.; Tonda-Turo, C.; Chiappone, A.; Sangermano, M.; Hakkarainen, M., Light Processable Starch Hydrogels. *Polymers* **2020,** *12* (6), 1359

CHAPTER III / CHAPITRE III

Introduction Chapitre III

La fabrication additive des hydrogels, une méthode prometteuse dans le domaine des biomatériaux, offre un contrôle précis sur la structure et les propriétés des matériaux. Cette approche permet non seulement la création de structures complexes mais également la réalisation de changements de forme programmés, connus sous le nom d'impression 4D. L'impression 4D représente une évolution significative de la fabrication additive, où les objets imprimés peuvent modifier leur forme ou leur fonction en réponse à des stimuli externes.

L'étape préliminaire avant toute impression en stéréolithographie c'est l'élaboration de la courbe de travail. Cette courbe décrit la relation entre l'exposition à la lumière et la profondeur de réticulation du matériau. Elle permet aussi de déterminer la sensibilité de la résine à l'irradiation. C'est souhaitable d'avoir une légère variation de la profondeur réticulée avec une légère fluctuation de l'intensité de la lumière. Plusieurs paramètres permettent de contrôler la tendance de la courbe de travail comme l'intensité de l'UV, la quantité de photo-initiateur ou la quantité de photo-absorber.

$$Cd = Dp\ Ln\left(\frac{E0}{Ec}\right) \qquad \leftrightarrow \qquad Cd = Dp\ lnE0\ - Dp\ lnEc$$

Avec Cd: Epaisseur de réticulation
Dp: Profondeur de pénétration de la lumière
Eo: Energie de la lumière à la surface
Ec: Energie critique

Dans ce chapitre, la quantité de photo-initiateur (LAP) a été fixée comme dans le chapitre précédent à 3.75% w/w par rapport au polymère. Ainsi, l'optimisation du procédé d'impression a été réalisée en modifiant la quantité de photo-absorbeur (Orange-G) ajoutée (qui permet de limiter la diffusion de la lumière) et l'intensité d'irradiation. Dans un premier temps, des essais d'impression ont été réalisés sur les trois lots d'alginate étudiés dans le chapitre 2 avec la même formulation (3% w/w). Malheureusement, à cette faible concentration, la courbe de travail n'a pas pu être établie en raison de la faible résistance mécanique des hydrogels, ce qui rendait impossible la mesure des épaisseurs réticulées de l'ordre de centaines de micromètres. Par conséquent, il a été nécessaire d'augmenter la concentration de polymère dans la résine. Vu l'enchevêtrement important des chaînes d'alginate à MVA, HVA g/mol, la concentration maximale était limitée à 4-5% w/w, insuffisante pour la stéréolithophraphie. Pour réussir

l'impression 3D de l'alginate, la masse molaire de 55 000 g/mol était la plus prometteuse. Plusieurs formulations ont été testées afin d'élaborer des matériaux à géométrie complexe sous différents taux de réticulation pour étudier leurs comportements une fois doublement réticulés. Ensuite, pour obtenir différentes déformations à partir d'un même design, des hydrogels ayant un profil anisotrope de réticulation ont été imprimés et caractérisés. Le procédé d'impression par stéréolithographie permet de contrôler le taux de réticulation sur un même objet, ce qui permet ensuite de programmer le changement de forme, qui pourra être prédit par l'équation de Timoshenko.

Chapter III

Shape-morphing Photo-crosslinked Alginate Hydrogels via 4D Printing

KEYWORDS
4D printing, hydrogel, stereolithography, digital light processing, dual-crosslinking, photo-crosslink, smart devices

ABSTRACT
Methacrylated alginate was prepared to create 3D-designed and photo-crosslinked hydrogels using stereolithography with digital light processing (DLP). Various degrees of photo-crosslinking were investigated and implemented during the 3D printing process to achieve either a uniform chemical crosslink density throughout the entire gel (isotropic) or spatially varied chemical crosslinked densities within the same printed hydrogel (anisotropic). Secondary physical crosslinking was introduced by coordinating the alginate guluronate moieties with Ca^{2+} ions, resulting in contraction of the hydrogels. Volumetric changes, water uptake and compression testing were first investigated on isotropic photo-crosslinked hydrogels using various degrees of crosslinking. The results indicated that increasing the chemical photo-crosslinking degree leads to a reduction in swelling in PBS. Conversely, in a calcium solution, an opposite behavior was observed, with greater contraction occurring at lower degrees of photo-crosslinking. This behavior, supported by calcium titration, can be attributed to evolutions in mesh sizes of the hydrogels. Consequently, applying a gradient of photo-crosslinking induces non-uniform volumetric deformations within the same hydrogel, leading to contrasting deformation responses when immersed in a calcium solution. This allows for specific programmed shape deformation of 3D printed hydrogels upon swelling or contraction depending on the medium. This behavior was first demonstrated using 3D printed films with a photo-crosslinking gradient profile. Bidirectional bending can be induced simply by switching the media from PBS to $CaCl_2$ solution. Moreover, more complex shape deformations were observed by varying the photo-crosslinking gradient in specially designed tubular structures and porous cubes. Finally, the 4D printed devices demonstrated cell compatibility, as evidenced by cytotoxicity assays conducted on fibroblast NiH 3T3 cells, thereby opening possibilities for smart hydrogel medical devices.

1. INTRODUCTION

4D printing of soft materials such as hydrogels is an advanced approach combining the programmable shape deformation of 3D printed structures under an external stimulus with the swelling behavior of the hydrogel matrix.[1] Based on the chosen matrix, the external stimulus can vary from temperature, pH, ionic strength, light, magnetic or electric field.[2–4] Upon an external stimulus, the 3D printed hydrogel will change shape or size throughout time providing the fourth-dimension aspect of the technology.[5,6] This processing technique is particularly interesting for biomedical applications to develop patient specific implants, adaptable for non-invasive delivery of smart devices or on command drug delivery systems.[7–9]

Sodium alginate is a naturally occurring polysaccharide composed of alternating mannuronate (M) and guluronate (G) units. It has a remarkable ability to form a physically crosslinked network between the G units in the presence of multivalent cations such as Fe^{3+}, Cu^{2+}, Ca^{2+}, Mn^{2+}.[10] The physically crosslinked network can dissociate in physiological media due to sodium-calcium ion exchange. Moreover, the hydroxyl and carboxyl groups present on alginate backbone can be easily functionalized enabling the formation of a chemically crosslinked network.[11] Chemically crosslinked alginate is most commonly produced by photo-polymerization following alginate methacrylation, resulting in stable hydrogels suitable for biomedical applications.[12] Moreover, this chemical crosslinking process can be conveniently achieved during 3D printing by photo-polymerization, allowing for the creation of more complex hydrogel architectures.

Photo-printing of hydrogels has already led to successful development of smart actuators capable of controlled and programmed shape deformations.[13–15] This manufacturing process highlights the potential of smart hydrogels, paving the way for innovative applications of 4D printing in advanced biomedical devices.[16,17] For alginate 4D photo-printing, the most common reported technique in the literature is by direct ink writing (DIW), where the resin is extruded through a nozzle and cured under UV layer by layer to obtain the 3D structure. Cao *et al* developed alginate-based actuators with a gradient crosslinking using DIW.[18] The system consists of a bilayer film where each layer required different formulation in order to obtain an anisotropic profile that leads to a shape deformation. Before the printing procedure, a complete rheological study was performed on the formulations of the bio-ink in order to adjust the printer parameters for high resolution printing. Similarly, Constante *et al.* fabricated circular bilayer films composed of a photo-crosslinked alginate bottom layer and a poly(caprolactone) second

layer.[19] The two-step process produces self-folding thin films, with the diameter of the resulting tubes being controllable by adjusting calcium concentrations. In addition to bilayer systems, actuating mechanism can also be generated by an anisotropic swelling behavior across the surface of a single material. Lai *et al.* generated an anisotropic swelling degree in alginate films by modifying the number of layers printed followed by a drying step.[20] They controlled the shape deformation by modifying the pattern orientation of the different layer compartments, but remains on a 2D film structures. Another example of a self-folding 2D film based on alginate was reported by Kirillova *et al.*.[21] Their crosslinking gradient was hypothesized to result from the different light penetration between the top and the bottom of the film. Thus, the actuating mechanism originates only from light diffusion within the formulation.

Most examples in the literature focus on 2D alginate films capable of deformation, produced through various manufacturing techniques, and reports of complex 3D hydrogel actuators are notably less common. Although, the use of additive manufacturing techniques becomes particularly significant when leveraging their ability to create complex 3D structures.[22] Specifically, additive manufacturing by photo-polymerization methods, such as stereolithography (SLA) techniques, enable the convenient fabrication of complex 3D architectures with specific deformation capabilities.[23,24] Indeed, one of the advantages of SLA printing is the ability to spatially control the chemical photo-crosslinking density not only on simple film-like structures but especially on more complex three-dimensional architectures.[25,26] By controlling the grayscale profile of each layer, the crosslinking profile and density can be tuned within different areas of the printed object, which translates into different shape deformations upon swelling or contraction. Jiang *et al.*, obtained various deformation profiles by designing a well-tuned crosslinking profile that induces site-selective deformation on polyethylene glycol diacrylate (PEG) based resin.[27] Similarly, Ji *et al.* controlled the degree of bending of a 2-hydroxyethyl methacrylate based hydrogels by modifying the photo-crosslinking time on a tubular structure.[28] Finally, varying the degree of photo-crosslinking *via* UV photo-exposure was another strategy to induce actuator deformations. Ren *et al.* implemented a crosslinking gradient by modifying the curing time on a commercial resin and fumed silica based composites,[29] and Odent *et al.* investigated anisotropy-encoded hydrogel actuators approach by, among other factors, manipulating the degree of photo-crosslinking in PNiPAAm-based resin.[30] However, this gradient approach remains underexplored and is not yet widely adopted for hydrogels. Therefore, this study aims to explore the remarkable potential of the SLA process for creating crosslinking gradients

combined with the well-known ability of alginate hydrogels to form reversible interactions with multivalent cations, with the goal of enabling shape transformation through controlled swelling effects as illustrated in Figure III-1. This innovative approach opens up promising possibilities for developing bio-sourced and biocompatible 4D printed hydrogels for biomedical applications. Various 3D chemically photo-crosslinked alginate hydrogels were produced by SLA with digital light processing (DLP) printing. The mechanical properties as well as the volumetric changes of the hydrogels were evaluated for various degrees of crosslinking. 4D printed structures exhibiting controlled shape deformation is achieved by managing the crosslinking gradient during the curing process by DLP. Cytotoxicity assays on the dual crosslinked hydrogels were done on NIH-3T3 fibroblast cells as preliminary biocompatibility for potential use of the resins to design 4D printed smart biomedical devices.

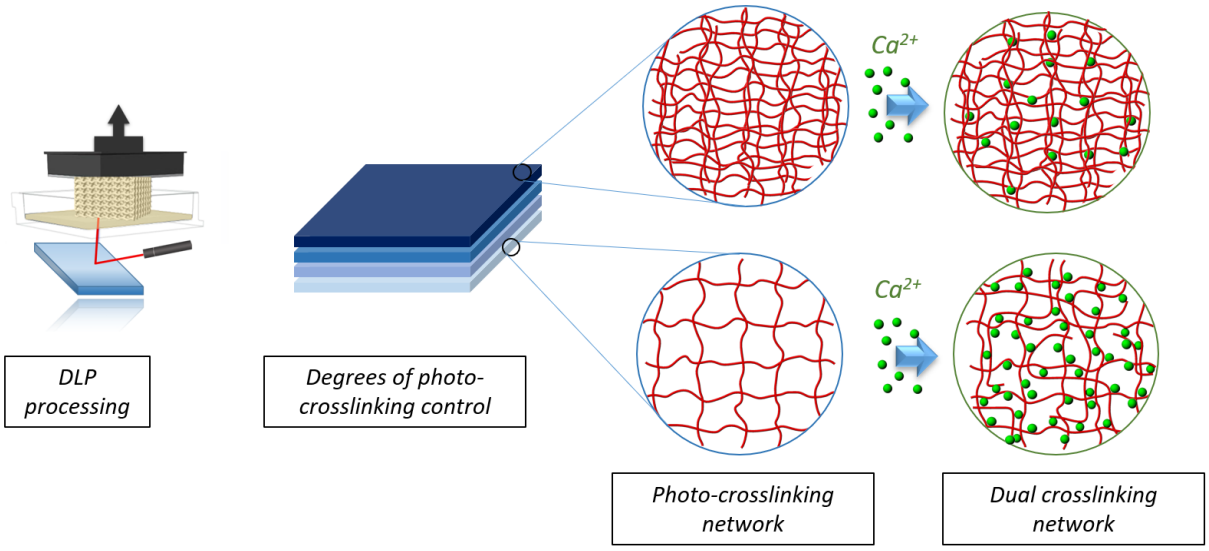

Figure III-1. Schematic illustration of 4D printing using DLP to obtain various crosslinking degrees and the resulting network before and after ionic stimulus.

2. MATERIALS AND METHODS

2.1. Materials

Low viscosity sodium alginate (LVA), methacrylic anhydride (MA), calcium chloride ($CaCl_2$), ethylenediaminetetraacetic acid tetrasodium salt dihydrate (EDTA $4Na^+$, $2H_2O$), Orange-G and phosphate buffered saline (PBS) were purchased from Sigma-Aldrich (France). Triethylamine (TEA) was purchased from Fisher Chemicals (France). Milli-Q water (conductivity = 18.2 mΩ.cm at 23°C) was used during this study. Lithium phenyl-2,4,6-trimethylbenzoylphosphinate (LAP) was synthesized as described by Majima *et al.*[31] All chemicals were used without further purification unless mentioned otherwise. Culture media

and additives were provided by Thermofisher (Gibco, France), Live/Dead cytotoxicity kit L3224 was purchased from Thermo Fisher (Invitrogen^{TM}, France) and NIH-3T3 CRL-1658TM cells were provided by ATCC (France).

2.2. Methods

Resin formulation and 3D Printing

All structures were printed by stereolithography using a digital light processing (DLP) printer (Max X27, Asiga Australia). The resins were prepared by dissolving the appropriate amounts of methacrylated alginate (Alg-MA) to obtain 6, 8 and 10% w/w aqueous solutions. The alginate methacrylation is described in our previous work[11] and reported in supplementary information (Figure III-S1) . The degree of methacrylation was calculated according to Equation III-S1. LAP was added at 3.75% w/w with respect to the alginate and Orange G at 0.2% w/v as photo-absorber. Orange G was added in order to control the UV light penetration for high resolution printing. UV intensity for DLP was fixed at 10 mW/cm^2 (after optimization Figure III-S2) and the printing layer thickness was 100 µm for all samples.

Uniform printing conditions

The swelling behavior, volumetric change and the mechanical properties were tested on 3D printed cylinders (8 mm diameter and 4 mm thickness). To obtain different degree of photo-crosslinking, the printing time of the individual 100 µm layer was chosen through the working curve (Figure III-S2) in order to optimize the UV penetration depths. The crosslinking time per 100 µm layer of each formulation is summarized in Table III-1. Upon printing, the hydrogels were washed in PBS.

Gradient printing conditions

To obtain an anisotropic swelling behavior, a crosslinking gradient is implemented by varying the crosslinking time over the thickness of the .stl designs generated by the Rhinoceros 3D software. To maintain a proper resolution, the gradient starts with the over-crosslinked section and decreases over the thickness when applicable. The details of each gradient section are provided in the discussion for the films, porous cubes, and cylinder designs.

Cyclic swelling studies

The equilibrium cyclic swelling degrees were measured starting from the washed hydrogels.The cycles comprised of the following sequences: (1) 5% w/v aq. $CaCl_2$ solution, and (2) PBS to mimic physiological conditions. For each measurement, the hydrogel was left

to swell in the specific media for 24 h at 25 °C The swelling degree was calculated using Equation III-1. The values are represented as the mean of triplicate sets.

$$Q = \frac{m_{swollen\ at\ time\ t}}{m_{\ dry}} \quad \text{(Equation III-1)}$$

Expansion coefficient measurements

The volumetric change of the hydrogels was assessed by evaluating the dimensional change in different medias (PBS and $CaCl_2$ solution). The expansion coefficient is calculated as the ratio of the dimensions of the swollen hydrogels and the dimensions of the .stl reference design (Equations III-2 and III-3).

$$\alpha_{xy} = \frac{diameter\ at\ swollen\ state}{diameter\ of\ STL\ design} \quad \text{(Equation III-2)}$$

$$\alpha_{z} = \frac{thickness\ at\ swollen\ state}{thickness\ of\ STL\ design} \quad \text{(Equation III-3)}$$

Compression testing

Compression tests on the 3D printed cylindrical samples (8 x 4mm) swollen hydrogels were performed on an Instron 3366L5885 mechanical tester equipped with a 100 N load cell. Hydrogels were taken at different points of the cycling swelling and the compression tests were done after measuring the dimensions. The compression speed was set at 1 $mm.s^{-1}$ with 200 ms sampling time. Each value is represented by the mean ± SD (n = 3). The Young's modulus was calculated from the slope of the initial 3% deformation in the linear domain.

Mesh size of the hydrogels at different degrees of photo-crosslinking was calculated following the rubber elasticity theory (RET) assuming incompressible elasticity according to the equation:

$$\xi = \left(\frac{E\ R\ T}{3\ N_A}\right)^{1/3} \quad \text{(Equation III-4)}$$

where E is the compression modulus, N_A is the Avogadro constant (6.022×10^{23}), R is the gas constant (8.314 J/K mol) and T is the temperature (298 K).

Photo-rheology analysis

Photo-rheology was done on a Thermo Fisher HAAKE MARS 60 rheometer using 20 mm parallel circular plate-plate geometry. The measurements were obtained during 500 s irradiation under 0.5 W/cm^2 UV mercury lamp equipped with a 320-480 nm filter. Before

testing, the samples were prepared to obtain 8% w/w Alg-MA solutions containing 3.75% w/w LAP and 0.2% w/v Orange G. The gap was fixed at 100 µm corresponding to the printing layer thickness and the temperature fixed at 20 °C. Results are obtained under a constant load of 0.1 N, strain of 1 % and 1 Hz frequency to ensure the linear viscoelastic domain.

Mesh size (ξ) was calculated according to Flory-Rehner rubber elasticity theory (RET):[32,33]

$$\xi = \left(\frac{R\,T}{G'\,N_A}\right)^{1/3} \qquad \text{(Equation III-5)}$$

where G′ is the storage modulus, N_A is the Avogadro constant (6.022×10^{23}), R is the gas constant (8.314 J/K mol) and T is the temperature (298 K).

Radius of curvature prediction

The radius of curvature of bisectional systems was predicted using the following simplified Timoshenko's equation[34]:

$$\frac{1}{\rho} = \frac{24\,(\Delta\alpha)(1+m)^2}{h\,(3(1+m)^2+(1+mn)(m^2+\frac{1}{mn})} \qquad \text{(Equation III-6)}$$

Where ρ is the radius of curvature, Δα is the difference of xy expansion between the section X4 and X1, m is the ration between the thicknesses of section X4 to section X1, h is the total thickness of the sample and n the ration of Young's modulus of section X1 to section X2.

Titration analysis

The calcium content in the hydrogels, submerged in 5% w/w $CaCl_2$ solution, was quantified by colorimetric titration with EDTA in presence of Eriochrome Black T. Briefly. Hydrogels photo-crosslinked at X1, X2, X3 and X4 were left in $CaCl_2$ solution for 24 h then placed in 10 mL PBS to release the calcium for 24 hours. The hydrogels were then removed (and dried) and the appropriate amount of PBS was added to compensate the quantity absorbed by the hydrogels. The pH of the solutions was adjusted to 11 with 1 M NaOH. 1 mL of the solution was titrated with 0.01 M EDTA solution. Equilibrium point is reached upon color change from dark blue to dark red.

Cytotoxicity assays

Cytotoxicity assays were performed on extracts from hydrogel actuators swollen in PBS and $CaCl_2$ solution according to the ISO 10993 standard. The hydrogel samples were sterilized in ethanol for 24h and then left to swell in filter sterilized PBS or $CaCl_2$. Extracts were prepared by incubating the hydrogel samples in a complete cell culture medium (Dulbecco's Modified

Eagle's medium 4.5 g L−1 D-glucose supplemented with 1 v/v% L-glutamine, 10 v/v% fetal bovine serum, and 1 v/v% penicillin /streptomycin) at a hydrogel concentration of 0.1 mg/mL for 24 hours at 37°C. Hydrogel samples were studied once immersed in PBS or in 5% w/w $CaCl_2$.

NIH-3T3 fibroblast cells were maintained in complete cell culture media at 37°C in a humidified atmosphere with 5 % CO_2. For the assay, cells were seeded into 12-well plates at a density of 10^5 cells/well and allowed to adhere for 24h.

After 24 hours of seeding, the culture media was replaced with 2 mL of hydrogel extracts. Control group includes cells treated with fresh culture medium (negative control) and cells treated with 70 % ethanol (positive control). After 24h of incubation at 37 °C with the extracts, cells were washed with PBS, detached using trypsin-EDTA, resuspended in PBS and stained using Live/Dead kit for 20 min at room temperature. Live/Dead assays were analyzed using a flow cytometer (FACS AccurciC6+ with Ex 488 nm; emission filters: 530/30 nm for live cells, and 610/20 nm for dead cells). The results were presented as mean ± standard deviation of three independent experiments.

Statistical analysis

All data are represented as the mean ± standard deviation unless otherwise specified. Statistical significance was assessed using two-tailed t-test assuming unequal variances. The t-test was conducted using Microsoft Excel (2021) with a significance threshold at $p < 0.5$.

3. RESULTS AND DISCUSSION

3.1. Study of the photo-crosslinked alginate hydrogel

Alginate hydrogels are commonly formed through physical crosslinking with multivalent cations such as Ca^{2+}. However, these physically crosslinked hydrogel systems exhibit low stability in physiological environment due to the decomplexation of the Ca^{2+} through Na^+ ion exchange. This limits their applicability as biomedical materials under physiological conditions. To overcome this limitation, chemical crosslinking of the alginate macromolecules produces more stable gels that can further be ionically crosslinked to tune certain properties of the hydrogels. By grafting methacrylate moieties onto the hydroxyl groups, a photo-crosslinkable resin can be produced, while the carboxyl groups remain available for complexation with Ca^{2+} ions.

In our study, we used sodium alginate with a molecular weight of 55.000 $g.mol^{-1}$, as this choice balances mechanical properties and viscosity effectively. Higher molecular weight alginates, such as those with molecular weights of 172.000 $g.mol^{-1}$ and 320.000 $g.mol^{-1}$, exhibited weaker mechanical properties and were unsuitable for increased concentrations due to their high viscosity, which limits the 3D processing by DLP (data not shown).[11] The degree of methacrylation achieved was 140% relative to a sugar moiety of alginate, ensuring both robust mechanical properties and high printing resolution. Based on these studies, the 8% w/w photo-crosslinked alginate hydrogels were the easiest to formulate, provided the best photo-printing conditions, and exhibited the most promising volumetric changes. We therefore focus the investigation on these hydrogel concentrations. To obtain various degrees of photo-crosslinking (X*n*), the curing time per 100 µm layer are summarized in Table III-1.

Table III-1. Irradiation time of the 100 µm printing layer to obtain different degrees of photo-crosslinking (Xn) for 8% w/w Alg-MA.

	Curing time			
Degree of photo-crosslinking (X*n*)	**X1**	**X2**	**X3**	**X4**
8% w/w	8 s	15 s	25 s	40

3.2. Physical properties of the photo-crosslinked hydrogel and impact on the dual crosslinking.

The influence of the printing conditions was investigated through swelling measurements and the volumetric change with respect to the designed dimensions of the 3D structures (cylinders with 8 mm of radius and 4 mm of thickness). In addition, such measurements were also performed to investigate the effect of the secondary crosslinking in the presence of Ca^{2+} ions.

As seen in Figure III-2A, increasing the X*n* gradually from X1 to X4, reduces the swelling ratio in PBS from Q = 31 to Q = 15, which is due a densification of the network, thereby reducing the PBS uptake. This is confirmed by the increase in gel content, which rises from 60% for X1 to 95% for X4, implying a corresponding difference in network density and mesh sizes (Figure III-S3A). Mesh sizes have been calculated following Flory-Rehner theory (Equation III-S1) and later on using the rubber elasticity theory (Equation III-4). Mesh sizes represent a number-average molecular weight of the linear chains between two network nodes (Mc). The results show a significant decrease in the mesh size when varying the crosslinking density where it decreases from 22 100 g/mol for X1 to 6873 for X4 (Table S3). Once immersed in Ca^{2+} solution,

secondary ionic crosslinking occurs between the guluronate units, which tends to further densify the network, reduces the mesh size, and results in expulsion of water. Interestingly, the swelling ratio for all X*n* is similar, with values close to Q ≈ 7. In consequence, the mesh sizes measured using Flory-Rehner theory are similar in the network generated by dual crosslinking and reach around 5500 g/mol. This suggests that a maximum level of dual crosslinking is achieved and the swelling properties of the network reaches a threshold. This effect should be observable through changes in Ca^{2+} complexation regarding the X*n*. Consequently, we measured the Ca^{2+} content of each dual crosslinked hydrogel using colorimetric titration. As shown in Figure III-2D, the Ca^{2+} content in the dry state of the hydrogel is 2.7% w/w when photo-crosslinked at X1. This value gradually decreases to 1.7% w/w as the X*n* increases to X4. The reduction in Ca^{2+} complexation in the hydrogels when the X*n* increases can be explained by the progressively limited chain mobility, which hinders the ability of the different guluronate units to further complex Ca^{2+} ions. Moreover, SEM images (Figure III-S4) reveals a distinguished aspect of the hydrogel's pores between the two swollen states. In PBS, the network demonstrates a thin film like structures whereas upon dual crosslinking, the walls become denser similarly to what reported by Li *et al.* in dual crosslinked Agar / PAAc hydrogels.[35]

This secondary ionic crosslinking is reversible and can be removed in PBS due to the Ca^{2+}-Na^{+} ion exchange, which increases the swelling ratio to almost its initial state. The swelling was seen to be reversible and cyclic as we previously demonstrated over several cycles.[11] This confirms that the dual crosslinking reaches a maximum limit, and the network cannot be further crosslinked, regardless of the level of the chemical photo-crosslinking. Shrinking and swelling kinetics was recorded for all hydrogels (Figure III-S5). As we previously demonstrated, altering the crosslinking time does not affect the time required to reach equilibrium, because the swelling mechanism of dual crosslinking alginate hydrogels follows a non-Fickian diffusion.[11]

Besides studying water uptake, it is important to distinguish the properties of the generated network and the shape change aspect of the hydrogels upon shrinking in Ca^{2+} solution. The volume changes are measured relative to the volume of the printed hydrogels swelled in PBS. As shown in Figure III-2B, we demonstrate that the volume of the printed hydrogels do show a difference in the shrinkage regarding the X*n.* Higher X*n* lead to less shrinkage, following the volume trend X4 > X3 > X2 > X1. Unlike the swelling ratio Q in Ca^{2+} solution, no threshold is observed among the four degrees of photo-crosslinking in Ca^{2+} rich solution. This aligns with

the idea that denser hydrogels have less chain mobility and therefore less potential for volume deformation. This difference can be explained by the initial swelling ratio of each degree of photo-crosslinked hydrogel, which varies significantly (Figure III-2A) and thus leads to a pronounced difference in volume after undergoing dual crosslinking.

Given that the driving force in hydrogel actuators is the differential expansion coefficient in the x-y plane in bilayer systems,[29,34] it is important to evaluate the dimensional changes of the hydrogels at different crosslinking conditions. The expansion coefficient (α_{xy}) values that influence the bending motion according to Timoshenko's principle (Equation III-6) are summarized in Figure III-2C.[34] All hydrogels swell and the diameter increase by 10 to 30% in PBS compared to their dimensions in the .stl design. As the X*n* gradually increases from X1 to X4, the x/y expansion coefficient (α_{xy}) decreases from 1.27 to 1.11. When photo-crosslinked at X1, the hydrogel's diameter is 27% larger than the .stl design, whereas at X4, the hydrogels exhibit only an 11% increase. Upon exposure to a Ca^{2+}-rich solution generating the secondary ionic crosslinking, the hydrogels shrink at different rates, resulting in varying final diameters (Figure III-S6). These values correlate with the volumetric change and expansion coefficient trend, where in Ca^{2+} solution, hydrogels with higher X*n* exhibit a lower shrinking behavior. Additionally, the expansion coefficient in the z-axis was found to follow the same trend, with slightly lower values (Figure III-S3B), due to the layer-by-layer printing process. From a single .stl design, several volumetric changes can be obtained in the equilibrium swelling state in PBS and Ca^{2+} solution by simply tuning the printing process by varying the photo-crosslinking time. This variable volumetric change of each X*n* allows designing controlled shape deformation when building hydrogel structure with an anisotropic crosslinking profile.

The study of the expansion coefficient of the hydrogels in different media, provides crucial insight to engineer and design hydrogel actuators with programmed and predicted shape deformations by implementing a crosslinking gradient. In PBS, increasing the photo-crosslinking time will result in a lower expansion trend due to the higher photo-crosslinking density of the network. On the other hand, when submerged in Ca^{2+} solution, hydrogels at higher X*n* show a lower shrinking behavior. The denser the network becomes, the more hindered Ca^{2+} diffusion into the matrix will become which was verified by quantifying the Ca^{2+} by colorimetric titration.

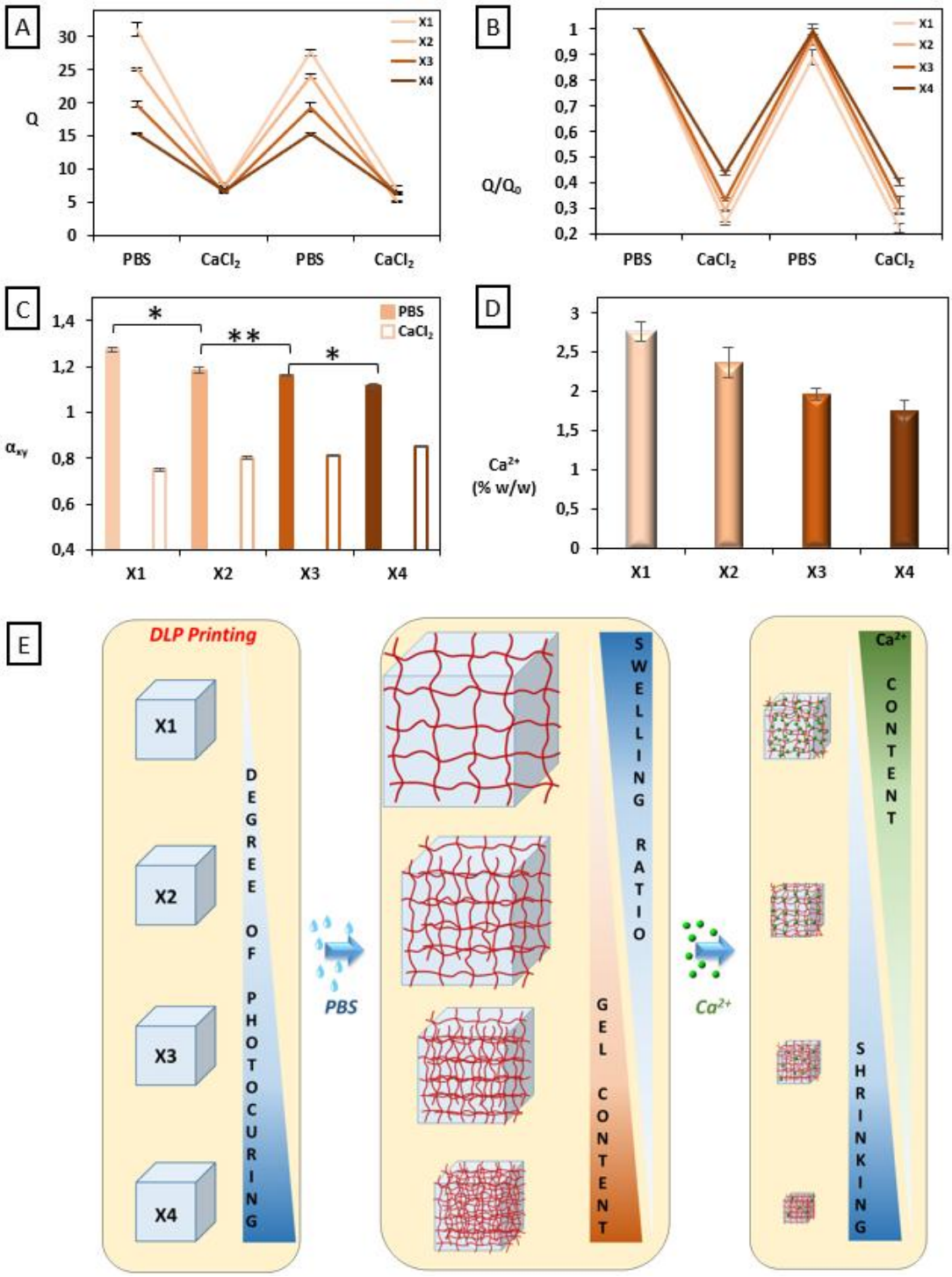

Figure III-2. A) Swelling ratio and B) ratio of swelling degrees with respect to the initial swollen state in PBS C) the expansion coefficient of 8% w/w Alg-MA hydrogels when swollen in PBS and Ca^{2+} solution. D) Calcium weight percentage in the dry hydrogels as obtained from colorimetric titration for freeze dried hydrogels photo-crosslinked at X1, X2, X3 and X4 after being submerged in a 5% w/w Ca^{2+} solution and reswollen in PBS and E) Schematic illustration of the evolution of the, gel content, swelling behavior and calcium content as the photo-crosslinking degree varies.

3.3. Mechanical properties studies related to the crosslink density

The influence of varying X*n* (from X1 to X4) as well as the dual crosslinking impact on the mechanical properties of the 3D printed structures was investigated. As seen in Figure III-3A, gradually increasing the degree of photo-crosslinking from X1 to X4 results in higher stress at break in PBS, increasing from 20 to 75 kPa, while the deformation remains similar around 25% for all the X*n*. The strength of the network is also depicted by the evolution of the Young's modulus, which increases significantly and gradually from 10 to 60 kPa as Xn increases. Therefore, the progression of mechanical properties of the printed hydrogels typically correlates with the X*n*. As the network density increases, mechanical resistance and stiffness also increase. Consequently, mesh sizes have been calculated using the rubber elasticity theory (Equation III-4). By increasing the X*n* from X1 to X4, the mesh size decreases from 7.6 nm to 4.3 nm confirming the higher crosslinking density (Table III-S1).

However, by immersing the printed hydrogel in a Ca^{2+} solution inducing an additional physical crosslinking, the mechanical properties are significantly improved, which logically results from a denser network (Figure III-3B). As a result, dual crosslinked hydrogels exhibit higher deformations at break, reaching approximatively around 70% for all the X*n*. The dual crosslinked hydrogels also demonstrate improved stresses at break reaching up to 900 kPa compared to a maximum of 80 kPa when swollen in PBS. Nevertheless, the progression of Young's modulus provides valuable insights into the network properties. Specifically, Young's modulus in Ca^{2+} solution increases for all X*n* compared to hydrogels in PBS. However, the ratio between Young's modulus in PBS and in Ca^{2+} solution decreases significantly as X*n* increases. This suggests that the main crosslinking at X1 is the physical, which gradually diminishes until X4, where photo-chemical crosslinking becomes dominant. However, as shown by the swelling properties of the network, which reach a threshold under dual crosslinking, Young's modulus also tends to be relatively close, ranging between 50 and 70 kPa with a large standard deviation. Increasing X*n* affects the ratio between physical and photo-chemical crosslinking, creating a non-equivalent network that may be responsible for the observed fluctuations in Young's modulus.

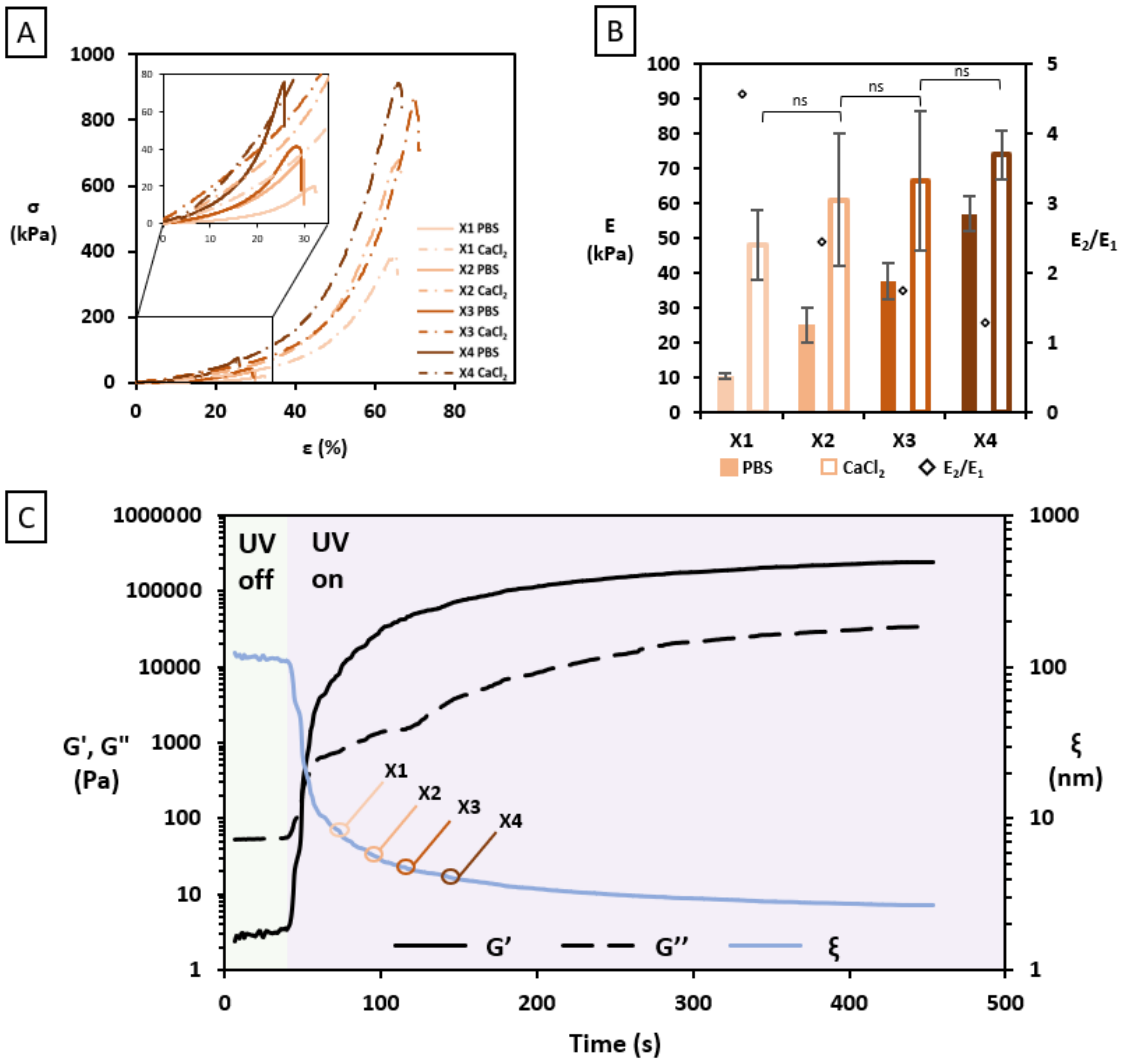

Figure III-3. A) Stress-strain curves for 3D printed cylinders 8% w/w Alg-MA at Xn depth for 100 µm layer printing process and B) the Young's modulus of hydrogels at Xn in PBS and Ca^{2+} solution calculated as the slope of the stress-strain curves at 3% deformation and the ratio E_2/E_1 of the Young's modulus in calcium to PBS. The values are represented as the mean ± SD (n=3) and C) Storage and loss modulus of 8% w/w Alg-MA resin during crosslinking under UV light and the evolution of the mesh size of the network. Circles refer to the mesh size of the hydrogels as calculated by RET from compression testing (Table S3).

Photo-rheology on the resin indicated a significant time range between the crossover of the storage modulus (G') and loss modulus (G") and the equilibrium as shown in Figure III-3C. This demonstrates the ability to tune the hydrogels mesh sizes by varying the photo-crosslinking time. Consequently, the exposure times determined initially using the working curve, align perfectly with the evolution of the mesh size, confirming the network differences between X1 (8 s), X2 (15 s), X3 -25 s) and X4 (40 s).

These values correlate to the evolution of the mesh size under UV irradiation (photo-printing) allowing us to position the hydrogels' X*n* on the photo-rheogram (Figure III-3C). The mechanical properties of these hydrogels are directly tied to the curing process, with longer photo-crosslinking times resulting in stronger and stiffer materials. The addition of Ca^{2+} ions further strengthens the hydrogels by creating additional physical crosslinking points. Understanding these mechanical properties is key to designing hydrogel actuators, as it helps predict and control the bending deformation.[36]

3.4. 4D actuators based on alginate hydrogel

The volumetric changes induced by varying environmental conditions of such hydrogels can be harnessed to achieve shape deformation in 3D printed designs. This capability enables the development of 4D printed alginate-based hydrogels. We previously demonstrated that the key feature is the progressive decrease of α_{xy} when increasing the X*n* from X1 to X4 in PBS and the progressive shrinking behavior in Ca^{2+} solution. Therefore, the variation in swelling behavior due to photo-crosslink density, further enhanced by the introduction of Ca^{2+}, can be exploited to generate gradients within a single structure fabricated by DLP. Various structures have been designed and fabricated using DLP, and the results are discussed in this section.

We initially start with simple film structures, similar to the studies on hydrogel actuators,[37] by incorporating a bisectional gradient on films and varying surface geometries: i) square surface (22 mm x 22 mm x 1 mm), ii) rectangular surface (33 mm x 22 mm x 1 mm), with one side featuring a regular topographical mesh, to easily identify the correct side visible in response to the stimulation medium (Figure III-4). The introduction of topography into these films also enabled the investigation of shape deformation effects on film actuators. This is particularly relevant for potential applications as medical devices, such as in wound healing, where the topography could be adapted to enhance tissue adhesion.[38,39] By combining the volumetric expansion coefficient with the compression modulus that were established earlier, shape deformation in a bisectional actuator design can be predicted using Timoshenko's equation.[11]

Therefore, through the modulation of X*n* in a bisectional film system, a curvature will be induced towards the section with the lowest expansion coefficient. Each section of film represents half of the total thickness, with one half-section photo-crosslinked at X1, X2 or X3 (section of the film containing the topography in the case of patterned films) and the other half-section photo-crosslinked at X4, respectively, to control the radius of curvature according to Timoshenko's principle (Equation III-6).[40] The radius of curvature is directly proportional to

the $\Delta\alpha_{xy}$; the maximum curvature can be obtained for the highest $\Delta\alpha_{xy,}$ which corresponds to films with section 1 photo-crosslinked at X4 and section 2 photo-crosslinked at X1. By modulating the X*n* of section 2 for X2 or X3, various bending curvatures can be obtained as seen in Figure III-4A leading to radii of curvatures similar to the predicted values obtained from Timoshenko's equation ranging between 3.1 to 8.1 mm.

Another parameter can be adjusted to control the degree of bending is the total thickness of the printed hydrogel. A rectangular bisectional film (X4/X1) was printed with a thickness of 2 mm. The printed hydrogel films swell anisotropically due to the implemented gradient, with X1 expanding more than X4. This differential behavior between the two sections causes the hydrogel to roll up. Both hydrogels with thickness of 1 mm (Figure III-3) and 2 mm (Figure III-S7) exhibit strong curvature toward the more crosslinked section which has a lower α_{xy} in PBS (corresponding to the patterned side, in case of films with topography). The radii of curvature obtained are 6.3 mm and 3.1 mm for thicknesses of 2 and 1 mm, respectively. The values obtained corresponds to the theoretical values from Timoshenko's model demonstrating the viability of the model for 4D printed alginate hydrogels. It is important to note that all the films behave similarly with a rolling motion of the actuators, and such independently to the geometries or the presence of topography. As seen in Figure III-4B-D, rectangular and square actuators were printed with and without the mesh design as well as a circular film where the same rolling motion is observed.

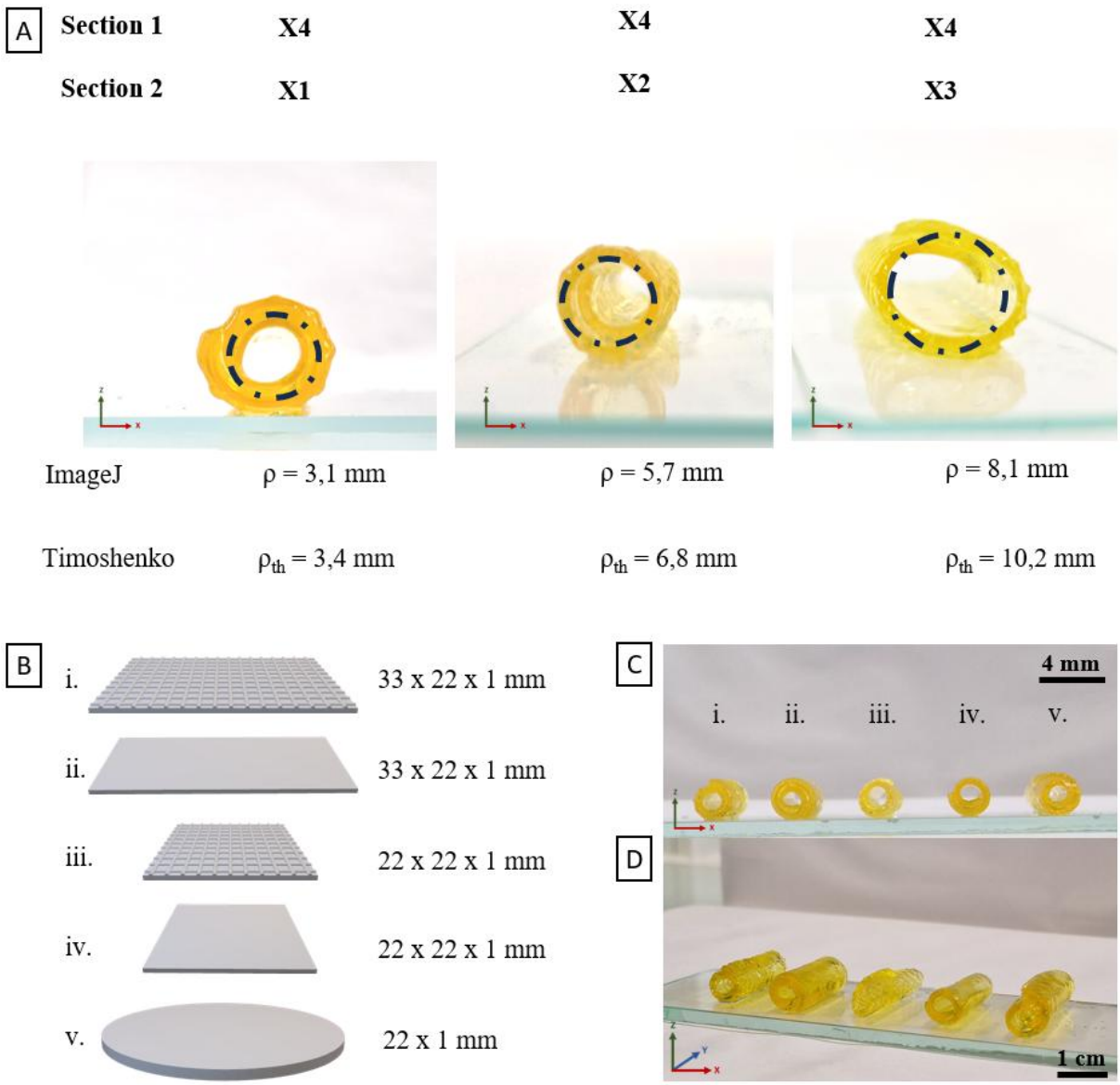

Figure III-4. A) 4D printed bisectional hydrogel actuators (33x22x1 mm) with different gradient profiles swollen in PBS at equilibrium and the radii of curvature obtained upon deformation which correlates to Timoshenko's mathematical model, B) .stl design and dimensions of the square and rectangular films with and without mesh and a circular film and B) face and C) side view of the rolled actuators in PBS.

Moreover, when the bisectional (33x22, X1/X4) film is immersed in a Ca^{2+} rich solution, a reverse actuation is observed as predicted in Figure III-5A. As showed and explained previously, hydrogels photo-crosslinked at X4 demonstrate a lower shrinking behavior than the one photo-crosslinked at X1, this forces the system to roll towards the X1 section (towards the patterned side for the structures with topographical mesh) as seen in Figure III-5B and S9,

leading to curvatures of 4.9 mm and 12 mm for the hydrogel having 1 mm thickness and 2 mm thickness respectively. Interestingly, an unexpected behavior was identified during the inverse rolling transformation. The hydrogels not only reverse the rolling actuation from X1 to X4, which was expected, but also exhibit an unexpected orthogonal curvature change in the X-Y planes of the film (Figure III-5C). The same orthogonal unfolding behavior was observed when switching the media from Ca^{2+} solution to PBS (Figure III-6). Additionally, such behavior was obtained independently to the geometries or patterned hydrogel films. Initially swollen in PBS, the hydrogel films roll towards the higher photo-crosslinked section (X4) where the section photo-crosslinked at X1 is on the outside. This rolling motion generates a stress profile with higher stresses in the curvature direction compared to the lateral direction. Upon immersion in a Ca^{2+}-rich solution, both sections of the hydrogel shrink simultaneously. This shrinkage triggers an unfolding motion of the film, followed by an orthogonal refolding. The actuator's motion begins at regions where the stress is minimal, allowing areas with high stress to gradually relax. This sequence results in a dynamic bidirectional bending: the film first unfolds in one direction due to the initial stress relief, and then refolds in a perpendicular direction as the stresses redistribute. This complex motion showcases the actuator's ability to respond adaptively to changes in its environment, optimizing its performance through the controlled redistribution of stress.

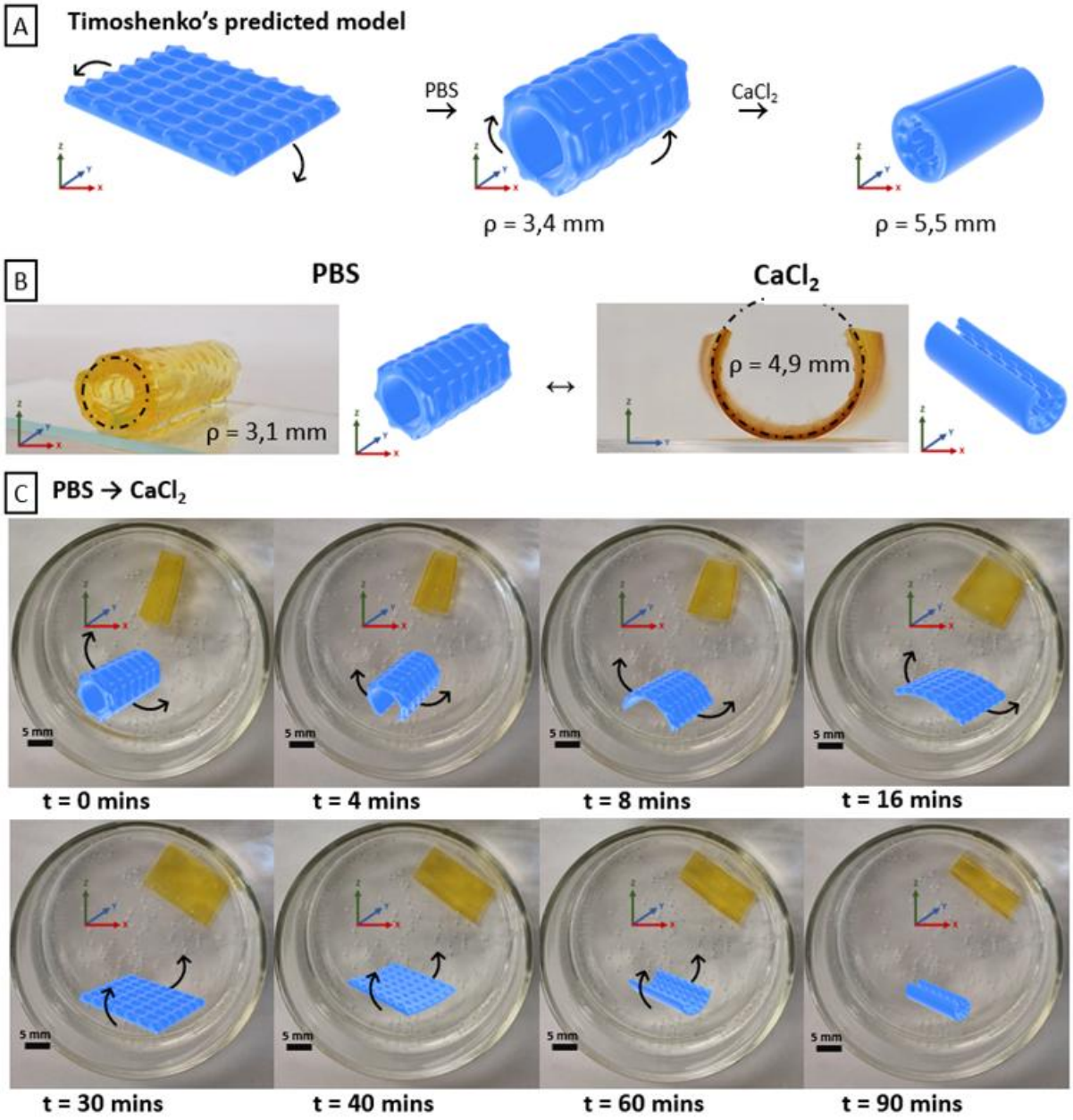

Figure III-5. A) Predicted radius of curvature of 4D printed 33x22x1 mm bi-sectional actuators X1/X4 when swollen in PBS and in 5% w/w Ca^{2+} solution and B) physical representation of the bisectional actuation when submerged in PBS and Ca^{2+} solution with the radii of curvature as measured by ImageJ and C) timelapse unfolding of the bisection actuator when transferred from PBS to Ca^{2+} solution.

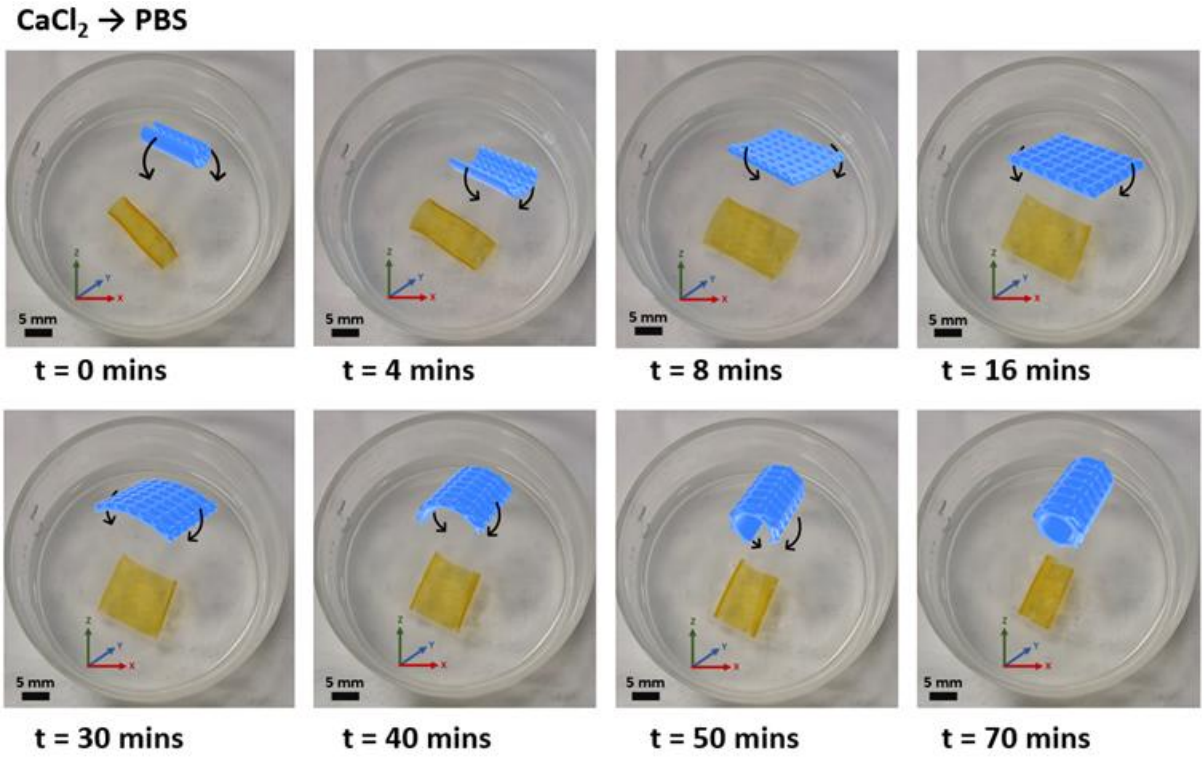

Figure III-6. Timelapse images of the rolling deformation of the 33x22x1 mm hydrogel actuator X1/X4 at 1 mm thickness when switching the media from Ca^{2+} solution to PBS.

We successfully obtained and studied a stimulated transformation of 3D printed film structures, by DLP technology enabling the elaboration of complex architectures with highly specific, and programmable shape deformations. As a second design, we envisioned to investigate more volumetric 3D structures by designing a porous cube .stl design shown in Figure III-S8A. When subjected to homogeneous isotropic photo-crosslinking at X1, without any photo-crosslinking gradient, the cube exhibits a uniform swelling in PBS where its dimensions increase by 27% from the .stl design and shrinks uniformly in Ca^{2+} rich solution by 40% in size from its swollen state as observed in Figure III-7 according to the expansion coefficient previously determined.

In contrast, employing photo-crosslinking gradients result in a more sophisticated response. In this approach, the porous cube is photo-crosslinked with a gradient X4, X3, X2, and finally X1 across its compartments from bottom to top (Figure III-7). This gradient introduces varying expansion coefficients (α_{xy}) for each compartment. As a result, when immersed in PBS, the compartment of the porous cube photo-crosslinked at X1, which has the lowest degree of crosslinking, expands more significantly than the compartment photo-crosslinked at X4. This differential expansion transforms the cubic structure into a trapezoidal shape, with the

compartment photo-crosslinked at X1 bulging outward more than the X4 compartment, as illustrated in Figure III-7.

When this structure is subsequently submerged in a Ca^{2+} rich solution, secondary ionic crosslinking is introduced into the network. In this environment, the compartment initially photo-crosslinked at X1 shrinks more than the other compartments, due to higher physical crosslinking in X1 as previously discussed. This differential contraction reverses the initial observed trapezoidal deformation, demonstrating a reversible shape transformation. Consequently, the 4D printed cube demonstrates a primary deformation in PBS and a reversible secondary deformation upon exposure to the Ca^{2+} rich solution. The varying X*n* induce internal stresses that drive the structure to transition between the programmed shapes.

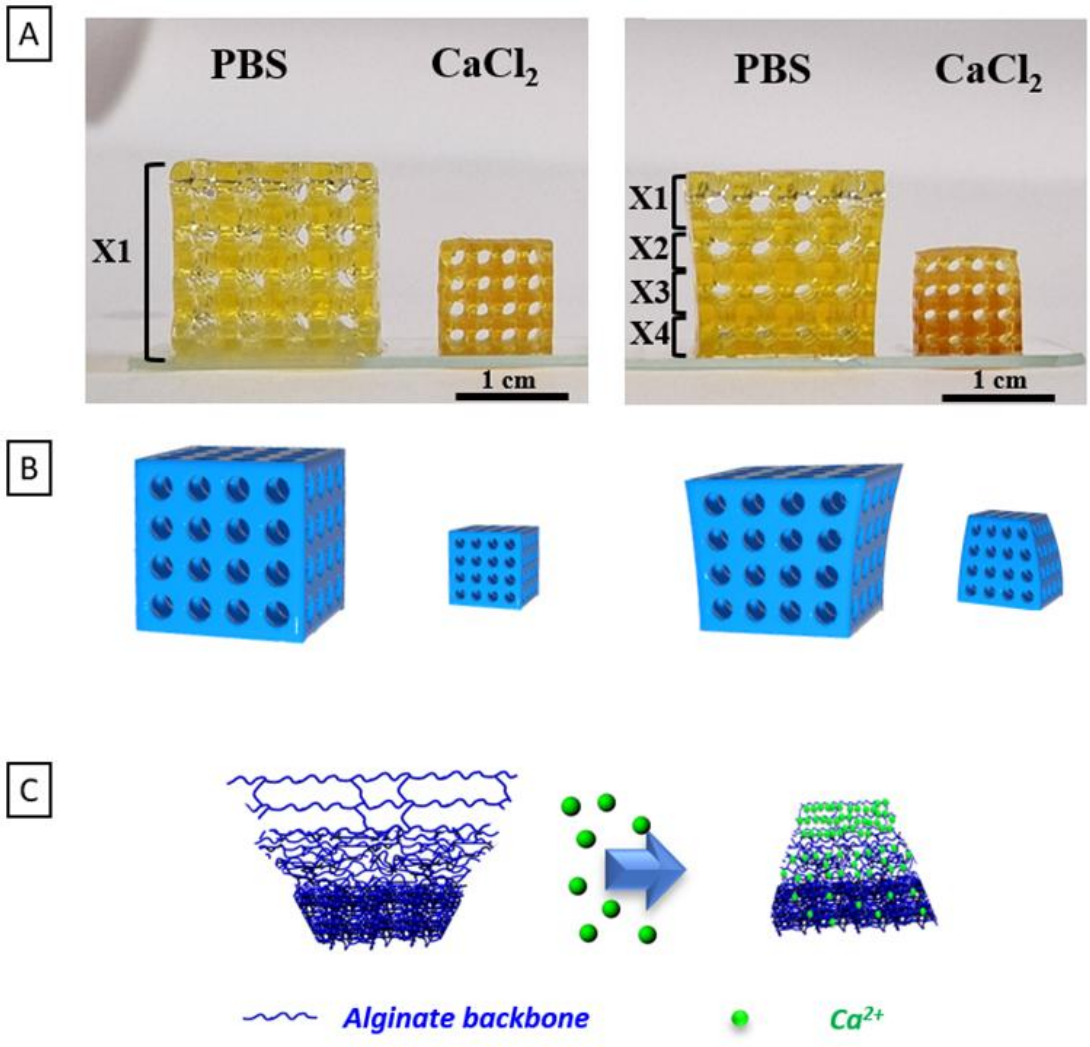

Figure III-7. A) Swelling behavior of a 3D printed porous cube uniformly photo-crosslinked at X1 and with 4 compartments crosslinking profile (X1, X2, X3 and X4 from top to bottom), and schematic illustration of the B) shape morphing of the hydrogels and D) crosslinked network when swollen in PBS and 5% w/w Ca^{2+} solution.

Another 3D structure, representing a tubular device, was designed and printed using DLP (Figure III-S8B). When subjected to an isotropic crosslinking at X1; this uniform photo-crosslinking induces a homogeneous volume expansion in PBS and a subsequent contraction of approximately 40% upon immersion in a Ca^{2+} solution. The versatility of the material is further demonstrated through anisotropic crosslinking, wherein a gradual gradient from X1 to X4 generates a conical morphology upon swelling in PBS (Figure III-8). This conical structure exhibits a reversible change in conicity when exposed to a Ca^{2+} rich solution, as observed in Figure III-8B, showcasing the material's versatile controlled response to environmental stimulation.

Additionally, the potential for creating alternated deformations can be achieved through the strategic incorporation of photo-crosslinking compartments arranged in sequences such as X4-X1-X4 or X1-X4-X1. A triblock gradient X4-X1-X4 will result in a convex deformation due to the higher expansion of the middle part. Whereas, the inverse deformation is obtained for X1-X4-X1 triblock gradient leading to a concave tubular structure. Furthermore, the deformation curvature switches direction upon submerging in Ca^{2+} solution. The X4-X1-X4 tubular structure tends to switch from convex to concave due to the lower expansion of X1 section than the X4 section while the X1-X4-X1 tubular structures tends to switch from concave to convex. This methodology enables the generation of complex printed architectures, highlighting the precision and versatility achievable through controlled crosslinking by DLP process. This approach enables a single .stl design to achieve a range of controlled and dynamic shape deformations.

In hydrogel engineering, manipulating crosslinking profiles offers unprecedented control over shape deformations. This approach enables the realization of complex and dynamic transformations from a single design. Such processing can only be obtained through a 3D additive manufacturing technology based on photo-polymerization.

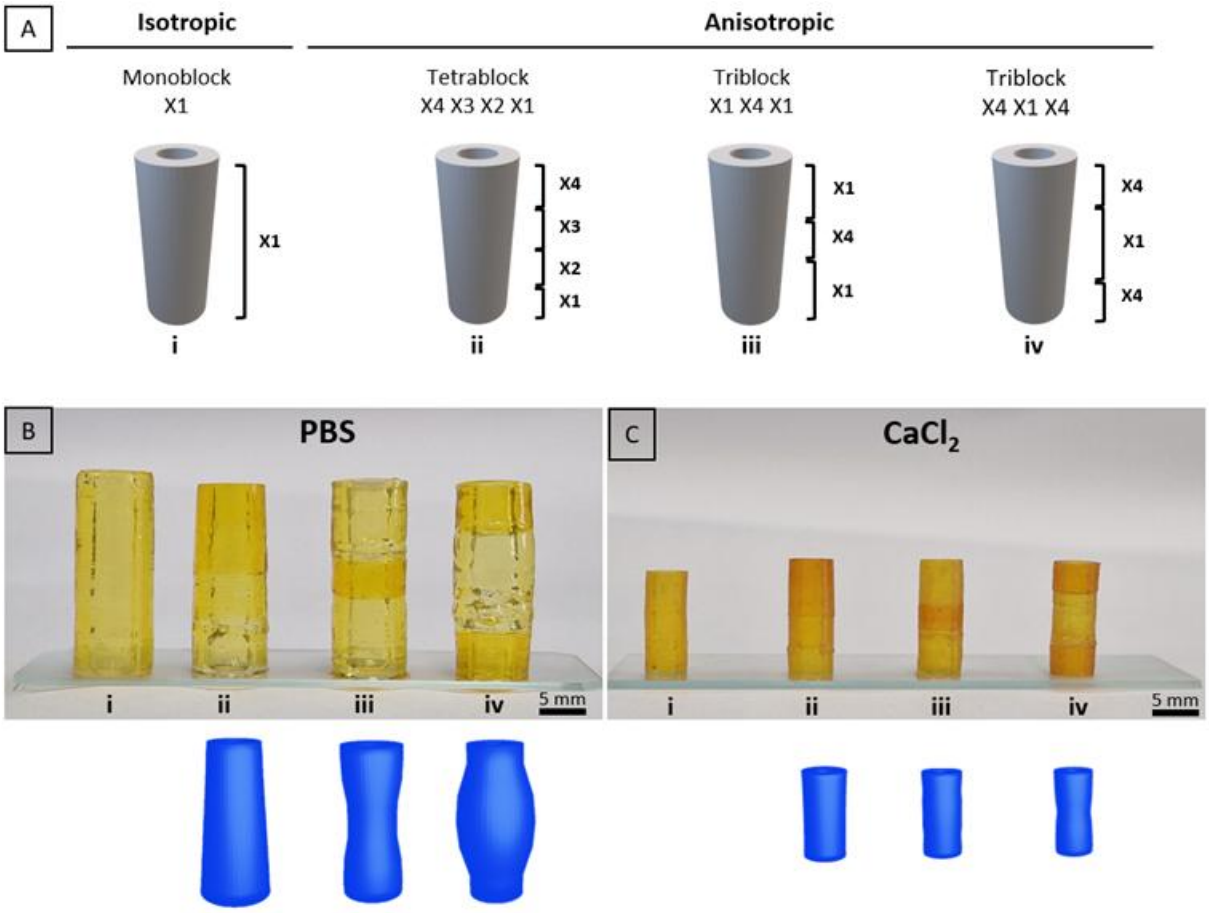

Figure III-8. A) Photo-crosslinking gradient profiles implanted on a tubular structure and their deformations when swollen in B) PBS and C) 5% w/w Ca^{2+} solution.

3.5. Cytotoxicity of the dual crosslinked alginate hydrogel

Given the macroscopic size of the hydrogels and the important Ca^{2+} concentration in the dual crosslinked network, it is important the evaluate the biocompatibility of the 4D printed devices. Therefore, cytotoxicity was evaluated according to ISO-10993 on alginate actuators swollen in PBS and Ca^{2+} solution. The dual crosslinked hydrogels are compared to printed hydrogels without Ca^{2+} addition. Live/Dead assays show that the cells remain viable in the medium containing the released Ca^{2+} that complexed in the hydrogels, comparable to the positive control (Figure III-8A). Quantification shows that NIH 3T3 fibroblast viability reaches 93% for the hydrogel swollen in PBS and decreases slightly, but not significantly, to 87% for the dual crosslinked actuator (Figure III-9B). Moreover, as shown in the Figure III-9C, the morphology of the cells does not change between the control medium and cells in contact of Ca^{2+}, confirming the absence of toxicity and potential biomedical applications.

4D printing hydrogels have already been explored for various biomedical applications.[17,41] Alginate hydrogel is well known to be a promising matrix in biomedical applications, such as tissue engineering scaffolds, drug delivery systems, or wound healing.[42,43] Therefore, our approach of using alginate hydrogels as a 4D printed structure with soft stimulation presents promising potential for biomedical applications.

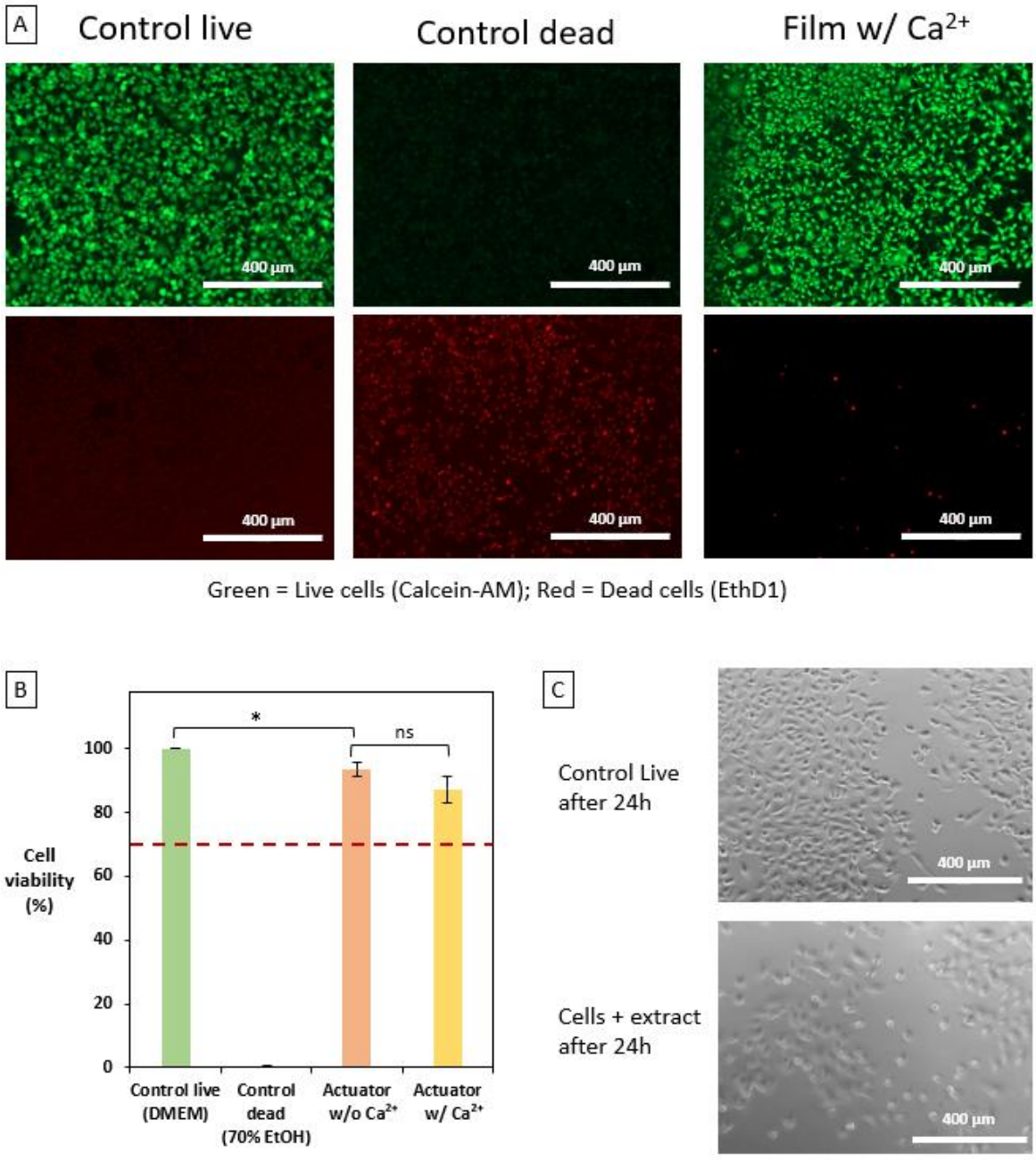

Figure III-9. A) NIH 3T3 cells as observed under an EVOS FL microscope after 24h incubation, B) Extract cytotoxicity essays on hydrogel films swollen in PBS and Ca^{2+} solution prior to extract (n=3) and C) cells morphology after 24h incubation at 37°C in the control group and with the extract. Red dotted line represents the 70 % threshold set by the European standard.

4. CONCLUSION

Sodium alginate (Mw = 55000 g.mol^{-1}) was functionalized with methacrylate units to obtain a photo-crosslinkable resin suitable for DLP. Resin formulation and printing conditions were optimized to have a high resolution and a fast-printing time. By tuning the degree of photo-crosslinking of the 3D printed structures, several dimensions at the equilibrium swollen state in PBS and Ca^{2+} solution can be obtained from a single .stl design. It was observed that by increasing the degree of photo-crosslinking, the hydrogels swell in PBS and expand greater than the .stl design where the hydrogels with the lowest degrees of photo-crosslinking have bigger dimensions. Moreover, it was observed that in Ca^{2+} solution the hydrogels shrinks and by increasing the degree of photo-crosslinking, the shrinking behavior was reduced due to a lower calcium complexation quantified by colorimetric titration. By implementing a crosslinking gradient on a single architecture, for example on a hydrogel film, a bidirectional bending motion can be obtained between PBS and Ca^{2+} solution. In addition, various precise and programmed transformations were obtained on a porous cube and a tubular structure by controlling the degree of photo-crosslinking profile. Lastly, the 4D printed architectures were observed to be biocompatible after cytotoxicity assays on NIH 3T3 cells. This study confirms the potential of the alginate-based hydrogel to create 4D printed structures suitable for biomedical applications.

Supplementary Information Chapter III

Shape-morphing Photo-crosslinked Alginate Hydrogels via 4D Printing

Sodium alginate chemical modification

Methacrylated alginate (Alg-MA) was obtained by reacting low viscosity Alg-Na^+ with methacrylic anhydride. A 4% w/w aqueous Alg-Na^+ was prepared by dissolving 12 g of sodium alginate in 300 mL milli-q water in a 1 L round bottom flask under mechanical stirring (600 rpm). In order to obtain a homogeneous mixture, the solution was left to stir for 4 hours. TEA was then added at 40 molar equivalents with respect to MA and the solution was left to stir for 30 minutes to ensure complete homogenization. Finally, MA was added at 20 molar equivalents with respect to the sugar unit. The reaction was maintained at 24 °C for 24 hours. Functionalized Alg-Na^+ was obtained by precipitating the mixture in cold acetone followed by drying at 24°C under reduced pressure at room temperature.

^{1}H NMR characterization

In order to quantify the degree of modification (DM), ^{1}H NMR was used. 20 mg of Alg-MA was dissolved in 1 mL D_2O and left to stir for 1 hour to obtain a homogeneous mixture. The ^{1}H NMR spectra were recorded on a Bruker Avance I 400 MHz (64 scans, 5 s relaxation time). The DM, defined as the number of methacrylate moieties per sugar unit, was calculated as the ratio of the protons of methacrylate (1.95 ppm, 5.8 ppm and 6.2 ppm) and H_{M1} proton of the alginate using the following equation and was found to be equal to 140% with respect to sugar moiety.

$$DM\ (\%) = M\% * \frac{I_{H\ vinyl\ 6.2\ ppm}}{I_{H_M\ 4.4\ ppm}} \qquad \text{(Equation III-S1)}$$

Where I_H represents the intensity of a vinyl proton of the grafted methacrylate at 6.2ppm, $I_{H_{M1}}$represents the intensity of the anomeric protons of the mannuronate units, and M% represents the fraction of mannuronate units in the polysaccharide. The M% is calculated by comparing the anomeric G proton at 5.8 ppm with the anomeric M proton at 4.47ppm and was found to be equal to 35 %.

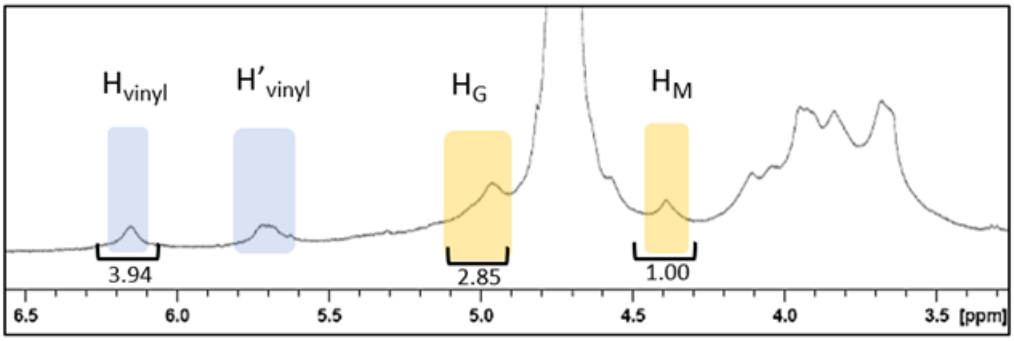

Figure III-S1. ^{1}H-NMR of methacrylated alginate in D_2O.

Optimization of printing conditions (working curves)

The printing conditions (photo-absorber quantity and light intensity) are first optimized on 10% w/w alginate resin. Following our previous study, photo-initiator amount (LAP) is fixed at 3.75% w/w with respect to the alginate[11]. Orange G amount and light intensity are varied and then fixed at 0.2% w/v and 10 mW/cm^2, respectively, to have the best conditions of printing. Next, the working curve of 6% w/w and 8% w/w Alg-MA resin were obtained, demonstrating a linear trend, which validates the chosen printing conditions.

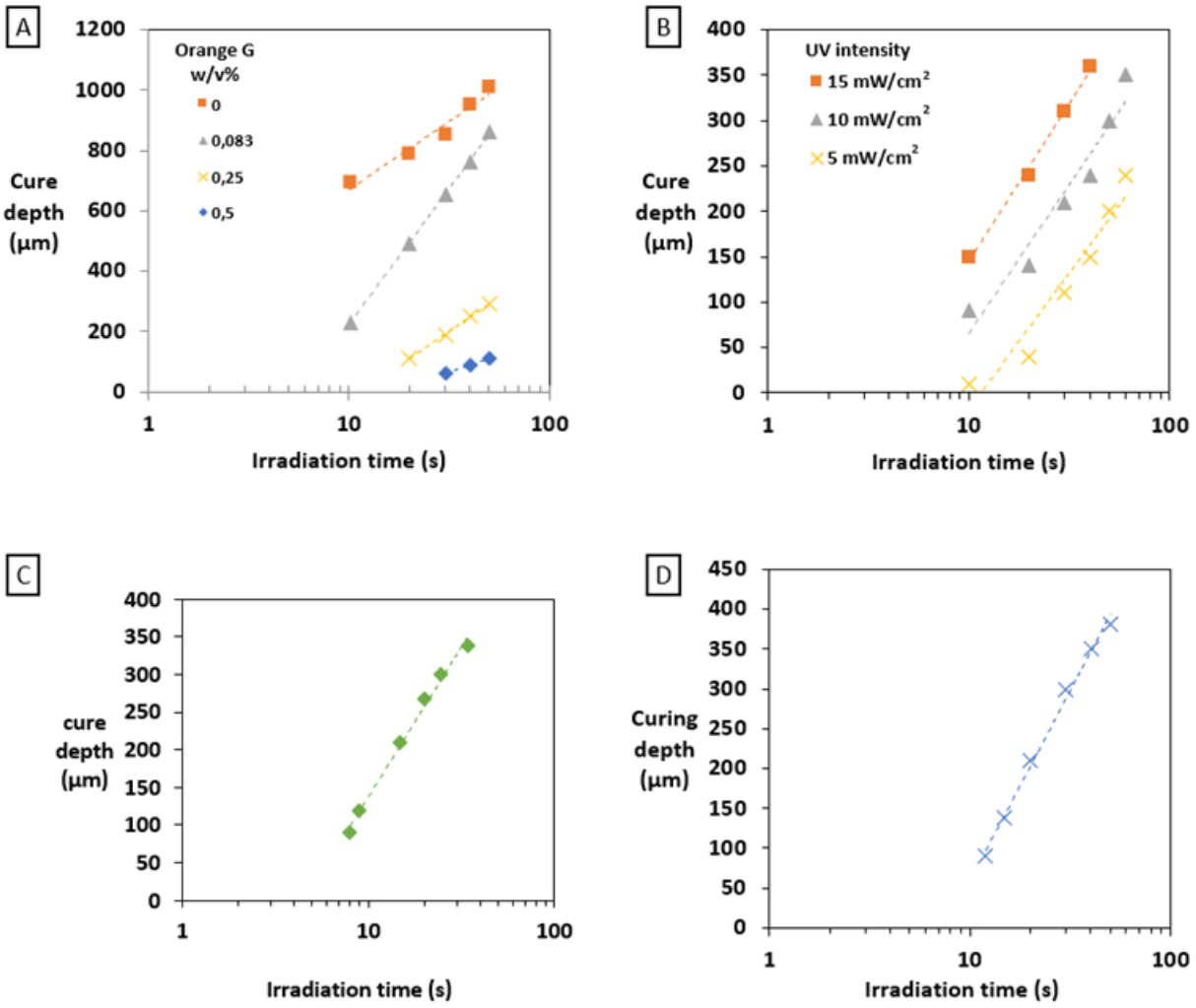

Figure III-S2. A) Influence of photo-absorber (Orange G) amount on the working curve of 10% w/w alginate resin under 10 mW/cm^2 irradiation. B) Influence of light intensity on 10% w/w alginate resin having 0.2% w/v Orange G and working curve of C) 8% w/w and D) 6% w/w Alg-MA resin having 0.2% w/v Orange G under 10 mW/cm^2 irradiation.

Gel Content

Gel content is calculated as the ratio of the dry mass of the hydrogel after washing and the total amount of polymers present in the hydrogel upon curing (resin concentration times volume of design). As seen, by increasing the degree of photo-crosslinking, the gel content increases for all formulations due to a higher efficiency in the crosslinking.

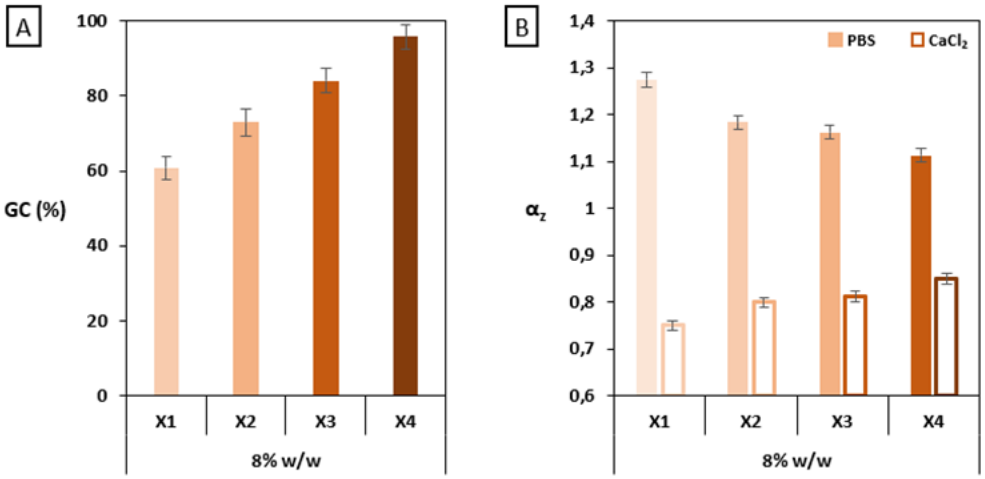

Figure III-S3. A) Gel content of the hydrogels obtained from the different alginate concentrations at various degrees of photo-crosslinking and B) expansion coefficient in the z direction of the hydrogel obtained from the different alginate concentrations at various crosslinking degrees.

Scanning Electron Microscopy and Energy Dispersive Spectrometry

Scanning electron microscopy (SEM) analyses were carried out to study the morphology of the hydrogel network. Prior to imaging, the hydrogel samples were left to swell in PBS or 5% w/w Ca^{2+} solution for 24 hours, washed in Millie-Q water for 2 hours and then freeze dried for 24 hours. Imaging was done using SEM (FEI Quanta FEG 200, Platform MEA, University of Montpellier) with a 10 kV operational acceleration voltage at vacuum to $4.5x10^{-1}$ Torr and a backscattered electron detector (BSED).

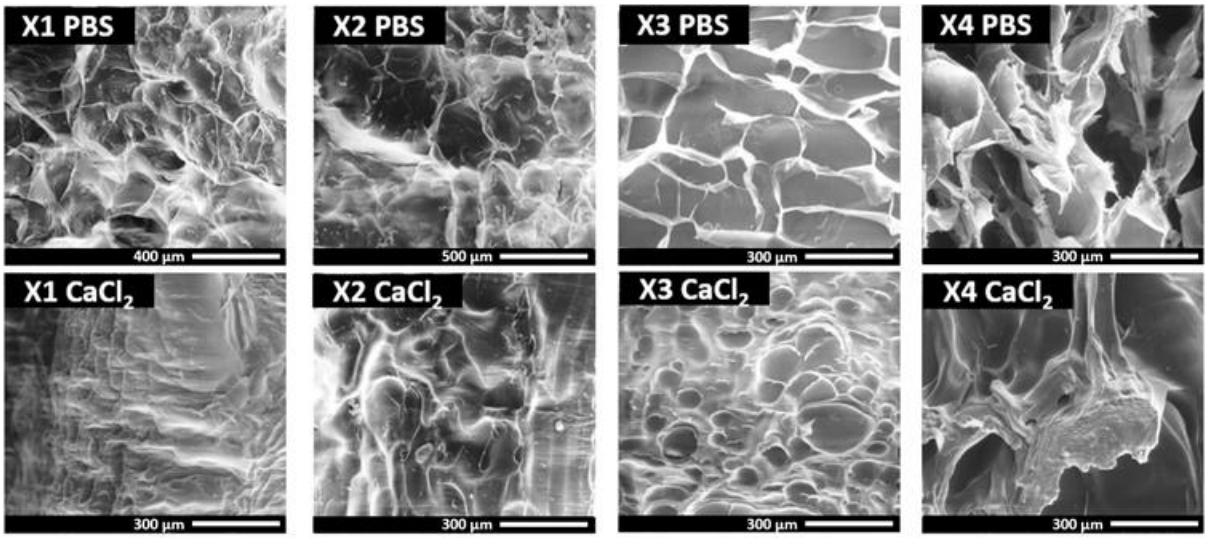

Figure III-S4. SEM images of freeze-dried 3D printed hydrogels at different crosslinking conditions when priorly swollen on PBS or 5% w/w $CaCl_2$ solution.

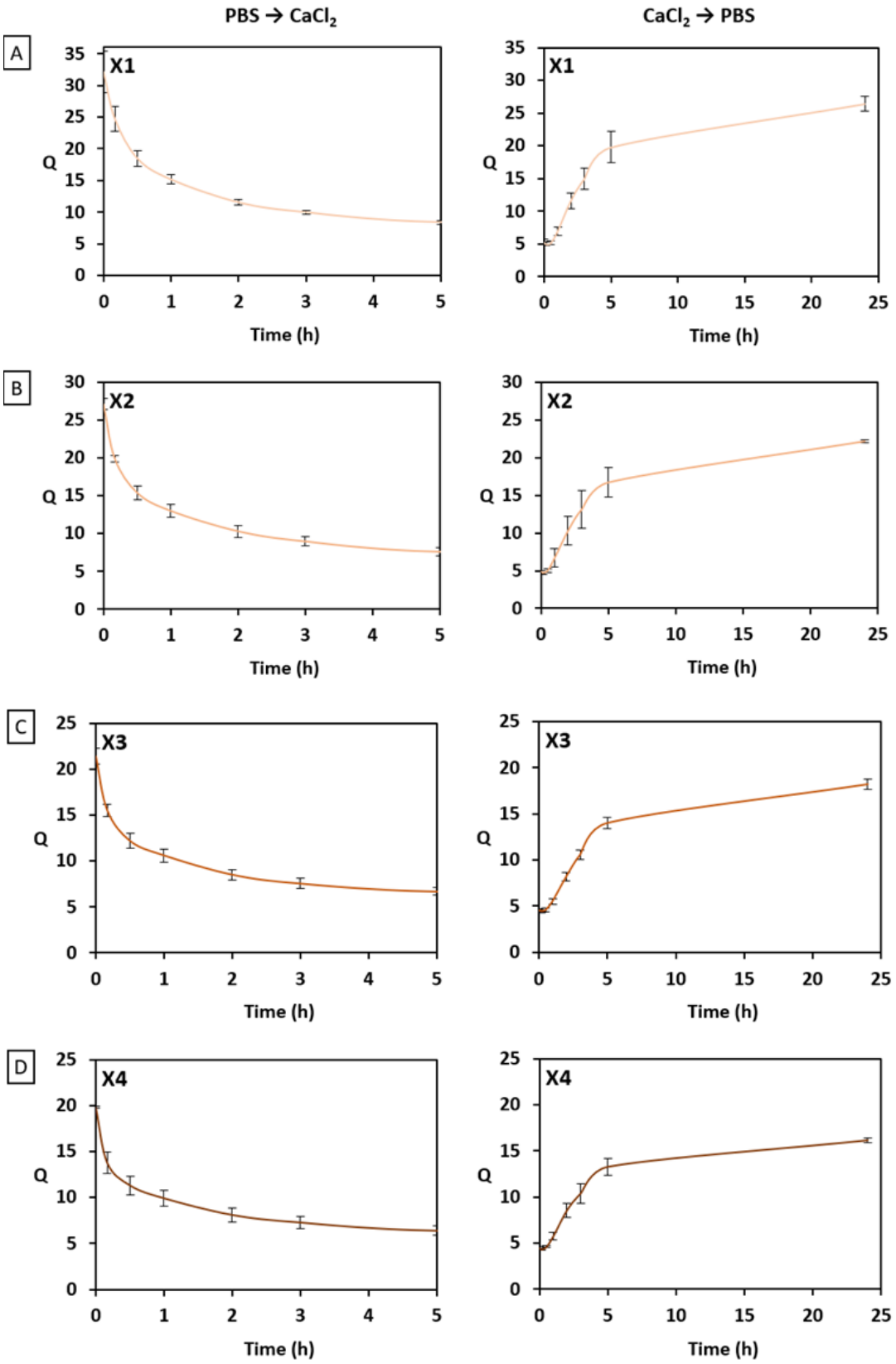

Figure III-S5. Swelling kinetics of 3D printed 8% w/w Alg-MA hydrogels photo-crosslinked at X1, X2, X3 and X4 when immersed in Ca^{2+} solution and PBS.

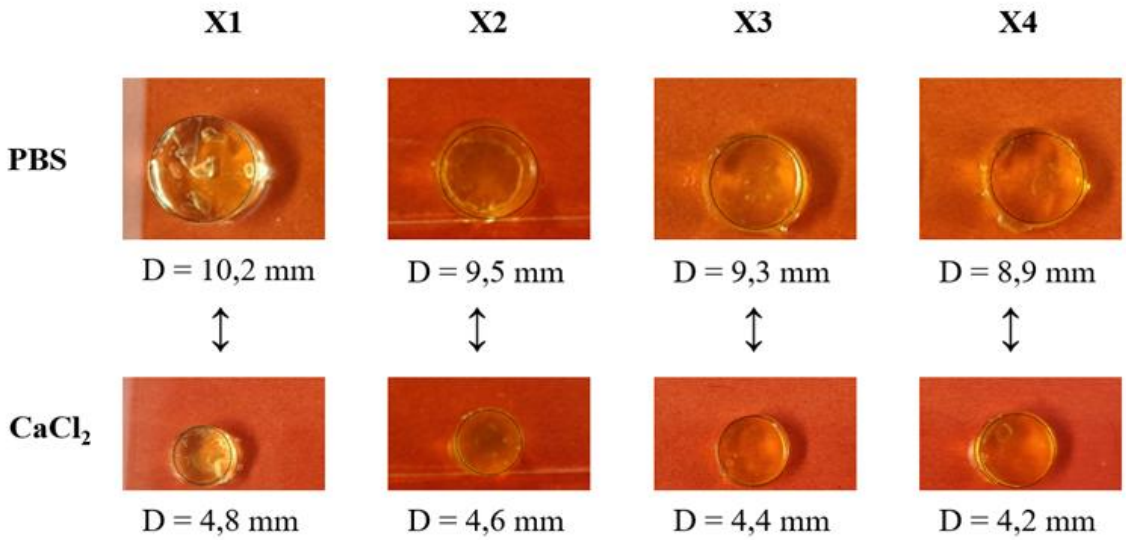

Figure III-S6. Radius of the 3D printed 8% w/w Alg-MA hydrogels photo-crosslinked at X1, X2, X3 and X4 when immersed in PBS and Ca^{2+} solution.

Mesh size

The molecular weight between crosslinking point (Mc) was calculated following the simplified Flory equation[44] for high degrees of swelling:

$$M_c = \frac{\rho V_1}{(0.5 - \chi)\, v_2^{5/3}} \qquad \text{(Equation III-S2)}$$

Where ρ is the dry polymer density (equal to 1.2 g/mL)[45], V_1 is the molar volume of water (equal to 18 ml/mol), χ is the Flory-Huggins parameter (equal to 0.2 in PBS and 0.4 in 5% $CaCl_2$)[46] and v_2 is the polymer fraction in the swollen hydrogel (equal to 1/Q).

Table III-S1. Mesh size calculation for 8% w/w Alg-MA hydrogels crosslinked at X1, X2, X3 and X4 from the compression modulus. a: calculated using RET theory and b. calculated using simplified Flory equation.

		ξ^a (nm)	Mc^b in PBS (g/mol)	Mc^b in $CaCl_2$ (g/mol)
8% w/w	**X1**	7.6	22 100 ± 1280	6240 ± 475
	X2	5.7	15490 ± 283	6025 ± 72
	X3	5	10 402 ± 405	5026 ± 295
	X4	4.3	6873 ± 120	5185 ± 86

4D Printing

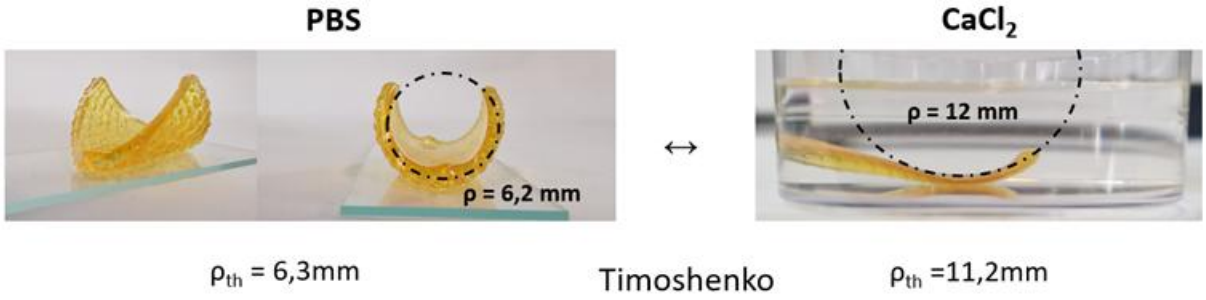

Figure III-S7. Rolling behavior of a 33x22x2 mm bisectional film photo-crosslinked at X1/X4 when submerged in PBS and Ca^{2+} solution with the respective radii of curvature as measured using ImageJ along with the predicted curvature calculated using Timoshenko's equation.

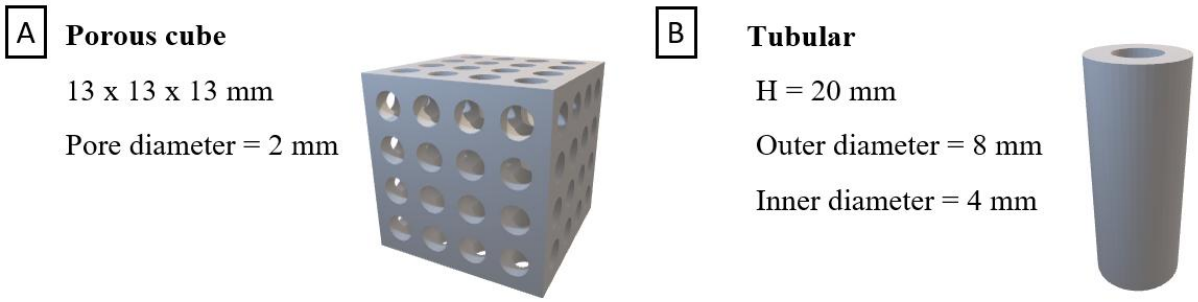

Figure III-S8. .stl design and dimensions of the A) porous cube structure and B) tubular structure.

REFERENCES

[1] M. Champeau, D. A. Heinze, T. N. Viana, E. R. de Souza, A. C. Chinellato, S. Titotto, *Adv. Funct. Mater.* **2020**, *30*, 1910606.

[2] J. Kopeček, J. Yang, *Polym. Int.* **2007**, *56*, 1078.

[3] Y. Dong, S. Wang, Y. Ke, L. Ding, X. Zeng, S. Magdassi, Y. Long, *Adv. Mater. Technol.* **2020**, *5*, 2000034.

[4] C. Benoit, S. Talitha, F. David, S. Michel, S.-J. Anna, A.-V. Rachel, W. Patrice, *Polym. Chem.* **2017**, *8*, 4512.

[5] J. Guo, R. Zhang, L. Zhang, X. Cao, *ACS Macro Lett.* **2018**, *7*, 442.

[6] T. Brossier, M. Habib, B. T. Benkhaled, G. Volpi, V. Lapinte, S. Blanquer, *Mater. Adv.* **2023**, 10.1039.D3MA00665D.

[7] S. H. Kim, Y. B. Seo, Y. K. Yeon, Y. J. Lee, H. S. Park, Md. T. Sultan, J. M. Lee, J. S. Lee, O. J. Lee, H. Hong, H. Lee, O. Ajiteru, Y. J. Suh, S.-H. Song, K.-H. Lee, C. H. Park, *Biomaterials* **2020**, *260*, 120281.

[8] W. Zhou, Z. Qiao, E. Nazarzadeh Zare, J. Huang, X. Zheng, X. Sun, M. Shao, H. Wang, X. Wang, D. Chen, J. Zheng, S. Fang, Y. M. Li, X. Zhang, L. Yang, P. Makvandi, A. Wu, *J. Med. Chem.* **2020**, *63*, 8003.

[9] H. M. El-Husseiny, E. A. Mady, L. Hamabe, A. Abugomaa, K. Shimada, T. Yoshida, T. Tanaka, A. Yokoi, M. Elbadawy, R. Tanaka, *Materials Today Bio* **2022**, *13*, 100186.

[10] C. Ouwerx, N. Velings, M. M. Mestdagh, M. A. V. Axelos, *Polymer Gels and Networks* **1998**, *6*, 393.

[11] M. Habib, S. Berthalon, L. Leclercq, A. Tourrette, T. Sharkawi, S. Blanquer, *Biomacromolecules* **2024**, *25*, 1660.

[12] M. Hasany, S. Talebian, S. Sadat, N. Ranjbar, M. Mehrali, G. G. Wallace, M. Mehrali, *Applied Materials Today* **2021**, *24*, 101150.

[13] T. Li, Z. Huang, G. C.-P. Tsui, C.-Y. Tang, Y. Deng, *REVIEWS ON ADVANCED MATERIALS SCIENCE* **2024**, *63*, 20240028.

[14] Z. Han, J. Zhang, *ACS Appl. Polym. Mater.* **2023**, *5*, 4605.

[15] D. Podstawczyk, M. Nizioł, P. Szymczyk-Ziółkowska, M. Fiedot-Toboła, *Adv. Funct. Mater.* **2021**, *31*, 2009664.

[16] J. Li, C. Wu, P. K. Chu, M. Gelinsky, *Materials Science and Engineering: R: Reports* **2020**, *140*, 100543.

[17] E. Yarali, M. J. Mirzaali, A. Ghalayaniesfahani, A. Accardo, P. J. Diaz-Payno, A. A. Zadpoor, *Advanced Materials* **2024**, *36*, 2402301.

[18] P. Cao, L. Tao, J. Gong, T. Wang, Q. Wang, J. Ju, Y. Zhang, *ACS Appl. Polym. Mater.* **2021**, *3*, 6167.

[19] G. Constante, I. Apsite, H. Alkhamis, M. Dulle, M. Schwarzer, A. Caspari, A. Synytska, S. Salehi, L. Ionov, *ACS Appl. Mater. Interfaces* **2021**, *13*, 12767.

[20] J. Lai, X. Ye, J. Liu, C. Wang, J. Li, X. Wang, M. Ma, M. Wang, *Materials & Design* **2021**, *205*, 109699.

[21] A. Kirillova, R. Maxson, G. Stoychev, C. T. Gomillion, L. Ionov, *Adv. Mater.* **2017**, *29*, 1703443.

[22] D. Han, R. S. Morde, S. Mariani, A. A. La Mattina, E. Vignali, C. Yang, G. Barillaro, H. Lee, *Advanced Functional Materials* **2020**, *30*, 1909197.

[23] G. Lu, R. Tang, J. Nie, X. Zhu, *Macromol. Rapid Commun.* **2024**, *45*, 2300661.

[24] M. Wang, W. Li, L. S. Mille, T. Ching, Z. Luo, G. Tang, C. E. Garciamendez, A. Lesha, M. Hashimoto, Y. S. Zhang, *Advanced Materials* **2022**, *34*, 2107038.

[25] H. Wang, Y. Xia, Z. Zhang, Z. Xie, *J. Mater. Chem. B* **2023**, *11*, 8883.

[26] Z. Zhao, J. Wu, X. Mu, H. Chen, H. J. Qi, D. Fang, *Sci. Adv.* **2017**, *3*, e1602326.

[27] P. Jiang, Y. Zhang, D. Liu, R. Guo, Z. Ji, X. Wang, X. Wang, *Advanced Materials Technologies* **2022**, *7*, 2101288.

[28] Z. Ji, C. Yan, B. Yu, X. Zhang, M. Cai, X. Jia, X. Wang, F. Zhou, *Adv. Mater. Technol.* **2019**, *4*, 1800713.

[29] L. Ren, Z. Li, Q. Liu, L. Ren, Q. Wu, B. Li, G. Li, Z. Song, X. Zhou, *Adv Materials Technologies* **2021**, *6*, 2001289.

[30] J. Odent, S. Vanderstappen, A. Toncheva, E. Pichon, T. J. Wallin, K. Wang, R. F. Shepherd, P. Dubois, J.-M. Raquez, *J. Mater. Chem. A* **2019**, *7*, 15395.

[31] T. Majima, W. Schnabel, W. Weber, *Makromol. Chem.* **1991**, *192*, 2307.

[32] A. Szarpak, R. Auzély-Velty, *Carbohydrate Polymers* **2023**, *320*, 121212.

[33] J. Karvinen, T. O. Ihalainen, M. T. Calejo, I. Jönkkäri, M. Kellomäki, *Materials Science and Engineering: C* **2019**, *94*, 1056.

[34] S. Timoshenko, *J. Opt. Soc. Am.* **1925**, *11*, 233.

[35] X. Li, Y. Zhang, Q. Yang, D. Li, G. Zhang, S. Long, *Iran Polym J* **2018**, *27*, 829.

[36] Q. Zhao, Y. Liang, L. Ren, Z. Yu, Z. Zhang, F. Qiu, L. Ren, *J. Mater. Chem. B* **2018**, *6*, 1260.

[37] F. Cheng, H. Chen, H. Li, *J. Mater. Chem. B* **2021**, *9*, 1762.

[38] H. Baniasadi, R. Abidnejad, M. Fazeli, J. Lipponen, J. Niskanen, E. Kontturi, J. Seppälä, O. J. Rojas, *Advances in Colloid and Interface Science* **2024**, *324*, 103095.

[39] J. Bai, X. Wang, M. Zhang, Z. Yang, J. Zhang, *Materials* **2024**, *17*, 2006.

[40] X. Wang, H. Huang, H. Liu, F. Rehfeldt, X. Wang, K. Zhang, *Macromol. Chem. Phys* **2019**, *220*, 1800562.

[41] Z. U. Arif, M. Y. Khalid, A. Zolfagharian, M. Bodaghi, *Reactive and Functional Polymers* **2022**, *179*, 105374.

[42] S. Lj. Tomić, M. M. Babić Radić, J. S. Vuković, V. V. Filipović, J. Nikodinovic-Runic, M. Vukomanović, *Marine Drugs* **2023**, *21*, 177.

[43] R. Ahmad Raus, W. M. F. Wan Nawawi, R. R. Nasaruddin, *Asian Journal of Pharmaceutical Sciences* **2021**, *16*, 280.

[44] L. R. G. Treloar, *The physics of rubber elasticity: by L.R.G. Treloar*, 3rd ed., Clarendon Press ; Oxford University Press, Oxford : New York, **2005**.

[45] B. Trica, N. Tritean, D. Constantinescu-Aruxandei, F. Oancea, *Coatings* **2023**, *13*, 562.

[46] A. W. Chan, R. J. Neufeld, *Biomaterials* **2009**, *30*, 6119.

CHAPTER IV / CHAPITRE IV

Introduction Chapitre IV

L'étude sur les hydrogels à base d'alginate méthacrylé (Alg-MA) présentée dans le chapitre précédent met en évidence les capacités de ces matériaux à subir des déformations programmables grâce à des gradients de réticulation et à des interactions ioniques en présence du calcium. Cette étude a permis d'ouvrir la voie vers de potentielles applications biomédicales innovantes, notamment dans la conception de dispositifs intelligents imprimés en 4D. Cependant, afin d'améliorer les propriétés de déformation de ces hydrogels ou encore de complexifier les transformations, l'ajout d'un second stimulus thermique au système pourrait s'avérer bénéfique, permettant ainsi une adaptation plus précise et efficace dans un environnement physiologique.

Dans notre quête de polymères thermosensibles, nous avons d'abord exploré la chimie des polysaccharides, notamment la kappa-carraghénane (k-carraghénane), connue pour sa transition sol-gel modulable. Les chaînes de k-carraghénane forment des hélices dans l'eau, qui vont par la suite se désorganiser avec a température, permettant la solubilisation du polysaccharide comme illustré dans la Figure IV-Ai. La réversibilité de la formation de double hélice se produit en baissant la température créant ainsi un hydrogel réticulé physiquement. En fonction de la concentration, cette transition peut être contrôlée, comme présenté sur les mesures rhéologiques dans la Figure IV-Aii. Cependant, après méthacrylation, nous avons observé une perte totale de la thermosensibilité de la k-carraghénane (Figure IV-Aii). La fonctionnalisation par des groupements méthacryliques sur les groupes hydroxyles inhibe donc la reformation des ponts hydrogène entre les chaînes, empêchant ainsi la formation des hélices et des doubles hélices. Cette limitation nous a conduits à explorer d'autres polymères reconnus comme thermosensibles, comme les Pluronics, pour étudier l'impact de cette double stimulation sur les propriétés des hydrogels d'alginate.

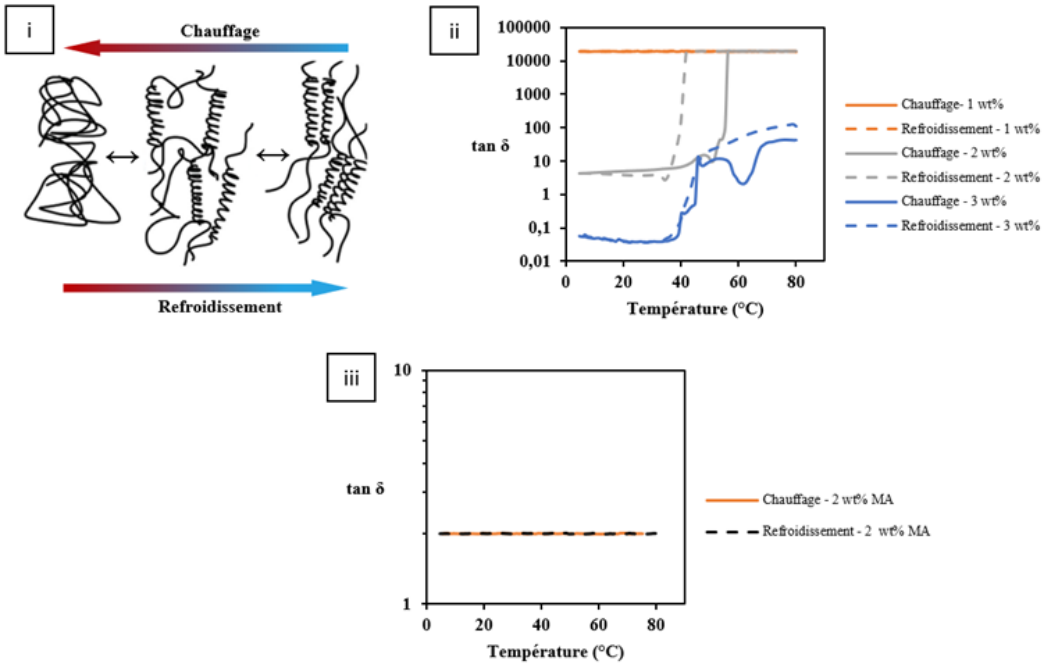

Figure IV-A. i) Schéma illustratif de la transition sol-gel et ii) balayage en température de la k-carraghénane non méthacrylé à différentes concentrations et iii) de la k-carraghénane méthacrylé à 2 wt% dans l'eau.

Le Pluronic est un copolymère tribloc formé de polyéthylène glycol (PEG) et de polypropylène glycol (PPG), connu pour ses propriétés thermosensibles et sa capacité à former des micelles dans l'eau. En plus de leur incorporation dans les résines pour leurs effets thermiques, les Pluronics sont souvent utilisés pour encapsuler des principes actifs dans les micelles afin de permettre une libération contrôlée. Afin d'anticiper cette combinaison d'hydrogel Pluronic et Alginate photo-réticulé, nous avons dans un premier temps étudier le comportement thermique des hydrogels de Pluronic photo-réticulés. C'est dans ce contexte que s'inscrit le chapitre suivant, consacré à l'étude de trois Pluronics différents : P123, P104 et F127, fonctionnalisés avec des groupes méthacrylates, et par la suite photo-réticulés. L'objectif de cette étude est donc d'étudier l'amplitude de déformation des hydrogels de Pluronic sous stimulation thermique.

Chapter IV

Photo-crosslinked Pluronic Hydrogels: Micellar Organization and Thermal Response

KEYWORDS

Methacrylated Pluronic, thermo-sensitive hydrogels, phase diagrams, rheology

ABSTRACT

Pluronic P123, P104, and F127, bearing hydroxyl groups (identified as -OH), were functionalized with methacrylic moieties (named -MA) at the chain ends to form chemically cross-linked hydrogels. Before crosslinking, the influence of the chain end functionalization was evaluated on the micellar solutions' phase diagrams using rheological measurements. Phase diagrams showed micellar organization shifts for the three Pluronics upon adding methacrylic moieties to the hydroxyl groups. Furthermore, photo-rheology showed that the micellar organization influenced the chemical crosslinking reactions. Organized micellar states showed faster photo-crosslinking reaction and produced higher gel content hydrogels. Moreover, temperature sweeps on the crosslinked systems showed that F127-MA, P123-MA, and P104-MA hydrogels lose their thermoresponsiveness to the corresponding phases when crosslinked in an organized state. Finally, the thermal behavior observed through the rheological study was correlated to the hydrogels' swelling behavior. Thermal responses of the Pluronic hydrogels corresponded to up to 30% and 20 % water release when crosslinked in an isotropic or organized state, respectively.

1. INTRODUCTION

Pluronic is a family of triblock copolymers composed of alternating polyethylene oxide (PEO) and polypropylene oxide (PPO) blocks.[1,2] They have gained much attention in scientific and industrial communities due to their atypic behavior in aqueous solution when their concentration or the temperature are increased. Indeed, Pluronic polymers self-assemble into micelles in aqueous solutions above their respective (critical micelle concentration) CMC. Based on the length of each block, Pluronic micelles can also organize themselves into different conformations under increase of the concentration and/or temperature producing gel-like materials.[3]

As a result, Pluronic copolymers have been used in a wide range of applications, such as cosmetics as thickening systems or hydrogels. Their biocompatibility has also led to their use in the biomedical field.[4]

From a scientific standpoint, the limits of the thermal regions related to the different lyotropic mesophases can be determined using complex light scattering techniques while their exact nature requires the use of Small Angle Neutron Scattering experiments (SANS). Several organizations are described such as cubic, lamellar, hexagonal, etc…[5–7] For example, Wanka *et al.* successfully obtained the phase diagrams of P104, L121, L122, P123, F127, PE 6200, PE6400, P65, and F68 in aqueous solutions using static light scattering.[8] Yardimci et al. studied the influence of the Pluronic chains on the thermal behavior of F68 and F108.[9] From SANS analyses, they obtained the phase diagrams of both Pluronics. They observed a shift of the micelles' organization towards lower temperatures and concentrations when increasing the Pluronic chain's molecular weight.

More accessible and simpler techniques can also be used to observe the physical changes that occur during micellar organization in aqueous solution. Indeed, such transition also influences the system's physical properties and in particular their viscoelastic behavior. Simple rheological measurements (thermomechanical analyses, spectromechanical experiments, viscosimetric measurements…) can detect these physical changes. Habas et al. compared temperature sweeps under shear stress with small-angle neutron scattering (SANS) studies.[10] They successfully observed the Pluronic phase transitions using rheology and precisely determined the organization states using SANS, confirming the use of rheology to detect Pluronic lyotropic transitions.[11–13]

One possible strategy to modify the properties of Pluronic is to functionalize the hydroxyl end groups. For instance, Park *et al.* functionalized F127 with carboxyl end groups to induce pH

sensitivity.[14] They observed that the phase diagram shifts to higher concentrations due to the increase of the hydrophilicity of the micelles using the inverted tube test method. For example, native F127 at 18% w/w gelifies above 27 °C, whereas functionalized F127 with carboxylic chain ends gels above 35 °C for the same concentration. Meng *et al.* functionalized F107 and F127 with phosphorylcholine end groups.[15] Using rheological experiments, they observed an increase in the gelling temperature of the modified Pluronics due to the hydrophilic nature of the phosphorylcholine groups.

Acrylic or methacrylic end groups can also be added at the chain ends to obtain chemically crosslinked Pluronic hydrogels. The crosslinked hydrogels present a thermal response due to the micelles' orgaization when temperature increases. Di Biase et al. studied the influence of acrylic units on the properties of photopolymerized Pluronic F127 under different crosslinking conditions.[16] They showed that diacrylated F127 did not lead to the formation of hydrogels between 5 and 25% w/w contrarily to native copolymers. Vendenhaute et al. obtained chemically crosslinkinked Pluronic hydrogels on methacrylated F127, L35, L43, and L62.[17] But, although differential scanning calorimetry showed specific thermal responses of the different crosslinked hydrogels, no thermal behavior was investigated on the methacrylated polymers before crosslinking.

Even though abundant studies concern Pluronic F127, further data are required about the other Pluronics and even less so on the structure-property relationship of the functionalized polymers before crosslinking. Volkmer et al. used functionalized P123 with hexamethylene diisocyanate, butane diisocyanate, and hydrogenated diphenylmethane diisocyanate as a cell carrier for its gelling ability at temperatures close to physiological conditions.[18] Garripelli et al. oligomerized Pluronics P104 and P85 to obtain higher molecular weights block copolymer chains.[19] Using the inverting test tube method, they could define the phase diagrams of the native and modified Pluronics. A notable shift towards lower temperature values was observed for both Pluronics once oligomerized due to extended and enforced chain entanglements.

In our own study, we investigated the thermal behavior of Pluronic F127, P123, and P104 before and after methacrylation and photo-crosslinking. We used rheology as a simple and effective method to compare the micellar organization of native copolymers with that of their methacrylated forms, and to examine the evolution of different phase diagrams more widely. In addition, we evaluated the influence of the micellar configuration on the chemical crosslinking using photo-rheology. Finally, the thermal responses of the crosslinked F127, P123, and P104 hydrogels were registered using rheological measurements. The swelling behaviors of each system under different crosslinking conditions were evaluated to investigate

the possible influence of the micellar organizational state on the thermal behavior of the photo-crosslinked network.

2. MATERIALS AND METHODS

2.1. Materials

Pluronics P123 (20 PEO – 70 PPO – 20 PEO), F127 (106 PEO – 70 PPO – 106 PEO), and methacrylic anhydride (MA) were purchased from Sigma-Aldrich. Pluronic P104 (27 PEO – 61 PPO – 27 PEO) was generously donated by BASF chemicals. Triethylamine (TEA) and dichloromethane (DCM) were purchased from Fisher Chemicals. Milli-Q water (conductivity = 18.2 mΩ.cm at 23 °C) was used during this study. Lithium phenyl-2,4,6-trimethylbenzoylphosphinate (LAP) was synthesized as described by Majima *et al.* All chemicals were used without further purification unless mentioned otherwise[20].

2.2. Methods

Pluronic Methacrylation

Pluronic P104, P123, and F127 were methacrylated by grafting methacrylate moieties on the hydroxyl groups present at the chain ends using the same reaction conditions. Each Pluronic (50 g) was dissolved in DCM (100 mL) under magnetic stirring (700 rpm) for 4 hours. Then, 20 eq TEA was added with respect to the hydroxyl groups, and the solution was left under stirring for 30 minutes to ensure complete homogenization. Finally, 10 eq MA were added with respect to the hydroxyl groups. The reaction was maintained at 25 °C for 24 hours. Consequently, the Pluronic was precipitated in petroleum ether, solubilized in water, and then purified by dialysis for 3 days in 500 Da membranes against distilled water while changing the water twice a day. Purified Pluronic was freeze-dried and then stored at -18 °C before use.

^{1}H-NMR

To quantify the degree of modification (DM), ^{1}H-NMR was used. 5 mg of methacrylated Pluronic were dissolved in 1mL of D_2O and stirred for 1 hour. The degree of modification (DM), defined as the percentage of methacrylate moieties onto the hydroxyl groups, was calculated by comparing the peaks of the grafted methacrylate protons at 1.95, 5.8, and 6.2 ppm to the methylene protons (-CH_3) of the PPO units at 1.07 ppm.

Phase diagrams

To establish the phase diagrams, rheological measurements were done on a stress-controlled rheometer (MCR302 from Anton Paar) using the standard couette measuring system CC27/T200/SS. 15mL of samples were used and covered with paraffin oil to prevent water evaporation. Temperature sweeps were done from 5 to 85 °C at a 2 °C/min heating rate under 100 Pa shear stress and 10 rad/s angular frequency. Such conditions were previously determined using stress sweep experiments to study the different systems in their linear viscoelastic domain. As explained previously, the change in the storage modulus G' and loss modulus G" were used to detect the different state change (i.e. micellization and organization).

Photo-rheology

All tests were done on a Thermo Fisher HAAKE MARS 60 rheometer using 20 mm parallel circular plate-plate geometry. We obtained measurements during 400 s irradiation under 0.5 mW/cm^2 UV with a mercury lamp equipped with a 320-480 nm filter. Before testing, the samples were prepared to obtain 25 % w/w aqueous Pluronic solutions containing 3.75 % w/w LAP, and were placed at 10 °C to maintain a homogeneous liquid solution. Tests were done at a 0.5 mm gap under a constant load of 0.1 N, strain 1%, and 1 Hz frequency to ensure the linear viscoelastic domain. Measurements were done at various temperatures corresponding to different zones of the phase diagrams.

Temperature sweeps on crosslinked systems

After irradiation during the photo-rheology, the sample temperature was slowly decreased to 10 °C. Then, thermomechanical analyses were performed between 10 and 80 °C at a 2 °C/min heating rate under a constant normal force of 0.1 N, 2% deformation, 0.5 mm gap distance, and 1Hz frequency to meet the conditions characteristic of the linear viscoelastic domain. The thermal response of the crosslinked hydrogels is registered by the evolution of the storage modulus (G') and loss modulus (G") versus temperature.

Hydrogel preparation

The photo-crosslinkable Pluronic resin consists of 25% w/w methacrylated Pluronic with 3.75% w/w LAP with respect to the Pluronic. The Pluronic resin was injected in a cylindrical Teflon mold (1 cm diameter and 4 mm thickness), covered with a glass slide to ensure a flat surface and avoid solvent evaporation. Before photo-crosslinking, the mold containing the resin was maintained at 10 °C or 50 °C (temperatures corresponding to two different organizational phases deduced from the corresponding phase diagrams) for 1 hour to

generate a homogeneous assembly of the Pluronic micelles. Then, the resin was cured under UV exposure (365 nm) for 10 minutes using a UV Crosslinker Bio-Link chamber (Thermo Fischer, France) at 2-3 $mW.cm^{-2}$. Before the swelling/mechanical assays, the hydrogels were left in water for 24 hours (changing the water twice) to ensure the removal of all unreacted species. Then, they were dried on a Teflon sheet in a 45 °C oven under vacuum for 24 hours to ensure the removal of water from the network.

Cyclic swelling

The water uptake was measured starting from the dried hydrogels. The swelling cycles were between 10 °C and 50 °C. For each measurement, the hydrogels were left to swell for 24 hours to reach an equilibrium state. The swelling ratio (Q) was determined using Equation IV1, where $m_{swollen}$ represents the weight of the hydrogel sample after reaching equilibrium swelling. In contrast, m_{dry} represents the weight of the hydrogel after a drying treatment. The drying process involved placing the hydrogel in an oven set to 45 °C under vacuum conditions for 24 hours to ensure the removal of the water.

$$Q = \frac{m_{swollen}}{m_{dry}} \quad \text{(Equation IV-1)}$$

Water release when heated is calculated as the percentage of the water expulsed from the hydrogels. It is calculated using equation 2.

$$water\ release = 100\left(1 - \frac{Q_{50°C}}{Q_{10°C}}\right) \quad \text{(Equation IV-2)}$$

3. RESULTS AND DISCUSSION

3.1. Elaboration of the Pluronic Methacrylation

To obtain chemically photo-crosslinked Pluronic hydrogels, the hydroxyl groups present at the chain ends of the unimers were functionalized with methacrylate group as illustrated in Figure IV-1. ^{1}H-NMR was used to determine the degree of methacrylation. The reference peak for integration was the PPO block present at 1.08 ppm in D_2O, as observed in Figure IV-1 (174, 210, and 201 protons for P104, P123, and F127, respectively). The degree of methacrylation of the three Pluronic batches was found between 89 and 93%.

Before methacrylation, the R_H of F127-OH was evaluated to be close to 7.9 nm, which is slightly higher than that characteristic of P104-OH and P123-OH (4.5 and 4.6 nm, respectively). This size difference is logically correlated to the higher molecular weights of the different

Pluronics, which are 13 388 $g.mol^{-1}$ for F127-OH, 5 900 $g.mol^{-1}$ for P104-OH, and 5 820 $g.mol^{-1}$ for P123-OH.

Table IV-1. Molecular weight, composition, hydrodynamic radius and aggregation temperature for each F127, P123 and P104 (PEO_x – PPO_y – PEO_x).

	Mw ($g.mol^{-1}$)	**x**	**y**	**PEO / PPO**	**R_H (nm)**	**$T_{aggregation}$ – OH (°C)**	**$T_{aggregation}$ -MA (°C)**
F127	13388	106	70	3.03	7.9	30	30
P123	5820	20	70	0.57	4.6	10	7
P104	5900	27	61	0.88	4.5	25	20

DLS experiments show that the methacrylation of Pluronics does not seem to affect the micelles' hydrodynamic radius (R_H), as seen in Figure IV-S1. Table IV-1 proposes the values registered for all samples at 5 °C. Moreover, it can be seen that aggregation of the micelles starts at 30 °C for F127-MA, 10 °C for P123-MA, and 25 °C for the P104-MA. Then, the aggregation temperature for F127-MA seems to be unaffected by the methacrylation contrarily to P123-MA and P104-MA, which decreased by almost 3 °C and 5 °C, respectively. This shows that the methacrylation of the hydroxyl groups has an effect on more hydrophobic Pluronics like P123 and P104 rather than the more hydrophilic F127. The difference in aggregation temperature can be correlated to length of the hydrophilic PEO segment and to the ratio of PEO/PPO. On one hand, by comparing F127 with P123, for a fixed PPO length, increasing the PEO segment will result in aggregation at higher temperatures due to the increase in hydrophilicity of the micelles. On the second hand, comparing P123 with P104, for a similar M_w, decreasing PEO / PPO will result in aggregations at lower temperatures. Moreover, upon functionalization, the methacrylate groups are more diluted in the PEO segment of F127 compared to the other two which reduces the impact on the aggregation temperature.

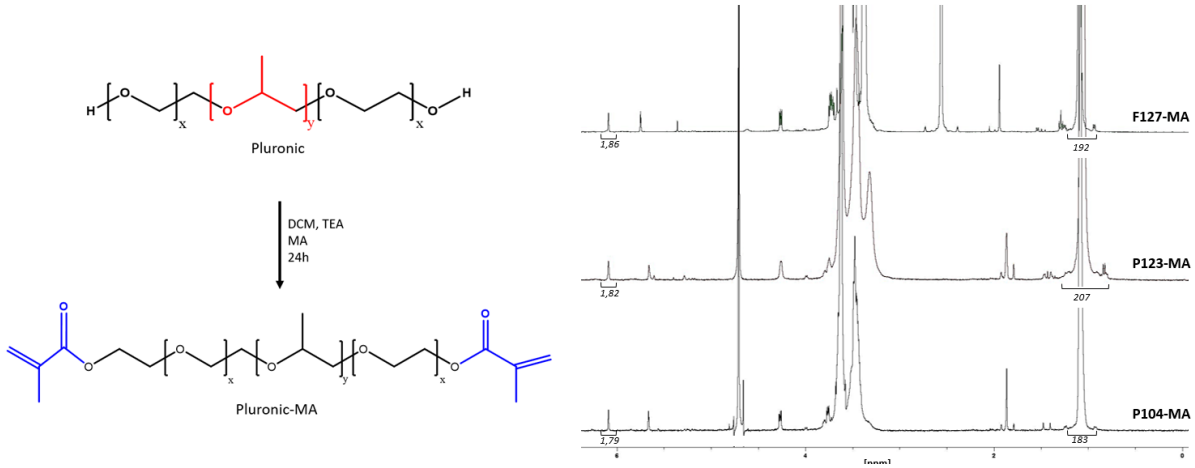

Figure IV-6. Methacrylation of Pluronic P104, P123, and F127 and 1H-NMR spectra of the methacrylated products F127-MA, P123-MA, and P104-MA from top to bottom.

3.2. Influence of the end functionalization on the Pluronics phase diagrams

Above the critical micellar concentration (CMC), Pluronic unimers self-assemble into micelles in water.[21] The inner core is made of aggregated PPO blocks while the external corona is constituted by PEO sequences. For higher temperature and if the concentration is high enough, these micelles adopt different conformational structures (cubic, hexagonal, etc.) as previously revealed by static light scattering.[8] Herein, we used rheological measurements to detect these different structural changes according a previous published methodology.[22] The attribution of the phases is done in accordance to the predetermined phase diagrams by Wanka *et al.*[8]

Figure IV-2 describes as an example, the results registered with the three different copolymers under native form on one hand and after methacrylation on the other, for a polymer concentration close to 30-35% w/w. Let's consider more precisely the case of P104-OH. For T <15 °C, the G' and G" values decrease with temperature. The aqueous solution is made of individual chains named unimers dissolved in water. Then, at T = 15 °C, the increase in both moduli indicates the micellization process due to the increase of the hydrophobic character of PPO blocks and their consecutive aggregation. At T = 27 °C, G' increases and even overtakes G" revealing the spatial organization of the micelles. The solution resembles a gel even if it is well-established that the system is rather a viscoelastic material with a high relaxation time. This "gel" state is observed until 40 °C. The consecutive decrease is due to a transition in the nature of the organized phase from a hexagonal phase to a lamellar phase.[23] For the higher temperatures (T > 70 °C), the significant increase in both G' and G" values is provoked by the solution demixing.[24] Then, during the temperature sweep, several phases of P104-OH at 35%

w/w were observed: unimer phase up to 17 °C, micellar phase up to 27 °C, cubic phase between 27 and 40 °C, hexagonal phase between 45 and 72 °C and demixing above 72 °C. For P123-OH at 35% w/w, the phases can be deduced: unimer phase up to 15 °C, micellar phase between 15 and 25 °C, cubic phase between 25 and 45 °C and demixing above 45 °C. For F127-OH 30% w/w the deduced phases are: unimer phase up to 17 °C, micellar phase between 17 and 23 °C, cubic phase between 22 and 87 °C and demixing above 87 °C.

Figure IV-2 shows that the grafting of methacrylic moieties at the PEO ends induces significant changes in the phase diagram of each Pluronic studied, as reported by Park et al with F127 modified with carboxylic end group.[14] In the case of P104-MA at 35%, the unimer phase is observed for T < 12 °C. The micellization produces itself for a temperature comprised between 12 and 18 °C. The divergence of both moduli due to the micellar organization is also shifted towards temperature (18 °C against 27 °C). But the organized phase (likely cubic) is observed for temperatures up to 50 °C and a probably hexagonal phase (due to the decrease of G' and G") appears above 50 °C. In other words, it is more thermally stable than that characteristic of the P104-OH at the same concentration. The transition of the consecutive phase is also more progressive. In the case of P123-MA at 35% w/w, the unimer phase is observed for T < 30 °C (against 15 °C) while micellization occurs between 30 and 38 °C, followed by cubic organization between 38 and 52 °C and hexagonal between 52 and 66 °C. Similarly, for F127, the micellization occurs between 14 and 23 °C (against 16 to 22 °C) and the cubic organization phase is observed between 22 and 70 °C compared to 23 to 87 °C for the native.

At a first conclusion, the different Pluronic functionalized with methacrylic moieties does not exhibit the same thermal response than that registered with the native copolymers. In other words, for each studied copolymer, the functionalization of the end groups with methacrylic moieties provokes important changes in the thermal response of the native copolymers by modifying the hydrophilic/hydrophobic aspect of the amphiphilic chains.

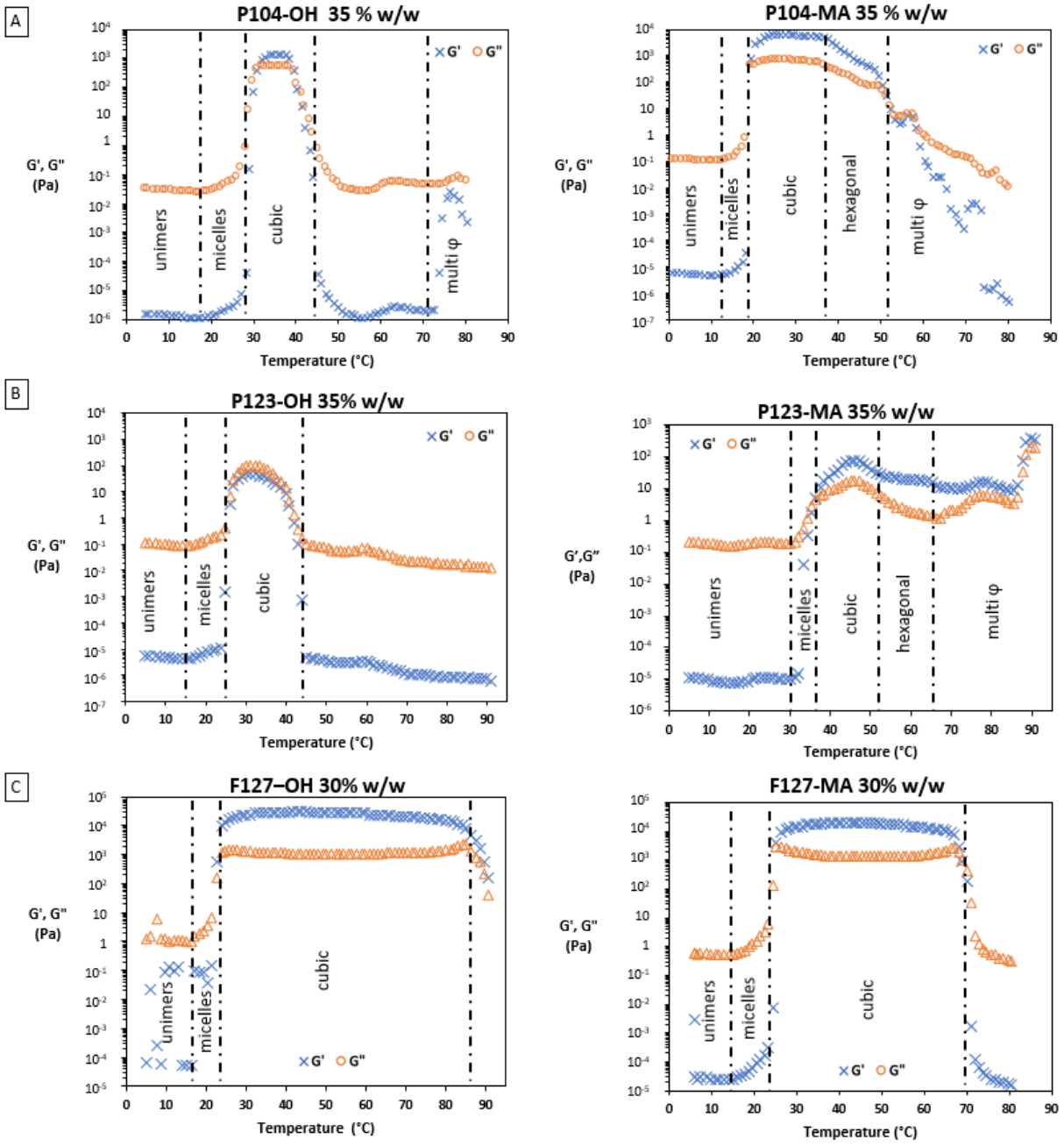

Figure IV-7. Temperature sweeps of A) P104-OH and P104-MA at 35% w/w, B) P123-OH and P123-MA at 35% w/w, and C) F127-OH and F127-MA at 30% w/w with the corresponding phases.

The same measurements were done on native (-OH) and methacrylated (-MA) F127, P104 and P123 at various concentrations. From the rheograms (Figure IV-S2, IV-S4, IV-S6), the phase diagrams of non-functionalized Pluronic F127-OH, P123-OH, and P104-OH were obtained up to 40% w/w as represented in Figure IV-8. Each phase transition corresponds to a significant change in the storage and loss modulus. The rheogram-derived phase diagrams of the non-functionalized Pluronics are similar to the ones obtained using static light scattering found in

the literature, which validates this methodology as a practical technique to detect Pluronic phase transitions[8]. Interestingly, it is essential to note that for P123-OH below 30% w/w, no phase transitions can be detected using rheological measurements, which was not the case from the literature with light scattering. However, the samples become cloudy upon heating solutions of 20 and 30% w/w, as represented in Figure IV-S8, while maintaining a liquid state. This effect may justify why light scattering can detect a phase transition. At the same time, no detection was measured by rheology as the thermal response of the micelles' assembly in this condition did not evolve mechanically. Combining all the rheograms (figures IV-S3, IV-S5, IV-S7), we observe that the methacrylated Pluronic exhibit a similar behavior to the non-methacrylated version with some slight modifications. The F127-MA phase diagram demonstrates a slight shift to higher concentrations, while P104-MA and P123-MA show a shift to lower temperature compared to the nonmethacrylated P104 and P123, respectively. The influence of the hydrophobic methacrylic units on the Pluronic chains can explain this shift. For P123 (20 PEO -70 PPO – 20 PEO) and P104 (27 PEO – 61 PPO – 27 PEO), the ratio of PPO to PEO is significantly higher than F127 (106 PEO – 70 PPO – 106 PEO). Increasing the hydrophobic aspect by adding methacrylic moieties will shift the phase diagrams for P123 and P104 towards lower temperatures, indicating a favored micellar configurational change. Moreover, for F127, the phase diagram slightly shifts towards higher temperatures due to the longer chains having a more hydrophilic nature where the micelles assembly is hindered to a certain degree.

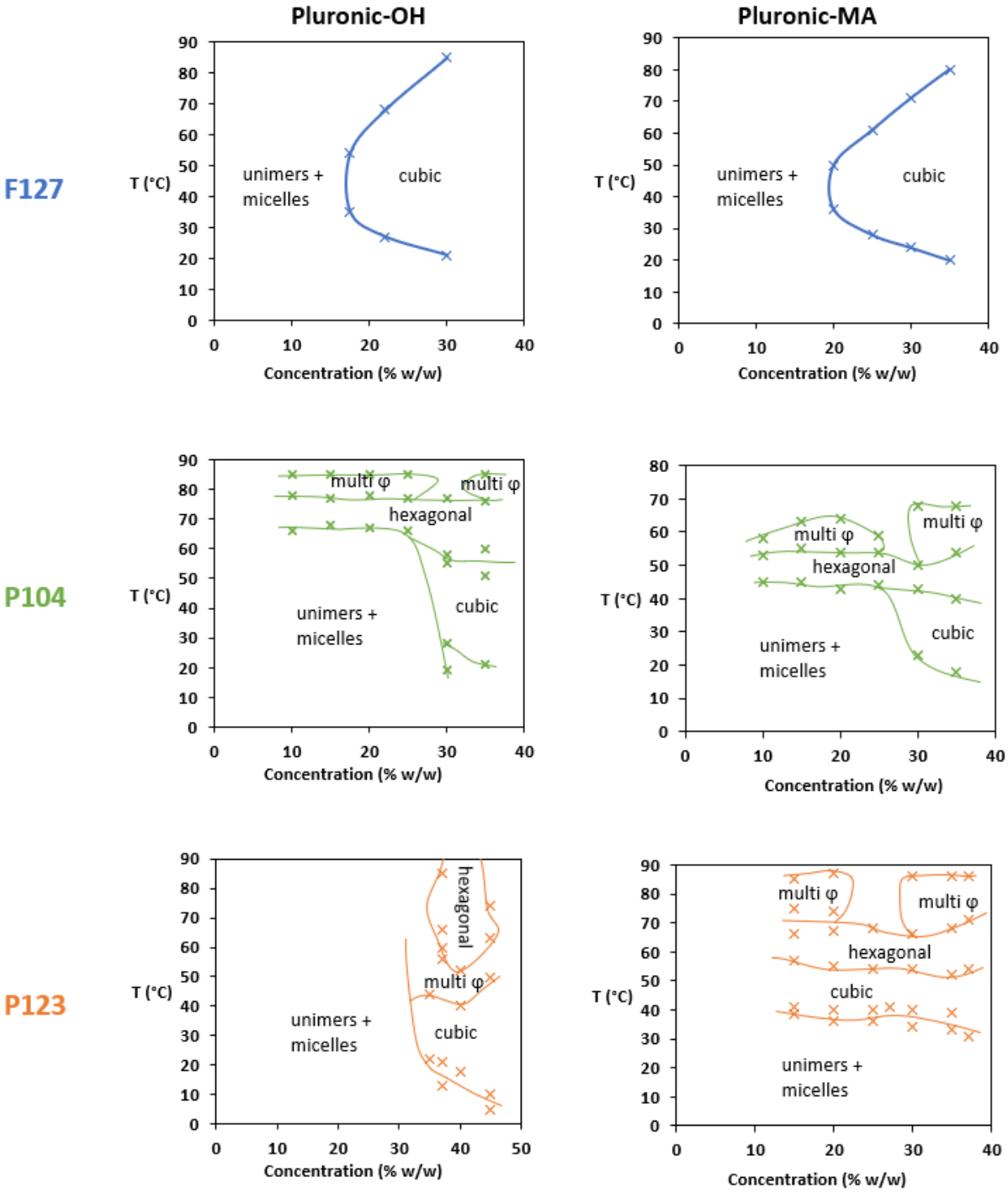

Figure IV-8. Phase diagrams of native (-OH) and methacrylated (-MA) Pluronics F127, P123, and P104 as obtained by rheological measurements.

3.3. Influence of micellar configuration upon photo-crosslinking

The impact of the photo-crosslinking process on the micellar conformational structure of methacrylated Pluronics was investigated. Pluronic concentration was fixed at 25% w/w for all samples, which exhibited a thermal response, and the crosslinking temperatures were chosen to correspond to different micellar structural organization states. Consequently, using photo-

rheology, the storage and loss modulus were recorded under UV irradiation at different temperatures corresponding to different micellar configurational phases. As shown in Figure IV-4, the formation of chemical crosslinking points improves the mechanical properties of the system, which can be seen by the increase in the storage modulus across all samples as soon as the UV lamp is turned on. When crosslinking the Pluronic micelles in an organized state (cubic or hexagonal) for P104, P123, and F127, the modulus reaches an equilibrium after 60 seconds of irradiation. When crosslinking occurs when the Pluronic is in its unimer states at 10 °C, 200 s of irradiation is needed for P104 to reach modulus equilibrium, and 320 s is necessary for both P123 and F127. In the unimer state, the Pluronic copolymers are disordered and free to move, which could explain the longer time required to form stable chemical bridges between them. The micelles are more ordered upon heating, and chemical crosslinking is facilitated and occurs faster.

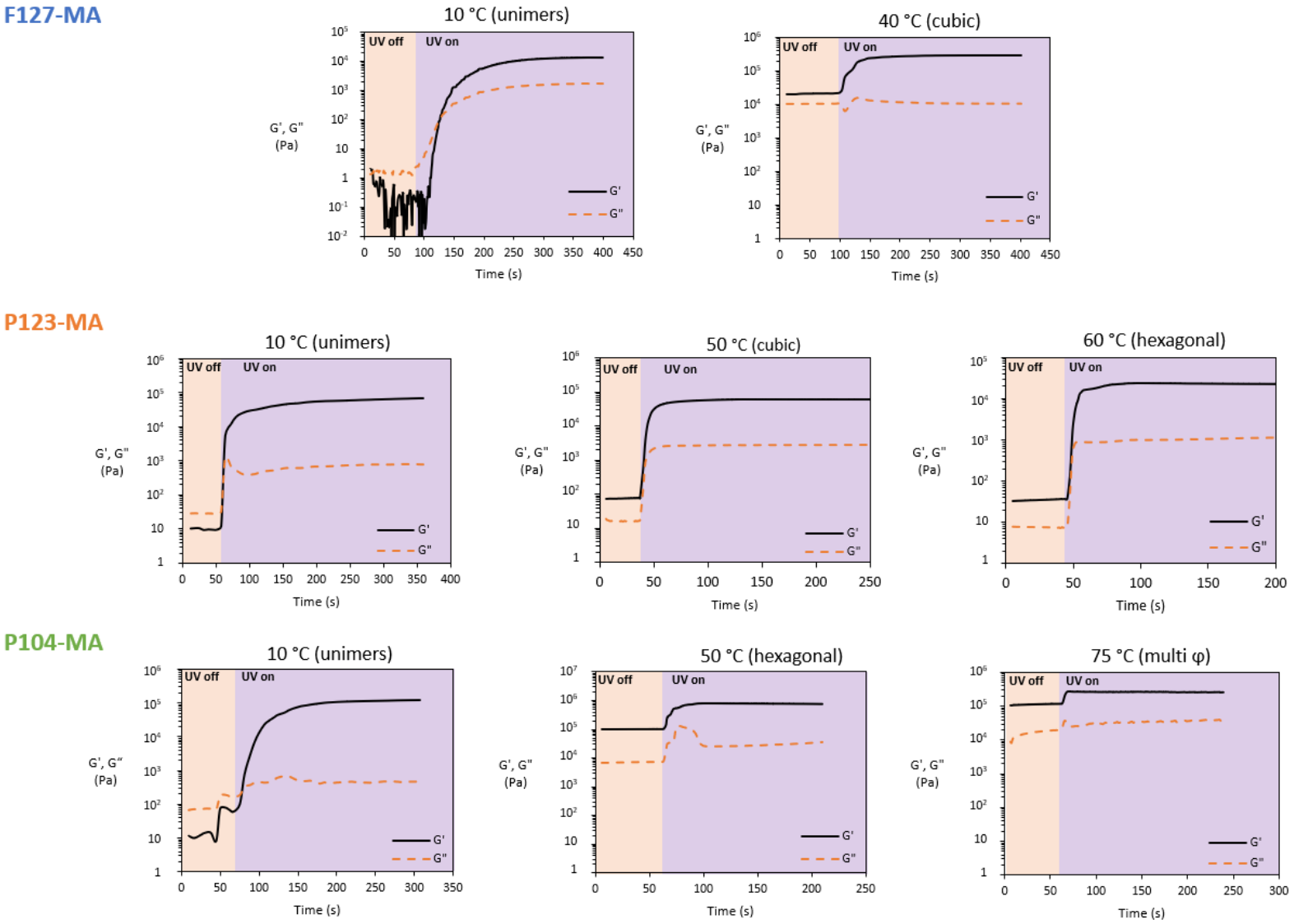

Figure IV-9. Storage and loss modulus of F127-MA, P123-MA and P104-MA at 25% w/w during crosslinking under UV irradiation.

3.4. Influence of photo-crosslinking on thermal responsiveness

Amphiphilic polymers can exhibit a thermal response upon temperature change.[25,26] When heating, the polymer-polymer interactions can be favored for lower critical solution temperature polymers. Herein, we investigate by rheology the micellar configurational change as a mean to induce a thermal response in a photo-crosslinked hydrogel system. After methacrylation, we showed that when heated, Pluronic P104-MA, P123-MA, and F127-MA demonstrated a conformational change in aqueous solution. The following step determines whether the system can still exhibit a thermal response similar to the non-crosslinked micelles following photo-crosslinking. Temperature sweep experiments were done on crosslinked hydrogels from different micellar configurational structures (unimer, cubic and hexagonal phases from the respective phase diagrams).

The thermal response can be detected as a modification of the hydrogels' storage and loss modulus, indicating a change in the gel's structural configuration. As seen in Figure IV-5, the most notable behavioral change of the hydrogels is detected when the hydrogels are crosslinked at 10 °C (in the unimer state) for the three Pluronic samples P104, P123, and F127. The thermal response starts at temperatures lower than the expected values from the methacrylated Pluronic phase diagrams. For instance, the temperature response occurs at around 44 °C for the P104-MA, 35 °C for P123-MA, and 30 °C for F127-MA, as seen from the phase diagrams at 25% w/w (Figure IV-3), while the thermal response starts at around 20 °C for the photo-crosslinked Pluronics. This thermal response shift can be explained by the chemical crosslinking of the micelles, resulting in a more compact arrangement of the chains at proximity that favors their structural phase change at lower temperatures.

Moreover, when the system is photo-crosslinked in an organized phase (cubic or hexagonal), the intensity of the thermal response of the crosslinked gels becomes less and less prominent and even absent. Chemical crosslinking was observed to favor the micelles' structural rearrangement at lower temperatures. However, it was seen that once crosslinked in an organized phase, the thermal response was present at lower temperatures but at a lower magnitude. Photo-crosslinking of the micelles can limit their mobility to rearrange at various temperatures, decreasing the thermal response's intensity. P104-MA photo-crosslinked in the cubic phase does not show a thermal response until 60 °C where the expected transition from cubic to hexagonal occurs; while photo-crosslinking in the hexagonal phase, the thermal response is wholly lost, as indicated by the constant G' and G" upon heating. As seen across the samples, if the system is photo-crosslinked in its unimer phase, the hydrogels present two thermal responses that can be correlated to the micelles movement to organize in a cubic or

hexagonal phase. However, when the system is photo-crosslinked in an ordered state cubic, the hydrogels do not show a thermal response at lower temperatures (that should have corresponded to the transition unimer to cubic) but exhibit a unique thermal response that tends to move the photo-crosslinked micelles to a higher organizational state corresponding to the transition cubic to hexagonal. Similarly, when the system is photo-crosslinked in the highest organizational state hexagonal, the hydrogels lose their thermal response due to the limitation of the micelles to move to a lower organizational state.

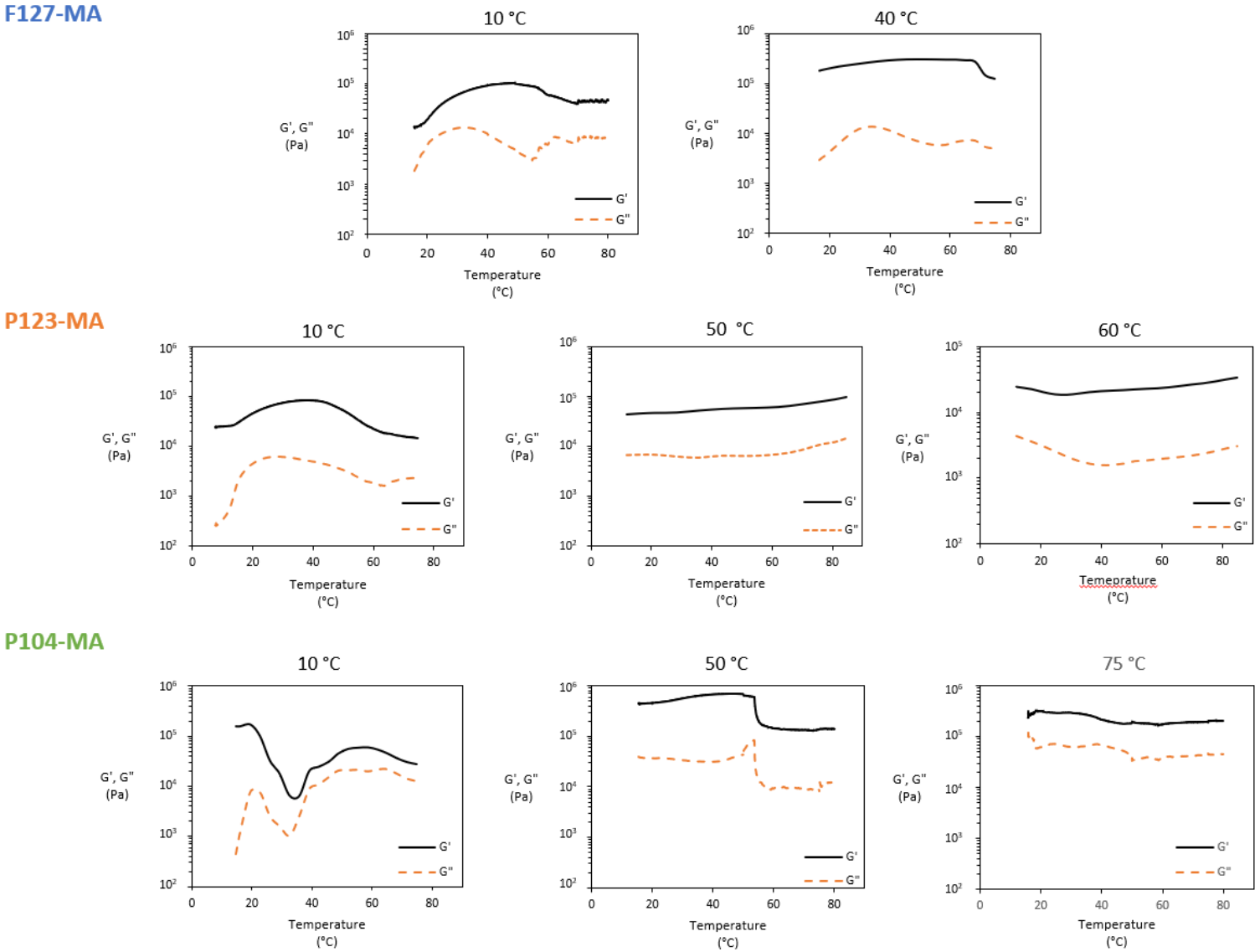

Figure IV-5. Storage modulus of 25% w/w photo-crosslinked P104-MA, P123-MA and F127-MA under shear stress at different temperatures.

3.5. Shape morphing hydrogels upon temperature variation

Pluronic cylindrical chemical hydrogels were prepared from 25% w/w methacrylated pluronics aqueous solutions in 8x4 mm Teflon mold and photo-crosslinked at different organization states (unimer and cubic corresponding to 10 °C and 50 °C respectively) in the presence of LAP as photo-initiator. The gel content of all hydrogels does not seem to be affected by the organizational state of the micelles, as seen in Figure IV-S9. To determine the thermal response, the photo-crosslinked hydrogels were swollen in water at 10 °C for 24 h, which corresponds to unimer phase, then the hydrogels were left to swell in water at 50 °C above the transition temperature (unimer to cubic) which was determined earlier (Figure IV-5). After 24 h, the hydrogels shrunk, and the mass difference and the diameters between the two swollen states were recorded. The water release and size (diameter) reduction after heating are summarized in Figure IV-6. Across all samples, whether crosslinked in the unimer or cubic state, a thermal response is observed through a water expulsion ranging between 30 and 60%. In addition, hydrogels crosslinked in the unimer state showed a higher water release profile when swollen at 50 °C, which can be explained by a higher degree of freedom in micelles' mobility in the crosslinked matrix. The water release is evidenced by water expulsion (figure IV-S10) and size reduction of the hydrogels, where the most noticeable shrinkage occurs when the system is photo-crosslinked in unimer state, as summarized in Figure IV-6. This correlates to the previously shown rheological study where the thermal response is more notable on photo-crosslinked hydrogels below the micellization temperature.

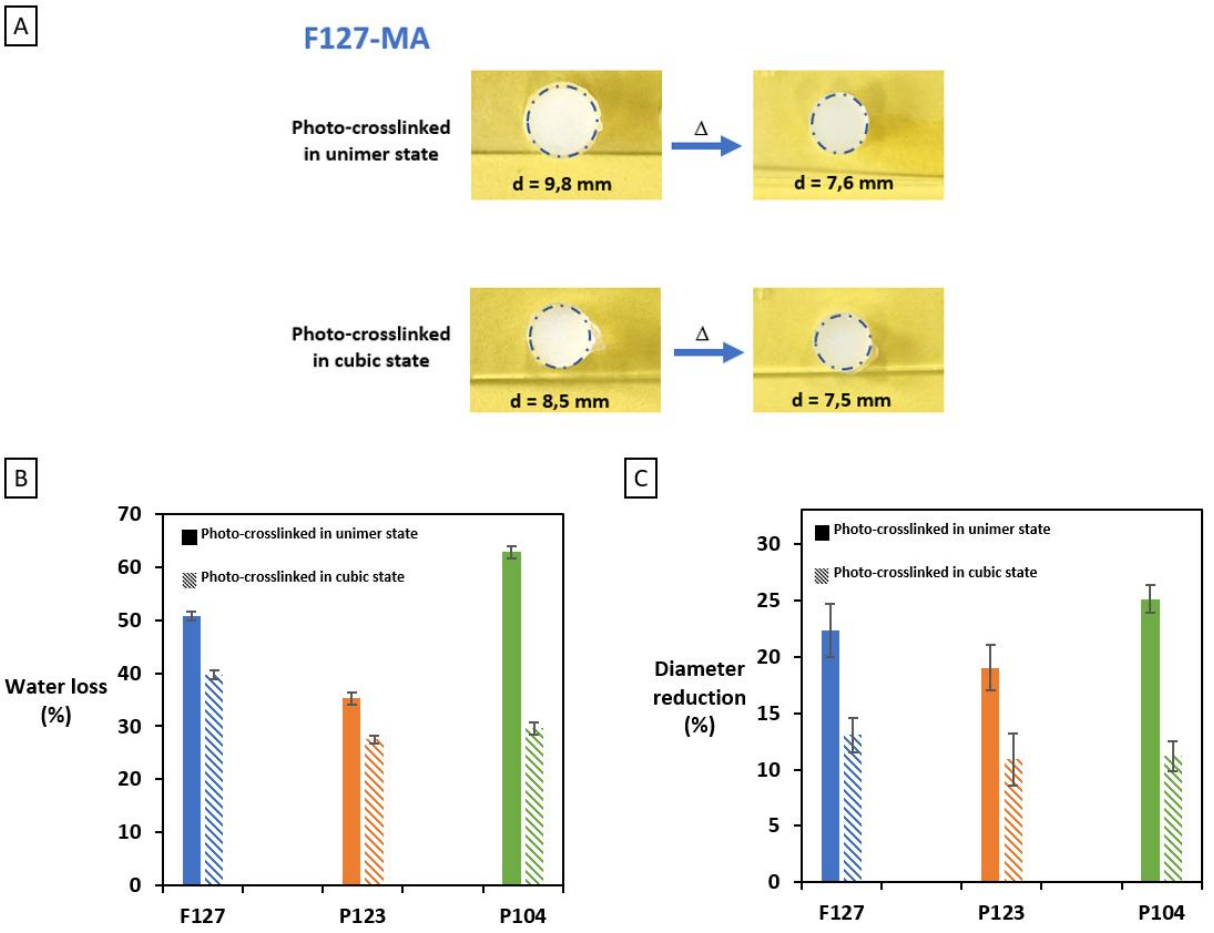

Figure IV-6. A) Physical representation of F127 25% w/w hydrogels swollen at 10 °C and 50 °C when crosslinked in unimer and cubic states, and B) water release and C) diameter reduction of the hydrogels containing 25% w/w Pluronics and photo-crosslinked at different conditions when heated from 10 °C to 50 °C.

4. CONCLUSION

In this study, we investigated the effect of the methacrylation on the thermal behavior of Pluronic F127, P104, and P123 before and after photo-crosslinking. It was demonstrated that the phase diagrams of the methacrylated Pluronics shift to lower concentrations for P104 and P123 and higher concentrations for F127. When the micelles present an organized state, the photo-crosslinking was observed to be faster and more efficient. Moreover, we noted that the thermal response of the hydrogels is highly dependent on the organizational state of the micelles. When photo-crosslinking occurs in an organized phase (cubic or hexagonal), the thermal response becomes less prominent and even lost in some cases, while photo-crosslinking in the unimer stateresulted in hydrogels with the most pronounced temperature response, which then leads to volume changing hydrogel. Chemical photo-crosslinking does not limit the

possible reorganization to a higher state; however, it was observed to limit the disorganization to lower organizational states. Methacrylated Pluronics are thus potential precursors to produce thermo-responsive photo-crosslinked hydrogels and could be used as potential resins for additive manufacturing techniques to lead to smart hydrogels[27].

Supplementary Information

Photo-crosslinked Pluronic Hydrogels: Micellar organization and Thermal Response

Dynamic Light Scattering (DLS)

Particle size measurements were performed on a NANO ZS Malvern nanoparticle size analyzer. The Pluronic solutions concentrations were optimized by continuous dilutions by a factor of 2 starting from a 10% w/v until the peak of interest disappears at 5 °C. The concentration was then fixed at 2.5% w/v and size measurements were done between 5 °C and 65 °C. The laser power, time interval, and number of channels were adjusted for each sample to obtain a good auto-correlation curve. The presented results are the average of three measurements.

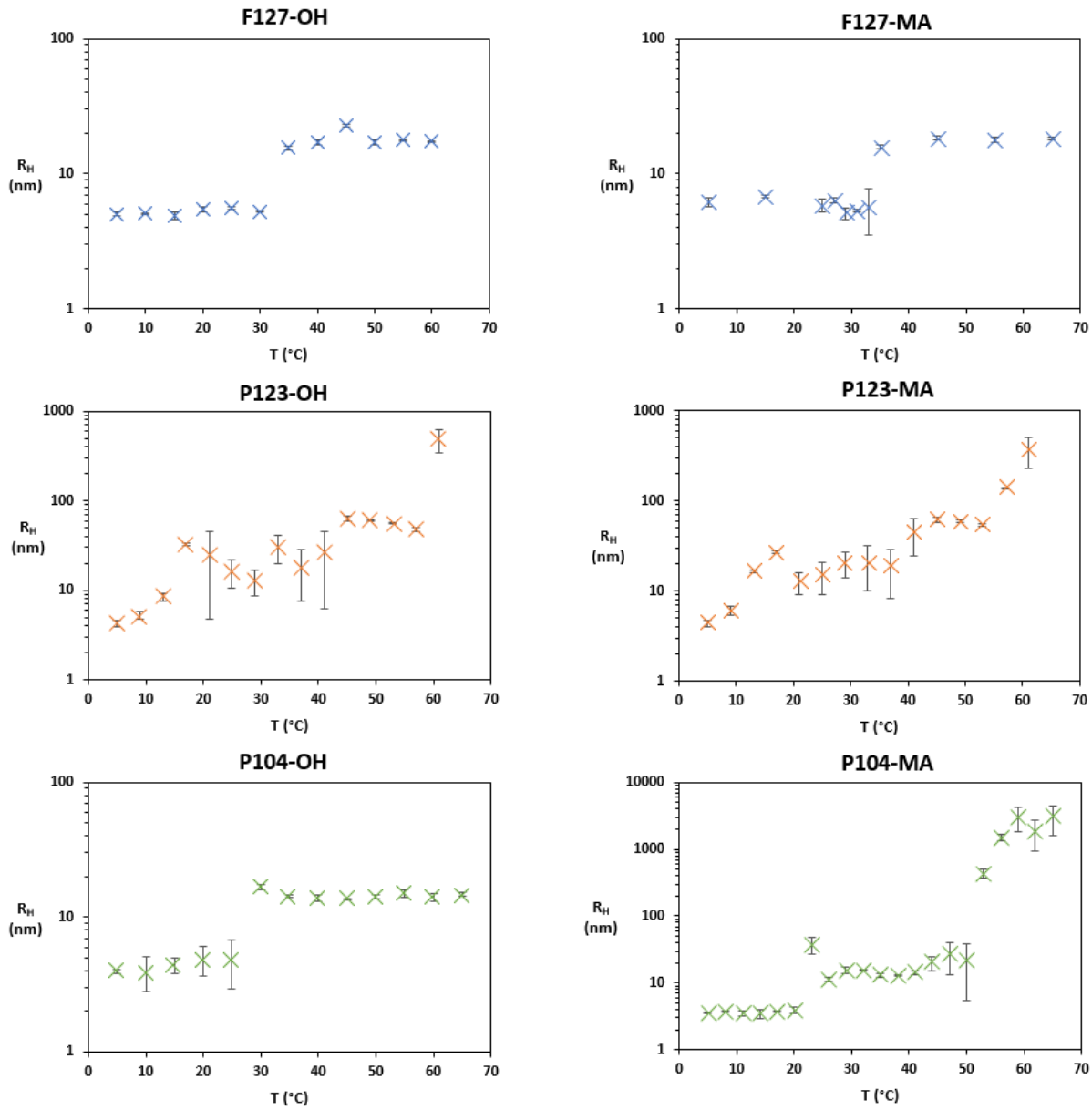

Figure IV-S1. Hydrodynamic radius (R_H) as obtained by dynamic light scattering for F127-OH, F127-MA, P123-OH, P123-MA, P104-OH and P104-MA at different temperatures for 2.5% w/w solutions.

Temeprature sweeps

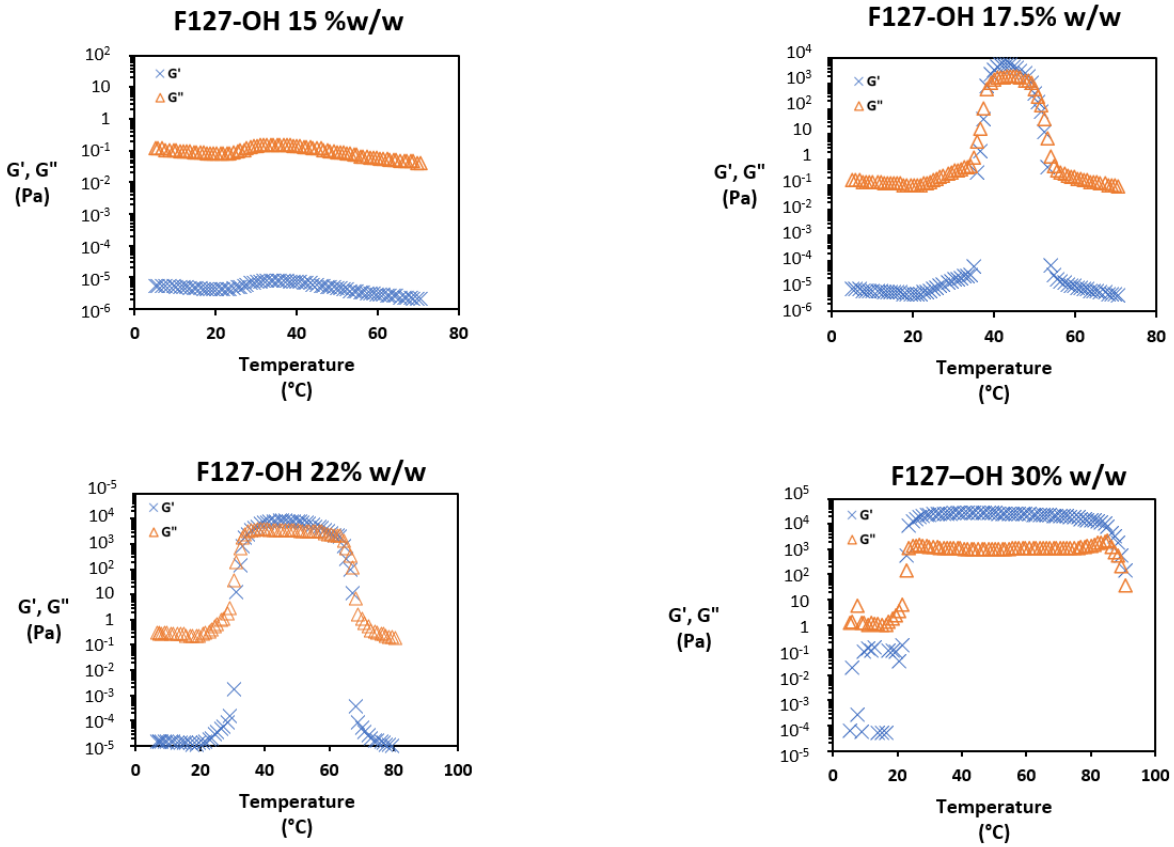

Figure IV-S2. Storage and loss modulus as function of temperature variation for F127-OH at various concentrations.

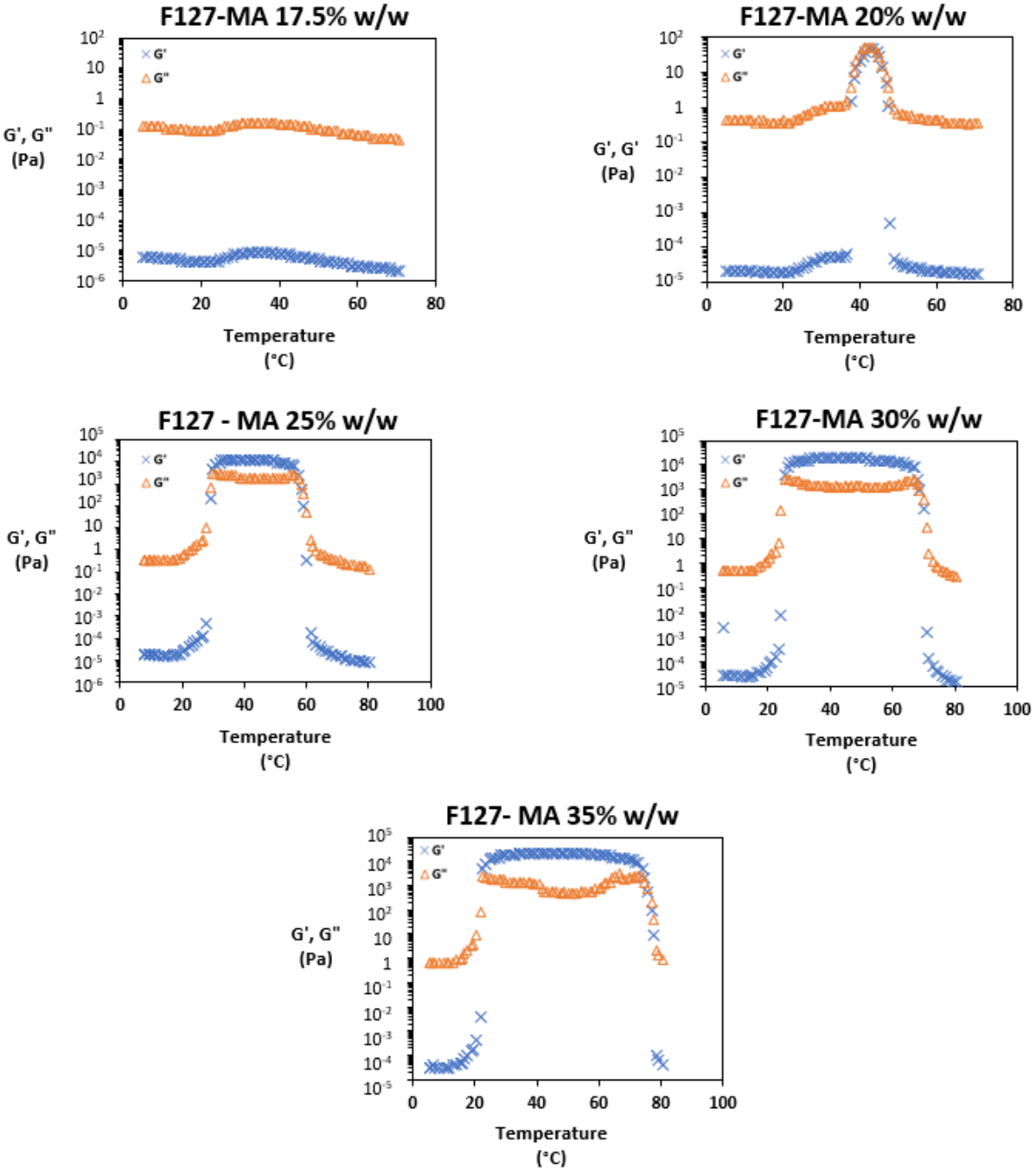

Figure IV-S3. Storage and loss modulus as function of temperature variation for F127-MA at various concentrations.

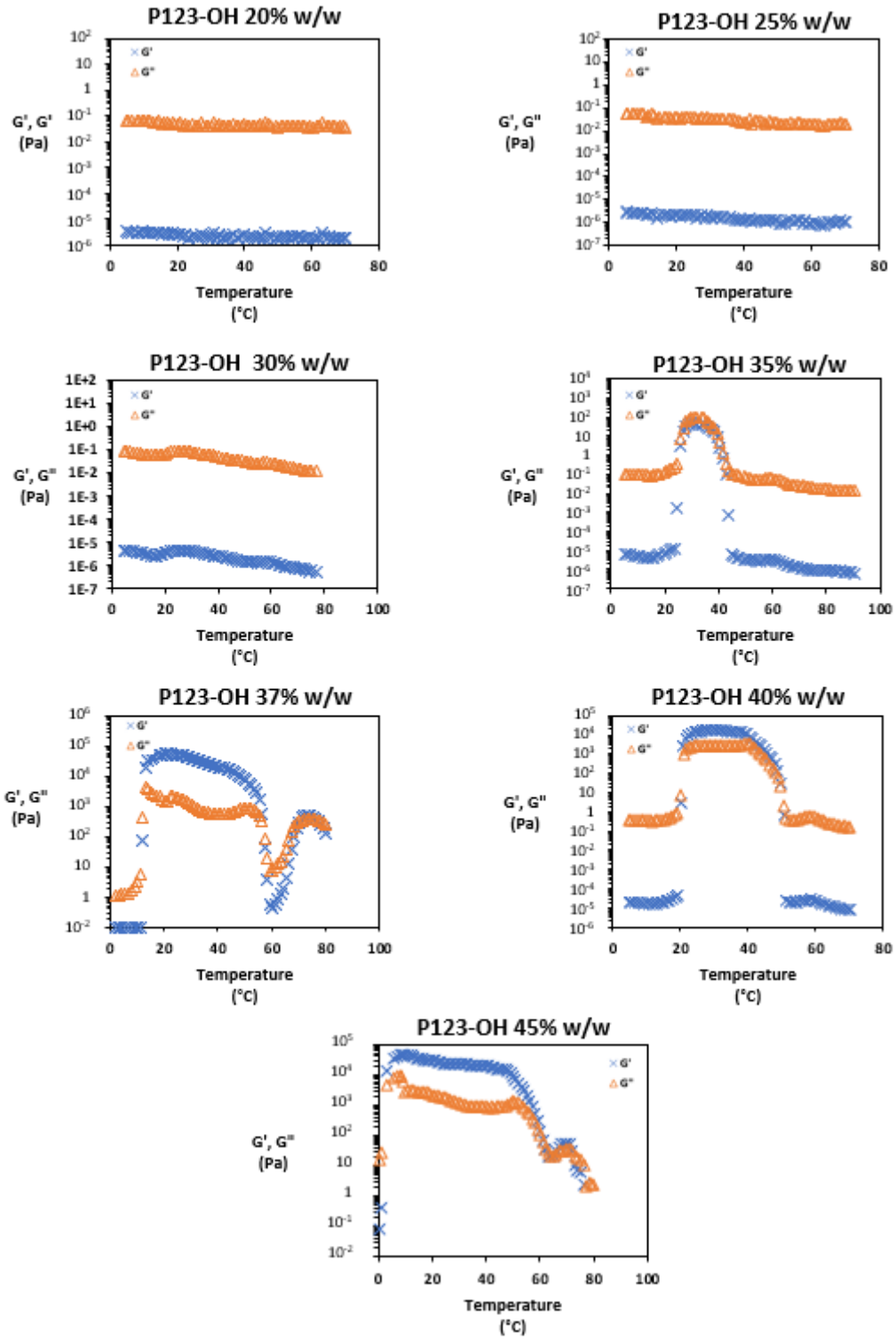

Figure IV-S4. Storage and loss modulus as function of temperature variation for P123-OH at various concentrations.

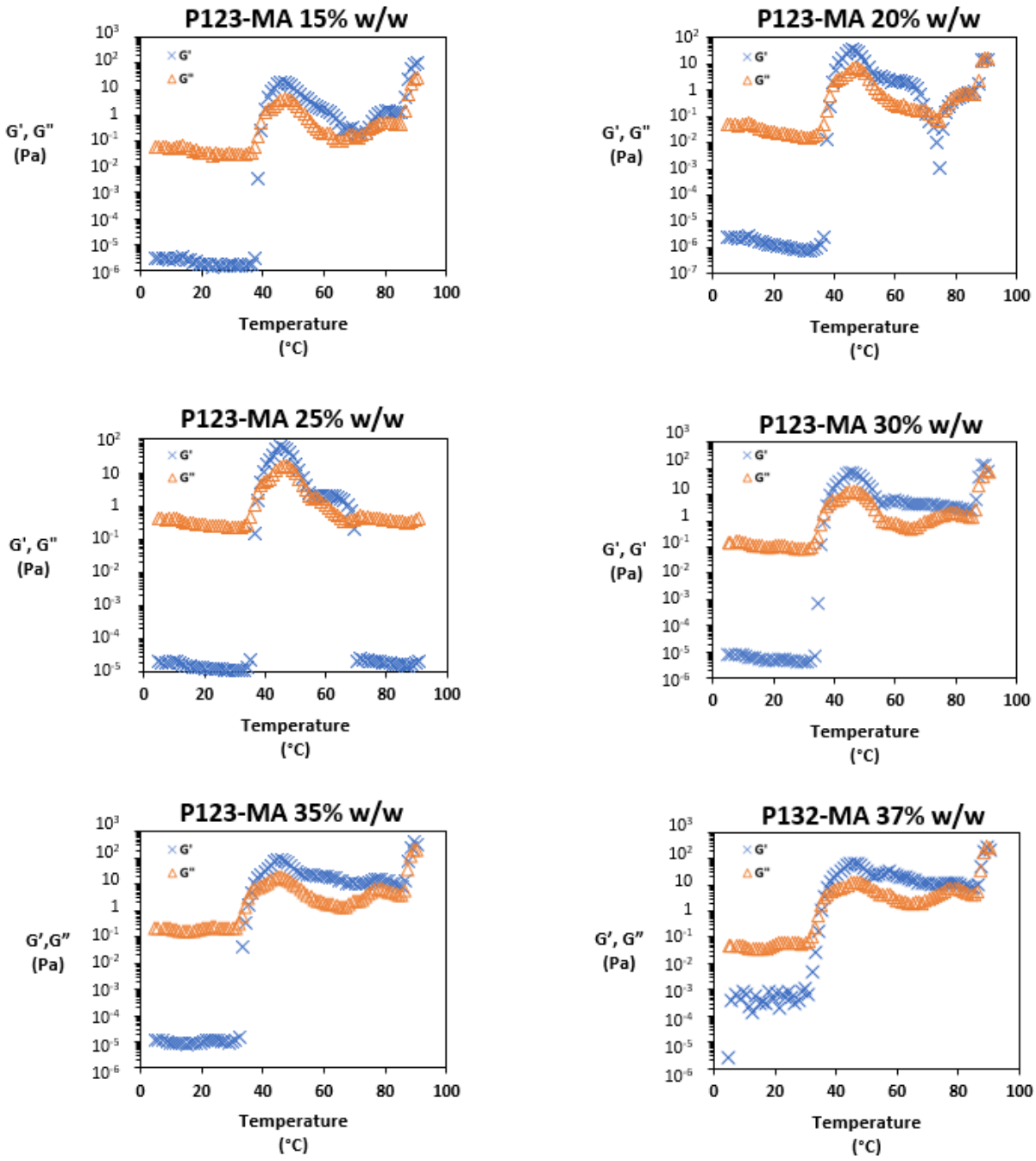

Figure IV-S5. Storage and loss modulus as function of temperature variation for P123-MA at various concentrations.

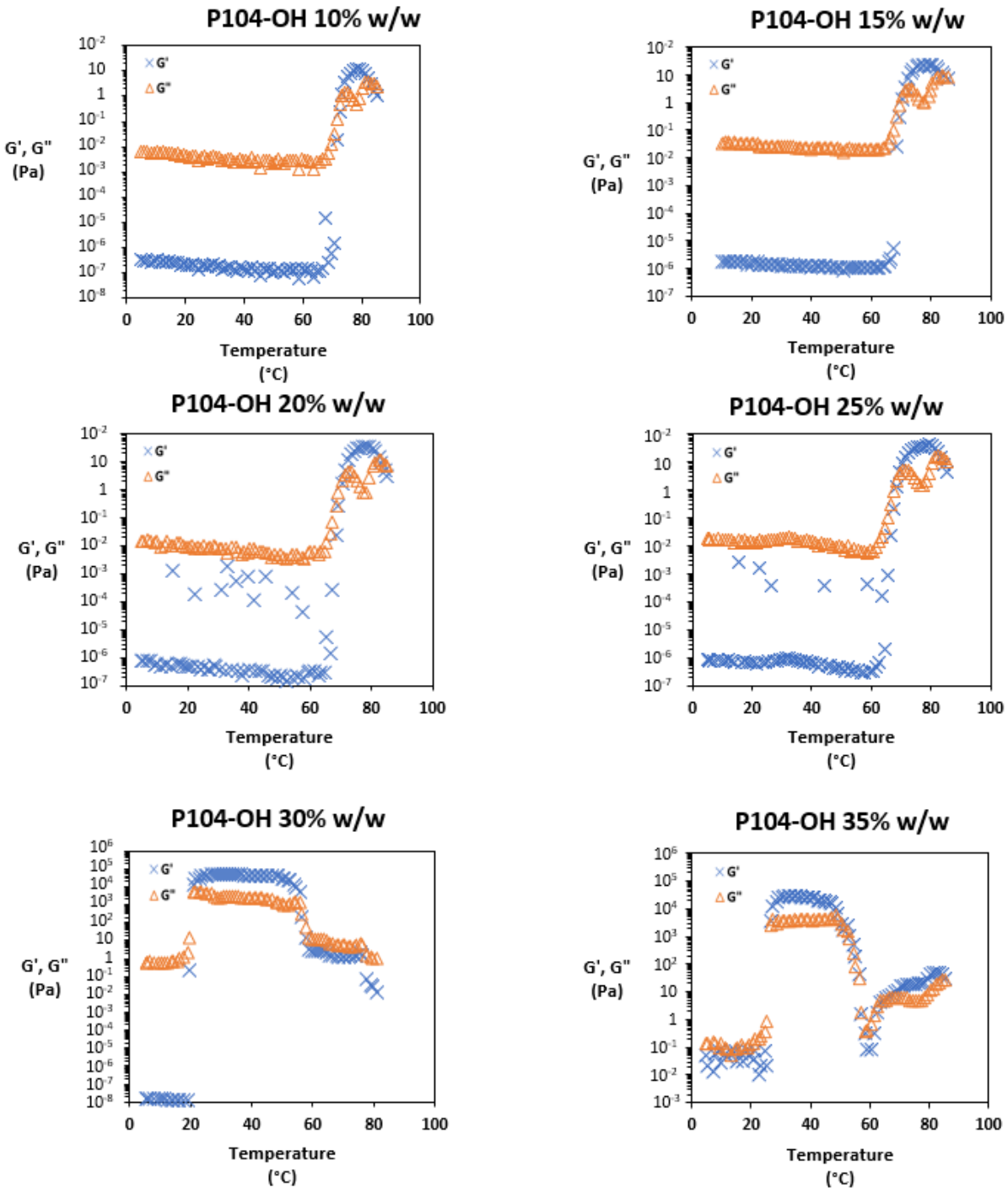

Figure IV-S6. Storage and loss modulus as function of temperature variation for P104-OH at various concentrations.

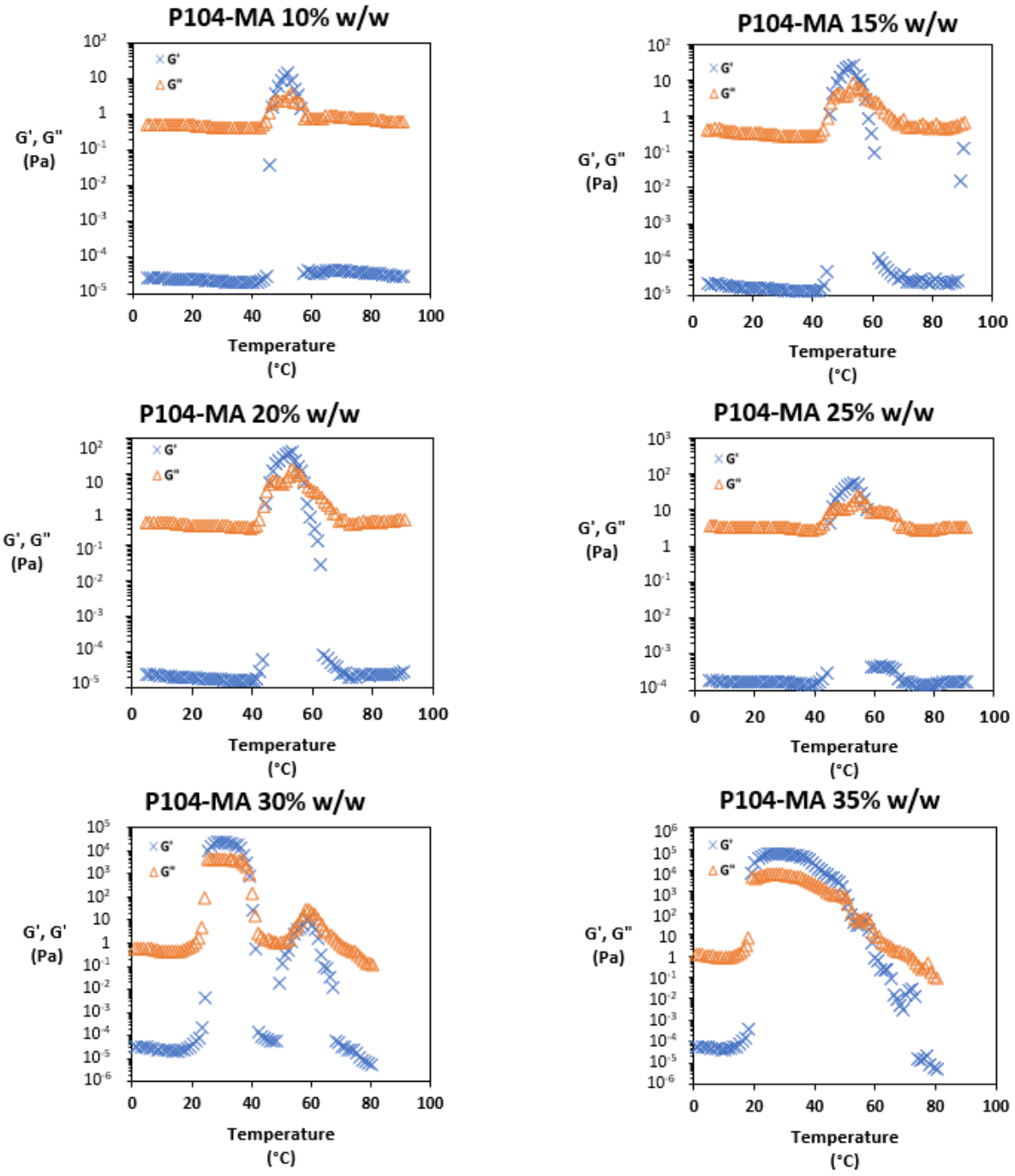

Figure IV-S7. Storage and loss modulus as function of temperature variation for P104-MA at various concentrations.

Figure IV-S8. Physical aspect of P123-MA solutions at 15% w/w (left) and 30% w/w (right) when heated to 70 °C.

Gel content (GC)

For this study hydrogels were used directly after UV curing. Upon photo-crosslinking, the hydrogels were dried under vacuum for 24 h then we recorded the mass denoted $m_{dry\,1}$. Then the hydrogels were left to swell in water for 24 h (changing the water twice) at 10 °C then 24 h at 50 °C recording the mass at each point. Finally, the hydrogels were dried and the recorded mass was denoted by $m_{dry\,2}$. The gel content (GC) was calculated using the following equation.

$$GC = 100 * \frac{m_{dry\,1}}{m_{dry\,2}} \qquad \text{(Equation S1)}$$

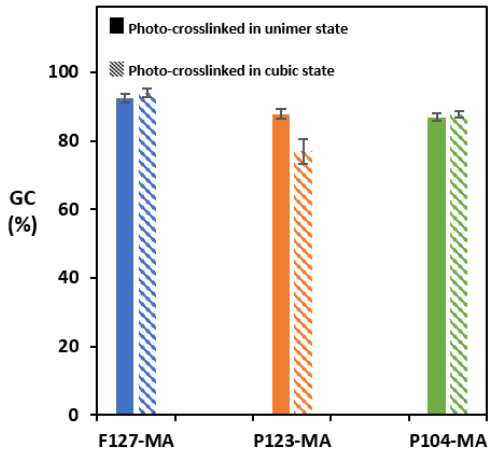

Figure IV-S9. Gel content of F127-MA, P123-MA and P104-MA hydrogels at 25% w/w when photo-crosslinked in ϕ_i and ϕ_{ii}.

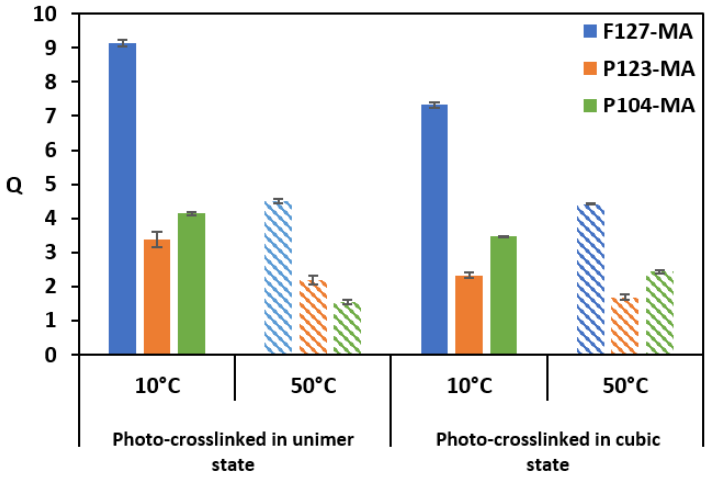

Figure IV-S10. Swelling degree of F127-MA, P123-MA and P104-MA hydrogels at 25% w/w when photo-crosslinked in ϕ_i and ϕ_{ii} when swollen in water at 10 °C and 50 °C.

REFERENCES

[1] B. Chu, *Langmuir* **1995**, *11*, 414.

[2] M. Newman, *Advanced Drug Delivery Reviews* **1998**, *32*, 199.

[3] R. K. Prud'homme, G. Wu, D. K. Schneider, *Langmuir* **1996**, *12*, 4651.

[4] E. Gioffredi, M. Boffito, S. Calzone, S. M. Giannitelli, A. Rainer, M. Trombetta, P. Mozetic, V. Chiono, *Procedia CIRP* **2016**, *49*, 125.

[5] K. Mortensen, *J. Phys.: Condens. Matter* **1996**, *8*, A103.

[6] C. Perreur, J.-P. Habas, J. Peyrelasse, J. François, A. Lapp, *Phys. Rev. E* **2001**, *63*, 031505.

[7] R. Linemann, J. Läuger, G. Schmidt, K. Kratzat, W. Richtering, *Rheola Acta* **1995**, *34*, 440.

[8] G. Wanka, H. Hoffmann, W. Ulbricht, *Macromolecules* **1994**, *27*, 4145.

[9] H. Yardimci, B. Chung, J. L. Harden, R. L. Leheny, *The Journal of Chemical Physics* **2005**, *123*, 244908.

[10] J.-P. Habas, E. Pavie, C. Perreur, A. Lapp, J. Peyrelasse, *Phys. Rev. E* **2004**, *70*, 061802.

[11] M. Zhang, M. Djabourov, C. Bourgaux, K. Bouchemal, *International Journal of Pharmaceutics* **2013**, *454*, 599.

[12] N. A. Di Spirito, N. Grizzuti, M. Casalegno, F. Castiglione, R. Pasquino, *International Journal of Pharmaceutics* **2023**, *644*, 123353.

[13] V. V. A. Fernández, N. Tepale, J. G. Álvarez, J. H. Pérez-López, E. R. Macı´as, F. Bautista, F. Pignon, Y. Rharbi, R. Gámez-Corrales, O. Manero, J. E. Puig, J. F. A. Soltero, *Journal of Colloid and Interface Science* **2009**, *336*, 842.

[14] S. Y. Park, Y. Lee, K. H. Bae, C. Ahn, T. G. Park, *Macromol. Rapid Commun.* **2007**, *28*, 1172.

[15] S. Meng, Z. Guo, Q. Wang, Z. Liu, Q. Wang, W. Zhong, Q. Du, *Journal of Biomaterials Science, Polymer Edition* **2011**, *22*, 651.

[16] M. Di Biase, P. De Leonardis, V. Castelletto, I. W. Hamley, B. Derby, N. Tirelli, *Soft Matter* **2011**, *7*, 4928.

[17] M. Vandenhaute, J. Schelfhout, S. Van Vlierberghe, E. Mendes, P. Dubruel, *European Polymer Journal* **2014**, *53*, 126.

[18] E. Volkmer, U. Leicht, M. Moritz, C. Schwarz, H. Wiese, S. Milz, P. Matthias, W. Schloegl, W. Friess, M. Goettlinger, P. Augat, M. Schieker, *J Mater Sci: Mater Med* **2013**, *24*, 2223.

[19] V. K. Garripelli, J.-K. Kim, R. Namgung, W. J. Kim, M. A. Repka, S. Jo, *Acta Biomaterialia* **2010**, *6*, 477.

[20] T. Majima, W. Schnabel, W. Weber, *Makromol. Chem.* **1991**, *192*, 2307.

[21] A. K. Rajasekharan, C. Gyllensten, E. Blomstrand, M. Liebi, M. Andersson, *ACS Nano* **2020**, *14*, 241.

[22] J.-P. Habas, E. Pavie, A. Lapp, J. Peyrelasse, *Rheol Acta* **2008**, *47*, 765.

[23] Y. Zhao, X. Chen, C. Yang, G. Zhang, *J. Phys. Chem. B* **2007**, *111*, 13937.

[24] E. B. Figueroa-Ochoa, L. M. Bravo-Anaya, R. Vaca-López, G. Landázuri-Gómez, L. C. Rosales-Rivera, T. Diaz-Vidal, F. Carvajal, E. R. Macías-Balleza, Y. Rharbi, J. F. A. Soltero-Martínez, *Polymers* **2023**, *15*, 2551.

[25] T. Brossier, M. Habib, B. T. Benkhaled, G. Volpi, V. Lapinte, S. Blanquer, *Mater. Adv.* **2023**, 10.1039.D3MA00665D.

[26] T. Pelluau, T. Brossier, M. Habib, S. Sene, G. Félix, J. Larionova, S. Blanquer, Y. Guari, *Macro Materials & Eng* **2023**, 2300305.

[27] M. Müller, J. Becher, M. Schnabelrauch, M. Zenobi-Wong, *Biofabrication* **2015**, *7*, 035006.

CHAPTER V / CHAPITRE V

Introduction Chapitre V

Suite à l'étude rhéologique sur la thermosensibilité des hydrogels de Pluronic, nous avons constaté que le Pluronic F127 présentait les meilleures transformations sous l'effet de la température. Cependant, ces transformations restent modestes. Elles sont bien moins marquantes que celles des hydrogels thermosensibles de type poly (N-isopropylacrylamide) (PNiPAAm) ou même les transformations de volume de l'alginate doublement réticulé. Malgré cela, nous souhaitons combiner l'alginate et le Pluronic dans une résine photosensible. Nous espérons obtenir un effet thermique plus marqué grâce à cette synergie, entre le stimulus ionique de l'alginate et la thermoréactivité du Pluronic. Cette combinaison pourrait améliorer la fonctionnalité et l'efficacité des dispositifs médicaux imprimés en 4D.

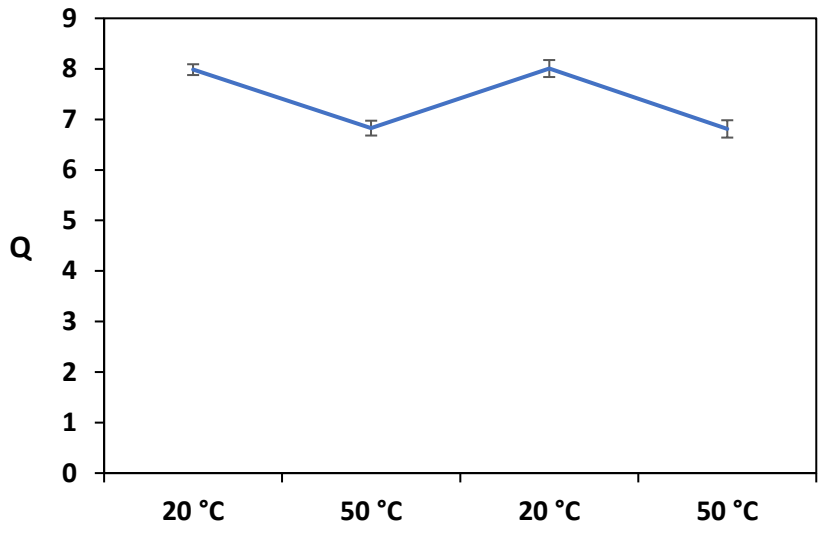

Figure V-A. Gonflement cyclique d'hydrogel avec 8% w/w Alg-MA et 25% w/w F127-MA en changeant la température entre 20 et 50°C. Les valeurs représentent la moyenne ± écart-type de 3 échantillons.

D'après les diagrammes de phases présentés dans le chapitre précédent, le candidat ayant une réponse thermique dans les conditions physiologiques (37 °C) est le Pluronic F127-MA à 25% w/w. Des tests préliminaires ont été réalisés sur des hydrogels contenant 8% w/w d'alginate méthacrylé et 25% w/w de F127-MA réticulés sous UV pour étudier l'effet thermique du Pluronic à température physiologique. Comme observé dans la figure V-A, en augmentant la température de 20 °C à 50 °C, les hydrogels dégonflent peu et le changement de taille est presque négligeable. En revanche, nous avons remarqué que les propriétés mécaniques des hydrogels ont été drastiquement améliorées. Dans ce chapitre, nous explorerons la synergie

entre l'alginate méthacrylé et le Pluronic méthacrylé dans le but d'améliorer les propriétés mécaniques des hydrogels à base d'alginate sans autant limiter sa complexation avec le calcium, plusieurs concentrations de F127-MA bien inférieur à 25% w/w ont été testé. Cette section se concentre sur le développement et l'optimisation de résines hybrides pour l'impression 4D. Les propriétés mécaniques et les comportements de transformation de forme par gonflement des structures imprimées seront analysés pour évaluer leur potentiel en tant que dispositifs médicaux.

Chapter V

4D Printed Alginate-Pluronic Hydrogels as Potential for Biomedical Devices

KEYWORDS
4D printing, methacrylated alginate, Pluronic F127, stereolithography, photo-crosslinking

Abstract:

Methacrylated pluronic F127 (F127-MA) was combined with methacrylated alginate (Alg-MA) to obtain a photo-sensitive resin for stereolithography DLP. The addition of Pluronic F127 significantly modified the swelling and improved the mechanical properties of the printed hydrogels. The printing process was optimized by controlling the degree of crosslinking as revealed by the gel content. Extended irradiation times resulted in a higher crosslinking degree, lower water uptake values and thus lower volumetric changes. The design of programmable 4D printed architecture by applying an anisotropic crosslinking profile in the printed structures was achieved. Tuning the crosslinking degree profile on a tubular structure result in various shape deformation when swollen in PBS. Moreover, another shape transformation can be revealed when submerging the hydrogels in a calcium rich solution. The complexation of Ca^{2+} ions with alginate results in the contraction of the matrix, causing the system to shrink by more than 40 % from its swollen state. 4D printed structures with various crosslinking profiles were developed and tested as potential biomedical devices such as stent as well as tissue filling device.

1. INTRODUCTION

4D printing is an innovating processing technique that builds upon 3D printing technology by incorporating the time factor.[1,2] 4D printed architecture can be designed to respond to an external stimulus such as temperature, pH, light, ionic strength, magnetic field… causing them to change shapes, functions or properties over time.[3] 4D printed structures can thus adapt to the dynamic nature of native tissues and represents a captivating technology that can be used for tissue engineering, drug delivery and smart implants.[4]

Hydrogels are three-dimensional networks of hydrophilic polymers capable of absorbing and retaining large amounts of water and have gathered considerable attention in the biomedical field due to their tunable mechanical properties, and ability to mimic the native extracellular matrix.[5] 4D printing of hydrogels for biomedical applications represents a promising processing technique to develop architectures that can change shape or function in response to an environmental stimulus.[6] This technology has significant potential for developing smart medical devices, such as implants that adapt to changes in the body or scaffolds that evolve during tissue regeneration.[7,8] One of the primary difficulties in 4D processing of hydrogels is finding the appropriate material that combines the suitable mechanical properties, biocompatibility and a responsive behavior.[9]

We previously demonstrated the shape morphing capabilities of 4D printed scaffolds and smart biocompatible actuators obtained by 4D processing of modified alginate. Chemically crosslinked alginate hydrogels demonstrated an important volumetric change when adding and reversing a physical crosslinking by exposing them to alternating physiological and Ca^{2+} ions-rich solutions through.[10] The reversibility of the dual crosslinking of the matrix have been used as a tool to induce shape deformations by the absorption or release of calcium ions. Despite their attractive properties, alginate hydrogels often exhibit limitations, including weak mechanical strength (particularly the yield strength), which can restrict their use in load-bearing tissues. The aim of this study is to improve the mechanical properties of 4D printed alginate devices without compromising their shape morphing ability and demonstrate a proof-of-concept applicative use for potential biomedical devices.

Improving the elasticity of hydrogels is commonly achieved by forming an interpenetrating network with complementary mechanical properties. For example, Yumin et al. developed a highly stretchable alginate hydrogel by including poly(vinyl alcohol) (PVA) in the calcium crosslinked matrix. By tuning the PVA content in the hydrogel, the deformation at break can

be improved by up to 20 % under tensile testing.[11] Similarly, Lei et al. improved the elasticity of oxidized sodium alginate by incorporating a physical crosslinked network of agarose.[12] The hydrogen bonds between agarose and alginate in addition to the helix structure of agarose when cooled resulted in a highly stretchable hydrogel with a 15 % increase in the deformation at rupture under compression testing. This approach demonstrates high potential to obtain a highly stretchable polysaccharide-based hydrogel. Among these various approaches to enhance the properties of alginates, none of them are easily compatible with 3D printing processes, particularly with photo-polymerization methods such as Digital Light Processing (DLP). The reinforcement of mechanical properties in 3D printed hydrogel devices has also been explored, particularly through the incorporation of nanocomposites[13] or by addition of assembled micelles such as Pluronic. While these methods have proven effective in enhancing the mechanical properties of gelatin or hyaluronic acid[14,15], they have rarely been applied to alginate. Bova et al. proposed to improve the mechanical properties of 3D printed methacrylated gelatin by incorporating Pluronic F127 in the resin[14]. The improvement of the mechanical properties was observed by rheological measurements where the elastic and storage modulus increased by an order of 2.

Herein we developed a methacrylated alginate-based resin with improved mechanical properties by integrating methacrylated Pluronic F127. The amount of Pluronic was optimized in order to enhance the mechanical properties while maintaining the ionic response of alginate in presence of Ca^{2+} ions. The volumetric change as well as compression tests were done on 3D printed cylinders at different crosslinking conditions. By investigating various degrees of crosslinking, structures with an anisotropic crosslinking profile were developed as biomedical devices. These include tubular structures that can adapt their shape to favor anisotropic vessel dilatation in vascular diseases, as well as custom structures that can serve as adaptable tissue fillers such for intervertebral disk repair.

2. MATERIALS AND METHODS

2.1. Materials

Low viscosity sodium alginate (LVA) and Pluronic F127 were purchased from Sigma-Aldrich. Methacrylic anhydride (MA), calcium chloride ($CaCl_2$), ethylenediaminetetraacetic acid tetrasodium salt dihydrate (EDTA $4Na^+$, $2H_2O$), Orange-G and phosphate buffered saline (PBS) were purchased from Sigma-Aldrich. Triethylamine (TEA) was purchased from Fisher Chemicals. Milli-Q water (conductivity = 18.2 mΩ.cm at 23 °C) was used during this study. Lithium phenyl-2,4,6-trimethylbenzoylphosphinate (LAP) was synthesized as described by

Majima *et al.*[16] Methacrylated alginate was obtained following the same protocol as our previous paper (chapter III). All chemicals were used without further purification unless mentioned otherwise.

2.2. Methods

Resin formulation and 3D Printing

All structures were constructed by stereolithography using a digital light processing (DLP) printer (Max X43, Asiga, KREOS supplier France). The resins were prepared by dissolving the appropriate amounts of Alg-MA (methacrylation in supplementary information Figure V-S1) and Pluronic F127-MA (methacrylation in supplementary information Figure V-S2) to obtain a solution with 8% w/w Alg-MA and 2.5, 5 and 7.5% w/w F127-MA. LAP was added at 3.75% w/w with respect to the polymers as photoinitiator and Orange G at 0.2% w/v as photo-absorber. Orange G was added in order to control the UV light penetration depth to attain high resolution printing. UV intensity was fixed at 5 mW/cm^2 (after optimization Figure V-S3) and the printing layer thickness was 100 µm for all samples. For post printing processing, the hydrogels were washed in PBS for 2 days while changing the media twice a day to ensure the removal of all uncrosslinked groups.

Printing conditions with DLP approach

The swelling behavior, volumetric change and the mechanical properties were tested on 3D printed cylinders having 100 µm printing layer. The STL files of the different 3D printed structures were generated using the Rhinoceros 3D software.

First of all, the lowest time irradiation to reach 100 µm photo-crosslinked layer was established by drawing the working curve (Figure V-S3). In order to obtain an anisotropic swelling behavior, a photo-crosslinking gradient is implemented by varying the irradiation time on the z axis. Typically, irradiation time of the individual 100 µm layer was varied to obtained different degrees of photo-crosslinking. The irradiation time per 100 µm layer of each formulation is summarized in Table V-S1.

Cyclic swelling

The equilibrium cyclic swelling degrees were measured starting from the washed hydrogels. The cycles were between PBS and 5% w/w $CaCl_2$. For each measurement, the hydrogel was left to swell for 24 hours at room temperature. The swelling degree was calculated using equation 1. The values are represented as the mean of triplicate sets.

$$Q = \frac{m_{swollen\ at\ time\ t}}{m_{\ dry}} \quad \text{(Equation V-1)}$$

Expansion coefficient

The volumetric change of the hydrogels was assessed by evaluating the dimensional change in different medias (PBS and $CaCl_2$ solution). The expansion coefficient is calculated as the ratio of the dimensions of the swollen hydrogels and the dimensions of the .stl reference design (Equations V-2).

$$\alpha_{xy} = \frac{diameter\ at\ swollen\ state}{diameter\ of\ STL\ design} \quad \text{(Equation V-2)}$$

Thermogravimetric analysis (TGA)

Thermogravimetric tests of the hydrogels were performed on a TA Instrument Q50 Thermogravimetric Analyzer. The analysis was conducted under 60 mL/min N_2 flux from 25 to 550 °C at a heating rate of 5 °C/min.

Compression testing

Compression tests of the swollen hydrogels were done on an Instron 3366L5885 mechanical tester equipped with a 100 N load cell. Cylindrical samples of 8 × 4 mm were 3D printed at different conditions as summarized in Table 1. Hydrogels were taken at different points of the cycling swelling and the compression tests were done after measuring the dimensions using a digital thickness caliper (DD-50-L, Henri R. LECLERCQ supplier, France). The compression speed was set at 1 $mm.s^{-1}$ with 200 ms sampling time and an initial load of 0.01 N. Each value is represented by the mean ± SD (n = 3). The Young's modulus was determined as the slope at 3 % deformation.

Crosslinking density

The crosslinking density (ν_e), describing the number of crosslinking points per hydrogel volume was calculated according to Flory-Rehner equation[17,18]:

$$\nu_e = \frac{2C_1}{RT} \quad \text{(Equation V-3)}$$

Where ν_e represents the crosslinking density in mol/cm^3, R the gas constant, T the temperature and $2C_1$ is the intercept with the y axis of the plot:

$$\frac{\sigma\ V^{1/3}}{(\lambda - \lambda^{-2})} = 2\ C_1 + \frac{2\ C_2}{\lambda} \quad \text{(Equation V-4)}$$

Where σ is the stress, V is the density of polymer in the swollen hydrogel and λ the extension ratio obtained from the compression testing.

Force generated from swelling

To measure the force exerted by the dual crosslinked hydrogels when releasing the calcium once submerged in a physiological media, a tubular structure is placed between the disks of the compression testing machine equipped with a 100 N load cell in a 1% w/w EDTA solution (to accelerate the calcium decomplexation from alginate and therefore optimize the data acquiring) and left to swell. The axial and radial forces are measured without initial load.

Biomedical device

To simulate the hydrogel's behavior as a self-expanding soft stent, a polydimethylsiloxane (PDMS) thin tube (mimicking a vessel like structure) was fabricated by mixing Sylgard 184 base and curing agent at a 10:1 ratio by weight, degassing the mixture under vacuum, dipping a glass rod (4 mm diameter in the PDMS mixture) and curing it at 50°C for 3 hours. The Alg8-F2.5 4D printed hydrogel tube, previously contracted in 5% w/w $CaCl_2$ solution, was then inserted into the PDMS thin tube prior to submersion in 1% w/w EDTA solution.

Similarly, to simulate the hydrogel as a filler for intervertebral disks, a thick PDMS film (5mm thickness) was fabricated, and a 3 mm diameter hole was drilled into it. The hydrogel was placed inside the void, and the entire setup was submerged in 1% w/w EDTA solution, allowing the hydrogel to swell within the confined space following anisotropic shape-morphing.

3. RESULTS AND DISCUSSION

3.1. Swelling behavior and mechanical properties

The aim of this study is to achieve significant shape deformation with optimal mechanical properties in shape-morphing printed hydrogel devices. First of all, an optimized formulation of 8% w/w Alg-MA and 2.5% w/w F127-MA (denoted as Alg8-F2.5) was chosen due to the significant expansion difference between the swollen state in PBS and the contracted state in 5% w/w $CaCl_2$ (Figure V-1C, Figure V-S4). Several degrees of crosslinking were achieved by increasing the UV irradiation time for each 100 µm layer during the printing process denoted as X1, X2, X3 and X4 were X1 refers to the lowest photo-crosslinking degree and X4 the highest.

The swelling behavior of Alg8-F2.5 hydrogels was studied in both PBS and calcium rich solution across different photo-crosslinking degrees (X1, X2, X3 and X4). When immersed in

PBS, the hydrogel with the lowest photo-crosslinking degree (X1) has the highest swelling ratio reaching up to 70 compared to 25 for the hydrogel crosslinked at X4. Increasing the crosslinking density of the hydrogels will result in a much denser network limiting the water uptake. Once submerged in calcium-rich solution, additional physical crosslink nodes are introduced to the hydrogel that contracts the network and releases water from it decreasing the swelling ratio to around 13 as seen in Figure V-1B. The swelling and contraction kinetics of the Alg8-F2.5 hydrogels was measured in $CaCl_2$ and PBS. As seen in Figure V-2, hydrogels at higher degrees of crosslinking require longer times to reach equilibrium due to the tighter network. Physical crosslinking induced by the calcium is reversible and the hydrogels recover their initial swollen state when immerged in PBS due to the sodium/calcium ion exchange. The water uptake difference across the hydrogels can also be observed by studying the dimensional changes of the hydrogel such as the diameter change. The main focus will be on the xy expansion given that the objective is to develop medical devices where the desired deformation occurs radially. As seen in Figure V-1C, hydrogels crosslinked at X1, exhibit the highest radial change with respect to the STL file and by varying the crosslinking degree various final sizes can be obtained. It is important to note that the expansion of the hydrogels radially and across the thickness varies (Figure V-S4) where the expansion in the z axis demonstrates lower values. Due to the layer-by-layer printing process, it is possible that the interface between layers behaves differently than the core of the layers with the presence of Pluronic micelles in the resin. In addition, once the hydrogels are submerged in $CaCl_2$ solution, they shrink and reach similar diameter sizes regardless of the crosslinking degree as seen in Figure V-1C, D. In fact, at high degrees of crosslinking, the chain mobility becomes more limited, thereby restricting the complexation of the adjacent alginate chains with the calcium ions hence reducing the shrinking ratio of the network. This can explain why all the hydrogels exhibit the same diameter in the calcium solution (Figure V-3D).

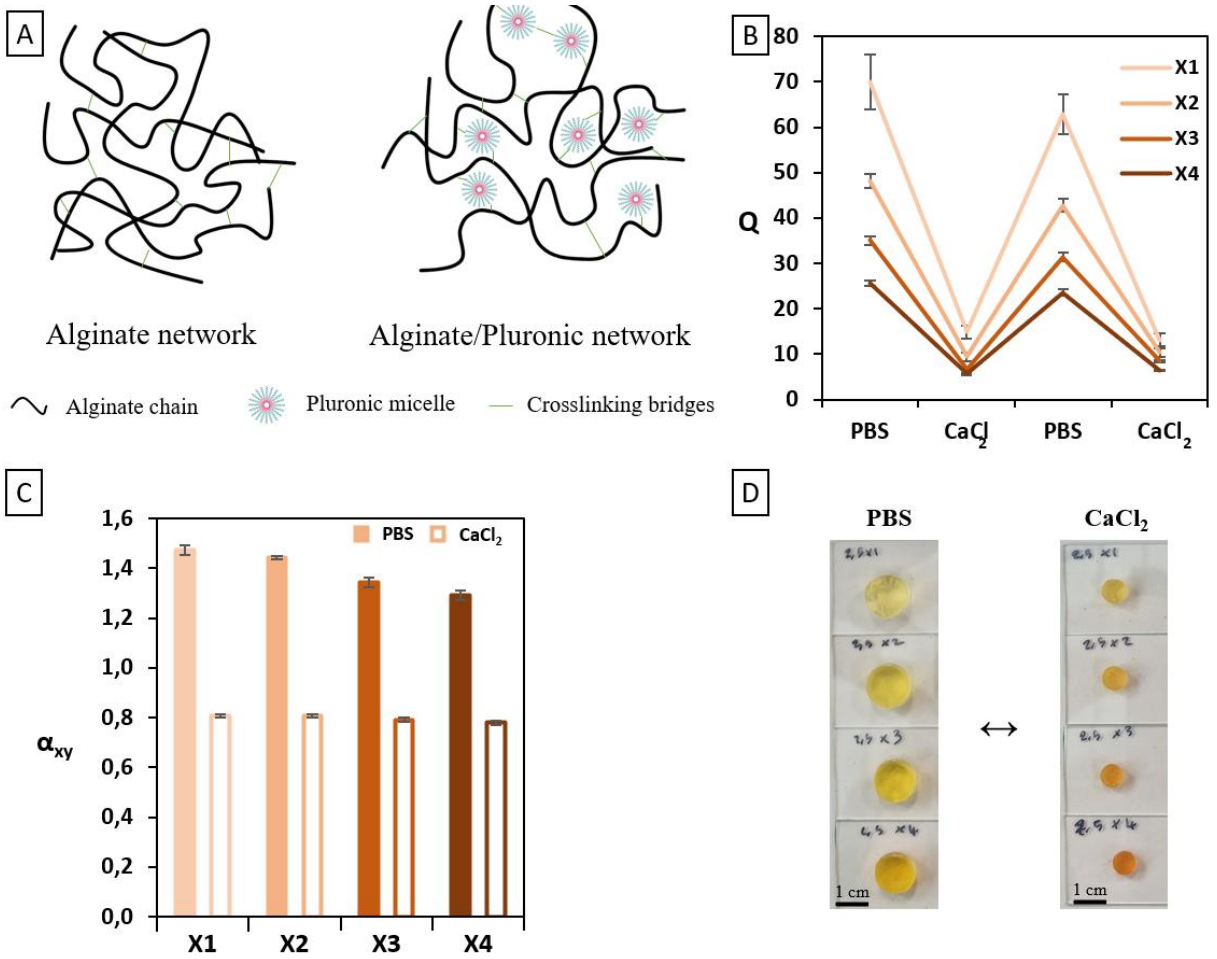

Figure V-1. A) Schematic representation of the Alg-MA crosslinked network with and without F127-MA. B) Cyclic swelling behavior of Alg8-F2.5 hydrogels with different crosslinking degrees when swollen in PBS and 5% w/w $CaCl_2$. C) xy expansion coefficient of the hydrogels at equilibrium when swollen in PBS and 5% w/w $CaCl_2$ solution and D) physical aspect of Alg8-F2.5 hydrogels in PBS and $CaCl_2$ solution when crosslinked at X1, X2, X3 and X4.

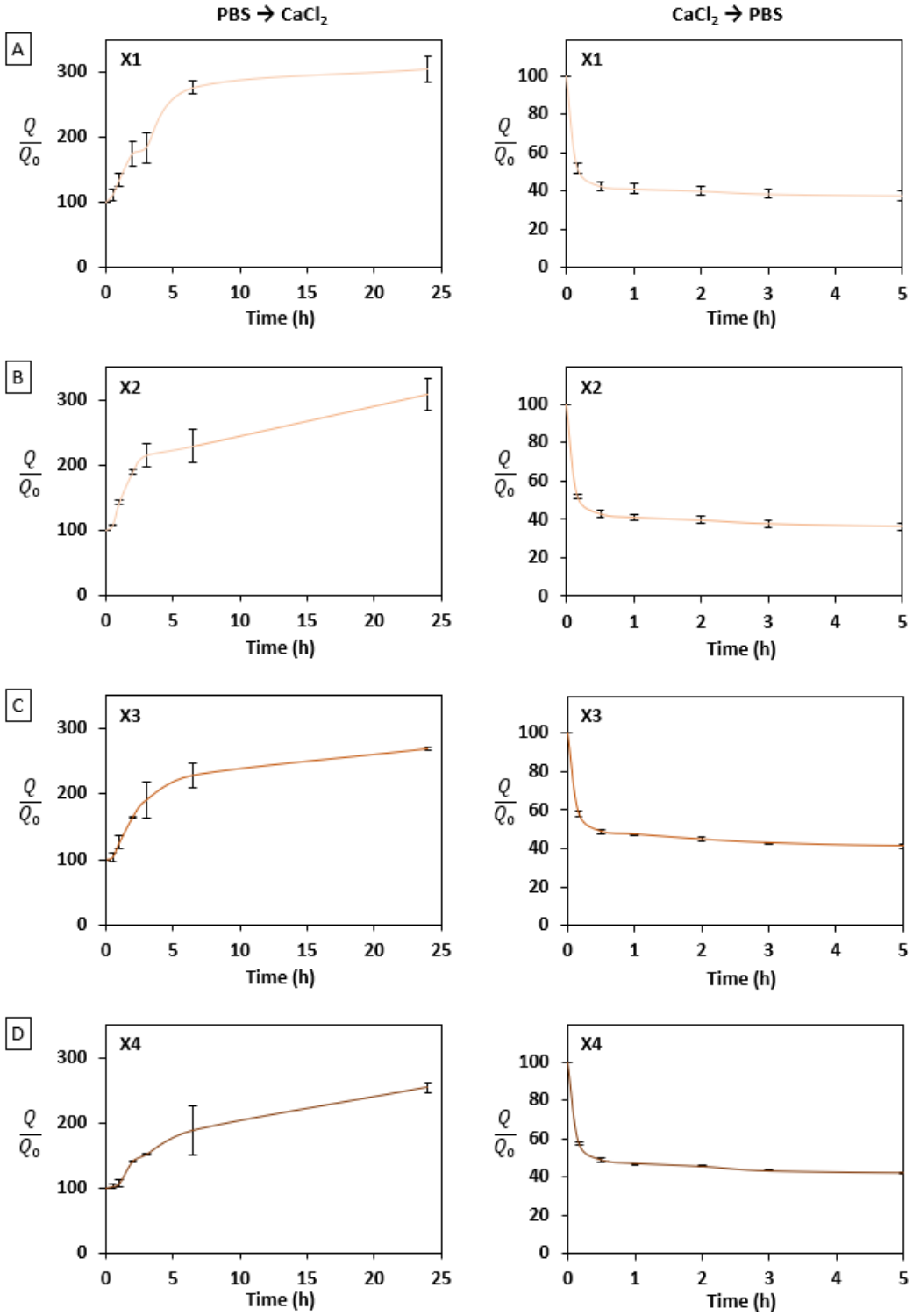

Figure V-2. Shrinking and swelling kinetics of Alg8-F2.5 hydrogels crosslinked at X1, X2, X3 and X4 when submerged in $CaCl_2$ solution (left) and PBS (right).

Moreover, compression testing revealed the differences in the mechanical properties of the hydrogels depending on the swelling media and crosslinking degree. In PBS, the deformation at rupture was around 30% for all hydrogels. The stresses at rupture increases with higher

crosslinking densities as seen in Figure V-3A. Increasing the crosslinking density will result in stronger and stiffer hydrogels seen by the increase in Young's modulus ranging between 7 kPa for X1 that increases to 30 kPa for X4 (Figure V-3B). In calcium solution, the mechanical properties of the hydrogels are significantly improved. The deformation at rupture of the hydrogels increased to reach 75% for X1 and around 65% for X2, X3 and X4 under significantly higher stresses. This improvement of the mechanical properties can be attributed to the addition of the secondary ionic crosslinking provided by the calcium ions which is also seen by the increase of the Young's modulus for all the hydrogels. The crosslinking density was calculated according to Flory-Rehner equation from the stress strain data. It can be seen that by increasing the irradiation time, an increase in the number of crosslinking points from 3 x 10^{-4} mol/cm^3 to 59 x 10^{-4} mol/cm^3 is achieved and that affects both the swelling behavior of the hydrogels and the mechanical properties as previously discussed.

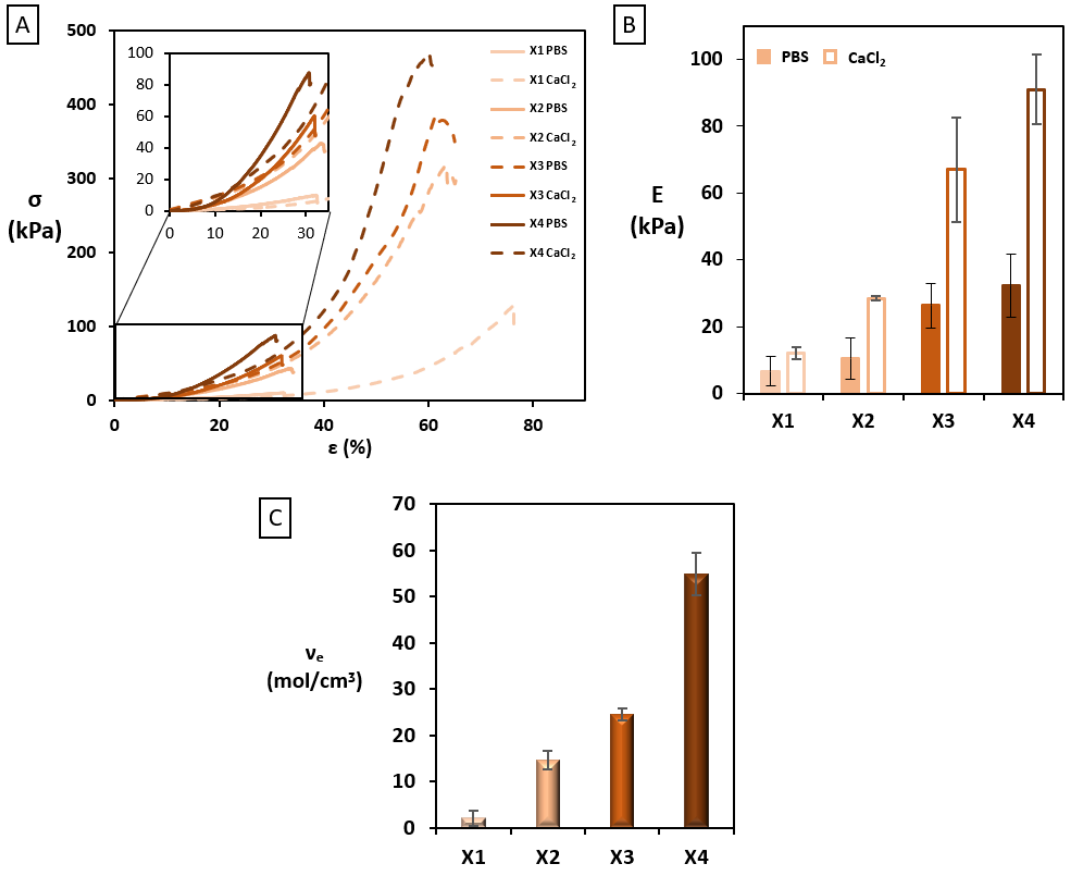

Figure V-3. A) stress strain curves of the hydrogels under compression testing B) compression modulus found at 3 % deformation of the hydrogels, C) crosslinking density as calculated using Flory-Rehner theory.

3.2. Thermogravimetric analysis (TGA)

From the thermograms of Alg8-F2.5 hydrogels crosslinked at various crosslinking degrees; several distinctive degradation zones are observed in Figure V-4A. First between 25 and 120 °C, weight loss is due to the evaporation of the remaining water in the hydrogels, between 200 and 300 °C, the first degradation of the alginate is observed and finally between 300 and 450 °C we observe the formation of alginate residue and the degradation of the Pluronic that is present in the hydrogel network as deduced from the separate thermograms of Alg8 and Pluronic hydrogels seen in Figure V-S5. Given that the alginate residue formation accounts for approximately 50% of the weight loss observed between 200 and 300 °C, the amount of degraded Pluronic can be deduced and is summarized in Figure V-4B. The hydrogels with the lowest crosslinking degree (X1) contain the highest percentage of Pluronic in the matrix around 40 %. Increasing the crosslinking density will result in the decrease of Pluronic quantity reaching 26 % for hydrogels crosslinked at X4. This difference can be attributed to the different reactivity between Alg-MA and F127-MA, where F127-MA photo-crosslinks at a higher rate, whereas Alg-MA requires a longer irradiation time to photo-crosslink.

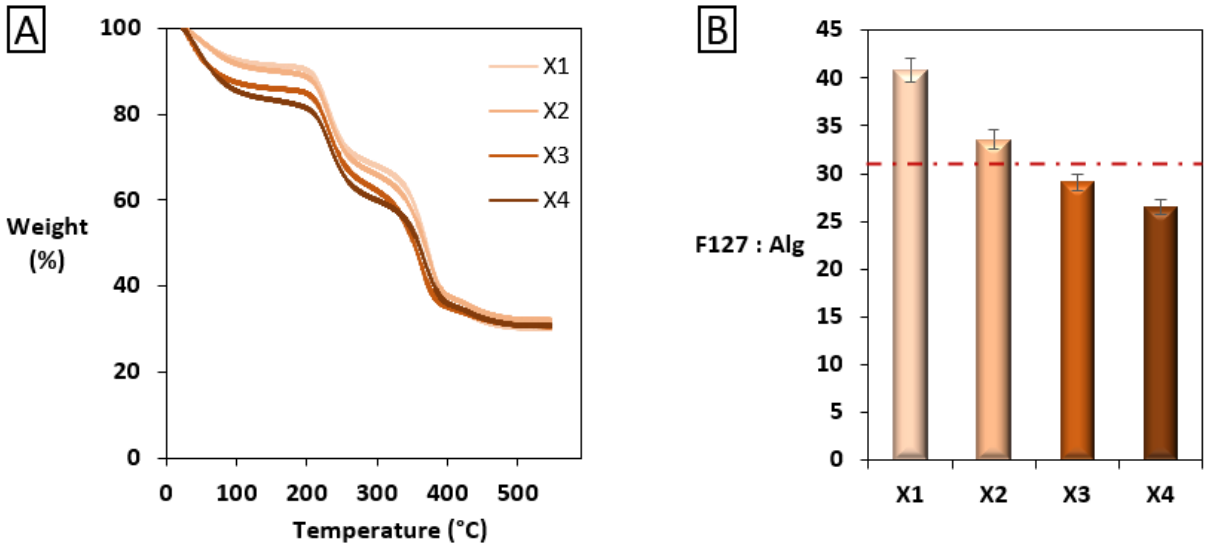

Figure V-4. A) Thermal degradation profiles of Alg8-F2.5 hydrogels crosslinked at X1, X2, X3 and X4 and B) mass ratio of F127-MA and Alg-MA in the hydrogels at different degrees of crosslinking as obtained from the thermograms.

3.3. Force Generated while swelling

Given that the hydrogels change dimensions when alternating between calcium solution to PBS, it is important to measure the force generated from the dual crosslinked hydrogel when submerged in PBS. This measurement will provide insight into the mechanical response and

potential applications of the hydrogels as biomedical devices. The force generated by tubular hydrogels at various degrees of crosslinking when releasing calcium was measured by allowing the hydrogels to swell in PBS in a confined environment. As the hydrogels expand by releasing the calcium ions, they exert a force on the compression disks (Figure V-5B). The radial forces generated by the hydrogel tubes were recorded as follows: X1 generated a force of 1.6 mN/mm over 80 minutes, X2 generated 2.7 mN/mm over 120 minutes, X3 generated 12.5 mN/mm over 250 minutes, and X4 generated 20 mN/mm over 280 minutes (Figure V-5A). These results indicate that the force generated during swelling increases with the crosslinking density, with higher crosslinked hydrogels taking longer to reach maximum force due to the tighter crosslinked network in accordance to the previously shown swelling kinetics. It is important to note that, Alg8 hydrogels generated higher radial forces as represented in Figure V-S6, however no plateau was reached due to the hydrogels rupture. Swelling in a confined environment results in the destruction of pure alginate hydrogel matrixes, where by the integration of Pluronic in the network, the hydrogels become more resistant.

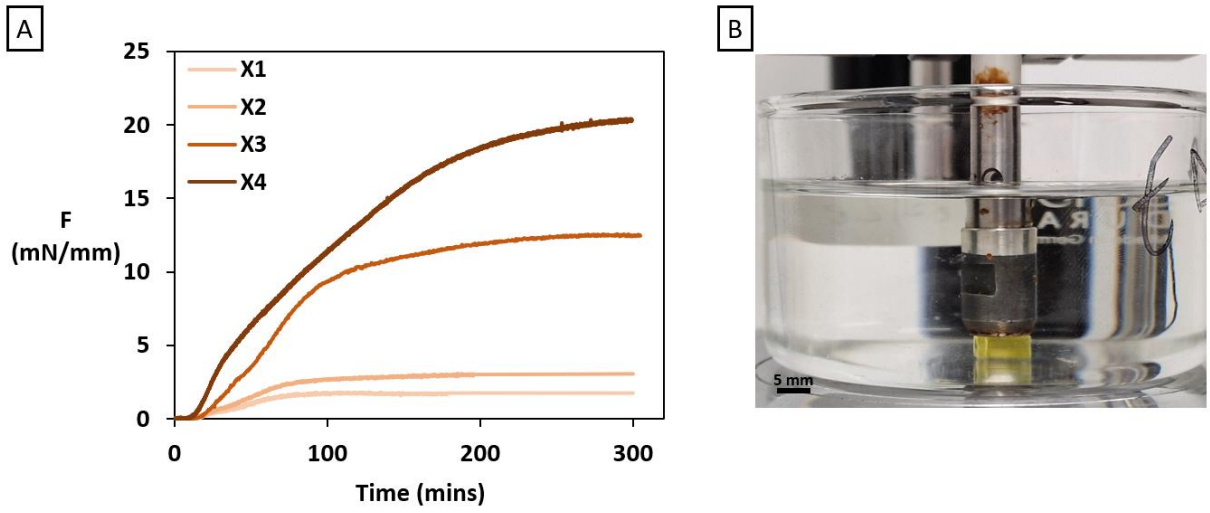

Figure V-5. A) Radial force generation from Alg8-F2.5 3D printing isotropic hydrogels photo-crosslinked at X1, X2, X3 and X4 when releasing calcium in a confined environment and B) a visual representation of the experiment.

3.4. Soft stent

Stenosisis the abnormal narrowing of a bodily channel that often occurs in blood vessels or ducts and can lead to severe health complications due to restricted flow. Traditional metallic stents are commonly used to maintain the patency of these channels, but they come with challenges such as rigidity, risk of tissue damage, the potential for long-term complications like restenosis and potential migration issues due to mal apposition to the narrowed duct.[19,20] To

address these issues, we have developed a 4D printed hydrogel stent, offering a softer and more adaptable alternative. The hydrogel material provides several advantages: its flexibility minimizes damage to surrounding tissues, and its biocompatibility reduces the likelihood of adverse reactions. In order for the 4D printed stent to maintain its position and adapt to the narrowed vessel for optimal duct apposition an anisotropic crosslinking gradient was implemented on a tubular architecture: X4 in the top and bottom sections and X1 in the middle section. Due to this anisotropic profile, the 4D printed hydrogels will exhibit a non-uniform expansion profile and will deform into a convex aspect in physiological conditions as seen in Figure V-6A. The device can be implanted in its shrunken state and when in PBS it will expand as schematized in Figure V-6B. Doing so, the force generated from the dual crosslinked hydrogel when placed in physiological conditions will be non-uniform and will avoid the migration of the device. To mimic extravascular tissue, the dual crosslinked hydrogel (in its shrunken form) was placed in a PDMS thin tube and submerged in 1% w/w EDTA solution. Throughout time, the calcium will be released from the hydrogel, and the device will swell and expand the PDMS tube as seen in Figure V-6C maintaining a flow in the PDMS tube.

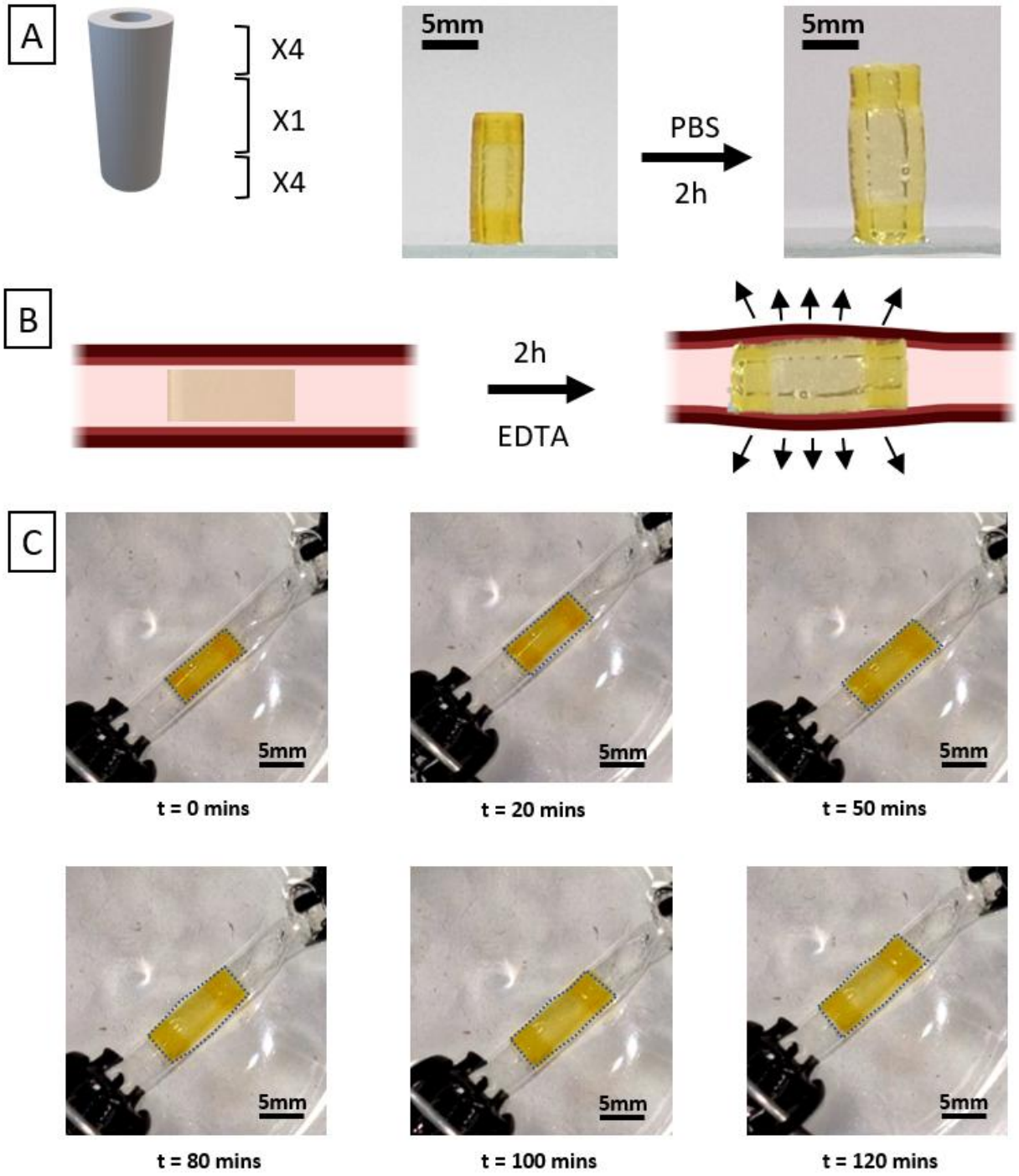

Figure V-6. A) The anisotropic crosslinking profile implemented on the STL tube design and the physical aspect of the hydrogel after printing when submerged in 5% w/w $CaCl_2$ solution and PBS. B) Schematic illustration of the soft stent as the 4D printed hydrogel is implemented in its shrunken state and C) timelapse of the expansion of the dual crosslinked hydrogel when placed a thin PDMS tube mimicking extravascular tissue.

3.5. Tissue filling

In tissue filling applications, particularly for intervertebral disc repair, the need for materials that can adapt and integrate seamlessly with the body's natural structures is crucial. Traditional fillers often face challenges such as insufficient adaptability to dynamic physiological environments and potential migration from the implantation site.[21] To address these limitations, we have developed 4D printed hydrogel based tubular structure designed to fill tissue voids effectively. The smart hydrogel is designed to shrink in calcium solution for noninvasive surgery and in physiological conditions it will expand and deform into a concave like structure. The design is obtained by implementing a triblock crosslinking gradient on a cylindrical STL design: the top and bottom sections of the hydrogel are crosslinked at X1 while the middle section is crosslinked at X4 as illustrated in Figure V-7A. This anisotropic crosslinking profile will induce a concave deformation of the cylinder where the 4D printed hydrogel is larger at the extremities than in the middle. This device can be used as tissue filler that will stay in place due to the non-uniform expansion profile. Once implemented in its shrunken form in a PDMS mold submerged in 1% w/w EDTA solution, the 4D printed device will expand throughout time as seen in the timelapse illustrated in Figure V-7C fill the missing part of the mold. Due to the anisotropic expansion profile, the 4D printed device will extend beyond the mold forming a plug at both extremities ensuring the stability of the device once implemented. This 4D printed hydrogels offer a significant potential as smart scaffold for the reconstruction of the annulus fibrosus tissue, providing targeted support and promoted tissue regeneration.

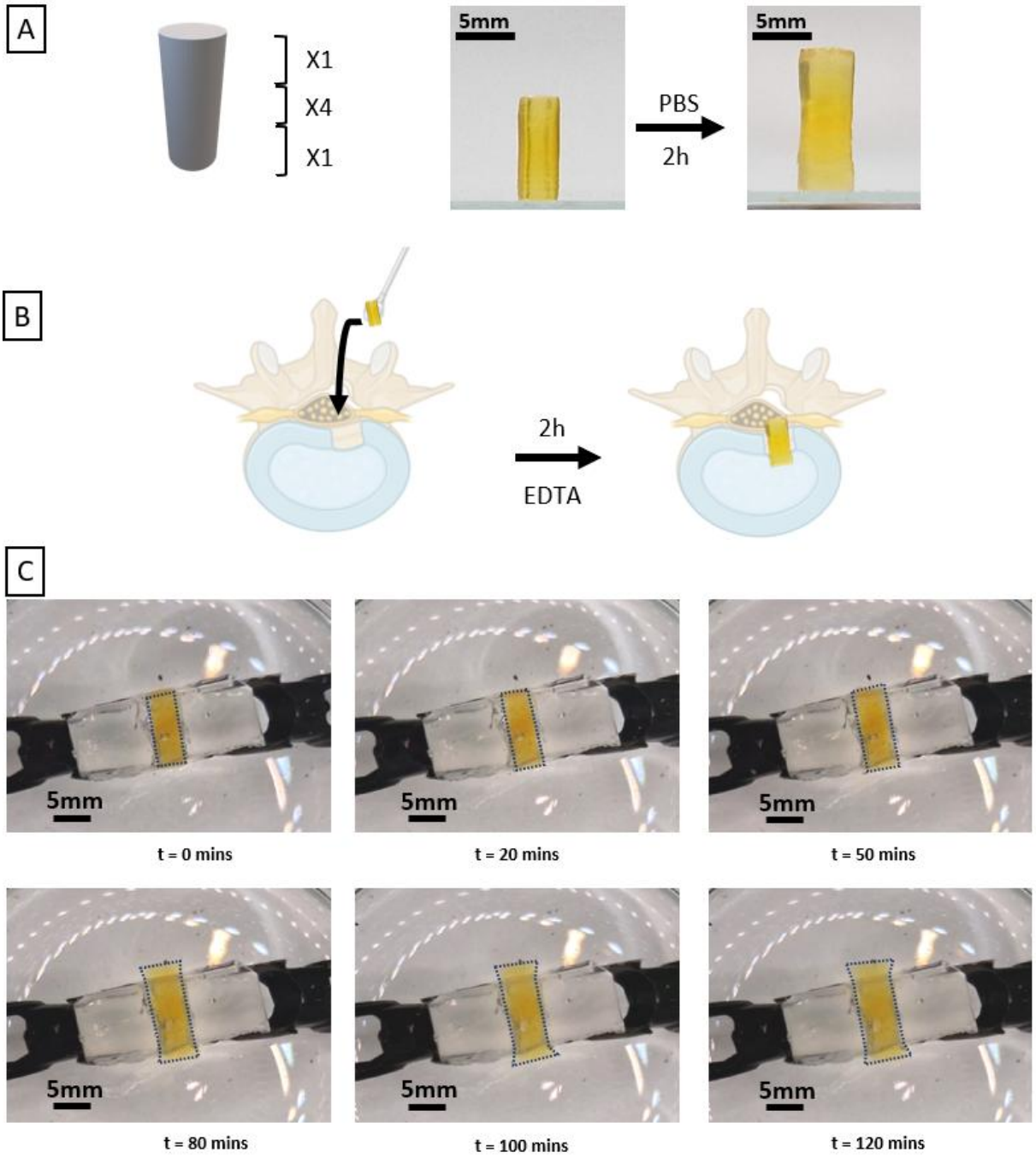

Figure V-7. A) The anisotropic crosslinking profile as implemented on the STL tube design and the physical aspect of the hydrogel in its shrunken and swollen state when submerged in 5% w/w $CaCl_2$ solution and PBS respectively. B) schematic illustration of 4D printed hydrogel as tissue filling and C) timelapse of the expansion of the hydrogel in a PDMS mold.

4. CONCLUSION

The mechanical properties of 3D printed alginate hydrogels were enhanced by incorporating Pluronic F127-MA into the formulation. The ability of the alginate to complex with calcium ions was not hindered by the Pluronic addition. The hydrogels shrunk in calcium

rich solution and regained their swollen state in physiological conditions. Several crosslinking degrees were achieved by varying the irradiation time during the printing process. It was observed that various dimensional changes of the hydrogels can be obtained from a singular STL design by simply adjusting the photo-crosslinking time, which in turn varies the crosslinking density of the network. The force generated due to the expansion of the hydrogels was measured, revealing a correlation between the exerted force and the crosslink density. Consequently, implementing a crosslinking gradient on a singular STL design will result in programmed shape deformations. Lastly, two models of 4D printed biomedical devices were designed as to simulate a soft stent for solution of stenosis disease and tissue filling in the model of intervertebral disk degeneration. Due to the anisotropic crosslinking profile, the devices were implemented in their shrunken state and reswollen in physiological media resulting in the adjusted expansion according to the morphology of a diseased site.

Supplementary Information Chapter V

4D Printed Alginate-Pluronic Hydrogels as Potential for Biomedical Devices

Sodium alginate and Pluronic F127 chemical modification

Methacrylated alginate (Alg-MA) was obtained by reacting low viscosity Alg-Na+ with methacrylic anhydride. A 4 wt/v% aqueous Alg-Na+ was prepared by dissolving 12 g of sodium alginate in 300 mL milli-q water in a 1 L round bottom flask under mechanical stirring (600 rpm). In order to obtain a homogeneous mixture, the solution was left to stir for 4 hours. TEA was then added at 40 molar equivalents with respect to MA and the solution was left to stir for 30 minutes to ensure complete homogenization. Finally, MA was added at 20 molar equivalents with respect to the sugar unit. The reaction was maintained at 24°C for 24 hours. Functionalized Alg-Na+ was obtained by precipitating the mixture in cold acetone followed by drying at 24°C under reduced pressure.

Similarly, Pluronic F127 was methacrylated by grafting methacrylate moieties on the hydroxyl at the chain ends using the same reaction conditions. 50g of Pluronic were dissolved in 70 mL of DCM to obtain a 71 w/w% solution in a 250mL round bottom flask under magnetic stirring (700 rpm) for 4 hours. 2 eq TEA was then added with respect to MA and the solution was left to stir for 30 minutes to ensure complete homogenization. Finally, 10 eq MA were added with respect to the hydroxyl groups. The reaction was maintained at 24°C for 24 hours. The Pluronic was precipitated in petroleum ether, solubilized in water and then purified by dialysis for 3 days in 500 Da membranes against distilled water while changing the water twice a day. Purified Pluronic was then recovered by freeze drying and then stored at -24°C prior to use.

^{1}H NMR characterization

In order to quantify the degree of modification (DM), ^{1}H NMR was used. 20 mg of Alg-MA was dissolved in 1mL D_2O and left to stir for 1 hours to obtain a homogeneous mixture. The ^{1}H NMR spectra were recorded on a Bruker Avance I 400 MHz (64 scans, 5 s relaxation time). The DM, defined as the number of methacrylates per sugar moiety, was calculated as the ratio of the protons of methacrylate (1.95 ppm, 5.8 ppm and 6.2 ppm) and H_{G1} proton of the

alginate using the following equation and was found to be equal to 140% with respect to a sugar moiety.

$$DM\ (\%) = M\% * \frac{I_{H\ vinyl\ 6.2\ ppm}}{I_{M\ 4.4\ ppm}} \qquad \text{(Equation V-S1)}$$

Where I_H represents the intensity of a vinyl protons of the grafted methacrylate at 6.2ppm, $I_{H_{G1}}$ represents the intensity of the anomeric protons of the guluronic moieties and G% represents the fraction of guluronic units in the polysaccharide. The M% is calculated by comparing the anomeric G proton at 5 ppm with the anomeric M proton at 4.4ppm and was found to be equal to 35%.

For methacrylated Pluronic, 5 mg of F127-MA were dissolved in 1mL D_2O and left to stir for 1 hour. The degree of modification (DM) defined as the percentage of functionalized hydroxyl groups was calculated by comparing the peaks of the grafted methacrylate protons at 1.95, 5.8 and 6.2ppm to the methylene protons (-CH_3) of the PPO units at 1.07 ppm and was found to be equal to 93%.

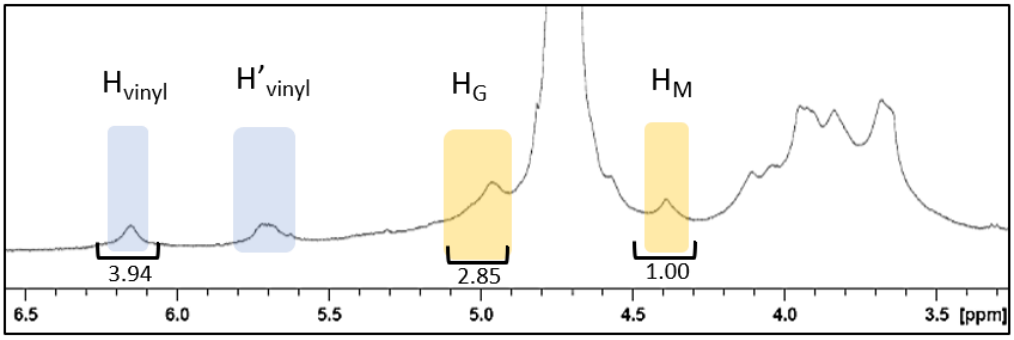

Figure V-S1. ^{1}H-NMR of methacrylated alginate in D_2O.

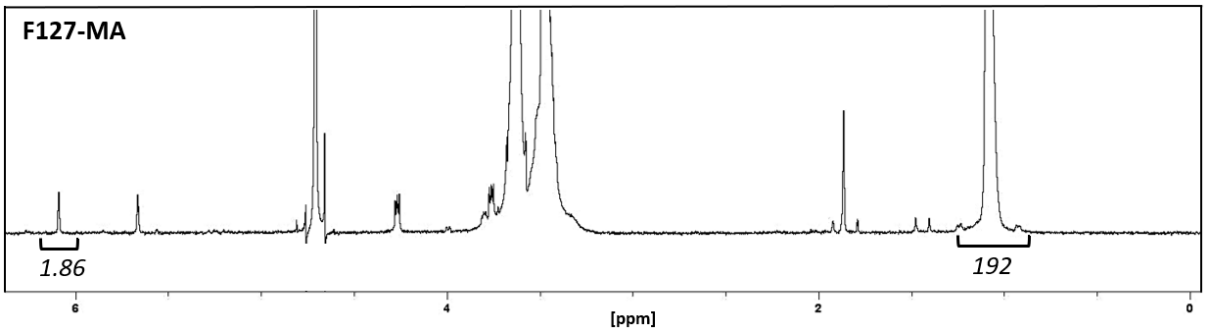

Figure V-S2. 1H-NMR spectra of the methacrylated F127-MA in D_2O.

3D Printing optimization

Light intensity during the printing process was tested at 5 and 10 mW/cm^2. The working curves correlating the irradiation time to the cured thickness were obtained for the Alg8-F2.5, Alg8-F5 and Alg8-F7.5 formulations. To ensure a good resolution printing and fast printing time, light intensity of 5 mW/cm^2 was chosen.

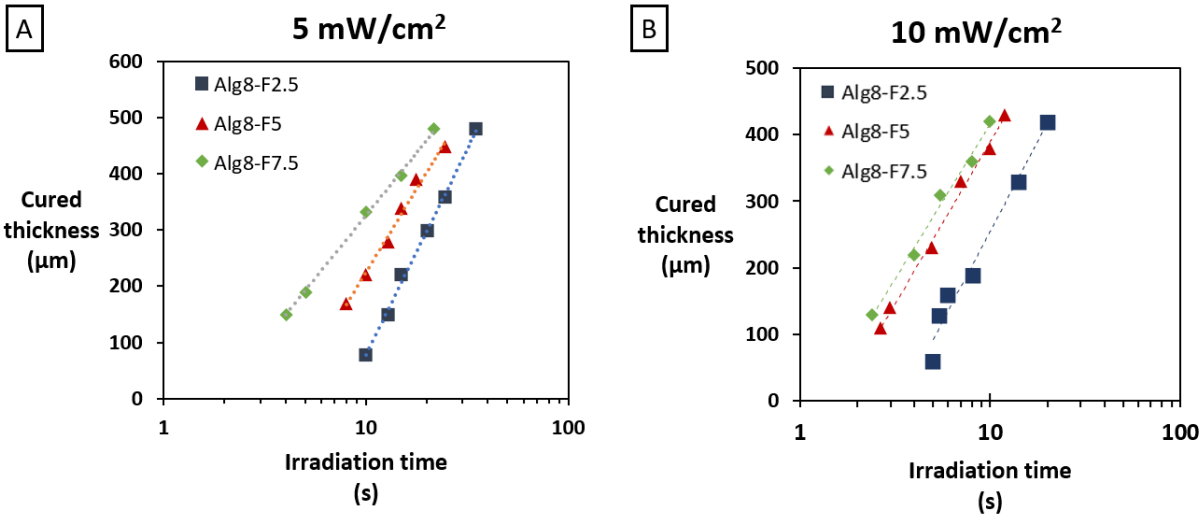

Figure V-S3. Working curves of the Alg8-F2.5, Alg8-F5 and Alg8-F7.5 under A) 5 mW/cm^2 and B) 10 mW/cm^2 UV intensity.

Table V-S1. Irradiation time of the 100 µm layer for the different alginate resins to obtain various degrees of crosslinking.

Curing time (s)	X1	X2	X3	X4
Alg8-F2.5	13	17	25	37
Alg8-F5	8	13	17	26
Alg8-F7.5	4,5	7,5	12,5	19

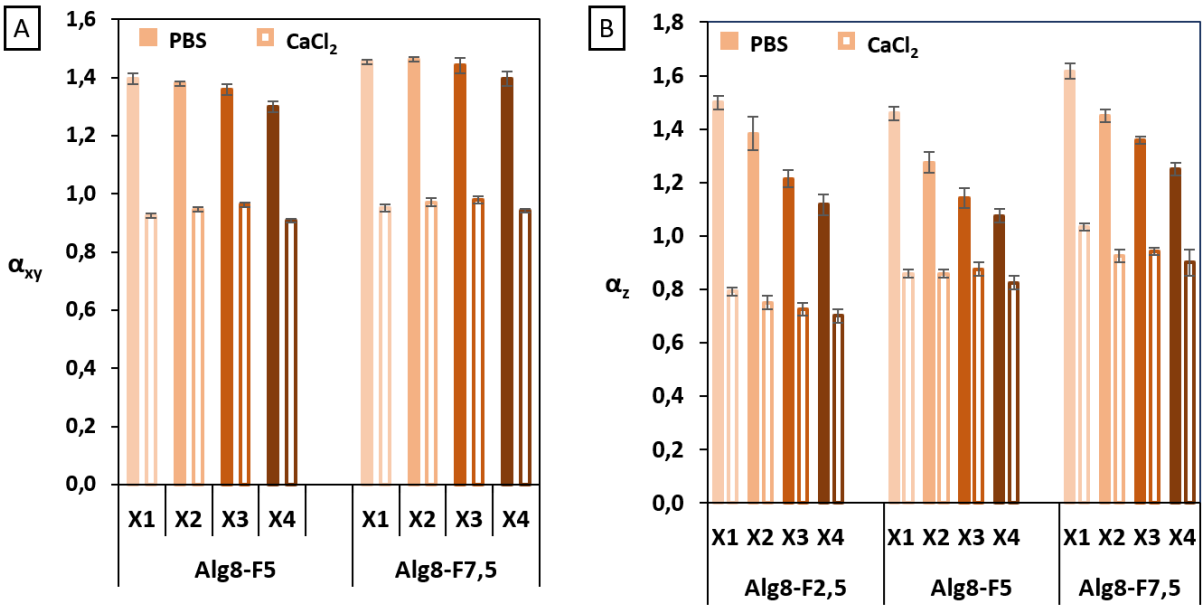

Figure V-S4. A) x-y expansion coefficient of the Alg8-F5 and Alg8-F7.5 hydrogels and B) z expansion coefficient of the Alg8-F2.5, Alg8-F5 and Alg8-F7.5 hydrogels at different degrees of crosslinking when swollen in PBS and calcium solution.

Thermogravimetric analysis

To quantify the amount of Pluronic in the crosslinked hydrogels TGA was performed. First, the tests conditions were optimized on alginate hydrogels that does not contain any Pluronic. Tests were done on sample oven dried or freeze dried. It was seen that freeze dried samples demonstrate a sharper curve due the sponge-like structure of the dried hydrogel. Moreover, heating rates of 10 and 5 °C/min were tested were the later showcased the best weight loss curve. From the alginate degradation spectra, several temperature ranges can be observed. Between 25 and 120 °C, weight loss occurs due to evaporation of moisture. The second weight loss occurs in the temperature range of 200 – 270 °C due to glycosidic bond cleavage. The final weight loss occurs between 300 and 470 °C attributed to the decomposition of the alginate backbone forming ashes as residue.[22,23] Across several samples, it was observed that the weight loss due to residue formation is about half of the weight loss occurring between 200 and 270 °C.

Moreover, TGA analysis was performed on 25% w/w Pluronic hydrogels, freeze dried at a 5 °C/min heating rate. As observed, before 100 °C, the evaporation of water occurs while the Pluronic demonstrate a sharp degradation between 320 and 400 °C leaving no residue.

From the individual degradation profile, distinctive peaks can be attributed to each component in the hydrogels containing both F127-MA and AlgMA. Hence, the percentage of Pluronic present in the hydrogels can be deduced.

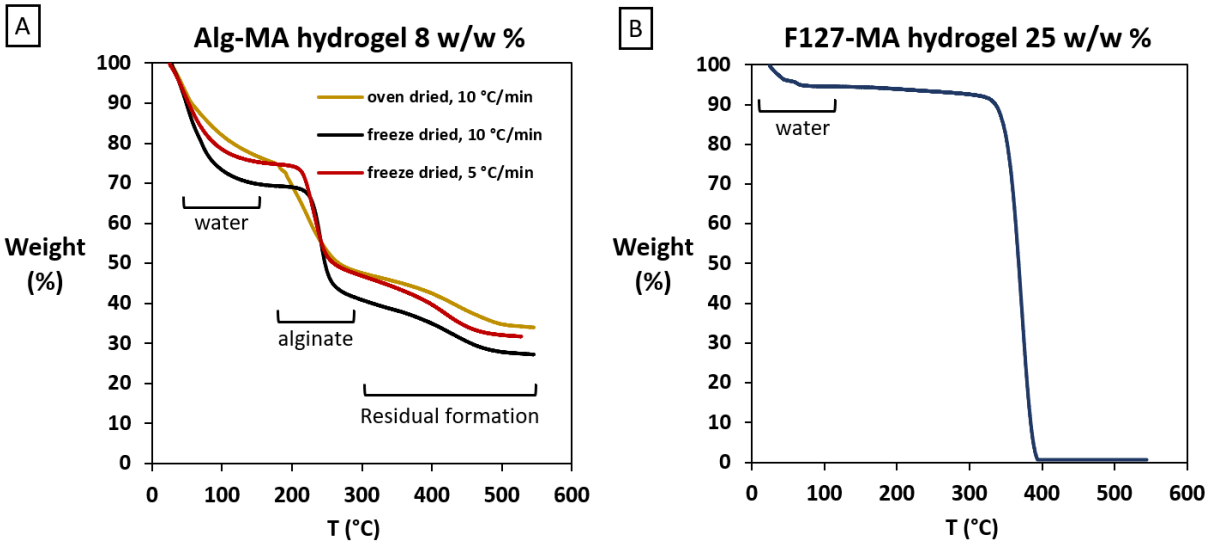

Figure V-S5. Thermograms of A) 8% w/w alginate hydrogels at different heating rates and drying conditions and B) 25% w/w freeze dried Pluronic F127-MA at 5 °C/min heating rate.

Force generated by swelling of Alg8

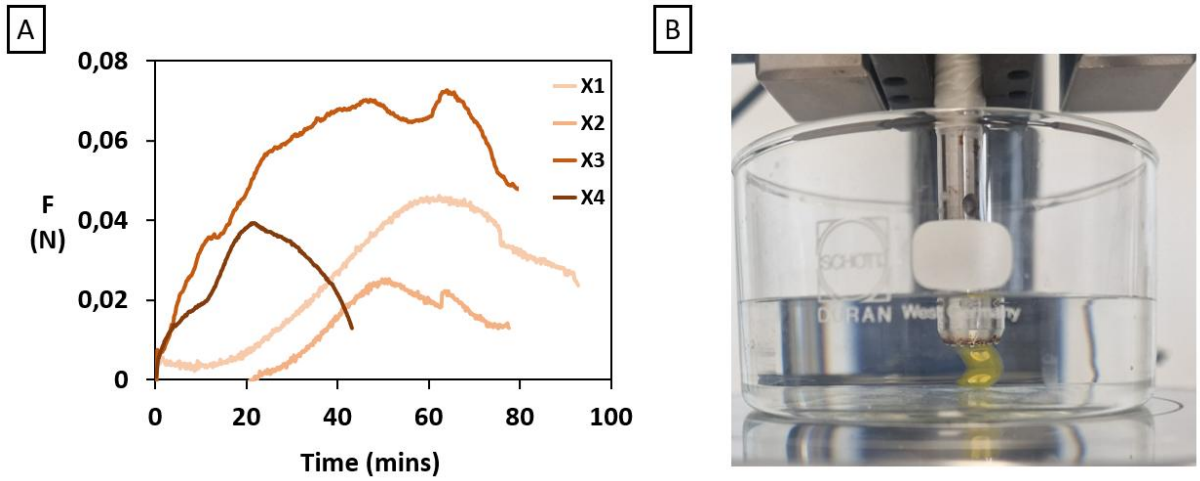

Figure V-S6. A) axial force generated from the shrunken hydrogels when submerged in 1% w/w EDTA solution and B) physical aspect of the bending of Alg8-F2.5 hydrogel crosslinked at X1 when expanding in a confined place.

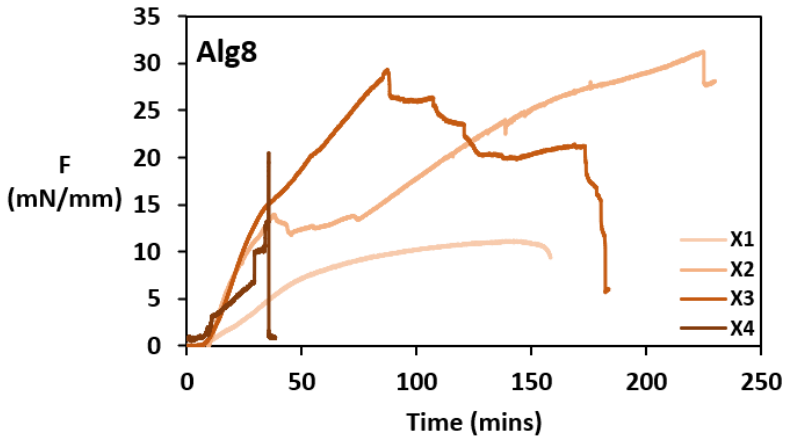

Figure V-S7. Radial force generated from the shrunken Alg8 tubular hydrogels crosslinked at X1, X2, X3 and X4 when submerged in 1% w/w EDTA solution. All hydrogels broke and did not reach equilibrium.

REFERENCES

[1] M. Champeau, D. A. Heinze, T. N. Viana, E. R. De Souza, A. C. Chinellato, S. Titotto, *Adv. Funct. Mater.* **2020**, *30*, 1910606.

[2] Z. U. Arif, M. Y. Khalid, A. Zolfagharian, M. Bodaghi, *Reactive and Functional Polymers* **2022**, *179*, 105374.

[3] P. Fu, H. Li, J. Gong, Z. Fan, A. T. Smith, K. Shen, T. O. Khalfalla, H. Huang, X. Qian, J. R. McCutcheon, L. Sun, *Progress in Polymer Science* **2022**, *126*, 101506.

[4] N. N. Ferreira, L. M. B. Ferreira, V. M. O. Cardoso, F. I. Boni, A. L. R. Souza, M. P. D. Gremião, *European Polymer Journal* **2018**, *99*, 117.

[5] E. M. Ahmed, *Journal of Advanced Research* **2015**, *6*, 105.

[6] E. Yarali, M. J. Mirzaali, A. Ghalayaniesfahani, A. Accardo, P. J. Diaz-Payno, A. A. Zadpoor, *Advanced Materials* **2024**, *36*, 2402301.

[7] A. Gevorkian, S. M. Morozova, S. Kheiri, N. Khuu, H. Chen, E. Young, N. Yan, E. Kumacheva, *Adv. Funct. Mater.* **2021**, 2010743.

[8] A. Sydney Gladman, E. A. Matsumoto, R. G. Nuzzo, L. Mahadevan, J. A. Lewis, *Nature Mater* **2016**, *15*, 413.

[9] Z. Chen, D. Zhao, B. Liu, G. Nian, X. Li, J. Yin, S. Qu, W. Yang, *Adv. Funct. Mater.* **2019**, *29*, 1900971.

[10] M. Habib, S. Berthalon, L. Leclercq, A. Tourrette, T. Sharkawi, S. Blanquer, *Biomacromolecules* **2024**, *25*, 1660.

[11] A. Yumin, D. Liguo, Y. Yi, J. Yongna, *RSC Adv.* **2022**, *12*, 11632.

[12] K. Lei, Z. Li, D. Zhu, C. Sun, Y. Sun, C. Yang, Z. Zheng, X. Wang, *J. Mater. Chem. B* **2020**, *8*, 794.

[13] W. Xing, Y. Tang, *Nano Materials Science* **2022**, *4*, 83.

[14] L. Bova, F. Maggiotto, S. Micheli, M. Giomo, P. Sgarbossa, O. Gagliano, D. Falcone, E. Cimetta, *Macromol. Biosci.* **2023**, *23*, 2200357.

[15] S. S. Sohn, V. Revuri, M. Nurunnabi, K. S. Kwak, Y. Lee, *Macromol. Res.* **2016**, *24*, 282.

[16] T. Majima, W. Schnabel, W. Weber, *Makromol. Chem.* **1991**, *192*, 2307.

[17] M. Mooney, *Journal of Applied Physics* **1940**, *11*, 582.

[18] D. L. Martin Jr, *Army Propulsion Laboratory and Center, Research and Engineering Directorate, U.S. Army missle command* **1970**, *Redstone Arsenal, Alabama*.

[19] H. Li, W. Wu, X. Liu, C. Wen, *Journal of Materials Science & Technology* **2023**, *152*, 148.

[20] I. Imaz-Iglesia, S. García-Pérez, A. Nachtnebel, B. Martín-Águeda, C. Sánchez-Piedra, B. Karadayi, A. R. Demirbaş, *Expert Review of Medical Devices* **2016**, *13*, 583.

[21] Y. Liu, Z. Zhao, C. Guo, Z. Huang, W. Zhang, F. Ma, Z. Wang, Q. Kong, Y. Wang, *Front. Cell Dev. Biol.* **2023**, *11*, 1286223.

[22] A. Salisu, M. Marsin Sanagi, A. Abu Naim, K. Juhanni Abd Karim, *Res. J. Pharm., Biol. Chem. Sci.*

[23] N. Işıklan, F. Kurşun, *Polym. Bull.* **2013**, *70*, 1065.

CONCLUSION GENERALE

Conclusion Générale

Ces travaux de thèse apportent une contribution majeure à l'avancement des technologies d'hydrogels par impression 4D, en ouvrant la voie au développement d'une nouvelle génération de dispositifs médicaux intelligents à base de polysaccharides (Figure A). Les actuateurs hydrogels, créés à l'aide de ces technologies avancées, offrent des perspectives inédites dans la conception de matériaux capables de déformations programmées en réponse à des stimuli externes. Cette capacité de réponse dynamique permet non seulement d'améliorer la fonctionnalité des dispositifs médicaux, mais aussi de créer des solutions plus personnalisées et adaptées aux besoins spécifiques des patients. En exploitant les propriétés réactives et adaptatives des hydrogels, ces travaux ouvrent de nouvelles avenues pour des applications biomédicales innovantes, telles que les implants intelligents et la chirurgie non invasive, marquant ainsi un progrès significatif dans le domaine de la biomédecine.

Le **chapitre I** a établi les bases de conception d'actuateurs en explorant les polymères utilisés dans les hydrogels intelligents mettant en évidence la nécessité de rechercher des alternatives aux polymères synthétiques dominants, en particulier les polymères naturels aux propriétés prometteuses. Ce chapitre a également abordé la variation des géométries des actuateurs, allant de structures unidimensionnelles (1D), telles que les barres, aux structures bidimensionnelles (2D), comme les films, jusqu'aux architectures tridimensionnels (3D). La compréhension et contrôle de l'actuation de ces systèmes deviennent de plus en plus complexes à mesure que l'échelle augmente, et ces systèmes tridimensionnels sont souvent moins étudiés, principalement ceux à base de polymères naturels.

Le **chapitre II** a approfondi l'élaboration d'hydrogels à base d'alginate par photo-réticulation, en examinant l'impact de la masse molaire et du degré de méthacrylation sur les propriétés des hydrogels. Cette étude a permis de mieux comprendre l'influence du stimulus ionique sur les propriétés de gonflement, mécanique et d'auto-réparation de ces hydrogels ainsi que la conception d'actuateur par une méthode simple et rapide ayant une déformation contrôlée et programmée.

Le **chapitre III** a mis en lumière les avancées dans l'impression 4D des hydrogels en contrôlant les gradients de réticulation pour générer des déformations programmées sur de diverse géométrie allant des films (2D) à des structures 3D plus complexe. Cette approche a démontré

une réversibilité et une capacité d'adaptation sous stimulus ionique, ouvrant la voie à de potentielles applications novatrices dans les dispositifs médicaux et les implants.

L'objectif du **chapitre IV** était de développer un système multi-stimulable en combinant l'alginate avec des composés thermo-stimulables. Le Pluronic semblait être une option prometteuse du fait de sa réponse thermique modulable. L'influence de la méthacrylation sur les propriétés thermiques des Pluronics P123, P104 et F127 a permis d'établir de nouveaux diagrammes de phases après modification chimique. Les résultats de l'étude rhéologique ont révélé que le meilleur candidat était le Pluronic F127 méthacrylé, par contre pour des concentrations élevées (20% w/w). Toutefois, nous avons observé des propriétés mécaniques prometteuses avec les Pluronics. C'est pourquoi, le **chapitre V** a consisté à améliorer les propriétés mécaniques de l'alginate en utilisant le Pluronic, tout en minimisant la quantité utilisée afin de ne pas altérer la réponse au stimulus ionique.

Ainsi, dans le **chapitre V**, nous avons tenté de compléter ces recherches en démontrant l'application de l'impression 4D pour créer des hydrogels à base d'alginate renforcés mécaniquement avec le Pluronic F127 méthacrylé. Ces hydrogels ont été utilisés pour développer des prototypes de dispositifs médicaux, tels que des stents vasculaires ou encore des scaffolds pour le comblement tissulaire, illustrant le potentiel de ces matériaux pour transformer les pratiques biomédicales.

Les perspectives de ces travaux de thèse sont prometteuses et ouvrent la voie à de nombreuses applications futures en tant que dispositifs médicaux de comblement tissulaire, cicatrisation de plaies ou encore ingénierie tissulaire par bio-impression. Ce système peut également coupler tous ces domaines avec un système de libération de principe actifs (PA) grâce à sa versatilité. En effet, la présence de groupements carboxyliques peut favoriser l'encapsulation de PA chargés positivement, et la présence des micelles de Pluronic permettrait l'encapsulation de PA hydrophobes. L'utilisation des hydrogels stimulables pour la libération contrôlée de médicaments offre un potentiel pour des traitements plus ciblés et efficaces, permettant d'adapter la libération des substances actives en fonction des besoins spécifiques du patient et des conditions physiologiques. En outre, il est possible d'améliorer encore les propriétés mécaniques des hydrogels en explorant les systèmes composites ou en testant des mélanges de polymères pour obtenir des systèmes multi-stimulables. L'intégration de différents types de polymères ou de charges dans les hydrogels peut permettre d'adapter leur comportement en réponse à une gamme plus large de stimuli, tels que la température, le pH, ou la lumière, tout

en renforçant leurs propriétés mécaniques. Ces développements pourraient conduire à la création de matériaux hybrides offrant une plus grande polyvalence et performance, et ouvrir de nouvelles possibilités pour des applications biomédicales avancées, allant des dispositifs médicaux intelligents aux systèmes de régénération tissulaire.

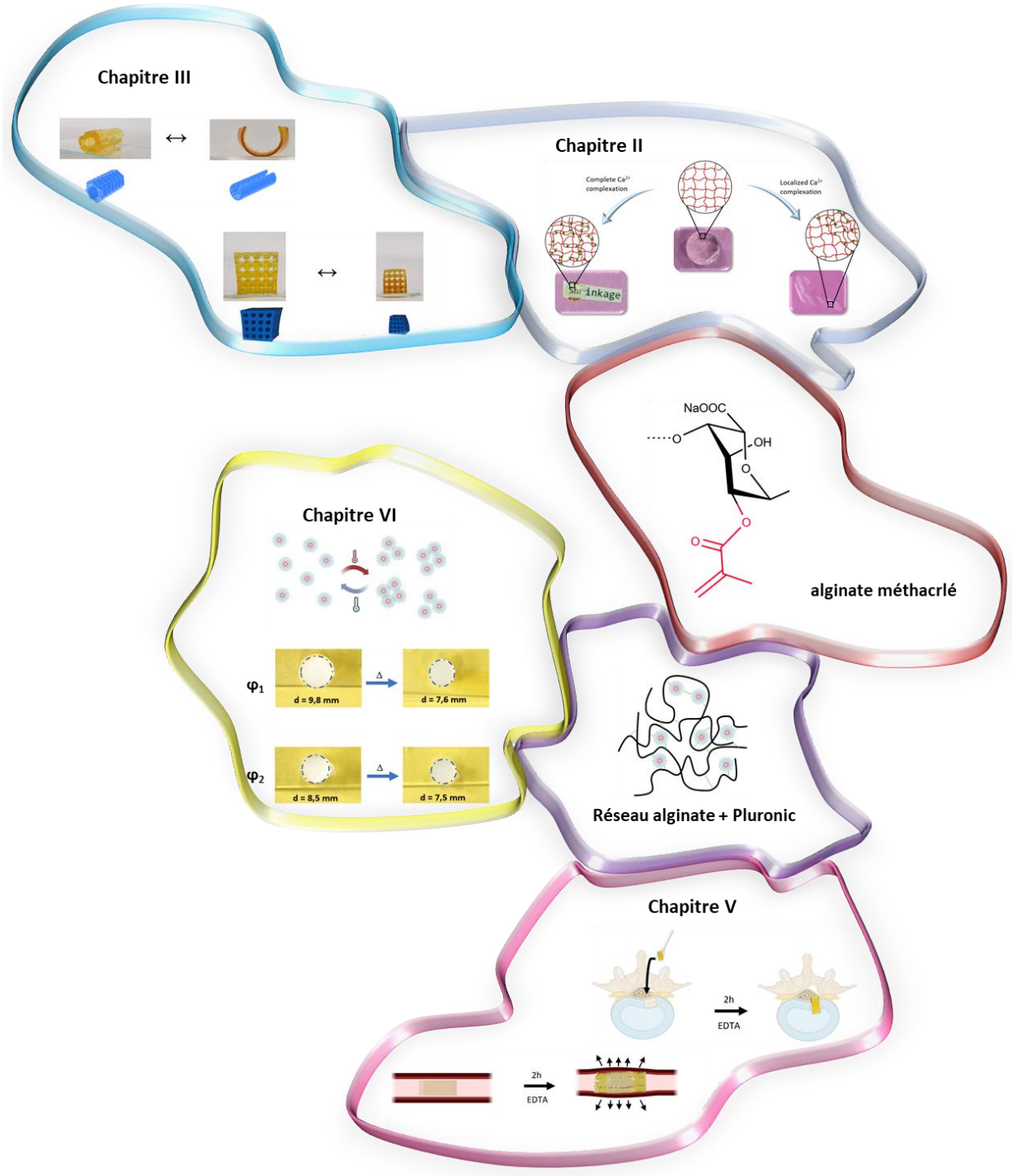

Figure A. Illustration des travaux effectués durant la thèse.

Dispositifs médicaux intelligents à base d'hydrogel de polysaccharide obtenus par Impression 4D

L'impression 4D est le processus par lequel un objet imprimé en 3D est transformé en une structure différente sous l'influence d'un stimulus. La possibilité d'imprimé des hydrogels en 4D permet d'envisager des applications potentielles dans le domaine biomédical. En effet, la conception de dispositifs médicaux capables de changer de forme et de fonction en réponse à des stimuli physiologiques ou externes spécifiques peut offrir des solutions de traitement personnalisées et évolutives, améliorant ainsi les thérapies en fonction des besoins spécifiques des patients. Les systèmes étudiés dans la littérature sont souvent conçus à partir de polymères synthétiques qui peuvent présenter certaines limites en termes de biocompatibilité et de biodégradabilité. Ce travail propose l'élaboration d'hydrogels à base de polymère naturel, l'alginate, obtenus par photo-réticulation. En modifiant des paramètres tels que la masse molaire et le degré de méthacrylation, il est possible de contrôler les caractéristiques des hydrogels et leurs réponses de changement morphologique lors d'un stimulus ionique. Cette flexibilité s'est révélée utile pour ajuster les propriétés morphologiques et mécaniques en fonction d'une application particulière. Il a donc été possible d'imprimer des hydrogels avec desdéformations programmées en contrôlant la photo-réticulation spatiale du gel. Afin d'ajouter un autre stimulus au système à base d'alginate, l'intégration d'un polymère thermosensible à base de Pluronic a été proposée. Pour ce faire, une étude approfondie a été réalisée pour comprendre l'influence de la méthacrylation sur les propriétés thermiques des Pluronics. Cette analyse a permis d'établir des diagrammes de phases pour les Pluronics P123, P104 et F127, démontrant comment ces matériaux réagissent aux variations de température. Les hydrogels à base d'alginate renforcés par le Pluronic F127 méthacrylé ont montré des propriétés mécaniques améliorées tout en maintenant des déformations programmées. Finalement, ce travail a permis de démontrer des preuves de concept de dispositifs commedes stents et des scaffolds pour le comblement tissulaire, capables de s'adapter aux sites d'implantation spécifiques du corps et répondre de manière dynamique aux stimuli.

Smart medical devices based on polysaccharide hydrogel obtained by 4D printing

4D printing is the process by which a 3D-printed object is transformed into a different structure under the influence of a stimulus. The possibility of printing hydrogels in 4D opens up potential applications in the biomedical field. Indeed, the design of medical devices capable of changing shape and function in response to specific physiological or external stimuli can offer personalized and adaptive treatment solutions, thereby improving medical therapies based on the specific therapeutic needs of patients. The systems studied in the literature are often designed from synthetic polymers, which may present certain limitations in terms of biocompatibility and biodegradability. This work proposes the development of hydrogels based on a natural polymer, alginate, obtained through photoreticulation. By modifying parameters such as molecular weight and the degree of methacrylation, it is possible to control the characteristics of the hydrogels and their morphological responses to an ionic stimulus. This flexibility has proven useful for adjusting the morphological and mechanical properties according to a specific application. It was therefore possible to print hydrogels with programmed deformations by controlling the spatial photoreticulation of the gel. To add another stimulus to the alginate-based system, the integration of a thermosensitive polymer based on Pluronic was proposed. To achieve this, an in-depth study was conducted to understand the influence of methacrylation on the thermal properties of Pluronics. This analysis enabled the establishment of phase diagrams for Pluronics P123, P104, and F127, demonstrating how these materials respond to temperature variations. The alginate-based hydrogels reinforced with methacrylated Pluronic F127 showed improved mechanical properties while maintaining programmed deformations. Finally, this work demonstrated proof of concept for devices such as stents and scaffolds for tissue filling, which can adapt to specific implantation sites in the body and respond dynamically to stimuli.